THE HONG KONG
POLYTECHNIC UNIVERSITY
香港理工大學

Department of Industrial and Systems Engineering

LASER STRUCTURING OF ULTRA-FINE CIRCUIT LINES IN PRINTED CIRCUIT BOARDS

by

Zhang Bin

A thesis submitted in partial fulfillment of the requirements for the degree of

DOCTOR OF PHILOSOPHY

July, 2006

CERTIFICATE OF ORIGINALITY

I hereby declare that this thesis is my own work and that, to the best of my knowledge and belief, it reproduces no material previously published or written, nor material that has been accepted for the award of any other degree or diploma, except where due acknowledgement has been made in the text.

(Signed)

ZHANG BIN (Name of student)

ABSTRACT

Laser structuring technique emerged in recent years for the need of fabricating fine circuit lines and spaces in printed circuit board. Most of the previous work only introduced laser structuring as a new method in the fabrication of fine circuit lines and mentioned that the width of circuit line can be reduced under 50 μm or below with this technique. Laser structuring technique will have a prosperous future only when the relationship between process parameters and fabrication results are deeply understood. In this work, the study focused on the control, optimization of process parameters and the prediction of circuit geometry in laser structuring technique. Also, the minimum width of circuit lines and circuit spaces fabricated with laser structuring technique that can pass quality and reliability tests were investigated.

In laser structuring of circuit lines (and circuit spaces), there are a number of process parameters. This study firstly focused on investigating the influences of the process parameters in the three main steps of this technique - the tin electroplating step, the laser writing step and the copper etching step. The effect of electroplating time and current density on the thickness of the tin layer in the tin electroplating step, the effect of laser power, repetition rate, number of repetitions and laser bite size of a frequency-tripled Nd:YAG laser (355-nm wavelength) to the geometry of the circuits in the laser writing step, the effect of time and circuit geometry (after the laser writing step) to final geometry of the circuits in the copper etching step were investigated. From these investigations, relations between the complex process parameters to the fabrication results in laser structuring have been identified.

Excimer laser (KrF, 248 nm wavelength) was used as another laser source in laser structuring. Excimer laser shows its advantages when the total width of circuit

line and space was as fine as below 60 μm, which cannot be achieved by Nd:YAG laser. When the total width of circuit line and circuit space was above 60 μm, it was more efficient to use Nd:YAG laser as laser source whose scanning velocity was about 120 times faster than Excimer laser.

Laser writing is the key step in the fabrication of fine circuit lines and circuit spaces in laser structuring. The laser parameters in laser writing step will directly influence the geometry of the circuit space. A set of experiments was designed using the Taguchi methodology, in which all parameters of interest are varied over a specified range, to obtain the quantitative estimations of the various parameters and the main parameters affecting the geometry of the circuit space. According to the analysis of variance (ANOVA), the main characteristic parameters that influence the geometry of the circuit space - depth of space, width of space and resolidification height - were investigated. Laser power and number of repetition are the most important parameters in the laser structuring process that have influences on all the experimental results—the space width, the space depth and the resolidification height. Some other parameters should also be considered in the experiment process according to the ANOVA analysis such as repetition rate and bite size.

A model of this non-linear system (laser writing step) might help the industry on the applicability of the laser structuring technique. Artificial neural network (ANN) is a useful tool for predicting outcome results and optimizing the operation parameters of the aforesaid non-linear process. ANNs are the fist time to be used in the study of laser writing step in laser structuring technique. Two artificial neural network (ANN) models were designed - ANN prediction model and ANN optimization model. The ANN prediction model is used to predict the geometry of the circuit space and the ANN optimization model is used to select optimum process parameters that can achieve an acceptable geometry for the circuit space in the laser writing step. In the ANN prediction model, the errors between the prediction results and experimental results were within ten percent. The optimum results from the ANN optimization model also matched the experimental results very well. With a new approach, by combining the characteristic parameters of circuit space predicted by the ANN prediction model and the mathematical description of the Gaussian profile, the geometry of the cross-sectional profile of the circuit space with the consideration of resolidification height in the laser writing step can be calculated.

After the laser writing and copper etching steps (tin layer was also stripped away), the final circuit lines and circuit spaces fabricated were tested using the quality and reliability tests – electrical open/short test, peel test and surface insulation resistance test (SIR test). The minimum width of circuit lines and spaces that passed the open/short test was as narrow as 25±5/40±5 μm. From the investigation, it was found that the variation of the width of the circuit lines and spaces was caused by the bite size of the laser, a splashing problem of melting materials in the laser writing step and a tin-layer cracking problem caused by etching in the copper etching step. When the variance of the widths of the circuit lines is ±5 μm, the variance of the width of the circuit line is just matching the IPC standard (IPC 6011) of ±20%. The copper circuit lines are found to be separate from the dielectric layer when the widths of circuit lines are under 10 μm. So the adhesion quality of circuit lines fabricated by laser structuring is acceptable only when the width of circuit lines is above 10 μm. When the widths of circuit spaces were above 45 μm, the resistance between isolated copper lines was above 10^6 ohm from the beginning to the end of the SIR test. The

minimum width of circuit spaces that can pass the SIR test was 45 μm. In general, the minimum widths of circuit lines and circuit spaces with good quality and reliability fabricated by laser structuring were 25 μm and 45 μm respectively.

The project is significant for both applied and academic fields. This study contributes to the understanding of the laser structuring technology and is of benefit in the fabrication of very fine line circuits in advanced printed circuit board industry.

ACKNOWLEDGEMENTS

Firstly, I wish to acknowledge the continuous support, valuable guidance and enthusiastic encouragement provided by my supervisor, Dr. K. C. Yung throughout my studies.

I also wish to express my sincere thanks to Mr. S. Y. Lau for his technical support in using some laboratory equipment, and to Mr. M. N. Yeung for his technical help in taking some SEM photos.

I would like to thank my colleagues and friends in The Hong Kong Polytechnic University for their help and technical support. Special appreciation is extended to Mr. Tam Siu Lim, Mr. Lee Chung Pang, Mr. Wong Chi Kui, Mr. Wong Wai Chung, Ms. Cheung Wan Sze, Mr. Guo Li Feng for their kind help.

Lastly, many thanks are due to my parents, Zhang Kui Ren and Lin Shu Qing, who have been most understanding and supportive throughout my study.

CONTENTS

LIST OF FIGURES

LIST OF TABLES

LIST OF SYMBOLS

A: absorbtivity of material

b: the bias

c: the specific heat

C: the concentration of the etchant

C^b: the bulk concentration

d: the width of circuit space

d_b: the bite size of laser beam

d' : axial coordinate

D: thermal diffusivity $D=k/c\rho$

D_d: the distance between two outer edges of circuit space

D_e: diffusion coefficient of etchant

E: the energy of laser beam

E_r: the energy passed through the aperture on mask

Err: error of unit in ANN

F: the ratio of variance

f: the focal length of the image lens

g: the width of the rectangular beam of Excimer laser

h: the resolidification height of circuit space

h_m: the heat required to vaporize the unit mass of material

$h_l^{\max}$: the maximum melt depth of material

H_1: the smallest width of circuit space

H_2: the difference between the largest space width and the smallest space width

I_0: laser intensity

I_a: the laser intensity absorbed by material

k: thermal conductivity

κ: the rate constant of chemical reaction

k_A: number of levels for factor A

k_r: a constant determined by a chemical reaction

k^*: function of wavelength and temperature for metallic materials

l: the length of the rectangular beam of Excimer laser

L_d: the heat diffusion length

L': the latent heat per unit mass

L_m: the melting heat

L_v: the evaporation heat

m: the number of molecules of active etching component required to dissolve one molecule of the solid

M_s: the molecular weight of solid

m': a complex refractive index

n: functions of wavelength and temperature for metallic materials

P_{out}: the output laser power

Q_a: the energy absorbed by material

r: radius

r': the distance

r_0: the half width of circuit space before etching step

r_e: the half width of circuit space after etching step

R: the spectral and intensity-dependent reflectivity for a defined surface

R_s: the number of repetitions

R_r: the repetition rate of laser

R_T: the reflectivity of tin

R_C: the reflectivity of copper

S: the surface area under irradiation

SS: sum of squares

t: time

t_b: the time needed to reach the evaporation point

T_m: the melting temperature

T_v: the evaporation temperature

T_0: the initial temperature

u: the distance from the mask plane to the image lens

V: variance

v: the velocity of laser $v=R_r d_b$

$v_{A:}$ degrees of freedom for factor A

v_i: the distance from the image lens to the workpiece

v_s: the ablation velocity

W: the laser power of per pulse

W_{ij}: the weight

w: the radius of laser beam

w_1: the effective width of a conductor

x,y: axial coordinate

X: the input of node in ANN

Y: the output of node in ANN

z: the depth of circuit space before etching step

z_e: the depth of circuit space after etching step

z_1: the distance from focal plane to material

z_r : the Rayleigh length

Greek letters

ρ: the specific weight

α: the linear absorption coefficient of solid

α^{-1}: light penetration depth

β: dimensionless parameter in chemical etching process

β_a: the angle

γ: a constant in chemical etching process

τ: the duration of laser pulse

θ: the angle on the cross sections of circuit lines

λ: the wavelength

ω: factor, the physically reasonable values of ω are within $0.25<\omega<1$

δ: the etching thickness in etching process

σ: correction factor, $0<\sigma<1$

ε: a constant for material $\varepsilon = cT_v / L_v$

v : the speed of boundary in the evaporation-controlled limit

η: dimensionless time

η_0: the demagnification ratio

ξ: dimensionless position of the laser structuring front

ζ: dimensionless axial coordinate

ϕ : dimensionless temperature

CHAPTER 1

INTRODUCTION

1.1 The trends in printed circuit board manufacture

Global trends and challenges that affect the electronics industry have a substantial influence on printed circuit board (PCB) manufacturers because of the growing demand for portable products such as mobile phones, notebook computers, and personal digital assistants (PDAs). The PCB industry follows the famous Moore's Law (chip density doubling every 18 months) as in semiconductor industry (Terliuc & Benron, 1999). The printed circuit board (PCB) industry is experiencing a tremendous increase in demand for high-density boards and multiplayer boards, which will allow new IC component types to be properly and reliably interconnected to PCBs. Considering that it is much cheaper, quicker and has more flexibility to produce smaller features than additional layers, the trend is towards finer circuit lines and pads and not to increase the layer counts (Kimpfel, 1999).

Circuit lines and the size of pads both have significant impact on component density. Two parameters indicate the circuit patterning capabilities of a PCB manufacturer: minimum achievable lines/spaces (L/S) and pad-to-hole ratio. Roadmap data published by leading electronics equipment suppliers- such as the one published by Ericsson, presented in Figure 1.1 (Taff et al., 2001)- charts the demand for performances in these two parameters.

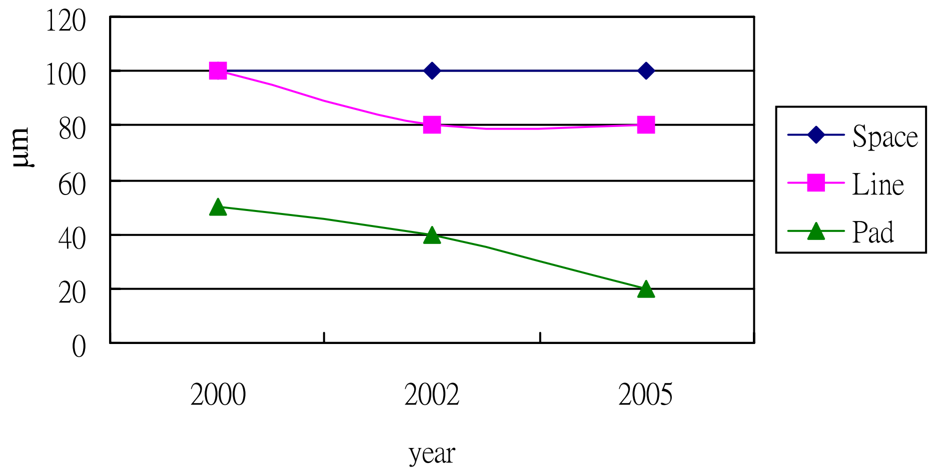

Fig.1.1 Ericsson Pad-Size and L/S Density Road Map

Fine line circuits are used in high-speed electronic applications. The requirements for higher signal speeds increase, with device rise time decreasing to the sub-nanosecond region and with operating frequencies increase to somewhere near the higher GHz region. Some critical signal factors at high signal speeds are signal loss and integrity (DK), signal speed (DF), transmission line characteristics, electrical noise, crosstalk, reflections, line and interconnection impedance, propagation delay, transient current and others. For very high frequency applications, it is crucial that conductor signal losses are minimized. This normally implies high conductivity, high backlit density, ultra fine circuit lines with a constant width and height (cross-section) along the entire length of the critical signal line (Keusseyan et al., 1998).

In the manufacturing process of PCB production, photolithography is a vital step to produce circuit pattern. Fine-line photolithography processes and the accompanying registration improvement have been identified as high-priority technical needs in the PCB industry. Meeting the need of fine-line photolithography will not only make high-density interconnect (HDI, the size of line/space below 150/150 µm) and microvia (the size of via is below 150 µm) boards be more practicable, but also can improve quality on conventional boards. However, this need for finer lines, pads and vias, as well as more precise alignment/registration of such features, has reached to a level where even evolutionary improvements in conventional exposure equipment (predominantly contact photo-imaging printers) are no longer adequate (Partha et al., 2001).

As circuit feature sizes on circuits shrink below 50 µm lines/spaces, resolution, alignment and quality problems become increasingly difficult to handle. Defects that were previously insignificant to cause electrical opens or shorts in circuit lines now contribute to quality losses. Variations in line width and edge-definition due to uneven contact become intolerable. Enormous investments are necessary to make circuit features less than 50 µm with good quality using conventional technology. For instance, a starting capital of some $7.7 million for structures of 75 and 50 µm is inevitable for introducing fine-line technology with a new lithography production line (Krause, 2000). Adding to this are the running costs for the required clean room, films, masks, photoresists, and disposal of ecologically harmful materials and residues. Currently, the achievable quality is between 60 and 70 percent which is unacceptable (Krause, 2000).

1.2 New techniques in Fine-line fabrication

Many new imaging techniques have emerged for the fabrication of fine circuit lines and spaces (fine circuit lines and spaces are most commonly defined to be 75 µm and below (Terliuc & Benron, 2000)). These new imaging techniques emerged to meet the need of higher densities, greater functionality and higher speeds in PCB industry such as step-and-repeat systems (Bender et al., 2002; Thompson, 2003), laser projection imaging (LPI) (Jain et al., 2002; Zemel, 2002) and laser direct imaging (LDI) (Buchner et al., 2004; Barclay et al., 2001). These techniques have distinctly different technological characteristics and each has application areas for which they are more suitable than others. Step-and-repeat projection is suitable for applications where repeated imaging of a small high-resolution pattern is required and where high throughput is not critical. LPI is attractive for volume production of large-area panels and LDI appears best for prototyping and quick-turn jobs and small production runs (Partha et al., 2001). With a demand for shorter product turnaround times and frequent new product releases, LDI is a more promising technology than the others.

Laser direct imaging (LDI) for printed circuit board applications emerged in the mid 1980’s. With new advancements in LDI equipment, laser technology and the introduction of specialized photoresists, LDI has come to the forefront of today’s imaging technology (Wheeler, 2002). In LDI, special thin and high-sensitivity resists are needed to obtain acceptable throughputs, since the throughput are very low for conventional resists (Partha et al., 2001). However, special high-density resists are more expensive and not at industry-standard. On the other hand, a smooth planar substrate and advanced lamination machinery and processes are critical for effective use of thin dry resist of 20 μm and less. The limit dimensions by using dry film lamination for fine lines/spaces are about 50/50 μm. The more challenging imaging will rely on liquid resists (Taff, 2001).

Liquid resists have no cover sheets and thus there is no light diffusion through such a protective layer. They are also much thinner than dry film and provide a much higher resolution during imaging and during etching. However, from a practical point of view, the image on the film never really matches the targets perfectly with both dry or liquid film due to the film's own expansion and contraction, panel distortion and target placement errors (Terliuc & Benron, 2000). This is where the laser structuring (LS) technique comes in.

1.3 Feasibility of laser structuring

LS is an answer to the enormous microelectronics push for further miniaturization and cheaper packaging, as well on chip substrate as on PCB level. LS can expect a prosperous future because it eliminates many complex steps and requires less time and money compared with the conventional and other imaging methods, especially on small volume production.

Laser structuring of etch resist is an advanced technique used in addition or even as an alternative to photolithography in order to produce circuit lines and spaces on a circuit board that reach circuit features smaller than 50 µm. LS has the same flexibility with laser direct imaging. However, the most outstanding advantage of LS compared with LDI is that it does not need to use the expensive high-sensitivity resists and can avoid the surface defects related with films. A small layer of tin electroplated on copper layer is used as etch resist in the etching process. For the structuring of the circuit lines, no further tools are necessary and complex masking steps are avoided.

Laser has become one of the most important and available manufacturing tools in the electronics industry for chips, packages, connectors, PCB and MEMS (micro-electro-mechanical systems). A laser structuring system uses a focused laser beam at UV wavelengths (355 nm or 532 nm (Roelants, 2002)) to expose the PCB, one pixel at a time. The required pattern is defined in the form of digital image data. A workstation uses these data to control the beam that directly ‘write’ the pattern on the board. In the LS process, the resist is exposed in a pixel-by-pixel serial manner by the movement of laser beam which is controlled by a high speed controller. LS process can achieve 50 μm circuit lines and spaces – or even smaller –high yields and acceptable processing times without any need of clean room facilities.

The focused laser beam only has to contourize the circuit lines and pads and leaves all other copper planes unaffected. Doing this, the total laser track length is minimized and throughput maximized (as shown in Fig.1.2). This is very important to improve the efficiency of LS.

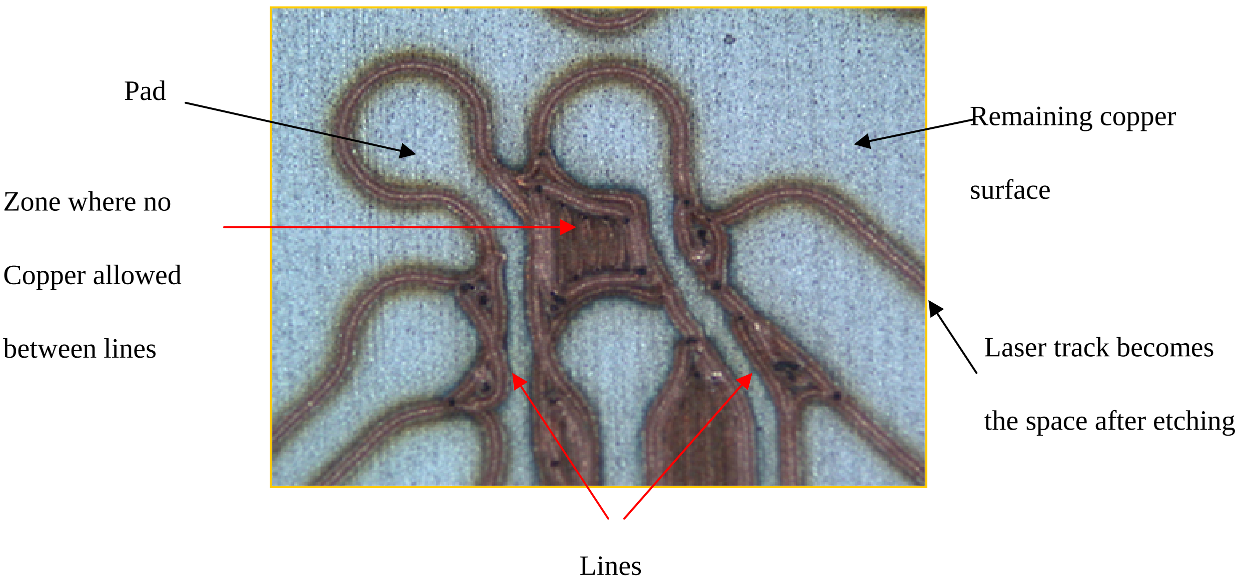

Fig.1.2 Circuit lines and circuit spaces fabricated by laser structuring

1.4 The worldwide market of laser direct imaging and laser structuring

Today's electronics industry is, in a word, demanding. Not only do many electronics products require smaller, faster, lighter, less expensive, more complex and reliable printed circuit boards, but PCB manufacturers have to continuously adapt to new product designs. The need for finer lines and spaces will only increase in the future and new fabrication techniques such as LDI and LS will have wide market.

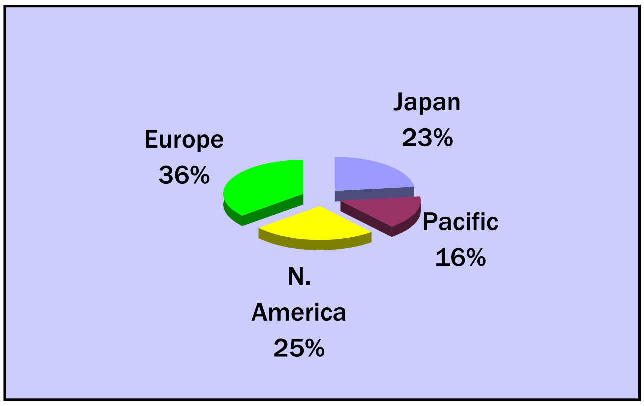

(a)

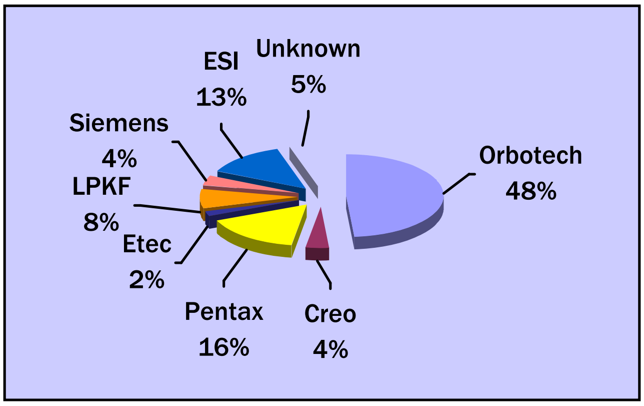

(b)

Fig.1.3 (a)Percent of laser direct imaging and laser structuring by area; (b)Estimated worldwide market shared by equipment manufacturer of LDI and LS (May 2002).

As shown in Fig.1.3a (Vaucher and Jaquet, 2002), Europe occupies the largest market of laser direct imaging and laser structuring. Then comes North America. In Asia, most players are in Japan. In Fig.1.3b, Vaucher and Jaquet (2002) have listed the key players in laser direct imaging and laser structuring. Orbotech is the undisputed leader in LDI. The second one is Pentax (Asahi Optical). Then comes the Electro Scientific Industries (ESI). The fourth one is LPKF Laser & Electronics AG.

The next one is Creo. Siemens is a company which produced Microbeam 3200, 3300 in laser structuring. The left five percent of the market includes the players of Etec, ManiaBarco, Dainippon Screen and so on.

These companies mentioned above are the most well-known companies which produce or utilize LDI & LS especially in LDI machine. It is clear that LDI and LS will have further utility prospect.

1.5 Comparison of LS & conventional PCB fabrication approach

Laser structuring is a promising technological alternative to conventional PCB lithographic process because it reduces many complex steps and spends less time and money, especially in small volume PCB production. So this technique may be widely used in PCB prototype design and production because of its flexibility and all the advantages mentioned above. Fig.1.4 gives the comparison between LS and conventional PCB fabrication processes (Krause, 2000).

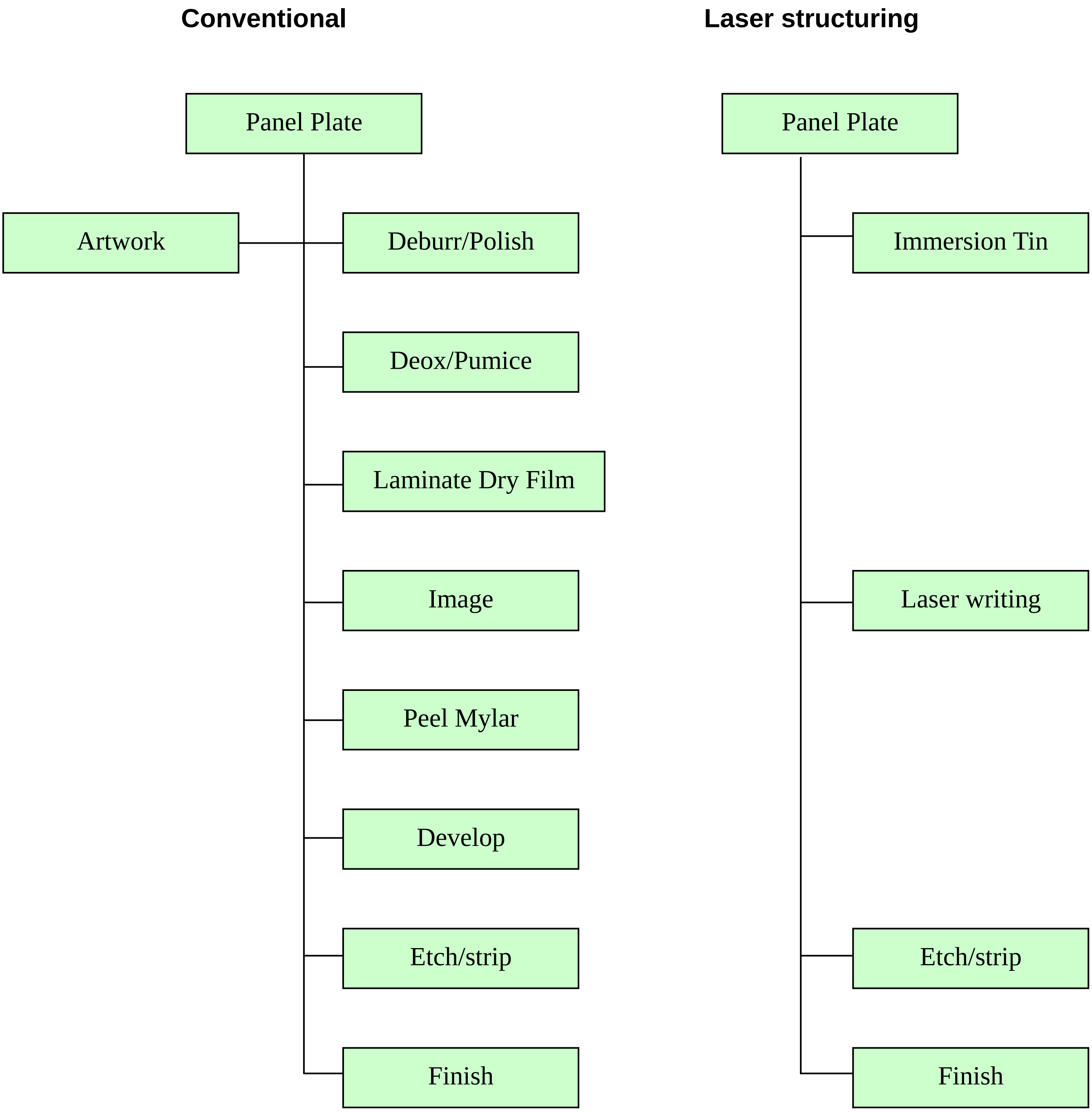

Fig.1.4 The comparison between LS and conventional PCB fabrication processes

Fig.1.5 and Fig.1.6 show the comparisons of LS, LDI and conventional PCB fabrication approach in the relationship between cost (time) and product yields by Vaucher and Jaquet (2002). From these figures, it is clear that LS exhibits great advantages when the product amount is below twenty-five pieces among these three approaches in this case. In fact, LS is still attractive when the product amount is less than 100 pieces. This volume can be considered a representative volume for a new prototype. As such, LS is the first choice in small volume production especially in the prototype design process.

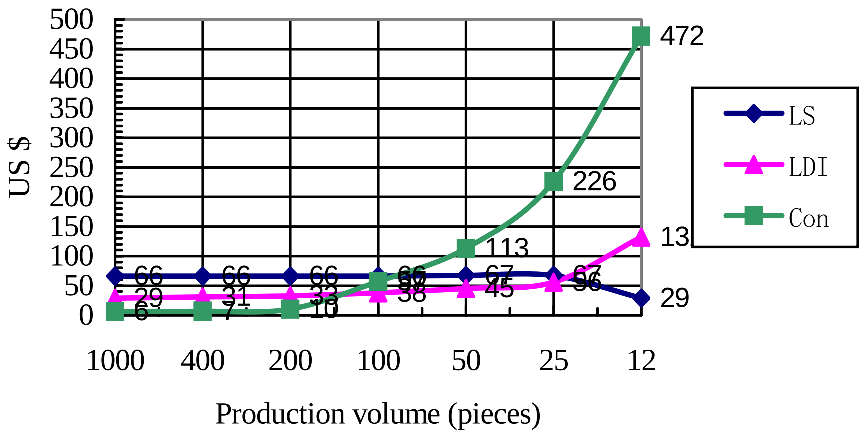

Fig.1.5 The comparison of the cost - production yields of LS, LDI and conventional PCB fabrication approach

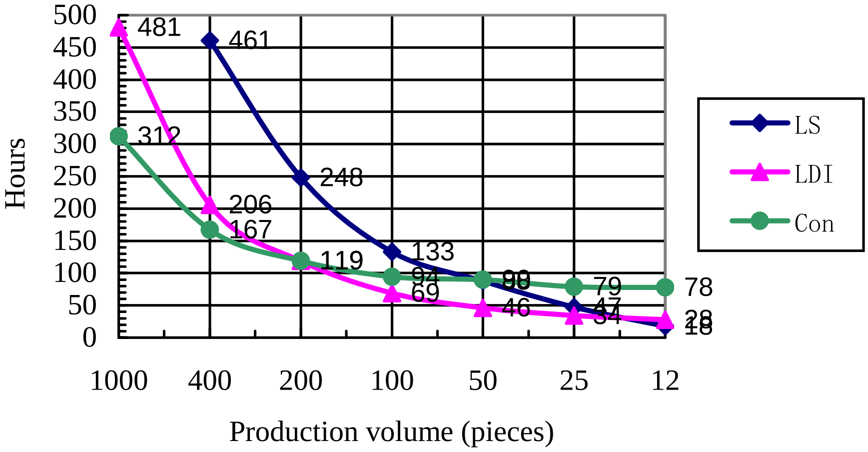

Fig.1.6 The comparison of the time - production yields of LS, LDI and conventional PCB fabrication approach

1.6 Laser used for material processing

The most common lasers used for material processing in industry are the carbon dioxide (CO_2) laser and the neodymium YAG (Nd:YAG) laser. These two lasers have stable output beam characteristics and are capable of operation in an industrial environment. In recent years, different lasers for material processing are emerging, including Excimer lasers, copper vapour lasers and special outputs from Nd:YAG lasers.

(i) CO_2 laser

CO_2 laser is a gas laser capable of delivering wavelength between 9 and 11 μm which is deep infrared invisible radiation. The high continuous wavelength (CW) output of CO_2 laser and the strong absorption of some materials (notably titanium and nonmetals) at 10 μm makes CO_2 laser ideal for cutting, welding and surface engineering purposes.

(ii) Nd:YAG laser

Nd:YAG lasers complement CO_2 laser because they have different wavelengths and output characteristics. Nd:YAG lasers are widely used in electronics fabrication such as for resistor trimming and marking where the energy must be focused precisely onto a small spot. Nd:YAG lasers can operate in several pulsed modes depending on both excitation and energy control in the laser cavity. Modes of Nd:YAG lasers include long pulses, Q switched pulses and mode-locked pulses. Q switched pulses, lasting a few nanoseconds, generates much higher peak powers. By passing Nd:YAG laser through nonlinear crystals, the frequency of the input laser can be doubled or tripled with the output wavelength of 533 nm and 355 nm. The high peak powers and short wavelength of Nd:YAG lasers often make them better for spot welding and laser marking.

(iii) Excimer laser

Excimer lasers, introduced in the mid-1970s, are pulsed gas lasers that use a mixture of gases to provide emission at a series of discrete wavelengths in the ultraviolet region of the spectrum. Together with frequency-converted Nd:YAG lasers, these UV lasers offer a wide range of material processing capabilities. Both the short wavelength and short pulse duration of UV lasers contribute to the reduction of thermal damage of materials. UV lasers can often remove a target material with minimal heat transfer to the surrounding material.

Table 1.1 Parameters of some industry lasers

Laser		Wavelength (μm)
Excimer laser	F_2	0.157 (UV)
	ArF	0.193 (UV)
	KrF	0.248 (UV)
	XeCl	0.308 (UV)
Nd:YAG laser	freq. tripled	0.355 (UV)
	freq. doubled	0.53 (Vis)
	fundamental	1.06 (IR)
CO_2 laser		9.24-10.64 (IR)

The wavelengths of some industry lasers are listed in Table.1.1. All the Excimer lasers (F2, ArF, KrF, XeCl) and the frequency tripled Nd:YAG laser are worked in the UV region of the wavelength spectrum.

1.7 Objectives of this research work

The main factors that influence the geometry of circuits and the relationship between the process parameters and the fabrication results of fine circuit lines and circuit spaces in laser structuring technique are investigated in this work. By controlling process parameters, the optimum geometry of circuits can be achieved with small width of circuit space (<50 μm), proper depth of circuit space (constraint by the thickness of tin layer and the total thickness of tin and copper layer) and less melting materials. The control and optimization of process parameters and the prediction of the geometry of circuits in laser writing step are the emphasis of this work. The minimum widths of circuit lines and circuit spaces fabricated with laser structuring technique that could pass the quality and reliability tests are also investigated in this work. The study comprises the following parts:

(i) The control, optimization of process parameters in laser writing step

- Construction of the relationship between process parameters and fabrication results with experiments and mathematical method;
- Investigation of the main factors affecting the three characteristic parameters of circuit spaces respectively (the width of space, the depth of space and the resolidification height) in laser writing step for the control of each characteristic parameter;
- Optimization of process parameters in laser writing step to achieve pre-designed geometry of circuit space.

(ii) The prediction of circuit geometry in laser writing step

- Prediction of the three characteristic parameters of circuit space—the width of space, the depth of space and the resolidification height with Artificial Neural Network;
- Prediction of the cross-sectional profile of circuit space with the consideration of resolidification height.

(iii) Quality and reliability tests of the final circuit lines and circuit spaces fabricated with laser structuring technique

- Investigation of the failure causes of the quality and reliability tests;
- Investigation of the minimum widths of circuit lines and circuit spaces (pass the quality and reliability tests) fabricated with laser structuring technique.

CHAPTER 2

LITERATURE REVIEW

2.1 Materials processing with laser

The current interest in the use of lasers is directly linked to the unique properties of laser light. The high spatial coherence achieved with lasers permits extreme focusing and directional irradiation at high energy densities (Bauerle, 2000). The applications of lasers in material processing are based mainly on the local conversion of the radiation energy into heat. Depending on the intensity and material parameters, four processing areas (Ifflander, 2001) including some recent researches in these areas are listed below:

--Heating: When the laser intensity is 10^4-10^5 W/cm^2, the material is only heated by the laser radiation. The laser with low intensity can be used for heat treatment of materials, hardening and oxidation (Wang & Lu, 2006; Pantsar & Kujanpaa, 2006; Tobar, 2005).

--Melting: When the laser intensity is 10^5-10^7 W/cm^2, the melting temperature at the material surface is reached very rapidly. Some techniques such as soldering, welding, melting cutting and surface treatment use laser intensity in this range (Thawari, 2005; Karatas et al., 2006; Stauffer et al., 2005; Kordas, Pap & Toth, 2006; Kuo & Lin, 2006)

--Vaporization: When the laser intensity is 10^6-10^8 W/cm^2, the material is vaporized rapidly with high intensity, mostly in the pulsed operation. The laser with high intensity can be used in drilling, trimming, penetration welding and so on (Fishburn

& Withford, 2005; Tan & Venkatkrishnan, 2005; Zhang & Tan, 2005; Luo et al., 2005)

--Plasma shielding: When the laser intensity is 10^8-10^9 W/cm^2, a plasma is produced by the vaporized material that shields the laser beam from the material (Bogaerts & Chen, 2005; Karnakis, 2005; Rodriguez, 2005; Siegel et al., 2005; Mao & Zeng, 2005)

In the previous work (Kimpfel, 1999; Higgins and Schreiner, 2000; Tadic, 2000; Krause, 2000; Roelants, 2002), laser structuring was introduced as a new technique in the fabrication of fine circuit lines under 50 μm or below. Laser structuring is a technique that is similar to laser drilling. The differences between these two techniques are: Firstly, the depth of cavity in laser structuring does not need to be as deep as that in laser drilling. The depth of cavities drilled by laser in laser structuring is about several micrometers (Kimpfel, 1999; Tadic, 2000). The depth of holes in laser drilling is from several micrometers to several millimeters (Dumitru, 2003; Tan & Venkatkrishnan, 2003; Bruneau & Hermann, 2005). So in laser structuring, it does not need many pulses at one spot and the shield affection to the laser from plasma is small. Secondly, the laser used in laser structuring is in the ultraviolet spectrum in order to get small spot size and high absorbtivity of laser beam (Krause, 2000; Tadic, 2000; Kimpfel, 1999). Some frequently used lasers in laser drilling such as CO_2 laser (Sciti & Bellosi, 2001; Low & Li, 2001; Rao, Kumar & Nath, 2005; Boutinguiza & Pou, 2005) are not used in laser structuring.

2.2 Laser structuring technique

The detailed laser structuring process is shown in Fig.2.1. In laser structuring, firstly, a small layer of tin (1-2μm) (Krause, 2000) is electroplated on the copper layer as the resist in the etching process. The properties of the tin deposit are of major importance. It should be thin to allow the highest possible ablation rate, but at the same time it must be thick enough to act as an effective etch resist. Then, the focused laser beam controlled by the CAD data contours the track or pad layout and removes the thin tin layer from the underlying copper. Even a few microns of copper layer will be removed. This exposed copper can subsequently be etched in chemical solution. Finally, the tin layer is stripped away. The technique of laser structuring removes a number of steps from the conventional PCB production process such as laminating photoresist, imaging and developing the circuit pattern.

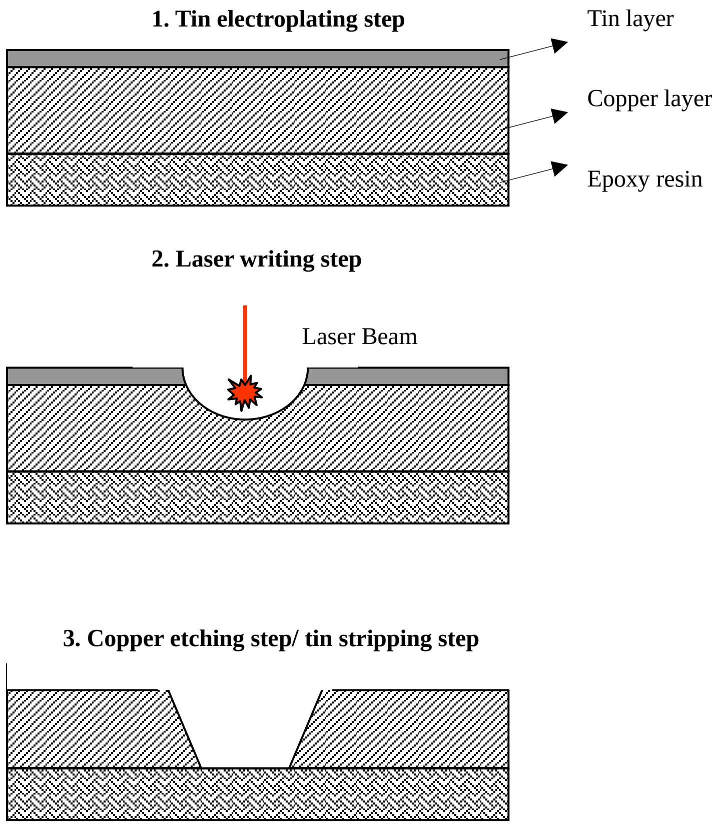

Fig.2.1 Laser structuring process

Laser structuring is a new technology in the fabrication of fine circuit lines/spaces. The previous work (Kimpfel, 1999; Higgins and Schreiner, 2000; Tadic, 2000; Krause, 2000 and Roelants, 2002) only introduced laser structuring as a new method in the fabrication of fine circuit lines and mentioned that the width of circuit line can be reduced under 50 μm or below with this technology. However, the control of process parameters and the minimum achievable width of circuit line/space were not available. As a new technique, LS is still immature. It is important to find out the relationship between process parameters and fabrication results in this technique to achieve fine circuit lines and circuit spaces with good quality and reliability. The control of process parameters in laser structuring and the prediction and optimization of the geometry of circuits fabricated with this technique will be studied in this work. Models of the interaction between laser and materials should be considered to help the control and analysis of the LS process.

In the previous research, only the 355nm Nd:YAG laser is taken as the laser source in LS. In order to enlarge the usage of this technique, some other lasers with shorter wavelength should also be considered as possible laser source.

2.3 Research work with Nd:YAG and Excimer laser

2.3.1 Research work with Nd:YAG laser

Nd:YAG lasers have different wavelengths and output characteristics, which make them widely used in industry. The Nd:YAG laser operating at 1.06 μm is often used when very high irradiance levels are required, which can only be achieved by producing a very small focused spot size. When the processed materials have too high a reflectance for a CO_2 laser beam, continuous wavelength Nd:YAG laser is sufficient for the particular application of surface treatment that required laser power up to 3 kW (Spawr, 2001). The high peak powers and short wavelength of Nd:YAG lasers also make them suitable in micromachining where the energy must be focused precisely onto a small spot.

Nd:YAG laser welding covers a large variety of techniques capable of producing welds in various metals, ranging from micrometers to tens of millimeters in thickness (Bransch, 1991). Both pulsed and CW Nd:YAG lasers can be used for welding of common engineering materials as the research of Bruno Martin in the laser keyhole welding processes (Martin, 2001).

Nd:YAG laser can also be used for both cutting and microcutting with the advantages of flexibility, high production rate and smooth cutting edges such as in the work of Rohde and Verboven (1995) and Steen and Kamalu (1983).

In micromachining system, Nd:YAG lasers are most often employed in the directed beam marking (McKee, 1995). The Nd:YAG laser marks most materials except for visually transparent materials such as clear plastics and glass. The largest market for Nd:YAG laser systems is to mark integrated circuits. The Nd:YAG laser is the best system to mark bare metal, including aluminum, copper, brass, stainless steel and most alloys (Scaroni, 1985). The Nd:YAG laser writing system is used to mark metal parts in the automotive, aerospace, medical industries, and in the electronics industry.

The Nd:YAG laser has frequently been used for hole drilling in metals (Tunna et al., 2005; Li & Zheng, 2005; Wang et al., 2004). The CO_2 laser is less often used because of the high reflectivity of metals in the far-infrared spectrum (Tohde &

Dausinger, 1996). Nd:YAG laser is also used in drilling non-metals with the available high irradiance to ablate or vaporize the workpiece material instantly with minimal heat-affected zone.

Pulsed-laser interaction with materials is important in a number of scientific and engineering applications. Particularly, short time scale and high spatial resolution achieved in pulsed Nd:YAG laser processing enable selective removal or deposition of materials with high precision, by minimizing the thermal-diffusion effect (Kim, 2004). The 2nd, 3rd, 4th harmonic laser wavelengths (generated at 532, 355, and 266 nm respectively) offer new opportunities in material processing applications. In particular, for drilling applications, solid-state lasers can provide very high peak irradiance (in the range of 10^8 to 10^{12} W/cm^2), good mode quality, low beam divergence and short pulse width in the nanosecond to femtosecond regime. These attributes greatly contribute toward their superior performance in achieving precise tolerances and repeatability.

As Nd:YAG laser has its advantages mentioned above, it is also used as a tool in the recently emerged technique--laser structuring-- for the fabrication of printed circuit board. In the research of Higgins and Schreiner (2000), Tadic (2000), Krause (2000) and Roelants (2002), they got fine circuit lines and circuit spaces under 50 μm and 50 μm with frequency tripled Nd:YAG laser (355 nm wavelength) as the laser source. So the Nd:YAG laser can be taken as an useful laser source in the fabrication of fine circuit lines in PCB.

2.3.2 Research work with Excimer lasers

Excimer lasers are increasingly being used for machining microstructures and devices (Metev & Veiko, 1994). In micromachining, Excimer lasers remove the material from a substrate through an ablation mechanism. They are capable of making microstructures with feature sizes in the order of 1 μm and they are applicable for all kinds of materials, including polymers, metals, and ceramics (Endert et al., 1995).

Ablation mechanism can be modeled by one or a mix of two processes: “photothermal” and “photochemical”. A photochemical process is often referred to as a non-thermal process because the removal of material is caused by a direct breaking of atomic bonds as energy is absorbed. In contrast, the absorbed laser energy may be converted to lattice vibrational energy (thermal) to melt and vaporize the material in a photothermal process. The two processes can occur in varying degrees of combination in micromachining in the case of using high-intensity Excimer lasers (Duley, 1996).

The photochemical process normally dominates in case of ablation of polymers, which have relatively low thresholds, while the photothermal process dominates for ablation of ceramics and metals, which possess high thresholds (Laude, 1994). By minimizing the heat-affected zone or the undesired thermal effect, a feature size in microscale levels can be accomplished.

Since the laser technology has improved substantially over the past decade, Excimer lasers now possess relatively high pulse energies, short pulse lengths, and high average and peak powers as compared to other laser sources. These attributes make them the most efficient and popular ablation tool for micromachining applications.

2.4 Taguchi methodology and Artificial Neural Network in the analysis and optimization of experimental results

2.4.1 Taguchi methodology

The orthogonal array methodology originated as an approach to quality engineering advocated by Genichi Taguchi (1986). The most commonly used orthogonal array designs are L8 (i.e. eight experimental trials), L16 and L18. The power of the Taguchi methodology is that it integrates statistical methods into the engineering process. Bendell et al. (1989) and Rowlands et al. (2000) reported success of the Taguchi method in the automotive, plastics, semiconductors, metal fabrication and foundry industries.

The combination of design of experiments with optimization of control parameters to obtain best results is achieved in the Taguchi Methodology. The Taguchi methodology consists of experimental planning with the objective of acquiring data in a controlled way to obtain information about the behavior of a given process. It gives a much reduced variance for the experiments with optimum settings of control parameters (Ross, 1989). Executing planned experiments and analyzing the data obtained can reveal information about the behavior of the given process. Optimum working conditions determined from the laboratory work can also be reproduced in the real production environment.

In the laser-material fabrication process, the Taguchi methodology has been widely used. Tam, Lim and Quek (1992) used the Taguchi methodology to optimize the laser-cutting process. Pandey, Shan and Bharti (1993) and Bandyopadhyay and Gokhale (2005) used the Taguchi methodology to determine process parameters in laser drilling process. In the work of Pan and Wang (2005), Casalino and Curcio

(2005) and Lee and Han (2006), they used Taguchi methodology for the investigation of laser welding process. The Taguchi methodology was also used in the analysis of laser surface hardening and laser casting process such as the work of Casalino and Filippis (2005) and Yang (2001).

LS as a new technique has some similar characters as other laser-material fabrication techniques such as the large number of process parameters. In existing studies, all the parameters affecting the laser structuring process have not been investigated in detail, because it requires a vast number of experiments, which enormously increases the experimental cost and the time required. In this work, the Taguchi methodology was used for quantitative estimations of the various parameters and the main factors affecting the performance of the laser structuring results.

2.4.2 Artificial neural network

An Artificial Neural Network (ANN) is an information processing paradigm that is inspired by the way biological nervous systems process information such as the brain (Stergiou & Siganos, 1996). The key element of this paradigm is the novel structure of the information processing system. It is composed of a large number of highly interconnected processing elements (neurons) working in unison to solve specific problems such as pattern recognition or data classification through a learning process (Anderson & McNeil, 1982). Learning in biological systems involves adjustments to the synaptic connections that exist between the neurons. The network adopts the following approach: change the weight by an amount proportional to the difference between the desired output and the actual output and can be represented by an equation:

$$\Delta W_i = \eta_l (D_y - Y) I_i \qquad (1)$$

where η_l is the learning rate, I_i is the input, D_y is the desired output, and Y is the actual output (Smith, 1996). This is called the Perception Learning Rule.

ANNs can be used to extract patterns and detect trends that are too complex to be noticed by either humans or other computer techniques with their remarkable ability to derive meaning from complicated data. A trained neural network can be thought of as an “expert” in the category of information it has been given to analyze (Fausett, 1994; Gurney, 1997; Haykin, 1999). ANN has the advantages of adaptive learning and self-organization. The first artificial neuron was produced by the neurophysiologist Warren McCulloch and the logician Walter Pits in 1943. But the technology available at that time did not allow them to do too much. The field of neural networks was pioneered by Bernard Widrow of Stanford University in the 1950s. Today, neural networks are used prominently in voice recognition systems, image recognition systems, industrial process control, medical diagnosis, quality control, financial forecasting and aerospace applications (Stergiou & Siganos, 1996; Orr et al., 1999).

The feedforward, back-propagation architecture (BP) was developed in the early 1970’s by several independent sources (Parker, 1987; Rumelhart, Hinton & Williams, 1985). Currently, the back-propagation architecture is the most popular, effective, and easy to learn model for complex, multi-layered networks. It is used in many different types of applications and is used more than all other ANNs combined (Anderson & McNeil, 2002). Its greatest strength is in non-linear solutions to problems. BP used the gradient steepest descent method to correct the weight of the inter-connective neuron. In the learning process of BP, the interconnection weights are adjusted using an error convergence technique to obtain a desired output for a given input.

The BP ANN models are widely used in the prediction of fabrication results and the optimization of fabrication process. Adhikary and Mutsuyoshi (2006) used the neural networks in the prediction of shear strength of steel fiber reinforced concrete beams. In the work of Ayata and his group (2006), they used ANN in the prediction of temperature distributions on layered metal plates. Al-Haik et al. (2006) used the ANN in the prediction of nonlinear viscoelastic behavior of polymeric composites. Fathi and Aghakouchak (2006) used ANN technique in the prediction of fatigue crack growth rate in welded tubular joints. ANN are also useful tools in the optimization of non-linear fabrication process, such as the work of Endelt, Nielsen and Danckert (2006) who used ANN in the optimization of a deep-drawing operation, the work of Xu et al. (2006) who used ANN in the optimization of heat treatment technique of high-speed steel and the work of Cus and Zuperl (2006) who used ANN in the optimization of cutting conditions.

Several researchers have adopted BP to model laser-material fabrication processes such as the work of Jeng, Mau and Leu (2000), Luo et al. (2005), Calslino and Jeng (2005) and Olabi et al. (2006) in laser welding. Olabi et al. used ANN in the optimization of CO_2 laser welding process. Luo et al. used ANN in the defect diagnosis in laser welding. Casalino and Jeng used ANN in the prediction of welding parameters in the laser welding process.

BP neural network is used to model the complex laser writing step of laser structuring technique in this work. The process parameters in laser writing step include the laser power, number of repetition, repetition rate, bite size and focal length etc. These parameters are controllable in the actual operation of laser structuring, but are interconnected and non-linear. Such problems limit the industrial applicability of the laser structuring technique. The artificial neural network is a useful tool for predicting fabrication results and optimizing the operation parameters of such a non-linear model.

2.5 Quality and Reliability tests of circuits

PCB testing methods have evolved along with the advance of PCB fabrication technology. Many testing methods which may have been of less concern in the past now require much attention because of the small size and the precision requirements (Zorich, 1991; Christou, 1994). Quality and reliability problems of circuits are related to the fabrication process and the size of circuit lines and circuit spaces. Quality is a measurement of the “goodness” of a device at time $t = 0$ (just completed manufacturing), whereas reliability is a measurement of the “goodness” of a device at some time $t > 0$ (some time after manufacturing) (Henderson, 2001). The main problems coming with the decreasing size of circuit lines and circuit spaces are the continuity of circuit lines, the insulation between lines under humidity and thermal cycling environment, the adhesion of copper lines on the dielectric layer and so on.

2.5.1 Quality tests of circuits

Open and short circuit interconnections create major IC yield and quality problems (Edward, 1999). The open/short problems will influence the electrical function of circuits. The electrical function is the basic and most important performance of circuits (McKenney & Numakura, 2001). With the decrease in the size of circuit lines and circuit spaces, the open/short problem will become more serious because even minor faults during the fabrication process will cause big problems.

The peel strength test is the most commonly used method to determine the adhesion of copper on the base material of PCBs (Jalonen, 2003). In laser structuring process, the copper etching and tin stripping steps involve exposure of the materials to chemical environments. Circuits fabrication process can degrade adhesion of copper to epoxy resin (Bergstresser & Hilburn, 2003). Metal/dielectric layer adhesion is a crucial factor of many applications in microelectronic or microsystem technologies and it depends on chemical and structural properties of the interface (Horn, Beil, & Wesner, 1999). In circuits fabrication process, adhesion between copper and base dielectric material is an important consideration because it will influence the minimum size of circuits which can adhere tightly on base material.

2.5.2 Reliability test of circuits

With the increasing focus on PCB reliability and miniaturized designs, failure mechanisms due to Conductive Anodic Filament (CAF), Electromigration Resistance (EMR) and Surface Insulation Resistance (SIR) are gaining a lot of attention. Smaller circuit geometries make the printed circuit board susceptible to conductive anodic filament growth and electromigration (Amla, 2002). Among the reliability test methods, CAF is mainly used in the detecting of dendrites and filaments through hole to hole (Neves, 2002). SIR is widely used as a line-to-line test method (Hauder, 2002).

Surface Insulation Resistance (SIR) is a test designed to expose a processed or unprocessed printed circuit substrate to elevated temperatures and humidity while applying an electrical potential. The goal is to determine if the printed circuit substrate measured by IC have the propensity for electromigration. Surface insulation resistance derived from EMR is widely used as line-to-line testing method in PCB fabrication. SIR is believed to be strongly dependent on fabrication conditions and techniques (Hauder, 2002).

With laser structuring, the size of circuit lines/ spaces can reach a level under 50/50 μm. Some quality and reliability problems emerge with the decreasing size of circuit lines/spaces at the same time. Open/short problem of circuit lines is related to the size of circuit lines/spaces and the results of peel test and SIR test will be influenced by fabrication process. So the quality and reliability of fine circuit lines and circuit spaces fabricated with the new approach – laser structuring-- should be considered in the further study.

2.6 Mathematical models in laser ablation of materials and chemical etching process

2.6.1 Mathematical models in laser ablation of materials

The modeling of the laser-target interaction always utilizes a classical treatment of heat transfer into a semi-infinite solid such as the work of Ready (1971), Paek and Bagliano (1972), Andrews and Atthey (1975). The work of Ready (1971) included some allowance for laser parameters and afforded predictions of the amount of material removal. Paek and Bagliano (1972) proposed a theoretical solution to predict the temperature profile and tangential stress distribution of the laser drilling process. The work of Andrews and Atthey (1975) remains a useful framework to start with, for it retains a simple formulation of the problem, allowing additional effects to be introduced without losing insight into the physical processes.

Allmen (1976) analyzed the effect of drilling velocity on drilling efficiency by using a 1-D dynamic model. Chan and Mazumder (1988) discussed the physics of vaporization and liquid metal expulsion during laser-materials interaction and presented a one-dimensional steady-state mathematical model for material damage. One-dimensional models of laser-induced vaporization and melting have been reported recently. On the other hand, several two- dimensional models deserve more interest.

Basu et al. (1988) studied the problems of laser melting in details and considered the heat transfer and flow field in the melting pool as well as the effect of the process parameters. In their work, the shape of the melting pool, the flow pattern and temperature profile were also discussed. Armon et al. (1989) also formulated a two-dimensional metal plate drilling model based on enthalpy balance, which they supported with experimental studies. Another two-dimensional model of material damage caused by melting and vaporization during pulsed laser irradiation was developed by Kar et al. (1990). Both solid-liquid and liquid-vapour interfaces were taken into account by defining the interface curve in the crater cross-section as a combination of a straight line and a parabola. Garnesh et al. (1997) also developed a very detailed numerical model and complete physical model for the laser drilling process by employing a free surface and phase change simulation. On the basis of Andrews and Atthey' analytical description of the drilling process in the evaporation regime, Solana et al. (1999) took a step forward to include laser absorption within the vapor as will as different types of time dependent laser sources.

In laser welding, laser cutting and laser drilling processes, when the recirculating velocity is so much higher than the scanning velocity, the flow field and heat transfer on a plane perpendicular to the scanning direction should also be considered. Such a motion cannot be obtained from two-dimensional models. Kou and Wang (1986) developed a three-dimensional model using the method of conjugate heat transfer. Chan, Mazumder and Chen (1988) developed a three-dimensional axisymmetric model for convection in a laser melt pool assuming Gaussian power distribution in a stationary circular laser beam. The models of laser ablation of materials are shown in Table 2.1.

Table 2.1 Models of laser ablation of materials (especially in laser drilling)

Investigator	Time	Dimension	Laser	Target material	Research emphasis of models
Paek & Bagliano	1972	1-D	CO_2 lasers operated in the pulsed mode	Alumina ceramic	Temperature profile and tangential stress distribution
Andrews & Atthey	1975	1-D	General	Metal	Drilling velocity in the evaporation regime
Von Allmen	1976	1-D	Nd:YAG	Metal	Drilling velocity, Drilling efficiency
Chan & Mazumder	1988	1-D	General	Aluminum superalloy, titanium	Damage caused by materials removal by vaporization and liquid expulsion
Ho et al.	1994	1-D	Pulsed laser, nanosecond	Metal	Heat transfer, Fluid flow
Basu & Srinivasan	1988	2-D	General	General	Laser melting
Armon	1989	2-D	CO_2	Al	Laser drilling on the enthalpy balance method
Kar & Mazumder	1990	2-D	Gaussian 10^7 w/cm^2 laser duration(s): micro	General	Melting and vaporization
Patel & Brewster	1991	2-D	General	General	Gas assist
Qiu et al.	1994	2-D	Nd:Glass	Al	Transient material behaviour in LMA
Ganesh& Faghri	1997	2-D	General	General	Numerical model and complete physical model, A free surface and phase change simulation
Zhang & Faghri	1999	2-D	Gaussian	General	Melting and vaporization phenomena
Paek & Gagliano	1971	3-D	CO_2	Fired-alumina	Temperature profile, thermal stress
Kou & Wang	1986	3-D	General	Metal	Surface tension
Zacharia et al.	1989	3-D	CO_2	Metal	Arc welding, DEA method
Chan, Mazumder & Chen	1988	3-D	Gaussian	General	FDM, vectorization

In this work, an analytical model previously developed for laser materials processing by Andrews and Atthey (1975) has been further developed to include the consideration of laser parameters and the two-layer structure of material (tin and copper) in laser structuring process.

2.6.2 Mathematical models in the etching rate of chemical etching

Etching is done either in “dry” or “wet” methods. Wet etching uses liquid etchants and dry etching uses gas phase etchant in a plasma. In wet-chemical etching (WCE) an etchant is used to dissolve the metal which is not protected by a mask (Rath & Chai, 2005). Chemical etching converts a solid insoluble material to a soluble form by dissolving the extended lattice of metal atoms so that these atoms can enter the solution as soluble compounds. This is accompanied by removal of electrons from the metal that is called oxidation. The types of etching processes includes isotropic and anisotropic. Isotropic etchants attack the material being etched at the same rate in all directions. Anisotropic etchants attack the material at different rates in different directions. Pure chemical etch is isotropic or nearly isotropic.

Mathematical models based on the fundamental principles of transport and reaction phenomena are useful in predicting the profile of the subject produced by the etching process and provide insight into the important mechanisms for chemical etching. This can be done using analytical techniques after some simplifying assumptions. Numerical simulations are more useful for more complicated structures and systems. But he numerical method should be able to analyze the fluid flow and transport phenomena in complex deforming geometries that is a non-trivial task (Sudirham & Damme, 2004).

Based on the rate of reaction, two possible cases namely—the diffusion-controlled etching (Notten, Kelly & Kuiken, 1986; Shin & Economou, 1991; Lam, Chai & Rath, 2004) and the reaction-controlled etching (Li, Shih & Mai, 1998; Kaneko et al., 2003; Rath & Chai, 2005) have been examined by various researchers. In diffusion-controlled etching, the reaction rate at the interface is infinitely fast compared to diffusion of etchant to the interface. Therefore for a given diffusion coefficient of etchant D_e, if $\kappa >> D_e$ (where κ is the reaction rate constant and D_e is the diffusion coefficient), the etching process can be assumed diffusion-controlled. In the reaction-controlled etching, the reaction rate is finite compared with the diffusion-controlled etching which is about 10^{-5} cm/sec (Rath & Chai, 2005). These two cases have been studied by Kuiken and Kelly (1986), Li, Shih and Mai (1998), Lam, Chai and Rath (2004) and Rath and Chai (2005) with one-dimensional models.

The etching rate is an important factor in the etching step of laser structuring. Mathematical models based on the rate of etching will be built. After the construction of the model of etching rate, the depth of circuit spaces in the etching step of laser structuring can be predicted quantitatively. With this model, the etching step can be controlled to achieve better cross-section profile of circuit spaces.

CHAPTER 3

MATERIALS, SAMPLES PREPARATION AND EXPERIMENT DETAILS

3.1 Introduction of laser structuring technique

Laser structuring of etch resist is an advanced technique used in addition or even as an alternative to conventional photolithography in order to produce circuit lines and spaces on a circuit board that reach circuit features smaller than 50 µm. In the conventional photolithographic process, the entire large PCB substrate is exposed at once. Whereas in laser structuring process a laser structuring system uses a focused laser beam at UV wavelengths to expose the PCB, one pixel at a time. The required pattern is defined in the form of digital image data. In the laser structuring technique, the process parameters will directly influence the cross-sectional profile and the geometry of circuits. The study of the relationship between process parameters and fabrication results will help to achieve optimum geometry of circuits by controlling process parameters.

Laser structuring technique is used in the fabrication of fine circuit lines and spaces in printed circuit board. The basic material of the printed circuit board used in this work is the FR4 laminate. The FR4 laminate is constructed from glass fabric impregnated with epoxy resin and copper foil. Firstly, a small layer of tin is electroplated on the copper foil to act as etch resist in the copper etching step. Secondly, frequency tripled Nd:YAG laser (355 nm) and KrF Excimer laser (248 nm) are used as laser source to remove the thin tin layer according to pre-designed CAD data. Different to the Nd:YAG laser, the Excimer laser can change the spot size of the laser beam conveniently to a smaller dimension by inserting a mask. Then the remaining copper uncovered by tin layer is then etched in alkaline cupric chloride solution. At last, tin layer is stripped away. The width of circuit lines and circuit spaces can be reduced to 50 μm with laser structuring technique.

Laser writing step is an important step in laser structuring technique. In laser writing step, the laser (in UV wavelength of spectrum) writes directly on a two-layer material (tin and copper). The laser source, material and the interaction of the laser and material in laser structuring technique are different from those in laser welding, laser cutting and laser drilling. The influences of the complex parameters on the geometry of circuits in laser structuring technique are studied by experiments in chapter four. The geometry of circuit space including the depth of space, the width of space and the resolidification height are measured with Boeckeler VIA-video and Talysurf PGI 1240 measurement system. In chapter five, Artificial Neural Networks and Taguchi methodology are firstly used in the control and optimization of process parameters in laser writing step. The Taguchi methodology consists of experimental designing with the objective of acquiring data in a controlled way to obtain information about the behavior of laser structuring process. Artificial neural network (ANN) is a useful tool for predicting outcome results and optimizing the operation parameters of non-linear process such as laser structuring. The experimental results about the relationship between process parameters and fabrication results in laser writing step are explained with mathematical method in chapter six. Also, the 2-D geometry of circuit space can be calculated with a new approach by combining the characteristic parameters of circuit space predicted by the ANN prediction model and the mathematical description of the Gaussian profile. The flow chart of the content in this work is shown in Fig.3.1.

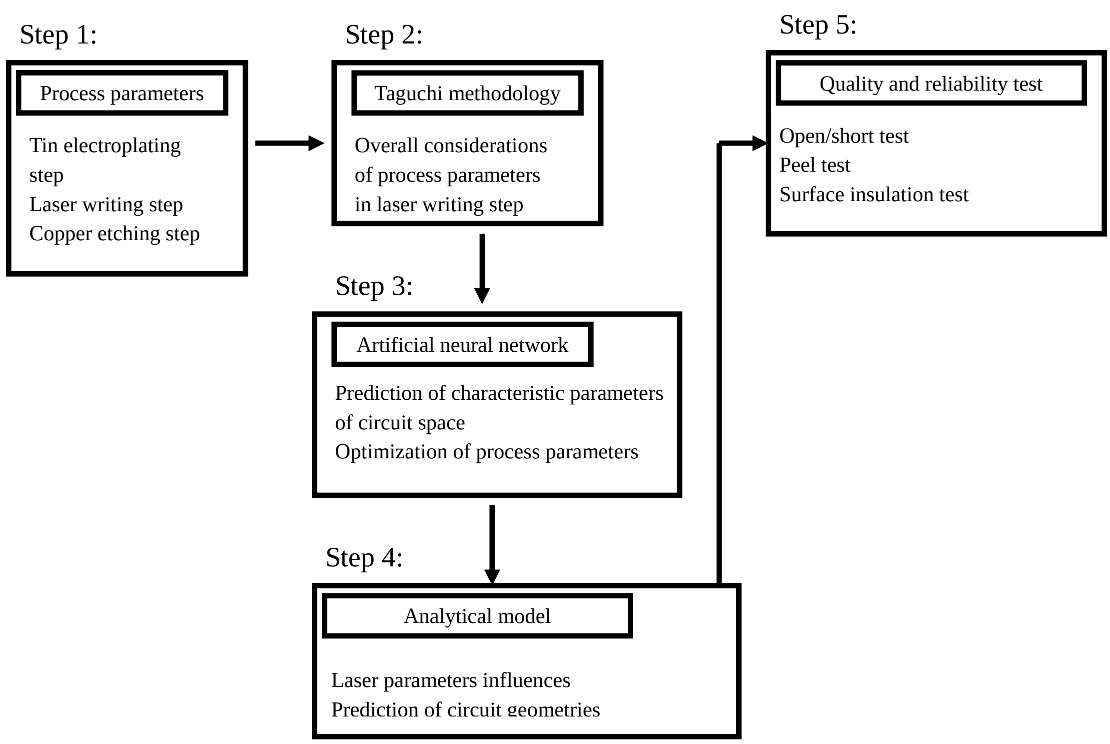

Fig.3.1 Flow chart of the content in this work

3.2 Materials used and preparation

The base dielectric material used in this work was FR4 laminate. FR4 laminate is the common base material from which multi-layer printed circuit boards are fabricated. “FR” means Flame Retardant, and Type “4” indicates woven glass reinforced epoxy resin. Other substrate materials such as PI/Ceramic can also be used as the base material in laser structuring and it is expected to achieve similar experimental results of the geometry of circuit space during laser-material interaction process. This is because, in laser structuring technology, laser beam only removes the electroplated tin layer and a small layer of copper. The underlying dielectric layer remains untouched. The laser-writing step is a laser-metal interaction process and the material of dielectric layer is of minor importance. So the experimental results of the geometry of circuit space on FR4 laminate can be considered applicable to other materials. The structure of the printed circuit board is shown in Fig. 3.2.

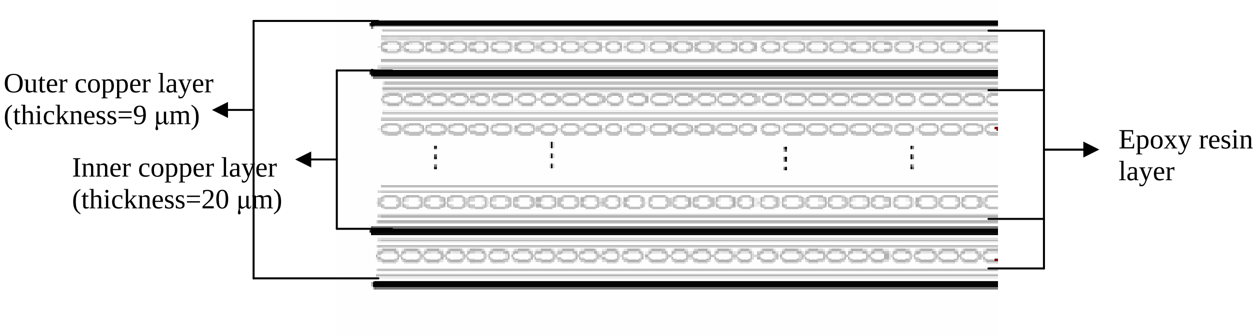

Fig.3.2 The structure of printed circuit board

The FR4 laminate is constructed from glass fabric impregnated with epoxy resin and copper foil. The thickness of the outer copper foil is about 9 μm with one surface pre-treated to promote the adhesion to epoxy resin.

On the surface of outer copper layer, a small layer of tin was electroplated on it. This tin layer was used as etch resist in the laser structuring technique. Some parameters of copper and tin are shown in Table 3.1.

Table 3.1 Parameters of tin and copper

	TIN		COPPER	
ρ (g cm^{-3})	7.30		8.96	
T_m (°C)	231.9		1083	
T_v (°C)	2270		2595	
L_m (J g^{-1})	60.7		212	
L_v (J g^{-1})	1945		4770	
k (W cm^{-1} K^{-1})	293(K)	0.65	293(K)	3.94
	373	0.63	373	3.94
	473	0.60	473	3.89
	505	0.30	773	3.41
	573	0.314	1273	2.44
	673	0.334	1356	1.656
	773	0.354	1373	1.661
	1273	-	1473	1.701
			1673	1.763
			1873	1.804
c (J g^{-1} K^{-1})	293(K)	0.222	293(K)	0.385
	373	0.239	373	0.389
	473	0.260	473	0.402
	505	0.250	773	0.427
	573	0.242	1273	0.473
	673	0.241	1356	0.495
	773	0.240	1373	0.495
	1273	0.260	1473	0.495
			1673	0.495
			1873	0.495
R_{355}	0.70		0.36	
R_{248}	0.68		0.38	

- ρ, the specific weight,
- T_m, the melting temperature,
- T_v, the evaporation temperature,
- L_m, the melting heat,
- L_v, the evaporation heat,
- k, the thermal conductivity,
- c, the specific heat,
- R, the spectral and intensity-dependent reflectivity for a defined surface.

3.3 Laser systems used in this work

Two laser systems were selected in this work—frequency tripled Nd:YAG laser and KrF Excimer laser -- for the comparison of the laser structuring results. An ESI 5100 laser processing system (Model 5100) was used in the experiments as the source of Nd:YAG laser. The Nd:YAG laser was frequency tripled and was operated at 355 nm equipped with an acousticoptical Q-switch. The maximum average power and the maximum pulse peak power of the laser were 1.2 W and 12 kW respectively. The pulse repetition rates vary from 0.1 kHz to 20 kHz. The pulse width was 30 ns and the focal length of lens was 80 mm and the divergence angle of the laser beam was about 3 mrads. In actual experiment, the diameter of spot size at the focusing point was fixed at 25 µm.

PulseMaster PM-848 laser system produced by Optec LightBench was used as another laser source in the experiments. The laser gases were Kr and F_2 and the Excimer laser was operated at 248 nm. The pulse repetition rate was 200 Hz and the pulse duration was 20 ns. The maximum average output power is 80 W. The effective focal length of the beam was 86.9 mm and the divergence of the laser beam is 1×3 mrads for the beam dimension of 25×12 mm^2. The position resolution of this system was 1 µm. The comparisons of KrF Excimer laser and frequency-tripled Nd:YAG laser are shown in Table 3.2.

Table 3.2 Comparisons of Excimer laser and Nd:YAG laser

	Excimer laser (KrF)	Frequency –tripled Nd:YAG laser
Wavelength	248 nm	355 nm
Beam size	25×12 mm (FWHM, long axis×short axis)	Diameter on the focal plane: 25 μm
Beam profile	Rectangular beam	Gaussian beam
Pulse width	20 ns	30 ns
Repetition rate	0-200 Hz	0.1 kHz to 20 kHz
Mode of operation	Pulsed	Pulsed

Nd:YAG laser and Excimer laser usually use different method in machining materials. Nd:YAG utilizes a focal point technique with focused lens. When Nd:YAG laser passes through lens, the material to be machined is placed at the focal point of the nearly Gaussian beam. The focused spot of Excimer beam will be very large and irregular in shape and cannot be directly used in micromaching. However when a mask with aperture is placed in the beam path it serves as a point source which is imaged onto the material surface with a prescribed demagnification. The size and shape of the laser spot on the material are determined by the aperture pattern and the demagnification.

3.4 Fabrication process in laser structuring

In the laser structuring process, firstly, a small layer of tin is electroplated on the pre-cleaned copper layer to act as etch resist in the copper etching step. Secondly, laser beam controlled by CAD data directly writes on the tin layer in a pixel-by-pixel serial way. The laser beam ablates the tin layer and at the same time a small layer of copper is also removed. Then the remaining copper uncovered by tin layer is etching away in chemical solution. At last, the tin layer is stripped. The whole flowchart of the laser structuring process is shown in the Fig.3.3.

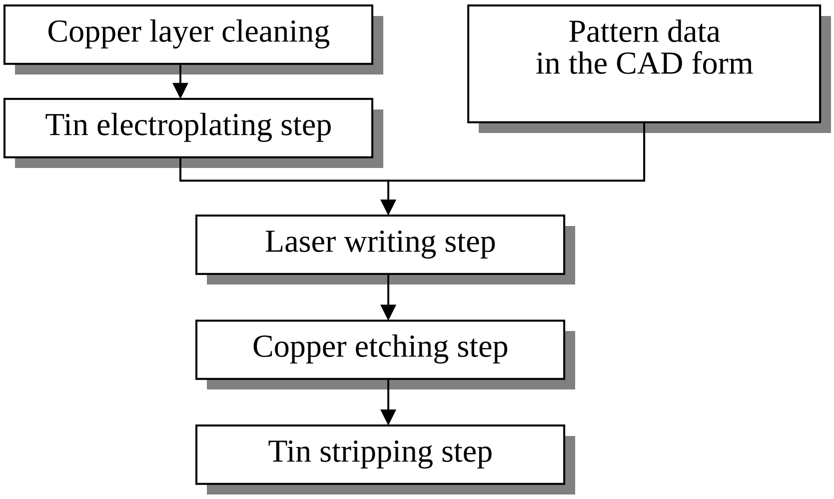

Fig.3.3 Flow chart of laser structuring process

3.4.1 Electroplating of tin layer

Electroplating is the process of producing a coating, usually metallic, on a surface by the action of electric current. The deposition of a metallic coating onto an object is achieved by putting a negative charge on the object to be coated and immersing it into a solution which contains a salt of the metal to be deposited. The metallic ions of the salt carry a positive charge and are thus attracted to the object. When they reach the negatively charged object (that is to be electroplated), it provides electrons to reduce the positively charged ions to metallic form.

The Ronastan EC electroplating solution is an acid based tin electroplating solution which produces smooth, fine grained, satin deposits over a wide plating range. The operation parameters of the electroplating solution are shown in Table 3.3.

Table 3.3 Operation parameters of electroplating tin solution

PARAMETER	RANGE
$SnSO_4$	35-45 g/l (40g/l)
H_2SO_4 (Sp. Gr. 1.84)	90-110 ml/l (100 ml/l)
Ronastan EC: Part A	15-25 ml (20 ml/l)
Ronastan EC: Part B	30-50 ml (40 ml/l)
Temperature	18-25 °C
Cathode Current Density	1-2 amps/dm^2
Deposition Rate	1 micron in 1.5 minutes at about 1.5 amps/dm^2
Agitation	Mild solution and slow mechanical agitation
Pretreatment	Use a 5-10% H_2SO_4 solution to keep bath concentration in H_2SO_4 at optimum range

The make up procedure of tin electroplating solution was as follows:

(1)Fill tank to 75% of volume with deionised water;

(2)Carefully add sulphuric acid;

(3)Add stannous sulphate. Be sure it is completely dissolved;

(4)Cool bath to 25 ºC;

(5)Add amount Ronastan EC Part B chosen from above formulation and mix well;

(6)Add amount Ronastan EC Part A chosen from above formulation and mix well;

(7)Adjust solution to final volume (1 L) using deionised water.

In the tin electroplating step of laser structuring technique, a small layer of tin needs to be deposited on the outer copper layer of printed circuit board. The printed circuit board is properly pre-cleaned and the cell is filled with tin electroplating solution. A wire is attached to the copper layer of the printed circuit board while the other end of the wire should be attached to the negative pole of a power supply. Another wire was connected to the positive pole of the power supply with its other end connected to two pieces of tin foil as shown in the Fig.3.4.

The printed circuit board then carries negative charge and tin foil carries positive charge. As the object to be plated is negatively charged, it attracted the positively charged tin cations. Electrons flew from the object to the cations to neutralize them to metallic form. At the anode electrons are removed from the tin metal, oxidizing it to the tin cations. Thus the tin dissolves as ions into the solution and replacement tin is supplied to the solution for that which have been plated out in the cell. By controlling electroplating time and electroplating current, a small layer of tin can be electroplated on the outer copper layer of the printed circuit board.

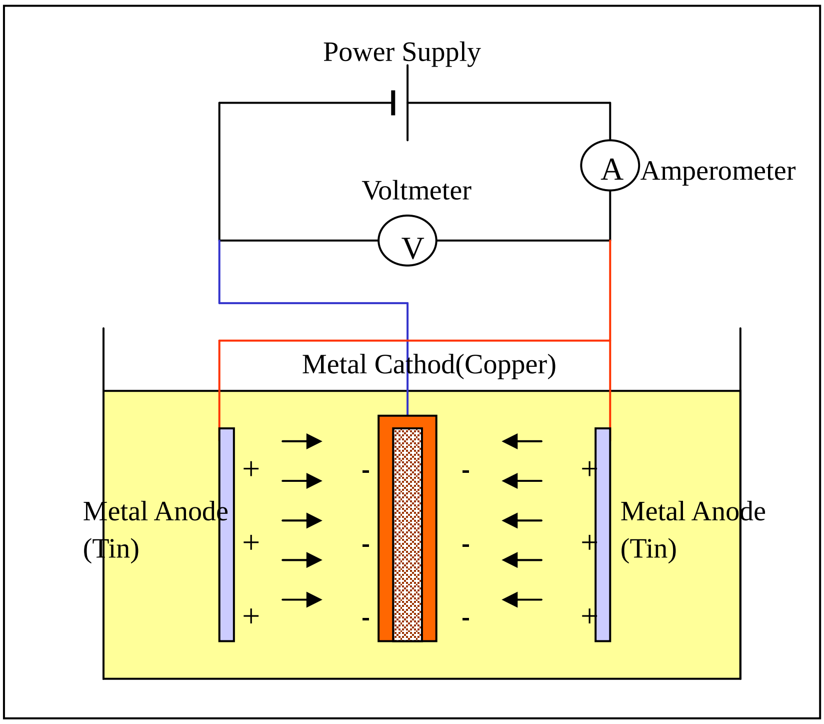

Fig.3.4 The tin electroplating process

3.4.2 The formation of circuit lines and spaces with Nd:YAG laser

In the LS technique, a pulsed UV Nd:YAG laser replaces the broadband light sources traditionally used to expose thin photoresist layers laid atop the PCB substrates. Rather than conventional photolithography, where the pattern in the resist is obtained by exposing it to an image projected through a mask, the laser beam writes directly on the tin layer in laser structuring technique. In the conventional photolithographic process, the entire large PCB substrate is exposed at once. Whereas in laser structuring process the laser beam only exposes small spots at any time. LS spot sizes must be kept small in order to keep the “pixel” (smallest exposed feature) size comparable to or better (smaller) than that obtained with lithography. As a result, the focused laser beam must move over the substrate with high speed in order to achieve satisfactory throughput.

Each laser pulse will ablate away a small layer of material and form a cavity on the substrate. With the serial moving of laser beam, cavities will formed in the appearance of a continuous groove. The formation of circuit lines and circuit spaces in laser writing process of LS can be explained by Fig.3.5. The spaces (b) between the circuit lines are constructed from a continuous series of small cavities fabricated by the moving of laser spot. The circuit lines (a) are then formed between the two spaces. The parameters in laser writing step will directly influence the geometry of circuit spaces. The geometry of circuit spaces will then influence the final geometry of circuit lines after the laser writing and copper etching steps.

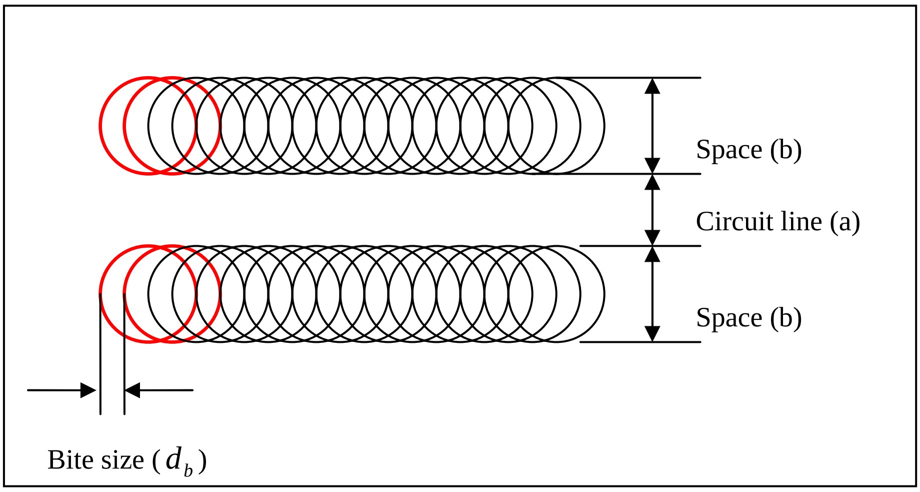

Fig.3.5 The fabrication of circuit lines and circuit spaces with the moving of laser beam

The uniformity of the space width means the variation of space width. This variation should be less than a certain value which is determined by bite size d_b. The uniformity of the space width is an important parameter which will influence the uniformity of the widths of circuit lines in etching step and will be discussed later.

3.4.3 The formation of circuit lines and spaces with Excimer laser

When the frequency-tripled Nd:YAG laser is used as the laser source, the diameter of the laser beam can be focused at 25 μm at the focal point. This focused laser beam can be used directly as a writing tool to fabricate fine circuit lines and circuit spaces in laser structuring. By contrast, the laser beam of the Excimer laser cannot be used directly to structure fine circuit lines and circuit spaces, because the size of the rectangular laser beam is very large (12 mm × 25 mm). In order to reduce the size of the laser beam for use as a writing tool, a mask with small apertures is used as shown in Fig.3.6.

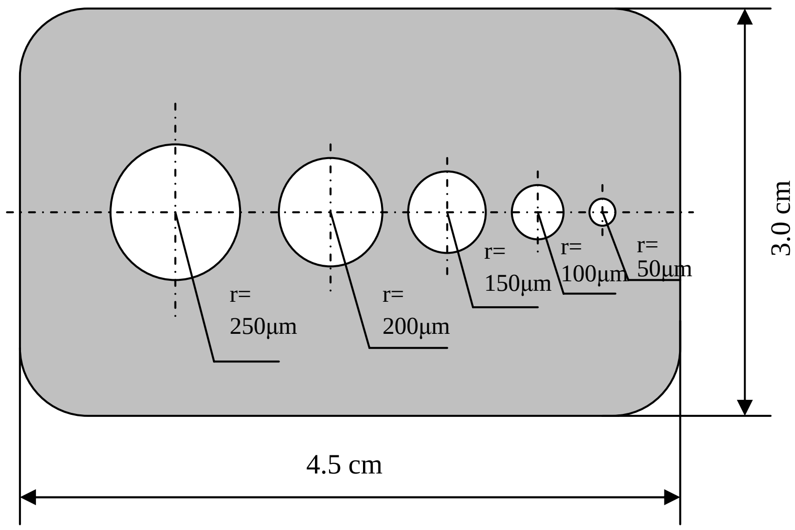

Fig.3.6 The masks used for the Excimer laser

The material of the mask is stainless steel and the dimensions of the mask are about 45 mm×30 mm determined by the mask holder of the Excimer laser system. Because the ratio of the pattern on the mask to the pattern written on the material is 10:1 in this work, the pattern size on the mask then would be ten times larger than the pattern size we obtained on material. For example, if the required diameter of the spot size on material is 25 μm, the diameter of the aperture on the mask is then ten times larger—that is 250 μm. In this work, the diameters of the apertures on the mask changed from 50 μm to 250 μm

The size of the aperture on the mask will influence the total size of circuit lines and circuit spaces. The diameter of the aperture cannot be reduced to an infinitely small dimension because it will affect the laser energy passing through it. When the size of the aperture is too small, the energy passing through it will be not strong enough to ablate materials. The minimum size of the aperture on the mask in laser structuring technology will be mentioned in Chapter Four. With a mask, the Excimer laser is reduced to a small spot and can be used to structure the circuit lines and circuit spaces directly.

3.4.4 Copper etching process

In the laser writing step of LS, laser only ablates away the tin layer and a small layer of copper. The circuit spaces fabricated after this step still connect circuit lines with remaining copper. In order to remove all the remaining copper uncovered by tin layer, copper etching step is used to create total insulation between circuit lines.

Printed circuit board entering the etch process have been coated with an etch resist (the tin layer). The resist layer selectively protects the circuit areas from etchant, whereas the remaining copper layer is etched away. Etchant on the surface of the panel removes the exposed copper, but cannot significantly dissolve the copper residing under the resist. In this way, a circuit space is formed between circuit lines.

As shown in Fig.3.7, the radius r_0 (half width of space) and depth z of circuit space before etching will change to r_e and z_e after the etching step. That is to say, the width and depth of space will both enlarge in the etching step. The remaining copper after laser writing step is etched away and the circuit spaces between circuit lines are finally formed.

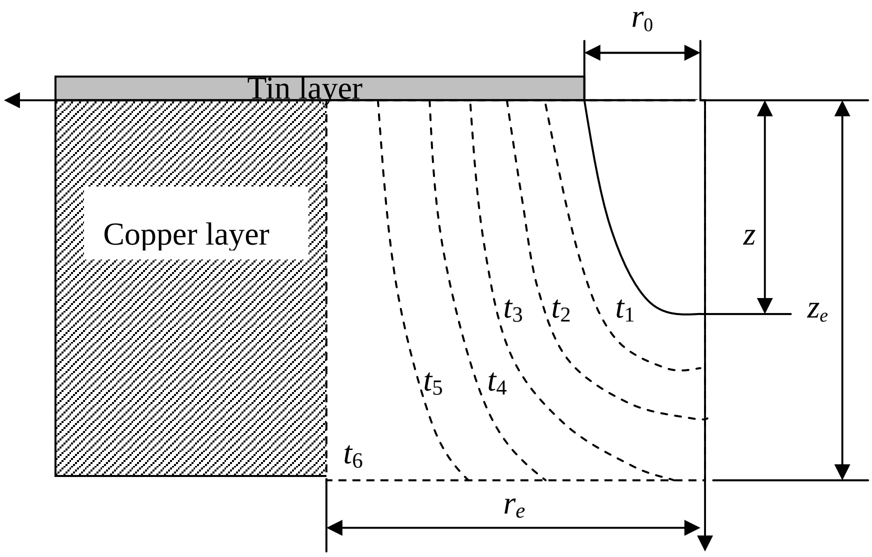

Fig.3.7 Width and depth of circuit spaces before and after copper etching step

By dissolving the extended lattice of metal atoms, chemical etching converts a solid insoluble material to soluble compounds that can enter the solution. This is accompanied by removal of electrons from the metal that is called oxidation. Copper can exist in three states, the elemental form, (Cu^0), the blue colored Cupric form, (Cu^{2+}), and the less common Cuprous form, (Cu^+). Copper can be etched using a solution of the copper itself depends on the transform of the copper salt from one state to the other.

The alkaline cupric chloride was selected as the copper etching solution in the laser structuring technique. When the cupric chloride was used as etchant, copper metal (Cu^0) from the surface of the circuit board was etched by cupric chloride ($CuCl_2$), resulting in the formation of cuprous chloride (CuCl). The high corrosive power of cupric chloride led to short etching times and little under-etching. The basic chemical reaction for alkaline cupric chloride chemistry (see Fig.3.8) was the oxidation of copper metal by cupric ions to form cuprous ions.

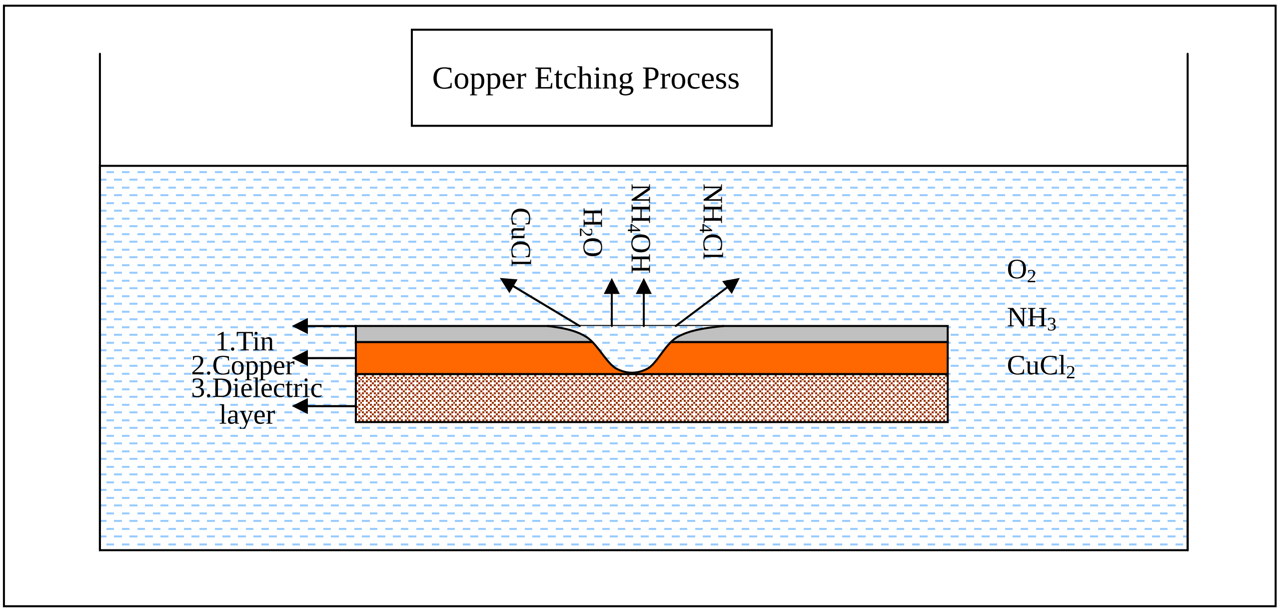

Fig.3.8 Copper etching process in the alkaline $CuCl_2$ solution

3.4.5 Tin stripping process

The goal in this process is to strip the tin layer on the copper layer. To facilitate this mechanism, the tin must be oxidized. Oxidation is the first step in any metal stripping process, and the purpose of which is to remove electrons from a substance. In the case of stripping tin, the oxidizer is nitric acid. Today's tin stripping solutions are always proprietary mixtures, but their compositions are quite similar (McKesson, 1999). The typical composition is as follows:

20% (w/w) Nitric Acid

5% (w/w) Ferric ion Fe^{3+}

<1% (w/w) Anti-tarnish

<1% Suspending Agent

The reaction for tin stripping is illustrated by:

$$2Sn+2HNO_3 \rightarrow 2SnO_2 + N_2O + H_2O \qquad (1)$$

Notice that each mole of tin is oxidized, losing four electrons. Water and nitrous oxide are produced as by-products of the reaction. All pure elements, like tin or copper, are neutral, meaning they do not carry any charge, and they have the same number of electrons as protons. For any metal to go into solution the metal must carry a positive charge. In the tin stripping reaction, removing electrons with an oxidizing agent give the elemental tin a positive charge. Tin has three different ionic charges or oxidation states that can occur:

1. Tin metal, Sn^0 (neutral)
2. Stannous Salts, Sn^{2+} (missing 2 electrons)
3. Stannic Salts, Sn^{4+}, (missing 4 electrons)

In the stripping process, the tin is oxidized to the stannic (Sn^{4+}) form. Once the metal had been oxidized, it must then be dissolved into solution. However most stannic salts were insoluble in water and even not soluble at any concentration of nitric acid. In order to keep the stannic oxide from precipitating out, it must be held by the suspending agent. The suspending agent kept the stannic oxide in solution by creating a fine dispersion of stannic oxides within the stripper solution.

A typical acid stripping solution also includes an inhibitor species to reduce any acid attack on the underlying copper substrate once the tin resist has been removed. Inhibitor is a substance that retards some specific chemical reaction. The addition of inhibitors in this experiment keeps the copper oxidation under control, leaving the unprotected tin under susceptible to oxidation by the nitric acid.

CHAPTER 4

FEASIBILITY STUDY OF LASER STRUCTURING

In the laser structuring process, there are three main steps – tin electroplating step, laser writing step and copper etching step. The process parameters (electroplating time and electroplating current in tin electroplating step; laser power, number of repetitions, repetition rate and bite size in laser writing step; the influence of space geometry and etching time in copper etching step) in these three steps will affect and determine the final dimension of circuit line and circuit space. In this section, the relationship between process parameters and electroplated tin thickness as well as the dimension of laser structured circuits will be discussed in detail in the tin electroplating step, laser writing step and copper etching step.

4.1 The electroplating of tin layer as etch resist

4.1.1 The variation of electroplating current

In the conventional photolithography technique, the thickness of photoresist are important factors, which influence the geometry and quality of circuit lines and circuit spaces. Tin-layer acts as the same function as photoresist to some extent in laser structuring, so the thickness of tin layer are also important parameters that will be discussed in this section.

In order to control the thickness of tin layer in electroplating process, two parameters are considered. One is the electroplating current and the other is the electroplating time. In this section, electroplating time is fixed to find out the relationship between electroplating current and the thickness of tin layer. The size of printed circuit board is 8×5 cm^2. The results of two groups of experiments are shown in Table 4.1. The electroplating time is fixed at 60 seconds in the first group and 120 seconds in the second group.

Table 4.1 The thickness of tin layer with the changes of electroplating current

Time	Current (A)	The thickness of tin layer (μm)
60 seconds	0.15	1.3
	0.25	1.7
	0.35	1.9
120 seconds	0.15	1.6
	0.25	1.9
	0.35	2.3

Fig.4.1 shows that the thickness of tin layer increases with the increase of electroplating current. When tin layer is too thick, the tin stripping step will take much time. If the tin layer is not thick enough, it will not act as the etch resist effectively during copper etching process. So the thickness of electroplated tin layer should be controlled between one to two micrometers which was also mentioned in the work of Meier (2001), Kimpfel (1999) and Tadic (2000).

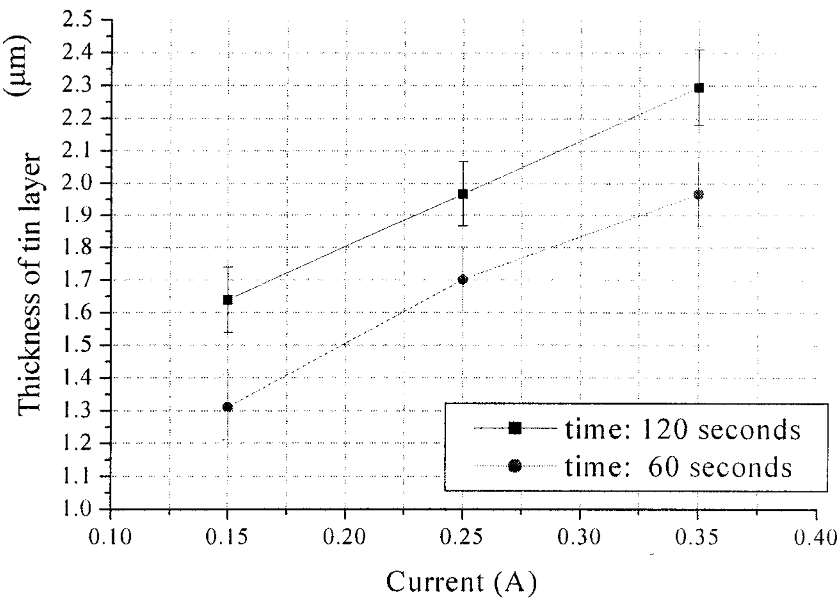

Fig.4.1 The thickness of tin layer with the changes of electroplating current

As shown in Fig.4.1, when the electroplating time is 60 seconds and electroplating current is from 0.15 to 0.35 A, the thickness of tin layer is from 1.3 to 1.9 μm (in the range of 1 to 2 μm). When the electroplating time is 120 seconds, the thickness of tin layer is in the range of 1 to 2 μm only when the electroplating current is from 0.15 to 0.25 A. In this experiment, most of the values of the thickness of tin were in the range of one to two microns, so these results were useful for further usage.

4.1.2 The variation of electroplating time

In this section, electroplating current is fixed and different thickness of tin layer is achieved by the controlling of electroplating time.

Table.4.2 The thickness of tin layer with the changes of electroplating time

Current (A)	Time (seconds)	Thickness of tin layer (μm)
0.2A	30	0.6
	90	1.5
	150	2.1
0.3A	30	1.5
	90	1.9
	150	2.8

The results of the influences of electroplating time on the thickness of tin layer are shown in Table 4.2. Two groups of experiments were carried out with the electroplating current was 0.2 A and 0.3 A respectively.

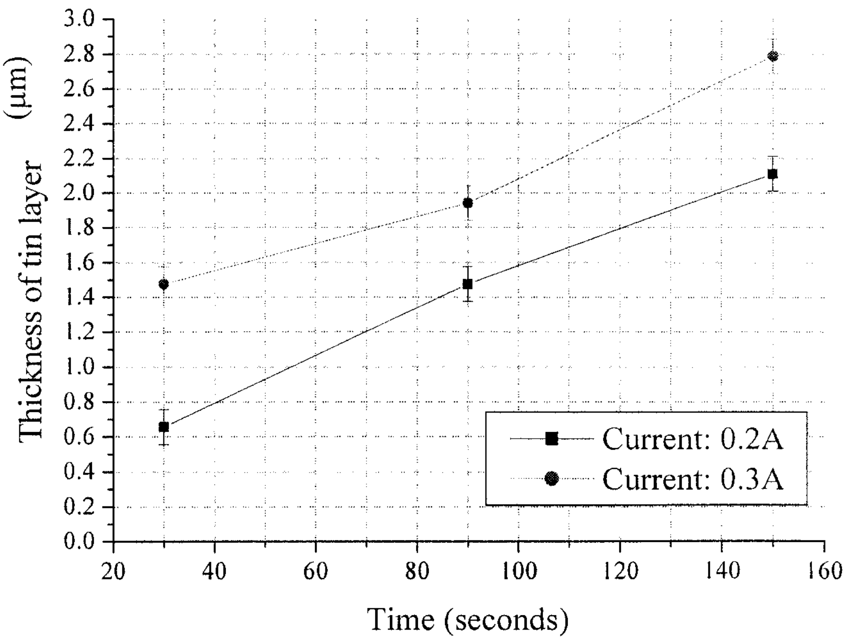

Fig.4.2 The thickness of tin layer with the changes of electroplating time

In Fig.4.2, it shows the relationship between the thickness of tin layer and the changes of electroplating time. It is clear that the thickness of tin layer increases with the increase of electroplating time. Electroplating time and electroplating current can both be used in the control of the thickness of tin layer.

In these experiments, the electroplating current was between 0.15 A and 0.35 A and the electroplating time was in the range from 30 seconds to 150 seconds, the thickness of tin layer varied from 0 to 3 μm. These experimental results provided experience in the controlling of the thickness of tin layer by selecting appropriate electroplating time and current. The thickness of tin layer between 1 μm to 2 μm would be accepted and used for further research.

4.2 Laser structuring with Nd:YAG laser

Laser parameters directly influence the geometry of circuit spaces in laser writing step. The geometry of circuit spaces in laser writing step (described by three characteristic parameters in this work: the depth of circuit spaces z, the width of circuit spaces d, the resolidification height h) is very important because it will influence the final geometry of circuit lines and circuit spaces. The detailed relationship between the process parameters and the geometry of circuit spaces (z, d and h) will be studied with Taguchi methodology in Chapter Five. The experimental results of the geometry of circuit space including the depth of space z, the width of space d and the resolidification height h were measured with Boeckeler VIA-video (with a resolution down to 0.1 μm) in this chapter. The quantitative relations between laser parameters and the depth of circuit spaces are studied to provide the range of process parameters for the subsequent study. The depth of circuit spaces is selected because it is strictly constraint by the thickness of copper layer. In order to protect the dielectric layer, the depth of circuit spaces structured by laser in laser writing step should be less than 10 μm.

Some frequently used laser parameters are discussed below, including laser power (P_{out}), number of repetitions (R_s), repetition rate (R_r) and bite size (d_b).

4.2.1 Effects of laser power

In general, a laser beam of circular cross-section is focused on the target surface by a lens, so that the spatial distribution of laser irradiance $I(r,t)$ at the focal plane can be expressed as,

$$I(r,t) = I(0,t)H(r) \tag{1}$$

The laser beam of Nd:YAG is Gaussian spatially, so

$$H(r) = \exp\left(\frac{-2r^2}{w^2}\right) \tag{2}$$

where r is the distance in the direction transverse to the direction of propagation, $I(0,t)$ is the laser irradiance at the center of the focal spot, and w is the focal spot radius for a Gaussian beam.

In this research, Q-switched pulsed laser is used so that the temporal profile of the irradiance at the center of the focal spot can be considered as

$$I(0,t) = I_0 G(t) \tag{3}$$

where I_0 is the maximum irradiance at the focal center point during the laser pulse duration τ, t represents time, and $G(t)$ is the time-dependent function. The laser beam irradiance $I(r,t)$ can be obtained in terms of the spatial and temporal profile as

$$I(r,t) = I_0 G(t)H(r) \tag{4}$$

Then the pulse energy Q can be expressed as

$$Q = I_0 \int_0^{\tau} \int_0^{\infty} G(t)H(r)2\pi r dr dt \tag{5}$$

In this research, I_0 is obtained by controlling the process parameters of the laser.

$$I_0 = \frac{2P_{out}}{\pi w^2 \tau R_r} \tag{6}$$

P_{out} is the average power of the laser, R_r is the repetition rate, w is the radius of the laser focal spot, and τ is the pulse duration.

Therefore, the pulse energy can be written as

$$Q = \frac{2P_{out}}{\pi w^2 \tau R_r} \int \int_0^\infty G(t)H(r)2\pi r dr dt \tag{7}$$

The pulse energy absorbed by a material is related to the reflectivity parameters of this material at a certain wavelength. If the reflectivity parameter is known as R, then the energy Q_a absorbed by the material (Zhang & Yung, 2006) is

$$Q_a = \frac{2(1-R)P_{out}}{\pi w^2 \tau R_r} \int \int_0^\infty G(t)H(r)2\pi r dr dt \tag{8}$$

In order to see the influence of laser power (P_{out}) on the depth of circuit spaces, some experiments were carried out. As the depth of circuit spaces structured by laser are only several micrometers, the laser power is set at a small value. In this research, the range of laser power was selected between 0.1 W and 0.4 W and other parameters were fixed at certain values (laser power=0.1-0.4 W, repetition rate=10 kHz, v=50 mm/s, bite size=5 μm and number of repetitions=1). From Fig.4.6, it can be seen that the depth of circuit spaces increases with each increase in laser power. As shown in Equation (8), when the laser power is increased, the material absorbs more energy at the same time. The relationship between the depth of circuit spaces and the laser power are shown in Fig.4.3.

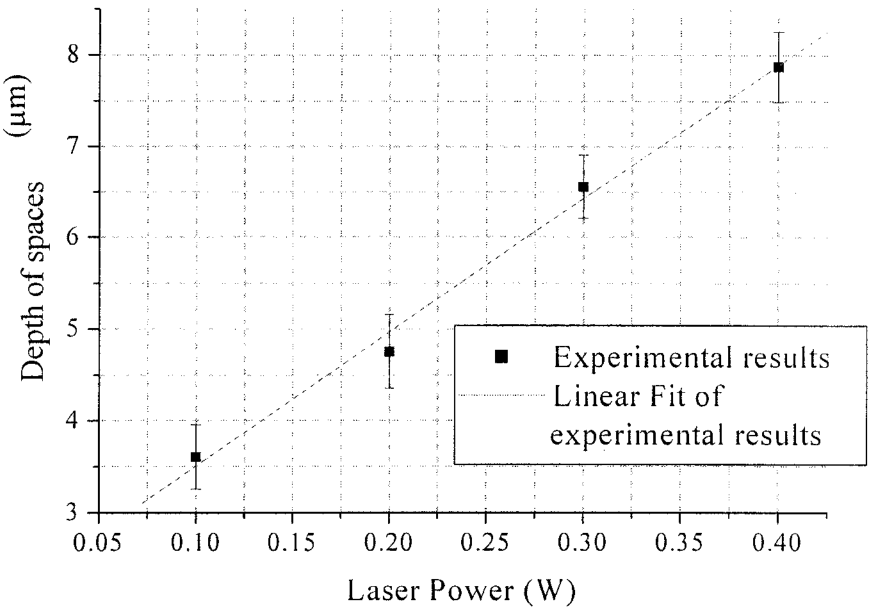

Fig.4.3 Curve fit of the experiments of laser power & depth of space

The depth of circuit spaces with the increase of laser power closely follows a positive linear relationship as shown in Fig.4.3, so a polynomial formula is taken to fit the experimental results. Table 4.3 lists the results for the SSE (the sum of squares due to error), R-square (the coefficient of multiple determination) and adjusted R-square (the degree of freedom-adjusted R-square). SSE is a statistic measuring of the deviation of the fitted values from the experimental results. A value closer to 0 indicates that the fit will be more useful for prediction of experimental results. R-square is used to measure how successful the fit is in explaining the variation of the data. R-square can take on any value between 0 and 1, with a value closer to 1 indicating that a greater proportion of variance is accounted for by the fit. The adjusted R-square statistic is generally the best indicator of the fit quality where a value closer to 1 indicates a better fit. These three quantified results are used to examine the goodness-of-fit from statistics.

Table.4.3 Accuracy of the curve fit – laser power & the depth of circuit space

Data set	Function Type	SSE	R-square	Adjusted R-square
Depth of space vs. laser power	Polynomial	0.88973	0.97709	0.97556

4.2.2 Effects of number of repetitions

In order to see the influence of number of repetitions on the depth of space, some experiments were carried out in which the number of repetitions were changed and other parameters were fixed at certain values. A set of experiments was shown below with laser power=0.1 W, repetition rate=10 kHz, v=50 mm/s, bite size=5 μm and different number of repetitions to see the influence of number of repetitions on space depths. A low value was selected for the laser power because this would permit a larger range for the increase of number of repetitions. The experimental results and the curve fit are shown in Fig.4.4. The function type of the curve fit is polynomial. The SSE and adjusted R-square results present the accuracy of the curve fit in Table 4.4.

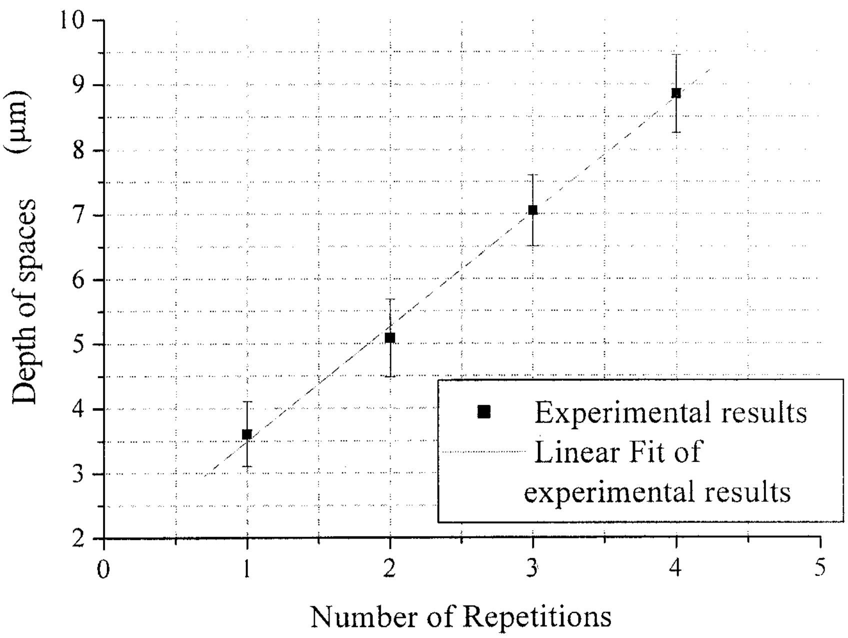

Fig.4.4 Curve fit of the experiments of number of repetitions & depth of space

Table.4.4 Accuracy of the curve fit – number of repetitions & the depth of circuit space

Data set	Function Type	SSE	R-square	Adjusted R-square
Depth of space vs. repetitions	Polynomial	0.04841	0.99692	0.99538

In the laser writing step, the splashing problems exist. The problem of the splashing of materials becomes more serious with increasing number of repetitions. The cross sections of circuit spaces structured by laser are shown in Fig.4.5 with number of repetitions were 2, 3 and 5 times separately. It can be seen that copper splashing increases with increasing number of repetitions.

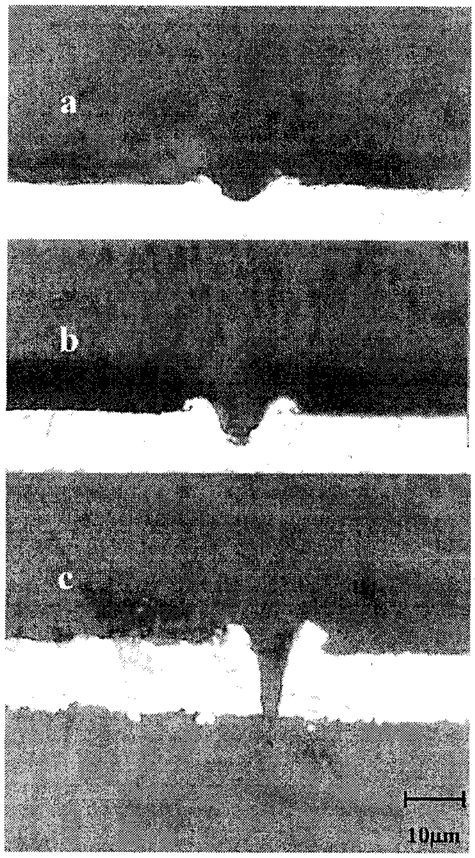

Fig.4.5 Cross section of circuit space with (a) number of repetitions=2, (b) number of repetitions=3, and (c) number of repetitions=5, at laser power=0.1 W, repetition rate=10 kHz, v=50 mm/s, bite size=5 μm.

The splashing of copper can melt and damage the tin layer near the circuit spaces and make the tin layer cannot act as resist effectively in the copper etching step. The splashing problem should therefore be avoided during laser writing step. That is to say, the number of repetitions should be selected at a small value. Further, because a higher velocity translates to higher efficiency, which is preferred in the industry, the number of repetitions should also be less. In this work, the number of repetition is selected as one. If it is necessary to increase the depth of circuit spaces, increasing the laser power or decreasing the repetition rate will be considered as better alternatives.

4.2.3 Effects of repetition rate

In the laser writing process, besides laser power and number of repetition, the influences of the parameters of repetition rate, bite size and velocity also need to be considered.

Repetition rate, bite size and velocity have a relationship that velocity is equal to the multiplication value of repetition rate and bite size ($v = R_r d_b$). Thus, when considering the repetition rate, we also need to consider its relations with velocity and bite size. In this section, bite size was fixed at a certain value and velocity changed with the variation of repetition rate.

In order to know the influences on the depth of space of the repetition rate, a set of experiments were performed in which the laser power=0.1 W, number of repetition=1, and bite size=5 μm. With the increase in the repetition rate (and the bite size set as constant), the peak power of the laser pulse decreases as shown in Equation (8), and the laser velocity is increased as mentioned above. From Fig.4.6, we can see when the laser repetition rate is 1 kHz or 2 kHz, the tin and copper layers are penetrated by the laser (the thickness of the tin and copper layers is about 10 μm). In order to achieve a higher velocity and protect the dielectric layer, which is under the copper layer, the repetition rate should be set above a certain level. For example, in this experiment, it should be set at equal to or higher than 3 kHz.

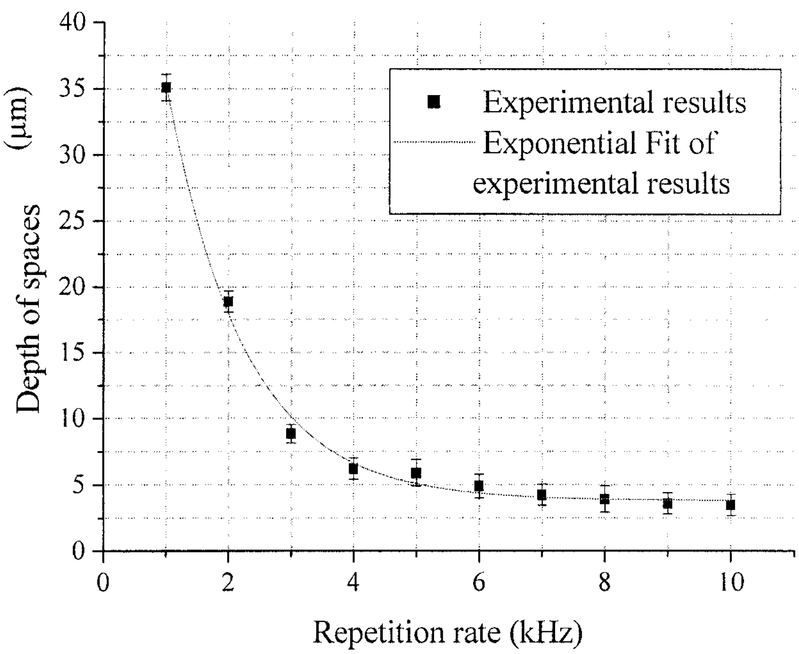

Fig.4.6 Curve fit of the experiments of repetition rate & depth of space

When the number of repetition is one, the acceptable repetition rate should be higher than 2 kHz to avoid any possible damage to the dielectric layer underneath the copper layer. The relationship between the depth of circuit spaces and repetition rate can be described with an exponential function. The SSE and adjusted R-square values are shown in Table 4.5.

Table.4.5 Accuracy of the curve fit -- Repetition rate & the depth of circuit space

Data set	Function Type	SSE	R-square	Adjusted R-square
Depth of space vs. repetition rate	Exponential	3.78469	0.99587	0.9938

4.2.4 Effects of bite size

As we mentioned above, velocity is equal to the multiplication value of repetition rate and bite size ($v = R_r d_b$). If it is necessary to increase the laser structuring velocity, besides the method of increasing the repetition rate, increasing the bite size can also have the same function. When the repetition rate is above a certain value, the depths of circuit spaces are very shallow, which may affect the efficiency of the copper etching process. Thus, at this time, the bite size can be changed to increase the structuring velocity.

With the increasing of the laser bite size (setting the repetition rate as constant), the velocity of the laser is increased at the same time. Achieving a faster fabrication progress is what we wanted, but the uniformity of the space should be considered at the same time. The uniformity of the width of space means the variation of the width of space. This variation should be less than a certain value, which is determined by bite size d_b.

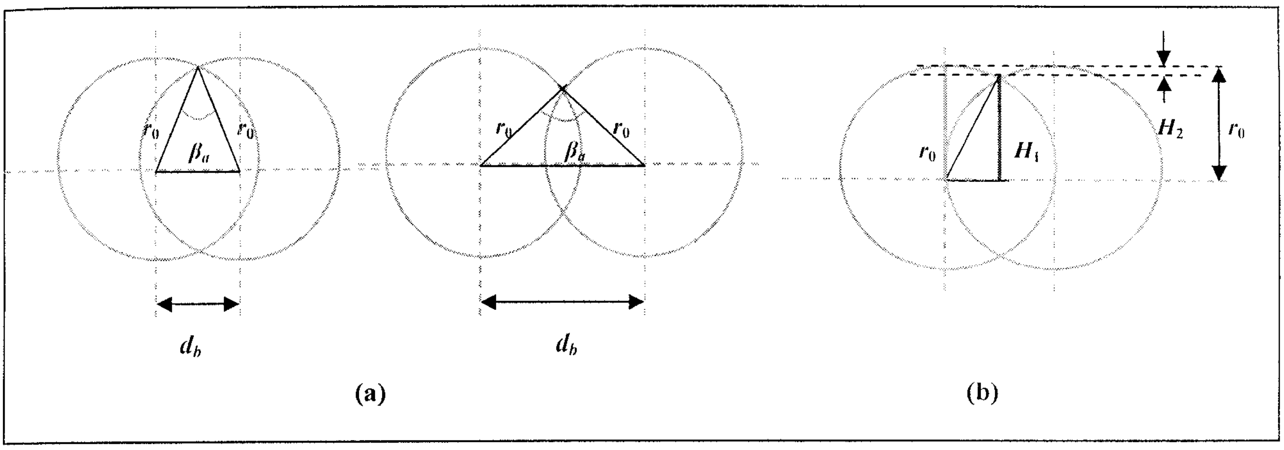

Fig.4.7 (a) The relations between bite size and angle β_a,

(b) The calculation method of the uniformity of space width.

The variation of space width (X) can be calculated by the Equations (9)-(12). From Fig.4.7a, it is clear that the angle β_a increases with the increase of bite size d_b. The relation between bite size d_b and angle β_a is shown in Equation (9).

$$\sin\frac{\beta_a}{2} = \frac{\left(\frac{d_b}{2}\right)}{r} = \frac{d_b}{2r_0} \tag{9}$$

Then, the angle β_a can be computed by

$$\beta_a = 2\arcsin\left(\frac{d_b}{2r_0}\right) \tag{10}$$

The difference between r_0 (the largest space width) and H_1 (the smallest space width) can be calculated by

$$H_2 = r_0 - H_1 = r_0 - r_0\cos\left(\frac{\beta_a}{2}\right) = r_0\left[1-\cos\left(\frac{\beta_a}{2}\right)\right] \tag{11}$$

The variation of the space width X is:

$$X = \frac{H_2}{r_0} \times 100\% = \left[1 - \cos\left(\frac{\beta_a}{2}\right)\right] \times 100\% \qquad (12)$$

In order to keep the uniformity of space width, the bite size d_b should be selected with the calculation results of angle β_a and variation X at low value. When angle β_a is too large i.e. bite size d_b is large, the circuit space was laser-structured by a set of obvious cavities instead of a continuous line as shown in Fig.4.8c-d. From experimental results, it is observed that in order to keep the uniformity of space width, the bite size d_b should be equal to or less than the radius of laser beam on material. When the bite size d_b is equal to the radius of laser beam, the angle β_a is 60° and the variation of the space width X is 13%.

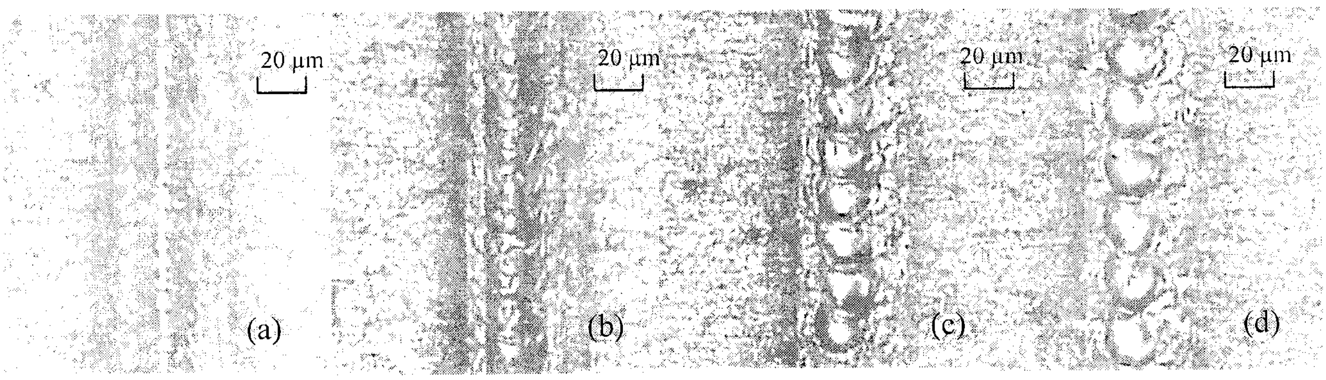

Fig.4.8 Laser structuring with (a) Bite size=7 μm and (b) Bite size=11 μm and (c) Bite size=15 μm and (d) Bite size=19 μm.

The uniformity of the width of space is influenced by the bite size, at the same time, the depth of space is also influenced by this factor. In order to know the relationship between the depth of space and the bite size, a set of experiments were performed in which the laser power=0.2 W, number of repetition=1, and repetition rate=5 kHz. With the increase of the bite size, the depth of spaces decreased first. When the bite size was equal to the radius of laser beam, the depth of spaces maintained nearly at the same value (as shown in Fig.4.9). The relationship between the depth of circuit space and bite size can be described by an exponential function. The SSE and adjusted R-square values are shown in Table 4.6.

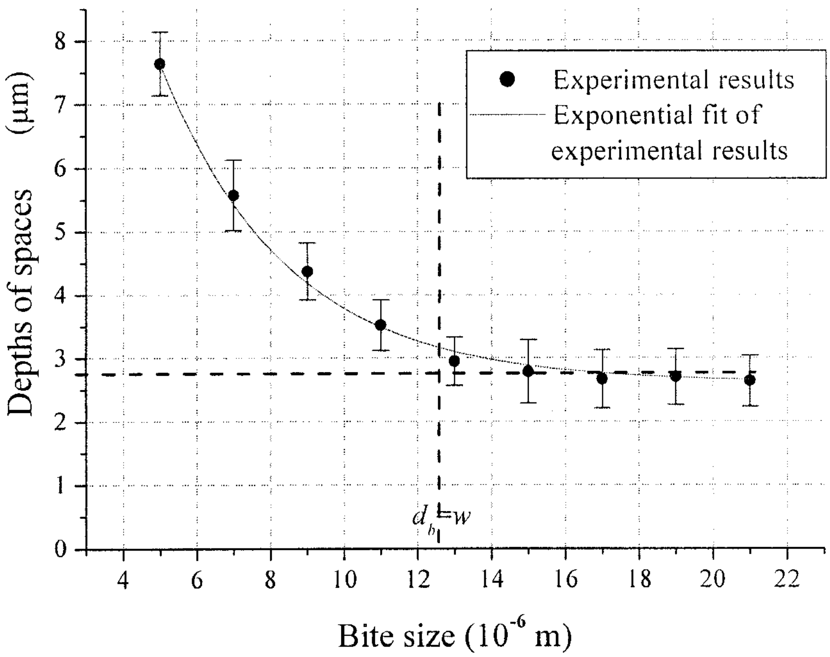

Fig.4.9 Curve fit of the experiments of bite size & depth of spaces

Table.4.6 Accuracy of the curve fit -- bite size & the depth of circuit space

Data set	Function Type	SSE	R-square	Adjusted R-square
Depth of space vs. bite size	Exponential	0.02133	0.9973	0.9952

4.3 Laser structuring with Excimer laser

The Excimer laser can also be considered as a laser source in laser structuring because of the advantages of its shorter wavelength and shorter pulse duration. There are three advantages to using the Excimer laser in laser structuring. Firstly, the diameter of the laser beam can be reduced to a small size by controlling the aperture on a mask. By doing this, the width of circuit spaces can be reduced to a smaller dimension. Secondly, when the laser interacts with heat conducting materials, the machining process is subject to thermal degradation. Both the short wavelength and the short pulse duration of the Excimer laser reduce the thermal damage to the materials. This laser ablation process results in sharply-defined features and smaller thermal-damage zone. Finally, the Excimer laser is taken as a laser source because it has a smaller reflection factor and thus better absorption by most materials. Considering the extent of the laser-induced surface damage, the Excimer laser seems to perform better than the Nd:YAG laser in this respect. And with the usage of a mask to control the diameter of the laser beam, Excimer lasers have the flexibility and convenience to fabricate smaller circuits than the Nd:YAG laser in laser structuring. In this section, the influences of the parameters of Excimer laser on the fabrication results are discussed in detail.

4.3.1 Effects of laser energy

From Fig.4.9, it is clear that the depth of space increases with each increase in laser energy. These results agree with those proposed by Andrews (Equation (13), Andrews, 1975). According to Andrews' theory about the laser ablation of materials, it is assumed that the laser power W is distributed uniformly over some area of the surface S and is applied normally to the surface. In a time interval δt, the depth of the space can be expressed as

$$z(t) = \frac{1}{h\rho S}\int_0^t W dt \quad \text{or} \quad z(t) = \frac{E(t)}{h\rho S}, \tag{13}$$

where h is the heat required to vaporize unit mass of material, and ρ is the density of the material. From Equation (13), it is clear that the depth of the space depends on the total energy supplied to the surface.

The depths of circuit spaces and the increase of laser energy exhibit a linear relationship as shown in Fig.4.10 (laser energy=80-180 mJ, number of repetitions=4, bite size=5 μm, spot size=25 μm, laser fluence=26-60 mJ/cm^2). The SSE and adjusted R-square results present the accuracy of the curve fit in Table 4.7.

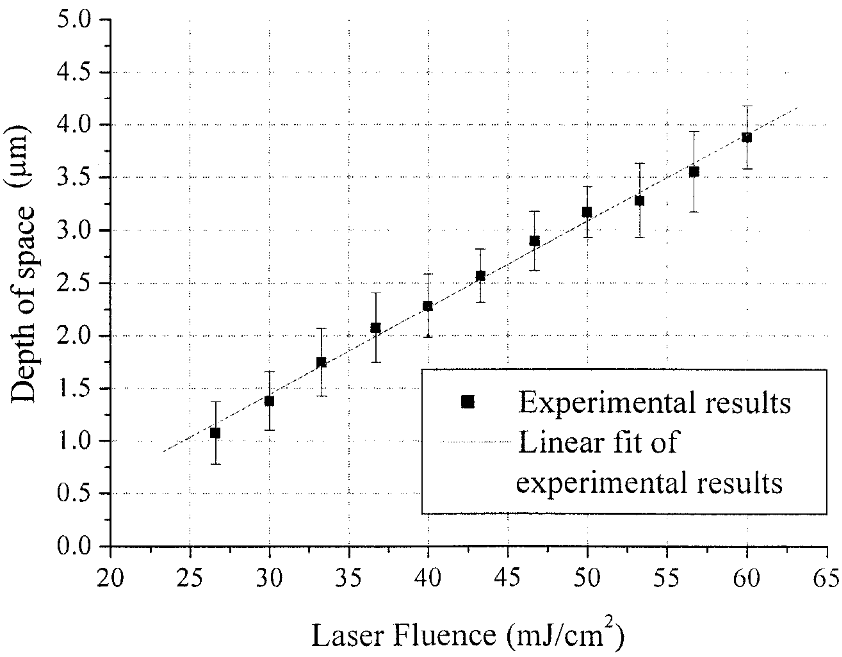

Fig.4.10 Relations between laser energy & depth of space

Table.4.7 Accuracy of the curve fit -- laser energy & the depth of circuit space

Data set	Function Type	SSE	R-square	Adjusted R-square
Depth of space vs. laser energy	Polynomial	0.04848	0.9941	0.9935

The depth of space with increasing laser energy is shown in Fig. 4.10. In our research, the depth of space should be larger than the thickness of tin layer in order to etch the copper under tin layer in etching step (1 μm) and smaller than the total thickness of tin and copper layer so as to protect the dielectric layer under copper layer (10 μm). The maximum laser energy of this Excimer laser system with stable output is about 180 mJ. In order to reach the depth of space above 1 μm, large number of repetitions was needed.

4.3.2 Effects of number of repetitions

Except for laser energy, number of repetition is an important factor that will influence the fabrication results of laser structuring. In order to see the influence of number of repetition on the depth of space, some experiments were carried out in which the number of repetition was changed and other parameters were fixed at certain values. The results between number of repetition and the depth of spaces are shown in Fig.4.11. The SSE and adjusted R-square results present the accuracy of the curve fit in Table 4.8.

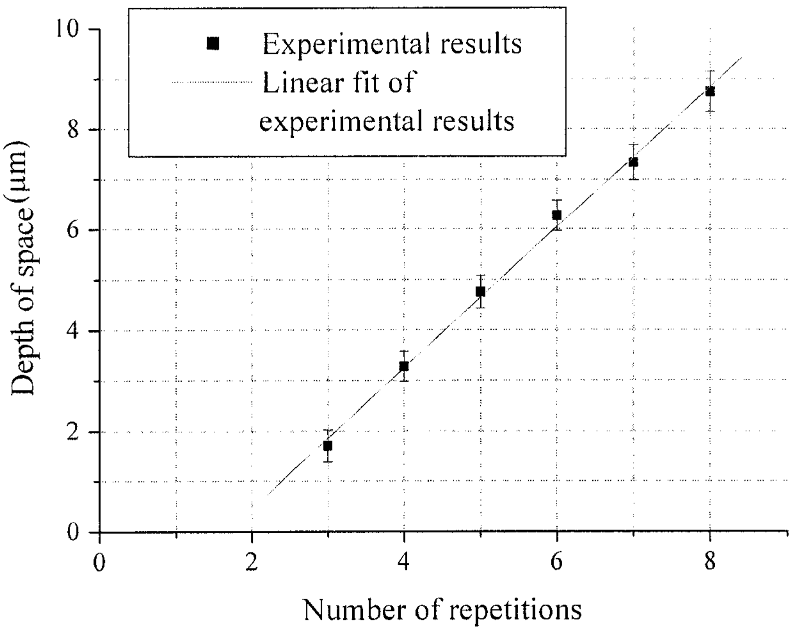

Fig.4.11 Relations between number of repetitions & depth of spaces

Table.4.8 Accuracy of the curve fit -- number of repetition & the depth of circuit space

Data set	Function Type	SSE	R-square	Adjusted R-square
Depth of space vs. number of repetition	Polynomial	0.1057	0.9969	0.9961

The depth of circuit space with the increase of number of repetition closely follows a positively linear relationship as shown in Fig.4.11 (laser energy=160 mJ, number of repetitions=3-8, bite size=5 μm, spot size=25 μm, laser fluence=53 mJ/cm^2). The thickness of the copper is ablated away by about 1.5 μm at each repetition.

From Fig.4.12, we can see the influence of number of repetition on the cavities structured by the Excimer laser. With the increase in number of repetitions, more laser energy was supplied to the material surface and caused enlargement of thermal damage. When the number of repetition was one, the edge of the cavity was not clear (as shown in Fig.4.12a). This is because the Excimer laser can only ablate a very small layer of materials at one time. When the number of repetitions was from five to seven, dark circular areas emerged around the cavities because the thermal damage zones increased with the increase in number of repetitions (as shown in Fig.4.12c). When the number of repetitions was increased from twice to four times, the edges of the cavities were clear and the thermal damage zones were not obvious (as shown in Fig.4.12b).

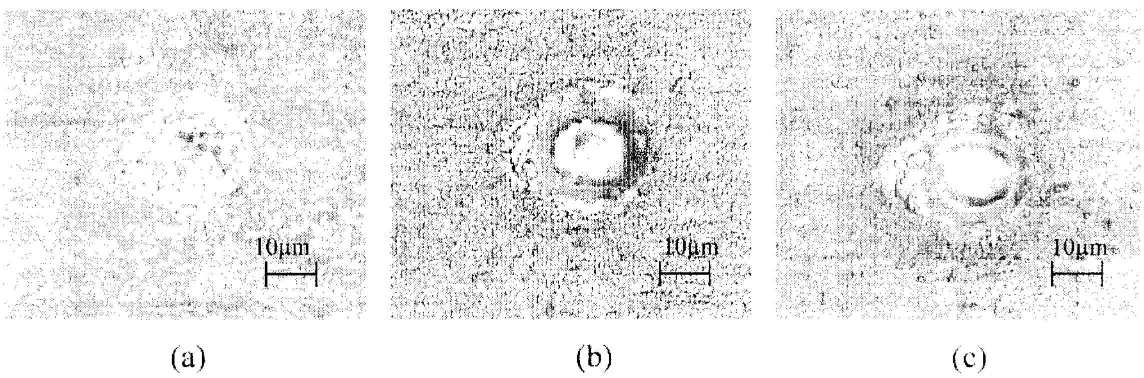

Fig.4.12 Cavities structured by Excimer laser with (a) number of repetition=1; (b) number of repetitions=4; (c) number of repetitions=6; at laser fluence=53 mJ/cm^2.

The enlargement of the thermal damage zone will affect the tin layer around the circuit spaces and influence the quality of the final circuit lines and circuit spaces. The tin layer can easily be melted away because of its low melting point. If the tin layer gets thinner, it will not act well as the etching resist during the etching process.

It is therefore better to take measures to reduce the thermal damage zone during the laser structuring process, such as by restricting the number of repetitions from two to four times, as in this work.

4.3.3 Effects of spot size of laser beam

With the need for a smaller size of pattern, the Excimer laser is more flexible and able to provide a smaller spot size of laser beam with the use of a mask. In the experiment to get the minimum widths of circuit lines and circuit spaces, smaller apertures on the mask are preferred, which will produce a smaller spot size. As shown in Fig.3.3, the small spot size of the laser beam will produce small widths of circuit spaces 'b' between circuit lines 'a'. The size of the circuits which is constructed by 'a' and 'b' will then be reduced. However, the aperture on the mask cannot be reduced to infinite small dimensions by considering the energy passing through it.

When the diameter of the aperture on the mask changes, the energy passed through the aperture also changes as shown in Table 4.9 calculated by Equation (14).

$$E_r = \frac{\pi r^2 E}{gl} \tag{14}$$

where E_r is the energy passed through the apertures on the mask, E is the pulse energy of the Excimer laser, g and l are the width and length of the rectangular beam of Excimer laser, and r is the radius of the aperture on mask.

Table 4.9 Laser energies with changes of aperture diameters on the mask

Diameter of the aperture on the mask (μm)	25	20	15	10
Energy of the laser beam (mJ)	$1.9\times10^{-6}E$	$1.2\times10^{-6}E$	$0.7\times10^{-6}E$	$0.3\times10^{-6}E$

This phenomenon that laser energy passed through mask changes with the change of the diameter of aperture on mask will influence the depths of circuit spaces to be structured. The depth of spaces will affect the final geometry of circuit lines and circuit spaces after etching and affect the etching time in the etching step. If the depth of spaces is small, it takes much more etching time and will enlarge the width of the spaces. In Fig.4.13, when laser energy and number of repetition were the same, the depths of spaces were different with the changes of apertures (laser energy=140 mJ, number of repetitions=4, spot size=10 μm-25 μm). In Fig.4.13a, the configuration of the cavity is not very clear because of the low energy passed through the mask (the diameter of the aperture is 100 μm). When the diameters of the apertures were under 100 μm, the configurations of cavities were almost unseen. When the size of aperture is small, in order to increase the depth of spaces, it needs more number of repetitions along the pattern. In order to keep high efficiency and decrease thermal damage of materials, we did not adopt the method of increasing number of repetition to increase depth of space. Then the minimum diameter of aperture with acceptable result of space depth was above 100 μm.

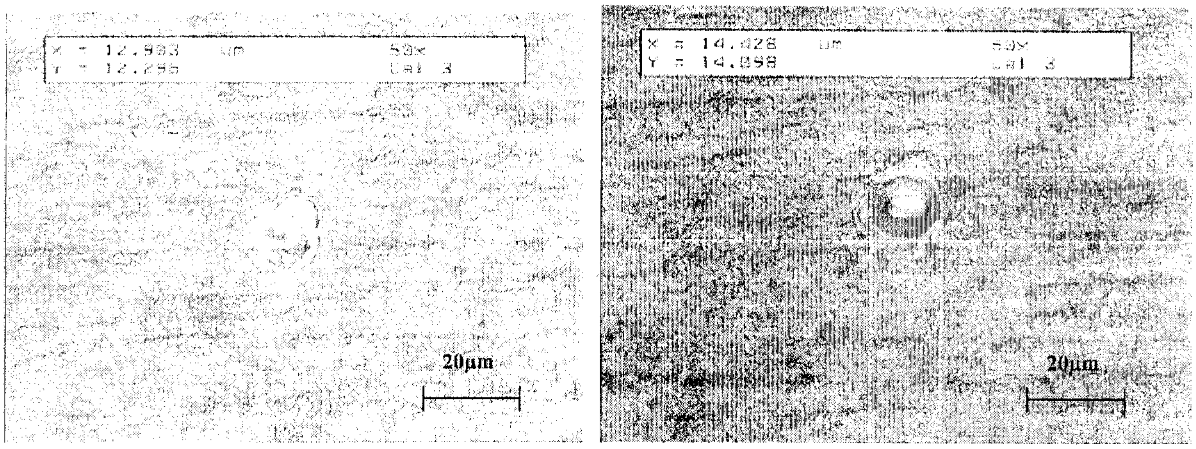

(a) (b)

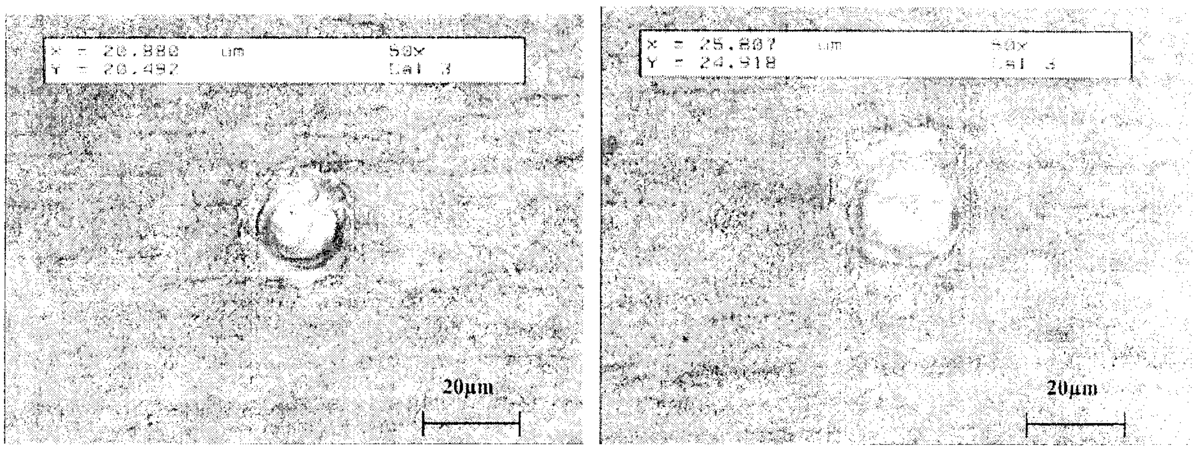

(c) (d)

Fig.4.13 Cavities structured by different diameters of the laser beam when (a) aperture diameter=100 μm, (b) aperture diameter=150 μm, (c) aperture diameter=200 μm, and (d) aperture diameter=250 μm.

The relation between the size of laser beam on material and the size of aperture on mask can be got based upon the following paraxial lens Equation:

$$\frac{1}{u}+\frac{1}{v_i}=\frac{1}{f}, \quad \eta_0=\frac{u}{v_i} \tag{15}$$

$$w=r/\eta_0 \tag{16}$$

where u is the distance from the mask plane to the imaging lens; f is the focal length of the image lens; v_i is the distance from the image lens to the workpiece; η_0 is the demagnification ratio; w is the radius of laser beam on material and r is the radius of aperture on mask. In this experiment, the demagnification rate η_0 was 10. The diameters of cavities on material were 1/10 of the diameter of aperture on mask.

4.4 Copper etching process

4.4.1 The influence of space geometry in copper etching step

Etching process will influence the geometry and cross-sectional profile of circuit lines and circuit spaces. Three configurations of circuit lines are shown in Fig.4.14, which are rectangular profiles and trapezoid profiles with positive and negative slopes. The configuration of circuit lines can be described by two parameters -- the effective width of a conductor w_l and angle θ (IPC-A-600G). The effective width of circuit lines w_l is the dimension measured at the top or the bottom of circuit lines, whichever is maximum as shown in Fig. 4.14.

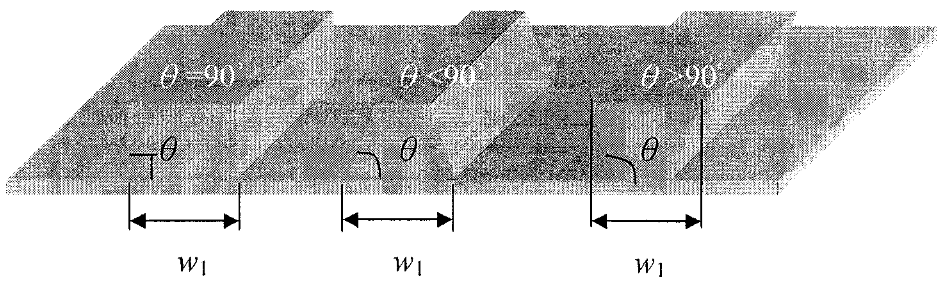

Fig.4.14 Three kinds of results of the cross-sectional profile of copper line after etching

When the effective width w_l is the same for the three configurations and angle θ is above 90°, the width of circuit line is smaller at the base material than at the top. In this situation, the contact areas between materials (circuits and base material) are smaller than that when the effective width w_l is the same and angle θ is equal or less than 90°. The adherence of circuit lines on base material will decrease with the decrease of the contact area between metal and polymer (Siau, 2005) The decrease of adherence will cause circuit lines more easily to separate from the base materials. In this work, one of the criteria on the quality of circuit lines is to observe the cross-sectional profiles of the circuit lines. The configuration with angle θ larger than 90° is thought to be unacceptable in consideration of adherence between circuit lines and base materials. So some relevant parameters at laser writing and copper etching steps should be determined to get copper circuit lines with good cross-sectional profiles (angle $\theta \leq 90°$).

Two kinds of parameters were considered in this section. Firstly, the parameters in laser writing step, which will influence the depth and width of circuit space, were studied about their further influences in the etching step. Secondly, the etching time that will influence the cross-sectional profile of circuit line was also studied.

In the laser writing step, the depth of space increases with increase of number of repetition, increase of laser power, decrease of repetition rate, and decrease of bite size. The depth and width of circuit spaces before etching process and the width of circuit spaces (the depth of circuit spaces is equal to the thickness of copper layer) after etching process are shown in Table.4.10. It is clear that deeper the depth of spaces in laser writing process, wider the width of spaces after etching under the same etching conditions.

Table 4.10 The influence of space depth (in laser writing step) on etching results

	Copper space Depth (μm)	Copper space Width (μm)	Space width (μm) (after 180 seconds etching)	Space width (μm) (after 600 seconds etching)
Laser power=0.2 W	6.1	20.3	34.1	48.6
Laser power=0.25 W	7.9	21.7	42.5	52.5
Laser power=0.3 W	9.0	19.9	45.2	56.1

Fig.4.15 and Fig.4.16 show the etching results after 180 and 600 seconds. When etching time was 600 seconds, the angle θ was almost 90 degree that was better than the etching time was 180 seconds.

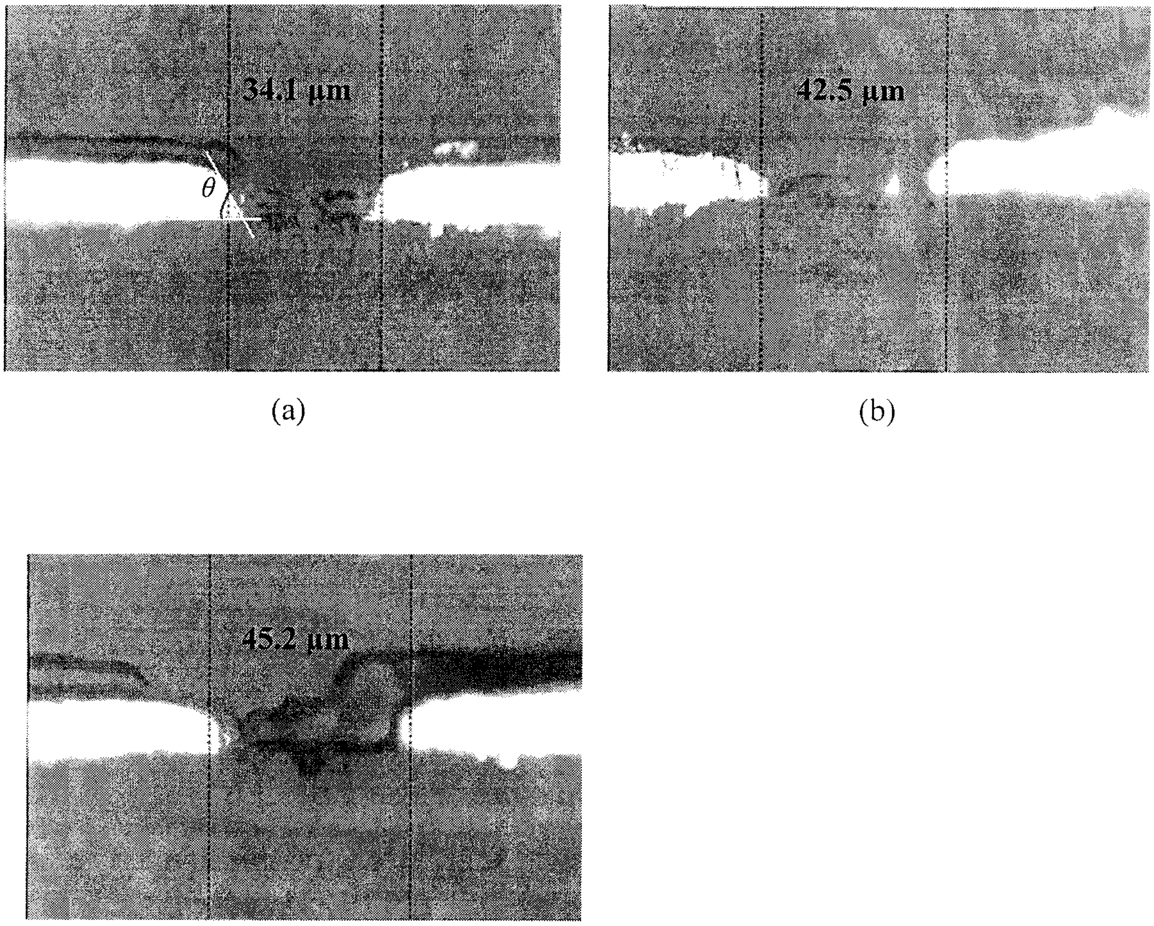

(c)

Fig.4.15 Cross section of circuit space after copper etching step (180 seconds) with (a) laser power=0.2 W, (b) laser power=0.25 W, (c) laser power=0.3 W at number of repetition=1, repetition rate=5 kHz, v=25 mm/s, bite size=35 μm in laser writing step.

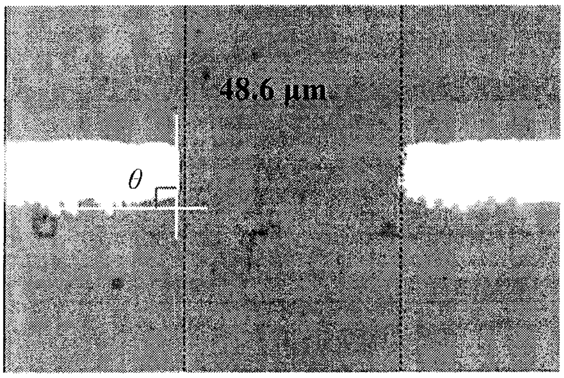

(a)

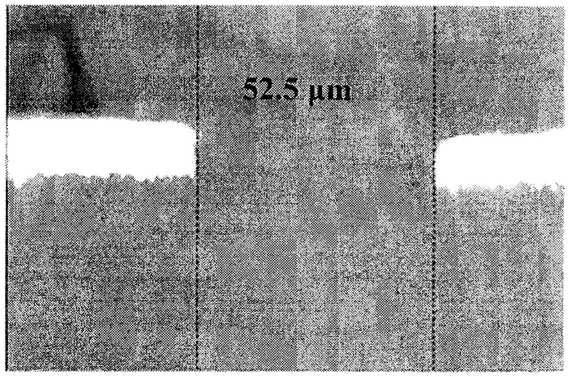

(b)

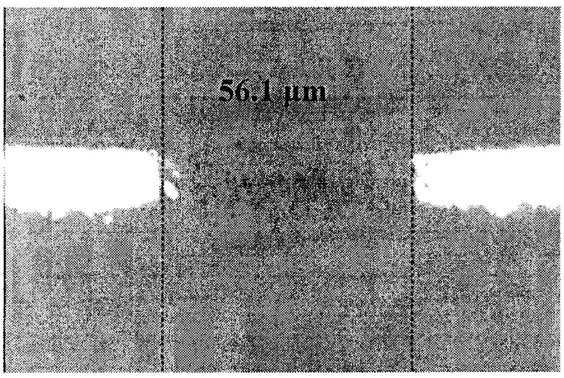

(c)

Fig.4.16 Cross section of circuit space after copper etching step (600 seconds) with (a) laser power=0.2 W, (b) laser power=0.25 W, (c) laser power=0.3 W at number of repetition=1, repetition rate=5 kHz, v=25 mm/s, bite size=35 µm in laser writing step.

4.4.2 The influence of etching time on copper etching process

In the etching process, the circuit spaces increase in both width and depth directions, as shown in Fig.4.17. When the depths of spaces increase in the etching step, the widths of spaces increase at the same time. When the remaining copper in circuit space is etched away (the insulation between circuit lines formed), the width of circuit space after etching step will become larger than that after laser writing step.

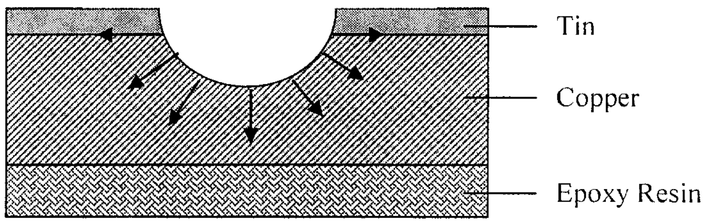

Fig.4.17 The copper etching process after laser writing step

In the copper etching step, etching time is an important factor that will influence the final geometry of circuit lines and circuit spaces. Fig.4.18 shows the cross sections and width of circuit spaces at different etching time. Etching solution first enlarged the width and depth of laser-structured space (as in Fig.4.18a). Then the copper layer was etched through (as in Fig.4.18b). With the etching time increased, the angle θ of the copper line increased from acute angle to right angle (as in Fig.4.18b-Fig.4.18d).

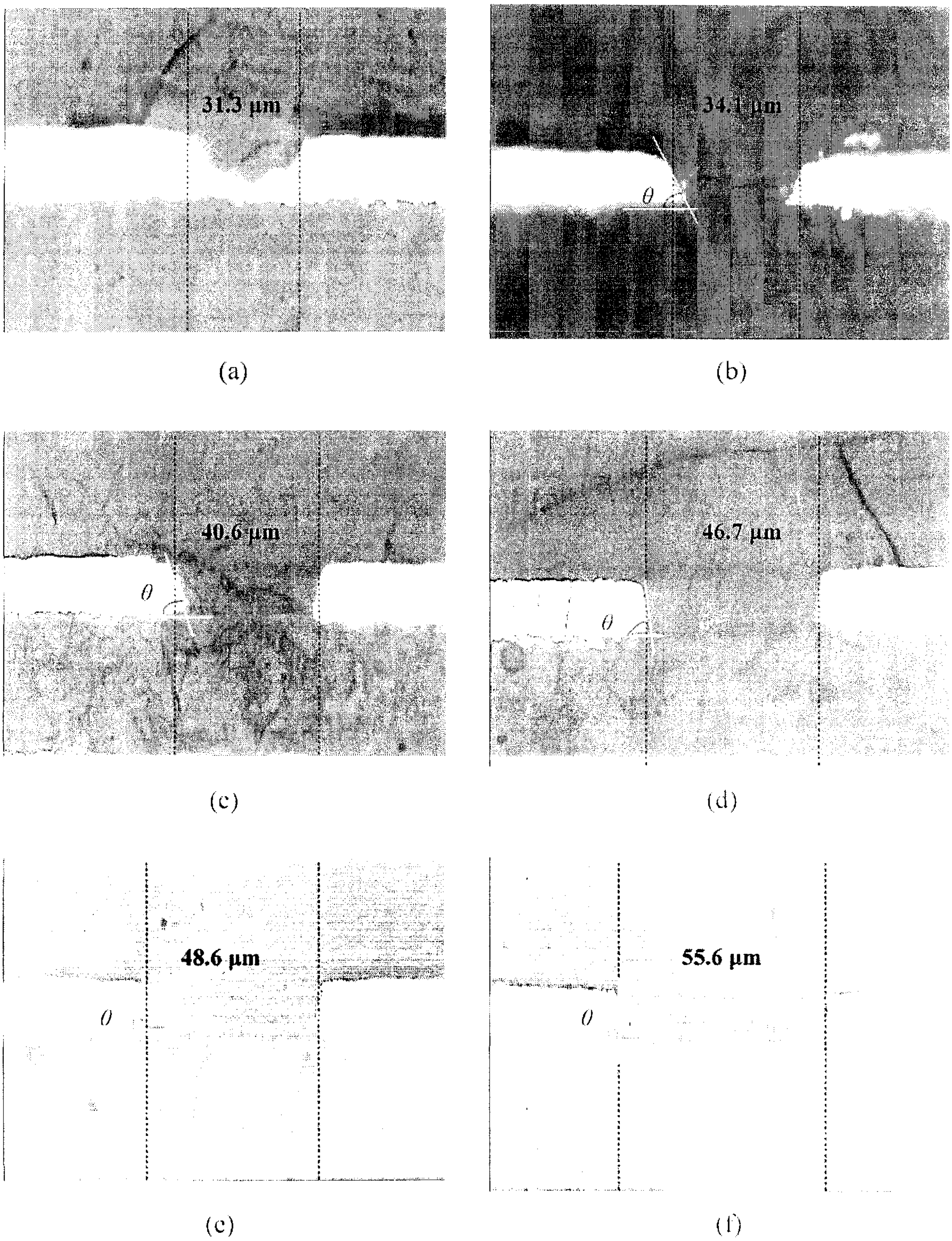

Fig.4.18 Cross section of circuit spaces with etching time is (a) 120 seconds, (b) 180 seconds, (c) 300 seconds, (d) 600 seconds, (e) 780 seconds, (f) 1200 seconds at number of repetition=1, laser power=0.25 W, repetition rate=5 kHz, v=25 mm/s, bite size=35 μm.

The changes of the widths of circuit spaces and angle θ with the etching time are shown in Table 4.11.

Table.4.11 The influence of etching time in the width of copper space and angle θ

Etching time (seconds)	120	180	300	600	780	1200
Width of copper space (μm)	31.3	34.1	40.6	46.7	48.6	55.6
Degree of angle θ	--	65°	70°	83°	90°	90°

From Table 4.11, it is clear that the width of circuit spaces increases with the etching time. Because the etching time was not exceedingly long, the angle θ was below or equal to 90 degree. That means all these etching results with the etching time above 180 seconds and under 1200 seconds are acceptable in industrial standard.

4.5 The comparisons of fabrication results with Nd:YAG laser and Excimer laser

4.5.1 Circuit spaces fabricated with Nd:YAG laser and Excimer laser in laser writing step

In this section, the circuit spaces fabricated by Excimer laser and Nd:YAG laser were compared. In order to make the etching process comparable between the Excimer laser and the Nd:YAG laser after laser writing step, the laser parameters in the laser writing process of these two laser sources should be selected to fabricate the depths of spaces at nearly the same value. The pulse energy of the Nd:YAG laser and the Excimer laser can be calculated by Equations (17) and (18) separately (Zhang & Yung, 2006).

$$Energy = (1000P_{out})/R_r \tag{17}$$

$$Energy = Energy\ intensity \times beam\ size = \frac{\pi w^2 E}{gl} \tag{18}$$

R_r—repetition rate of Nd:YAG laser, w—the radius of the laser beam

g—the width of the rectangular beam of the Excimer laser

l—the length of the rectangular beam of the Excimer laser

P_{out}—average power of Nd:YAG laser

E—pulse energy of Excimer laser

In this work, the laser parameters were selected according to the previous experimental results to get the depth of space at about 4 to 5 μm. The laser parameters were as follows. For the Excimer laser, the laser energy was 140 mJ; the number of repetitions was four times; the repetition rate was 50 Hz, the diameter of aperture on mask was 250 μm and the bite size was 5 μm. When the Nd:YAG laser was used as the laser source, the laser energy was 0.12 W, the number of repetition was one; the repetition rate was 6 kHz and the bite size was the same as with the Excimer laser. When these laser parameters were selected, the depth of circuit spaces could be controlled at about 4 μm for both laser sources. When the bite size fixed, the velocity increased with repetition rate. The repetition rate was 50 Hz and 6 kHz respectively with Excimer laser and Nd:YAG laser. Then the fabrication velocity with Nd:YAG laser was 120 times faster than with Excimer laser.

The profile of the laser output will influence the cross-sectional profile of the spaces structured by laser beam. The output of the Nd:YAG laser is a TEM_{00} beam mode (Gaussian profile), while the Excimer laser beam is rectangular in cross section and exhibits a reasonably flat topped profile. In Fig.4.19a, the experimental results of the circuit spaces fabricated by Nd:YAG laser and Excimer laser were measured by contact type measuring system—Talysurf PGI 1240 measurement system. The characteristic parameters of the circuit spaces including the width d and the depth z of circuit spaces and the resolidification height h are shown in Fig.4.19b.

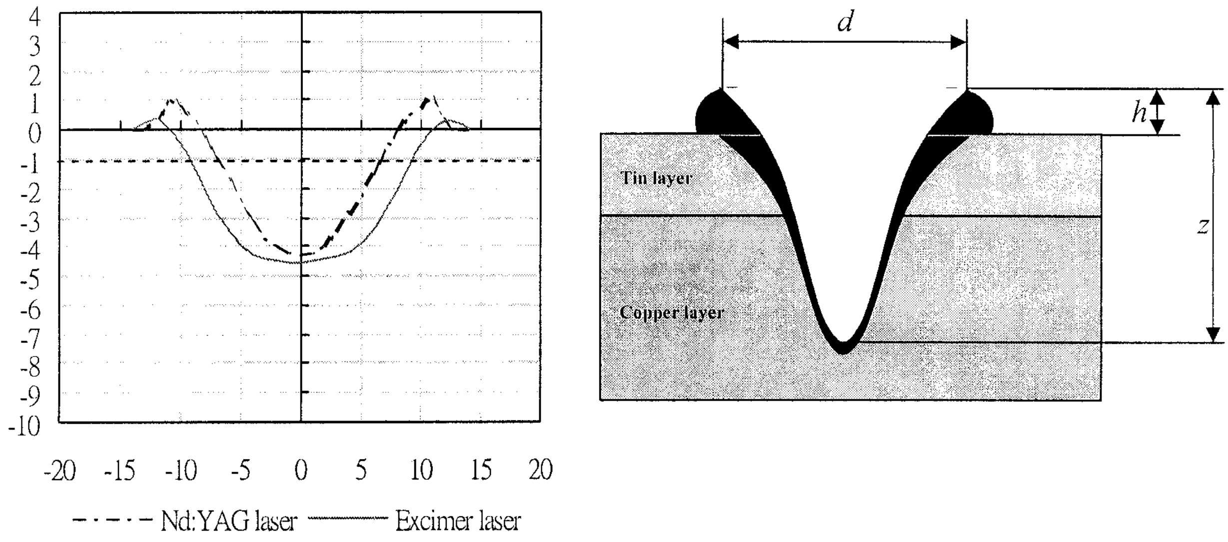

(a) (b)

Fig.4.19 (a) Comparison of cross-sectional profile of circuit space with Excimer laser and Nd:YAG laser; (b) Definition of the width of space *d*, the depth of space *z* and the resolidification height *h*.

As shown in Fig.4.19, the cross-sectional profile of circuit space structured by the Excimer laser is a little wider and much flatter at the bottom than that structured by the Nd:YAG laser. This is because the energy distribution of the Excimer laser is more uniform than that of the Nd:YAG laser. When the Excimer is used as the laser source, the aperture on the middle of the mask let the uniform laser energy pass through it. The material under the irradiation of the laser beam then absorbs almost the same energy. This will contribute to the flatter profile at the bottom of the circuit space with the Excimer laser than with the Nd:YAG laser, which has the Gaussian beam output. The width of circuit space is determined by the diameter of the aperture on the mask with the Excimer laser, but by the laser diameter and the energy distribution with the Nd:YAG laser. When the energy at the edge of the Nd:YAG laser beam cannot reach the damage enthalpy of the material, the width of circuit space structured by the Nd:YAG laser will be smaller than the diameter of the laser beam (the diameter of the Nd:YAG laser and the diameter of the laser beam of the Excimer laser were both 25 μm in this work).

The resolidification height *h* reflects the volume of resolidification material after melting. The laser structuring process with UV laser is dominated by material vaporization but accompanied with melting at the edge of space. Vaporization of material will bring clean pattern with less debris which is preferred in laser structuring. So it is better to reduce the amount of resolidification material. As shown in Fig.4.19, the resolidification height is smaller fabricated with Excimer laser than with Nd:YAG laser. So Excimer laser is more desirable for laser structuring process with respect to reducing the resolidification height.

4.5.2 Comparison of laser structuring results between Excimer and Nd:YAG lasers

On the basis of the circuit spaces fabricated by Excimer laser and Nd:YAG laser in last section, the final geometries of circuit lines and circuit spaces are compared after copper ethcing process. When the diameter of Excimer laser beam was 25 μm on the material which was equal to the diameter of Nd:YAG laser, the widths of circuit spaces were a little larger after laser writing step with the Excimer laser than with the Nd:YAG laser (Fig.4.19). And the widths of the spaces were a little wider during and at the end of the etching process when the Excimer laser was used as the laser source as shown in Table 4.12.

Table 4.12 Widths and depths of spaces after etching process

Etching time (seconds)		30	60	120	200	270
Excimer laser	Width (μm)	33.8	35.3	38.0	43.6	49.6
	Depth (μm)	6.4	9.3	10.5	__	__
Nd:YAG laser	Width (μm)	29.4	30.7	33.1	37.6	45.4
	Depth (μm)	4.9	8.4	9.5	__	__

To conclude, the etching speed (the ratio of depth to time) in copper etching process were almost the same after laser writing with these two lasers, as shown in Fig.4.20.

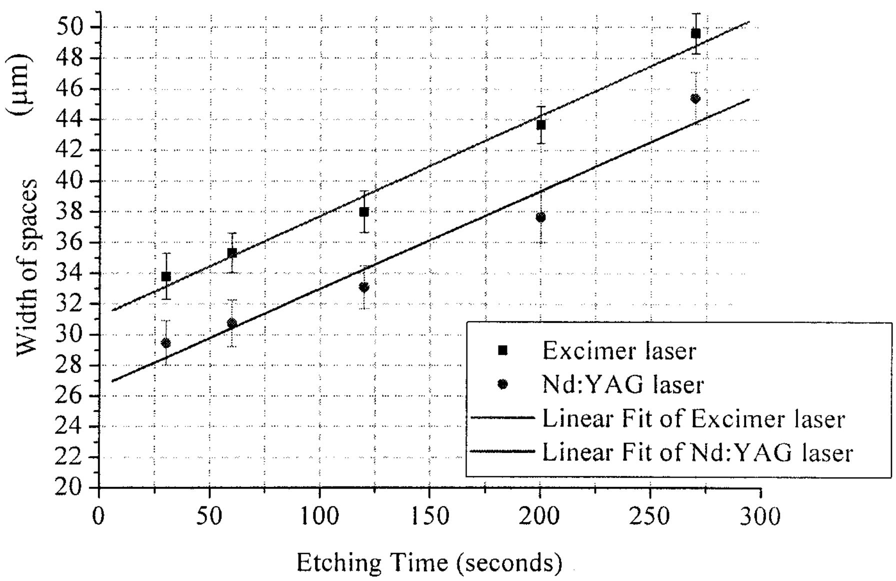

Fig.4.20 The width of circuit space with the changes of etching time after laser writing step with two laser sources

At the beginning of the etching process, the bottom of the spaces were much flatter when the Excimer laser was used as the laser source (in Fig.4.19). With the increase in the etching time, the cross section of the circuit spaces exhibited a similar profile, as shown in Fig.4.21. At the same time, with the etching time increased, the angle θ of the circuit lines increased from acute angle to right angle in both case.

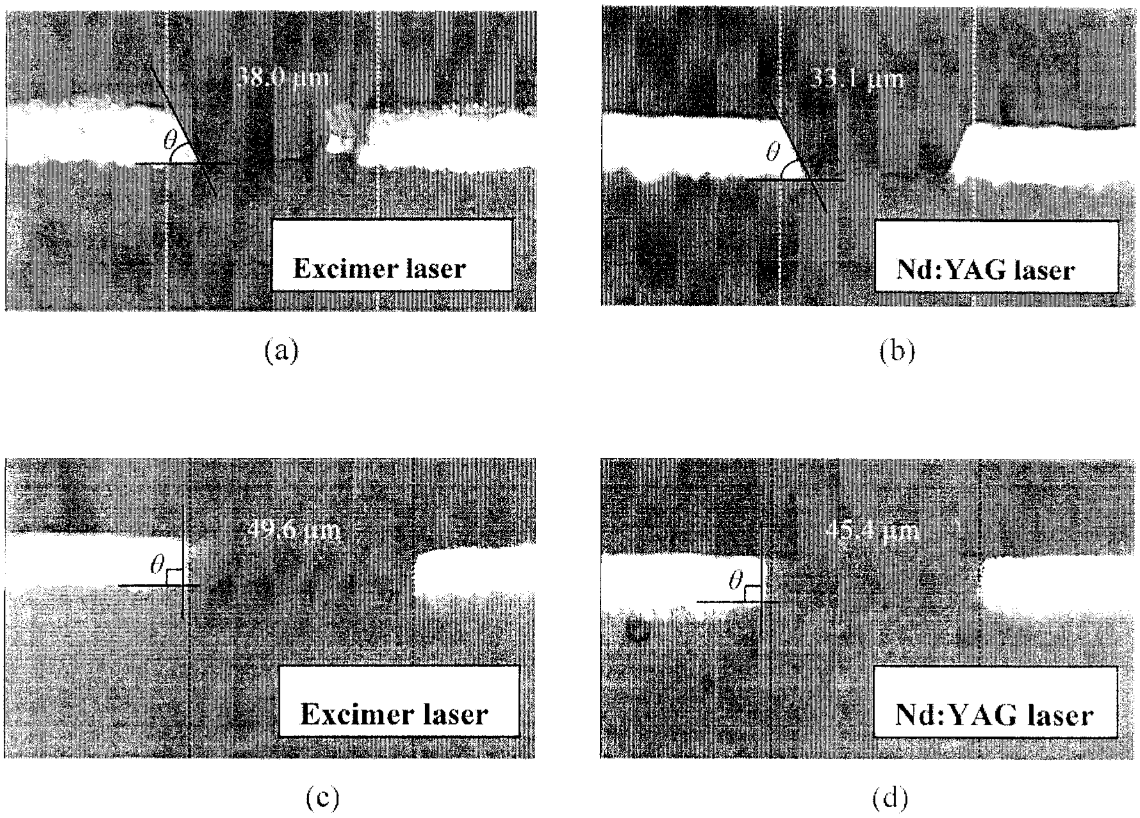

Fig.4.21 Comparisons of cross-sectional profile of circuit space during the etching process after laser writing step with Excimer laser and Nd:YAG laser: (a) and (b) after 120 seconds; (c) and (d) after 240 seconds

After the laser writing step and copper etching step, the main difference in the results for circuit lines and circuit spaces fabricated with Nd:YAG laser and Excimer laser was the minimum width of circuit space d. The minimum width of circuit space fabricated was 25 μm with Excimer laser, and 40 μm with Nd:YAG laser. The minimum width of circuit line can reach 20 μm fabricated with these two lasers. The minimum width of circuit spaces after etching step in laser structuring is shown in

Fig.4.22.

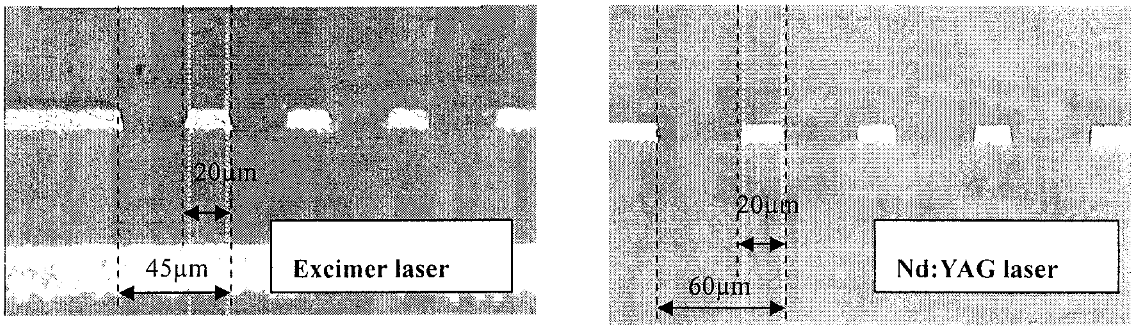

Fig.4.22 The minimum width of circuit lines and circuit spaces after etching step (with Excimer laser and Nd:YAG laser as laser sources)

Table 4.13 The comparisons of Excimer laser and Nd:YAG laser in laser structuring process

	Excimer laser (248nm)	Nd:YAG laser (355nm)
Control of laser diameter	better	fair
Fabrication efficiency	fair	better
Resolidification height	better	fair
Total width of circuit line and circuit space	≥ 60 μm	≥ 45 μm

The value of the minimum line width maybe varied a little with the changes of etching time and laser parameters. The minimum width of circuit lines and circuit spaces (circuit lines + circuit spaces) with Nd:YAG laser was 60 μm. The minimum width of circuit lines and spaces (circuit lines + circuit spaces) with Excimer laser can reach to 45 μm (when diameter of aperture was 100 μm). The comparisons of the laser structuring results with Excimer laser and Nd:YAG laser are shown in Table 4.13. Excimer laser shows its advantages when the total width of circuit lines and circuit spaces is under 60 μm, a small dimension that cannot be reached using

Nd:YAG laser. When the total width of circuit line and circuit space was above 60 μm, it was more efficient to use Nd:YAG laser as a laser source whose scanning velocity was about 120 times faster than the Excimer laser.

CHAPTER 5

THE USAGE OF TAGUCHI METHODOLOGY AND ARTIFICIAL NEURAL NETWORK IN LASER STRUCTURING TECHNIQUE

5.1 Taguchi methodology in laser structuring

5.1.1 Introduction of Taguchi methodology

Every experimenter has to design and conduct experiments to obtain enough and relevant data so that he can infer the relationship between process parameters and experimental results behind the observed phenomenon. People can do so by performing a series of experiments each of which gives some understanding. This requires making measurements after every experiment so that analysis of observed data will determine what to do next. However, the data obtained by this method is insufficient to draw any significant conclusions and the problem may still remain unsolved.

A well-designed set of experiments, in which all parameters of interest are varied over a specified range, is a much better approach to obtain systematic data. Mathematically speaking, such a complete set of experiments ought to give desired results. Usually the number of experiments and resources required are prohibitively large.

Dr. Taguchi of Nippon Telephones and Telegraph Company has developed a method based on “ORTHOGONAL ARRAY” experiments which gives much reduced variance for the experiment with optimum settings of control parameters. Thus the combination of Design of Experiments with optimization of control parameters to obtain best results is achieved in the Taguchi Methodology.

The Taguchi methodology consists of experimental designing with the objective of acquiring data in a controlled way to obtain information about the behavior of a given process. The advantages of Taguchi methodology is that optimum working conditions determined from the laboratory work can also be reproduced in the real production environment. Parameters affecting a given process may be divided into two groups as follows:

1. Controllable,
2. Uncontrollable.

Because of the very high cost, instead of determining uncontrollable parameters and removing them, values of controllable parameters that will improve the manufacturing process or fabrication result should be investigated.

5.1.2 Selection of factors and levels and the design of experiments

In previous work, all the controllable parameters affecting the laser writing process in laser structuring technique have not been investigated in details, because it requires a vast number of experiments, which enormously increases the experimental cost and time. However, quantitative estimations of the various parameters affecting the geometry of circuit spaces, and the main factors for optimum design of the laser writing process can be determined by the Taguchi methodology. The Taguchi methodology consists of designed experiments, with the objective of acquiring data in a controlled way, executing these experiments and analyzing data in order to obtain information about the behavior of the laser writing process.

This section discusses the use of the Taguchi methodology to obtain the quantitative estimations of the various parameters and the main parameters affecting the geometry of circuit space in the laser writing step using a Q-switched Nd:YAG laser. The process parameters, which will influence the geometry of the circuit space according to experimental results, are selected as the factors to see their influences on the fabrication results. Factors are considered from a process flowchart to answer the question of what factors may influence the geometry of circuit space. The effects of six key process parameters - laser power, number of repetition, repetition rate, bite size, focal length and the thickness of tin layer- are selected as shown in Fig.5.1.

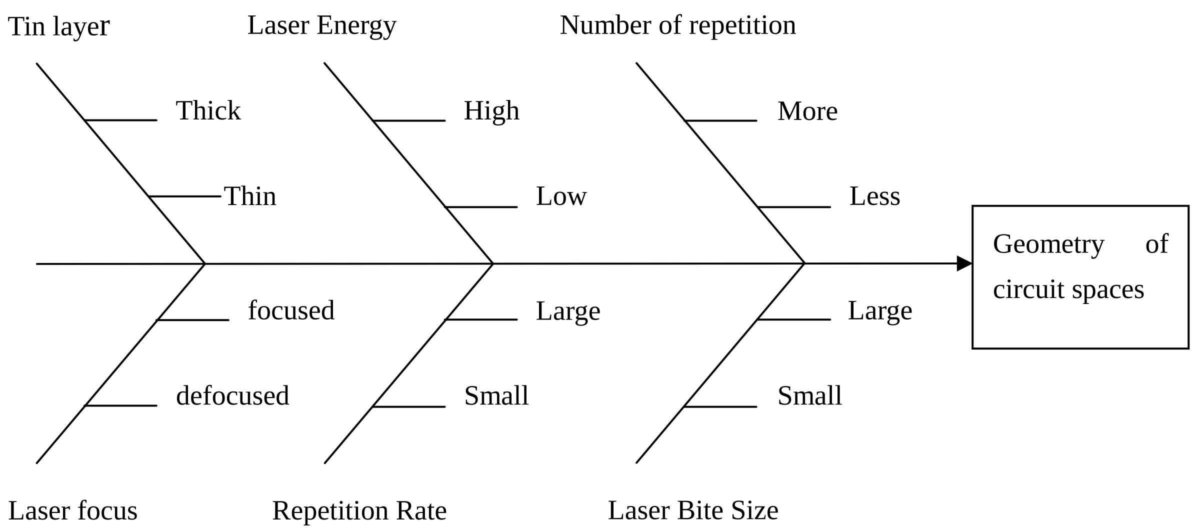

Fig.5.1 Experiment flowchart and fishbone diagram

The geometry of circuit space can be expressed in three characteristic parameters — the width of space *d* (the distance between the highest spot of circuit space), the depth of space z (from the highest spot to the lowest spot of circuit space) and resolidification height h (from the highest spot of the circuit space to the surface of tin layer) — which are shown in Fig.5.2. The width d and depth z of circuit space are important because they will influence the final geometry of circuit lines and circuit spaces. The resolidification height h reflects the volume of resolidification material after melting. The laser structuring process with UV laser is dominated by material vaporization. Vaporization of material will bring clean pattern with less debris. So it is better to reduce the amount of resolidification material by controlling experimental parameters. The height h is selected to represent the amount of melting and resolidification material. The good results of these three characteristic parameters ($d \leq 30$ µm, 2 µm$\leq z \leq$10 µm, $h \leq 3$ µm, achieved from experimental experience) can be achieved by selecting proper process parameters. The investigation of the main factors that affect the characteristic parameters will help to control the characteristic parameters more efficiently.

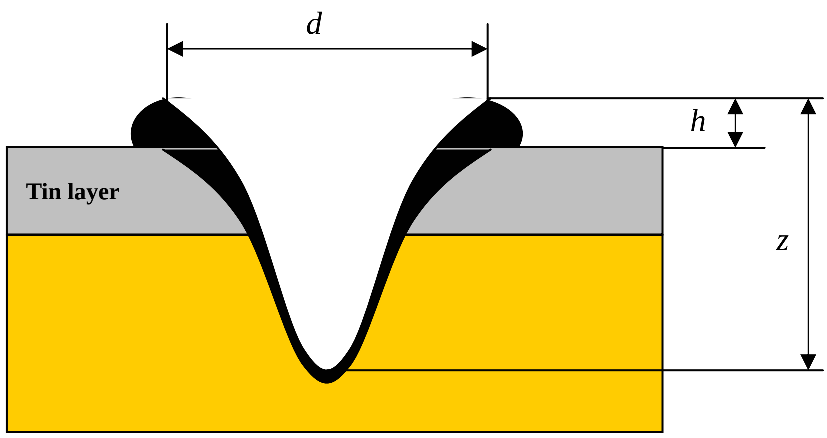

Fig.5.2. The cross-sectional profile and three characteristic parameters of circuit space

Experimental parameters and their levels to be studied, which were determined in the light of the preliminary tests (Zhang & Yung, 2006), are given in Table.5.1. In Chapter 4, some experiments were conducted to find out the relationship between process parameters and the geometry of circuit space. These experiments also provided information for the selection of the ranges of process parameters with Taguchi methodology.

Table 5.1 Factors and levels

Symbols and Factors	Level 1	Level 2	Level 3
A Laser Power (W)	0.15	0.25	0.35
B Number of repetition	1	2	3
C Repetition Rate (kHz)	6	8	10
D Bite Size (μm)	3	6	9
E Thickness of tin layer (μm)	1	1.5	2
F Defocused focal length (μm)	0	15	30

The choice of a suitable orthogonal array (OA) design is critical for the success of an experiment. Orthogonal arrays allow one to compute the main and interaction effects of factors via a minimum number of experimental trials (Moen, 1991; Ross, 1989). The selection of OA depends on the total degrees of freedom required to study the main and interaction effects of factors. The term "degrees of freedom" is used to describe the number of values in the final calculation of a statistic that are free to vary. In the context of statistical design of experiment (SDOE), the number of degrees of freedom is one less than the number of levels associated with the factor. In other words, the number of degrees of freedom associated with a factor at p-levels is (p-1). The number of degrees of freedom associated with an interaction is the product of the number of degrees of freedom associated with each main effect involved in the interaction. It is important to notice that the number of experiments must be greater than the total degrees of freedom required for studying the effects.

In this work, the effects of six factors (laser power, number of repetition, repetition rate, bite size, thickness of tin layer and defocused focal length, each has three levels) and three interactions between the factors (laser power & number of repetition, laser power & repetition rate, laser power & bite size) are studied. OA L27 is selected here to arrange the set of experiment (twenty-seven) to be greater than the total degrees of freedom (twenty-four). Here the notation 'L' implies that the information is based on the Latin square arrangement of factors. In this section, 27 sets of experiments were conducted under 27 sets of process parameters designed with Taguchi methodology. Under each set of process parameters, experiments were repeated five times. The size of the specimen was 8 cm$\times$ 5 cm.

Linear graphs are a tremendous help in quickly assigning factors and interactions to separate columns of orthogonal array table (Ross, 1989). Linear graphs can be modified to suit particular circumstances such as laser writing process. The first step is to draw the linear graph required for the experiment beginning with interactions and the non-interacting factors are then added as additional separate column locations as shown in Fig.5.3. According to the L27 Triangular table (Table 5.2), the complete required linear graph appears as in Fig.5.3.

Table 5.2 L27 Triangular Table (Interactions)

Column no.	Column no.											
	2	3	4	5	6	7	8	9	10	11	12	13
1	3 4	2 4	2 3	6 7	5 7	5 6	9 10	8 10	8 9	12 13	11 13	11 12
2	- -	1 4	1 3	8 11	9 12	10 13	5 11	6 12	7 13	5 8	6 9	7 10
3	- -	- -	1 2	9 3	10 11	8 12	7 12	5 13	6 11	6 10	7 8	5 9
4	- -	- -	- -	10 12	8 13	9 11	6 13	7 11	5 12	7 9	5 10	6 8
5	- -	- -	- -	- -	1 7	1 6	2 11	3 13	4 12	2 8	4 10	3 9
6	- -	- -	- -	- -	- -	1 5	4 3	2 12	3 11	3 10	2 9	4 8
7	- -	- -	- -	- -	- -	- -	3 12	4 11	2 13	4 9	3 8	2 10
8	- -	- -	- -	- -	- -	- -	- -	1 10	1 9	2 5	3 7	4 6
9	- -	- -	- -	- -	- -	- -	- -	- -	1 8	4 7	2 6	3 5
10	- -	- -	- -	- -	- -	- -	- -	- -	- -	3 6	4 7	2 7
11	- -	- -	- -	- -	- -	- -	- -	- -	- -	- -	1 13	1 12
12	- -	- -	- -	- -	- -	- -	- -	- -	- -	- -	- -	1 11

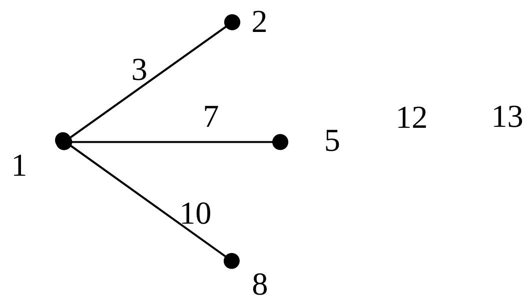

Fig.5.3. Linear graphs of factors

5.1.3 L27 orthogonal array and experimental results

The L27 orthogonal array and the experimental results are shown in Table 5.3. The parameters of laser power (A), number of repetition (B), repetition rate (C), bite size (D), thickness of tin layer (E) and defocused focal length (F) are inserted in column1, column2, column5, column8, column12 and column13. The interactions between A and B, A and C, A and D are inserted in column3, column7 and column10. Four columns (column3, column6, column9, column11) are empty which are used for calculation of error. Y_1, Y_2 and Y_3 are the results of space width *d*, space depth *z* and resolidification height *h*.

Table 5.3 Experimental design of the Taguchi analysis with L27 orthogonal array

TRIAL NO.	FACTORS													Y_1 DATA	Y_2 DATA	Y_3 DATA
	A	B		AB	C		AC	D		AD		E	F			
	Column no.															
	1	2	3	4	5	6	7	8	9	10	11	12	13			
1	1	1	1	1	1	1	1	1	1	1	1	1	1	23	4.230	1.742
2	1	1	1	1	2	2	2	2	2	2	2	2	2	16	2.688	0.599
3	1	1	1	1	3	3	3	3	3	3	3	3	3	15	2.164	0.619
4	1	2	2	2	1	1	1	2	2	2	3	3	3	25	6.758	2.095
5	1	2	2	2	2	2	2	3	3	3	1	1	1	20	4.422	0.611
6	1	2	2	2	3	3	3	1	1	1	2	2	2	17	4.790	1.970
7	1	3	3	3	1	1	1	3	3	3	2	2	2	27	7.650	2.456
8	1	3	3	3	2	2	2	1	1	1	3	3	3	21	7.901	5.281
9	1	3	3	3	3	3	3	2	2	2	1	1	1	16	5.412	1.082
10	2	1	2	3	1	2	3	1	2	3	1	2	3	29	11.230	3.889
11	2	1	2	3	2	3	1	2	3	1	2	3	1	22	4.694	1.478
12	2	1	2	3	3	1	2	3	1	2	3	1	2	18	3.239	1.032
13	2	2	3	1	1	2	3	2	3	1	3	1	2	33	10.039	2.149
14	2	2	3	1	2	3	1	3	1	2	1	2	3	26	6.338	2.195
15	2	2	3	1	3	1	2	1	2	3	2	3	1	21	8.716	3.434
16	2	3	1	2	1	2	3	3	1	2	2	3	1	35	12.825	3.371
17	2	3	1	2	2	3	1	1	2	3	3	1	2	26.5	10.054	6.365
18	2	3	1	2	3	1	2	2	3	1	1	2	3	23	8.009	3.008
19	3	1	3	2	1	3	2	1	3	2	1	3	2	33	11.692	3.783
20	3	1	3	2	2	1	3	2	1	3	2	1	3	27	6.767	1.700
21	3	1	3	2	3	2	1	3	2	1	3	2	1	21	4.160	0.753
22	3	2	1	3	1	3	2	2	1	3	3	2	1	35	12.723	2.215
23	3	2	1	3	2	1	3	3	2	1	1	3	2	31	9.437	2.837
24	3	2	1	3	3	2	1	1	3	2	2	1	3	26	10.066	7.025
25	3	3	2	1	1	3	2	3	2	1	2	1	3	35	13.000	3.411
26	3	3	2	1	2	1	3	1	3	2	3	2	1	34	11.828	6.788
27	3	3	2	1	3	2	1	2	1	3	1	3	2	27	11.485	4.032

Some experimental results of the cross-sectional profiles of circuit spaces measured by contact type measuring system -- Talysurf PGI 1240 measurement system (with a resolution down to 0.8 nm) -- are shown in Fig.5.4. When process parameters change, the geometry of circuit spaces including the width *d* and the depth *z* of circuit spaces and the resolidification height *h* are different.

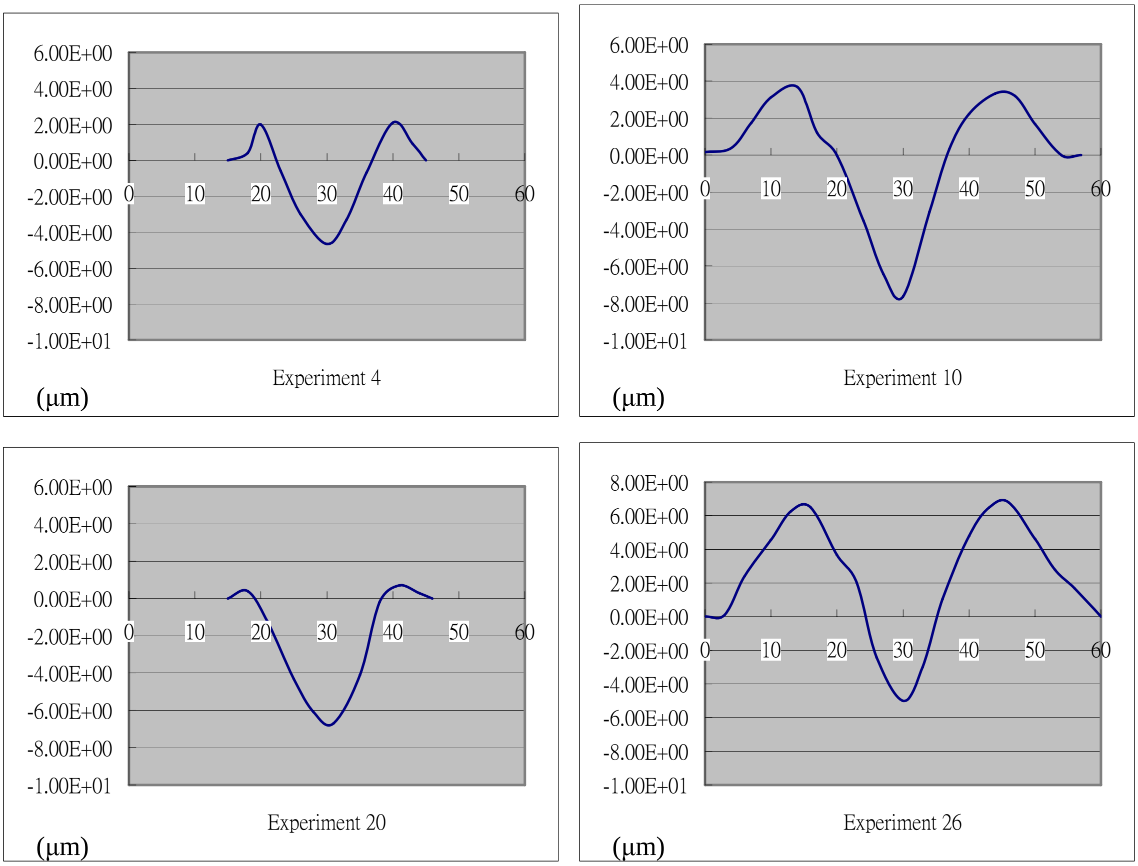

Fig.5.4 The cross-sectional profiles of circuit spaces under different experiment parameters

5.1.4 The relation between process parameters and experimental results

In order to find out the influences of process parameters on the laser structuring results, the experimental results were calculated in Table 5.4. In this table, Xi (i=1,2,3) is the sum of the results with the level is ‘1’, ‘2’ or ‘3’. x_i is the results of $X_i/9$. Y is the minus value of x_i(max)- x_i(min). Such as in the column one, X_1=the sums of A_1, X_2=the sums of A_2, X_3=the sums of A_3, $x_1=X_1/9$, $x_2=X_2/9$ and $x_3=X_3/9$. The value of Y is x_3 minus x_1. The value ‘Y’ indicates the influences of parameters on the laser structuring results. The parameters with bigger ‘Y’ values have greater influences on the results.

Table 5.4 The calculation of experiment results

		A	B	AB	C	AC	D	AD	E	F
Width *d* (μm)	X_1	180	204	230	275	223.5	230.5	226	224.5	227
	X_2	233.5	234	227.5	223.5	222	224	229	228	228.5
	X_3	269	244.5	225	184	237	228	227.5	230	227
	x_1	20.000	22.667	25.555	30.555	24.833	25.611	25.111	24.944	25.222
	x_2	25.944	26.000	25.278	24.833	24.667	24.889	25.444	25.333	25.389
	x_3	29.889	27.167	25.000	20.444	26.333	25.333	25.278	25.555	25.222
	Y	9.889	4.500	0.555	10.111	1.667	0.722	0.333	0.611	0.167
Depth *z* (μm)	X_1	46.015	50.864	70.488	90.147	65.435	80.507	66.26	67.229	69.01
	X_2	75.144	73.289	69.477	64.129	72.39	68.575	70.846	69.416	71.074
	X_3	91.158	88.164	72.352	58.041	74.492	63.235	75.211	75.672	72.233
	x_1	5.112	5.651	7.832	10.016	7.270	8.945	7.362	7.470	7.668
	x_2	8.349	8.143	7.719	7.125	8.043	7.619	7.872	7.712	7.897
	x_3	10.128	9.796	8.039	6.449	8.277	7.026	8.357	8.408	8.026
	Y	5.016	4.144	0.319	3.567	1.006	1.919	0.994	0.938	1.047
Height *h* (μm)	X_1	16.455	15.595	24.969	25.111	28.141	40.277	22.629	25.117	21.474
	X_2	26.921	24.531	23.656	27.854	23.374	18.358	27.97	23.873	25.223
	X_3	32.544	35.794	27.295	22.955	24.405	17.285	25321	26.93	29.223
	x_1	1.828	1.733	2.774	2.79	3.127	4.475	2.514	2.791	2.386
	x_2	2.991	2.726	2.628	3.095	2.597	2.040	3.108	2.652	2.802
	x_3	3.616	3.977	3.033	2.550	2.712	1.920	2.813	2.992	3.247
	Y	1.787	2.244	0.404	0.544	0.530	2.555	0.593	0.340	0.861

		Column 3	Column 6	Column 9	Column 11
Width d (μm)	X_1	230.5	229	229	228
	X_2	227	228	220.5	226
	X_3	225	225.5	233	228.5
	x_1	25.611	25.444	25.444	25.333
	x_2	25.222	25.333	24.5	25.111
	x_3	25	25.055	25.889	25.389
	Y	0.611	0.389	1.389	0.278
Depth z (μm)	X_1	72.196	66.634	70.298	72.255
	X_2	71.446	74.816	71.455	71.196
	X_3	68.675	70.867	70.564	68.866
	x_1	8.021	7.404	7.811	8.028
	x_2	7.938	8.313	7.939	7.911
	x_3	7.630	7.874	7.840	7.652
	Y	0.391	0.909	0.128	0.376
Height h (μm)	X_1	27.781	25.092	23.538	23.179
	X_2	25.306	27.71	24.465	25.444
	X_3	22.833	23.118	27.917	27.297
	x_1	3.087	2.788	2.615	2.575
	x_2	2.811	3.079	2.718	2.827
	x_3	2.537	2.569	3.102	3.033
	Y	0.550	0.510	0.486	0.457

According to the value x_1, x_2 and x_3, we can get the factors' influences on the experimental results. The six factors' influences on the width d and the depth z of circuit spaces and the resolidification height h are shown in Fig.5.5. The width d of circuit spaces increases with the increase of laser power, increase of number of repetition, decrease of repetition rate and decrease of bite size (in Fig.5.5a). When the value of defocused focal length increases, the width of circuit spaces increases at first because of the enlargement of laser diameter and then decreases because of the low laser energy caused by defocused length. The variations of space width are very small caused by thickness of tin layer and defocused focal length.

The influences of the six factors on depth of circuit spaces are shown in the

Fig.5.5b. The depth *z* of circuit spaces increases with the increase of laser power and number of repetition and decreases with the increase of repetition rate and bite size. The thickness of tin layer and the defocused focal length have small influences on the depth of circuit spaces.

The resolidification height *h* is mainly influenced by laser power, number of repetition and bite size. In order to get smaller resolidification height (less melting materials), it is better to select comparatively low laser power, small number of repetition and large bite size as shown in the Fig.5.5c.

From all these three figures, it is clear that laser power, number of repetition, repetition rate and bite size have the main effects on the space width *d*, space depth *z* and the height *h*. The thickness of tin layer and the defocused focal length have minor influences on the fabrication results. The detailed analysis of the experimental results will be made in the next section by ANOVA.

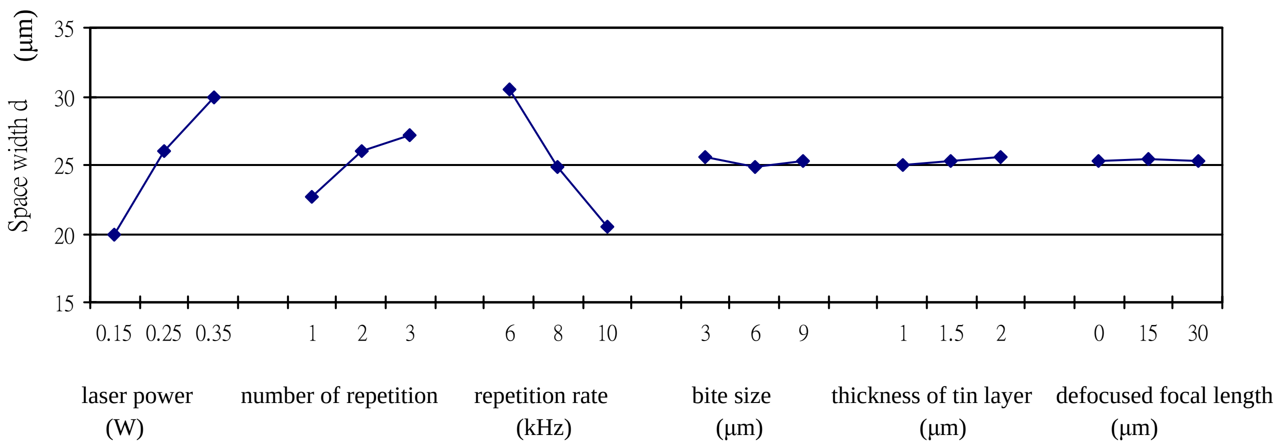

(a)

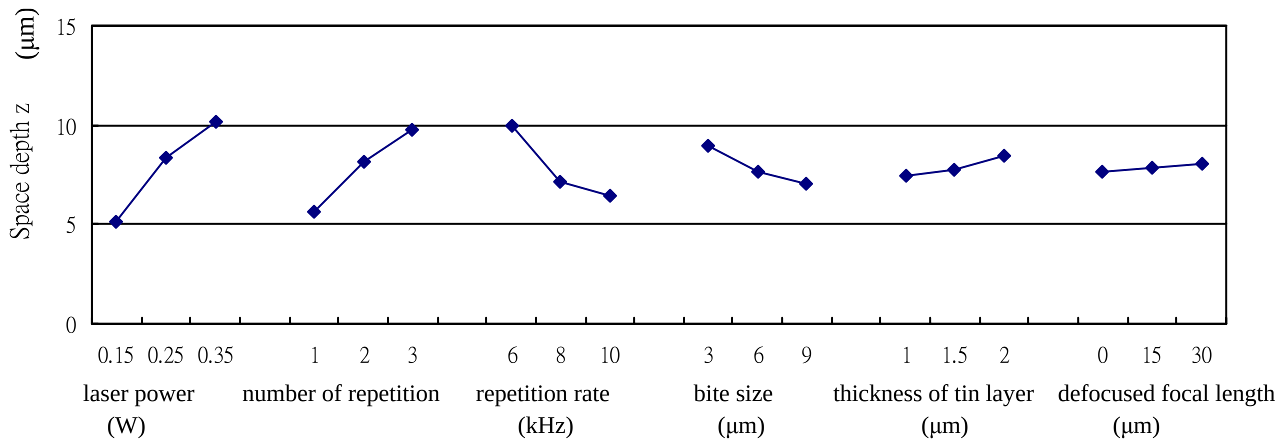

(b)

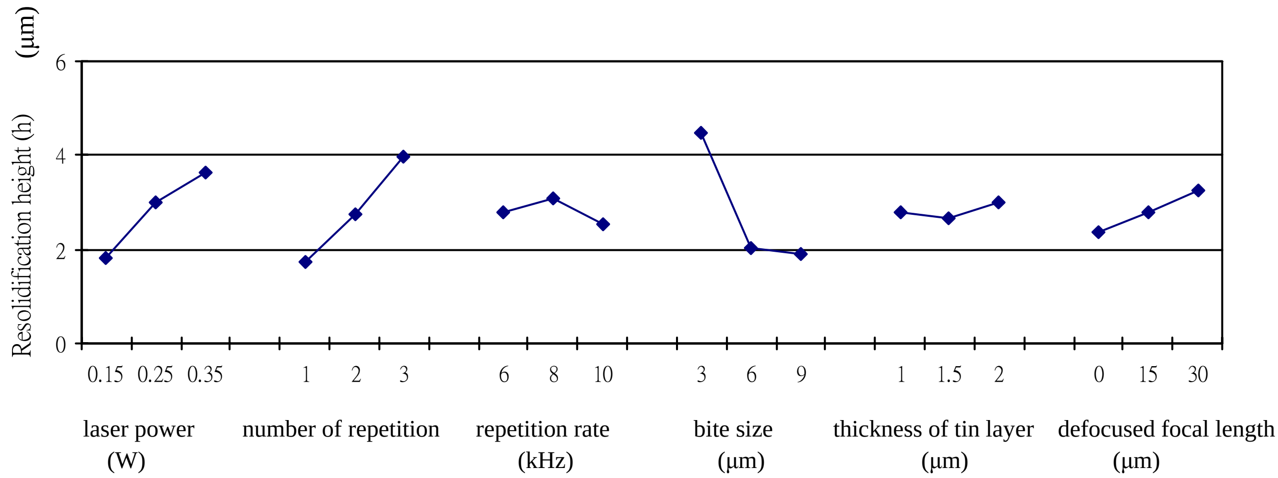

(c)

Fig.5.5 The relations between process parameters and characteristic parameters of circuit space

5.1.5 ANOVA analysis of experimental results

The purpose of experimentation should be to reduce or control variation of a product or process. Consequently, decisions must be made concerning which parameters affect the performance of the process. Since variation is a large part of the discussion relative to quality, analysis of variance (ANOVA) will be the statistical method used to interpret experimental data and make necessary decisions. ANOVA is a statistically based decision tool for detecting any differences in average performance of factors tested. Even thought to be important before experiment, some factors assigned to an experiment will not be significant at all. So ANOVA is used to see the significance of factors to experimental results. In other words, ANOVA helps assess the sources of variation that can be linked to the independent variables and determine how those variables interact and affect the experimental results.

The collected data were analyzed by using ANOVA for evaluation of the effect of each factor. Analysis of variance for A, B, C, D, E, F, AB, AC and AD are given in Table 5.4. The unassigned columns (column3, column6, column9, column 11) were also considered to estimate error variance in this section. When no factor or interaction was present in a column, the 1s, 2s and 3s were meaningless. Hopefully, this variation should be small. Excessive variation will indicate that a potentially important factor has been excluded from the experiment. The variation in the unassigned columns is small in this work. That is to say, the main factors to the fabrication results are included and considered.

The total variation may be decomposed into the following components:

1. Variation due to factor A, B, C, D, E, F (SS_A, SS_B, SS_C, SS_D, SS_E, SS_F);
2. Variation due to the interaction of factors A and B, A and C, A and D (SS_{AB}, SS_{AC}, SS_{AD});
3. Variation due to random error (SS_e).

$$SS_A = \frac{A_1^2}{n_{A_1}} + \frac{A_2^2}{n_{A_2}} + \frac{A_3^2}{n_{A_3}} - \frac{T^2}{N} \qquad (1)$$

$$SS_{AB} = \frac{(AB)_1^2}{n_{(AB)_1}} + \frac{(AB)_2^2}{n_{(AB)_2}} + \frac{(AB)_3^2}{n_{(AB)_3}} - \frac{T^2}{N} \quad (2)$$

$$SS_e = SS_{col3} + SS_{col6} + SS_{col9} + SS_{col11} \quad (3)$$

The degree of freedom v for each factor is the number of levels minus one.

$$v_A = k_A - 1 \quad (4)$$

The degree of freedom for an interaction is the product of the interacting factor's degrees of freedom.

$$v_{AB} = v_A v_B \quad (5)$$

The summary of the ANOVA results is shown in Table 5.5a-5.5c. *SS* is the sum of squares of each factor or interaction of factors; v_A is the degree of freedom for factor *A* and v_{AB} is the degree of freedom for the interaction of factor *AB*; *V* is the variance which is obtained by *SS/v*; *F* is the ratio of variance of each factor or interaction of factors due to random errors which is obtained by V_{factor}/V_e (V_{factor} is the mean square of each factor or interaction of factors, V_e is the mean square of random error). *F* value provides a decision at some confidence level of whether one factor causes significantly difference in the experiment results. When a factor (or interaction of factors) with small value of V_{factor} (near the value of V_e), this factor (or interaction of factors) is considered to be insignificant to the experiment results.

Table 5.5(a) ANOVA (analysis of variance) summary for width of circuit spaces *d*

Source	*SS* (Sum of Squares)	*v* (Degrees of Freedom)	*V* (Mean Square)	*F* (F-Statistic)
A	446.056	2	223.028	174.513#
B	98.167	2	49.083	38.406#
C	462.722	2	231.361	181.036#
D#	2.389	2	1.194	--
AB#	1.389	4	0.347	--
AC#	15.167	4	3.792	--
AD#	0.5	4	0.125	--
E#	1.722	2	0.861	--
F#	0.167	2	0.083	--
e	11.889	8	1.486	--
T	1040.167	32		
E pooled	33.222	26	1.278	--

At least 99% confidence.

Table 5.5(b) ANOVA (analysis of variance) summary for depth of circuit spaces *z*

Source	*SS* (Sum of Squares)	*v* (Degrees of Freedom)	*V* (Mean Square)	*F* (F-Statistic)
A	116.401	2	58.200	69.784#
B	78.349	2	39.175	46.972#
C	64.622	2	32.311	38.742#
D	17.378	2	8.689	10.418#
AB#	0.473	4	0.118	--
AC#	4.993	4	1.248	--
AD#	4.452	4	1.113	--
E#	4.267	2	2.133	--
F#	0.592	2	0.296	--
e	5.234	8	0.654	--
T	296.763	32		
E pooled	20.012	24	0.834	--

At least 99% confidence.

Table 5.5(c) ANOVA (analysis of variance) summary for resolidification height *h*

Source	*SS* (Sum of Squares)	*v* (Degrees of Freedom)	*V* (Mean Square)	*F* (F-Statistic)
A	14.815	2	7.408	23.517#
B	22.767	2	11.383	36.136#
C#	1.340	2	0.670	--
D	37.416	2	18.708	59.390#
AB#	0.755	4	0.189	--
AC#	1.398	4	0.349	--
AD#	1.585	4	0.396	--
E#	0.525	2	0.262	--
F#	1.337	2	0.668	--
e	6.668	8	0.583	--
T	88.605	32		
E pooled	8.203	26	0.315	--

At least 99% confidence.

The significance of the factors to the experimental results can be seen clearly in Table 5.5. Laser power, number of repetition and repetition rate are the most important factors that will influence the width of circuit spaces. In order to achieve smaller width of circuit spaces (achieve smaller size of final geometry of circuits), smaller laser power, smaller number of repetition and higher repetition rate are recommended. The most effective factors for identifying the depth of circuit spaces are laser power, number of repetition, repetition rate and bite size. Among these four parameters, laser power has the greatest influence and then are number of repetition, repetition rate and bite size. The resolidification height is caused mainly by laser power, number of repetition and bite size. So the resolidification height can be reduced by select low laser power, small number of repetition and large bite size. The conclusive results are shown in Table 5.6.

Table. 5.6 The significance of process parameters to the laser structuring results

	Width *d*	Depth *z*	Height *h*
Laser power	√	√	√
Number of repetition	√	√	√
Repetition rate	√	√	×
Bite size	×	√	√
Focal length	×	×	×
Thickness of tin layer	×	×	×
Interaction between laser power & number of repetition	×	×	×
Interaction between laser power & repetition rate	×	×	×
Interaction between laser power & bite size	×	×	×

Laser power and number of repetition are the most important parameters in the laser structuring process that have influences on all the experimental results—the space width *d*, the space depth *z* and the resolidification height *h*. Some other parameters are also should be considered in the experiment process such as repetition rate and bite size. The thickness of tin layer and the focal length have minor influences on the experimental results and can be ignored. The interaction between laser power and number of repetition, laser power and repetition rate, laser power and bite size can also be neglected according to the analysis of the ANOVA. The ANOVA analysis results have at least 99% confidence checked by F value (Ross, 1989).

5.2 Artificial neural network in laser structuring

5.2.1 Introduction to Back Propagation Networks

BPN (back propagate network), developed by Rumelhart et al. (1986), is the most prevalent of the supervised learning models of ANN (artificial neural network). BPN used the gradient steepest descent method to correct the weight of the inter-connective node. In the learning process of BPN, the interconnection weights are adjusted using an error convergence technique to obtain a desired output for a given input.

BP is most often applied in the modeling of non-linear and interconnected parameter systems (Jeng, 2000). Basically, the BP process consists of two passes through the different layers of the network: a forward pass and a backward pass. In the forward pass, an input vector is applied to the sensory nodes of the network, and its effect propagates through the network, layer by layer. Finally, a set of outputs is produced as the actual response of the network. During the forward pass, the synaptic weights of the network are all fixed, whilst during the backward pass, on the other hand, the synaptic weights are all adjusted in accordance with the error correction rule. The synaptic weights are adjusted so as to make the actual response of the network move closer to the desired response. The forward process, backward process and adjustment of weights are iterated until the error of the output is satisfied. Hence the mapping between the input vector and the output results can be established.

The multilayer BP network is shown in Fig.5.6. It includes the input layer (*i*), hidden layer (*j*) and output layer (*k*). Network is fully connected. That is to say each node provides input to each node in the next layer. Each layer consisted of several nodes and the layers were interconnected by sets of correlation weights. Each node can have incoming weight connections (from the previous layer) and outgoing weight connections (to the next layer). In addition, nodes can have a bias, or a thresholding unit. During testing each node evaluates its summary input by adding up the outputs from the previous layer, multiplied by their respective weights to the given node. The node's bias is finally added to obtain a net input, which is then passed to an activation function that produces the activation value of the given neuron.

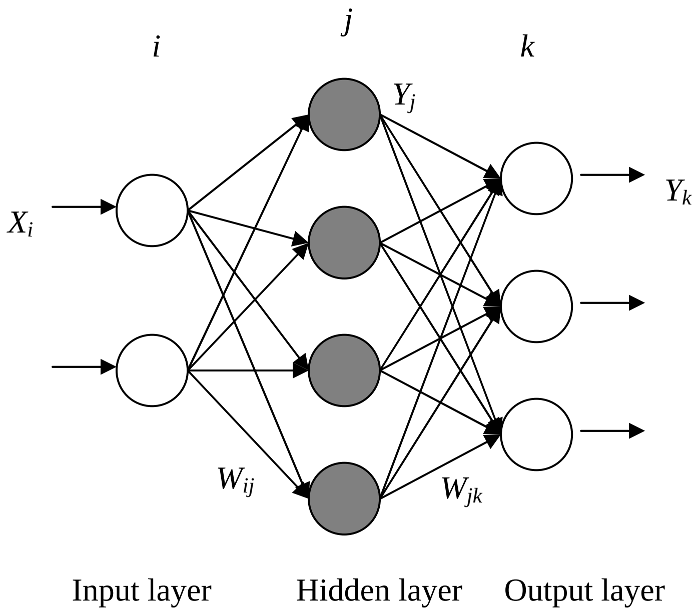

Fig.5.6 Structure of artificial neural network

Given a node *j* in a hidden layer or output layer, the net input is

$$I_j = \sum_i W_{ij} Y_i + b_j \tag{6}$$

where W_{ij} is the weight of the connection from node *i* in the previous layer to node *j*; Y_i is the output of node *i* from the previous layer; b_j is the bias of node.

Each node in the hidden and output layers takes its net input and then applies an activation function. It is also called a logistic, sigmoid, or squashing function. Given a net input I_j to node *j*, then

$$Y_j = f(I_j) \tag{7}$$

The output of unit j, is computed as

$$Y_j = \frac{1}{1+e^{-Ij}} \tag{8}$$

When reaching the output layer, the error is computed and propagated backwards. For a unit k in the output layer, the error is computed by a formula:

$$Err_k = Y_k(1-Y_k)(T_k - Y_k) \tag{9}$$

where Y_k is the actual output of node k; T_k is the true output; $Y_k(1-Y_k)$ is a derivative of activation function.

The error is propagated backwards by updating weights and biases to reflect the error of the network. For a node *j* in the hidden layer the error is computed by a formula:

$$Err_j = Y_j(1-Y_j)\sum_k Err_k W_{jk} \tag{10}$$

where W_{jk} is the weight of the connection from unit *j* to unit k in the next higher layer, and Err_k is the error of unit k.

Weights are updated by the following equations, where *l* is a constant between 0.0 and 1.0 reflecting the learning rate

$$\Delta W_{ij} = lErr_j Y_i, \quad W_{ij} = W_{ij} + \Delta W_{ij} \tag{11}$$

Biases are updated by the following equations

$$\Delta b_j = lErr_j, \quad b_j = b_j + \Delta b_j \tag{12}$$

The ANN integrated with backpropagation formulas is shown in Fig.5.7.

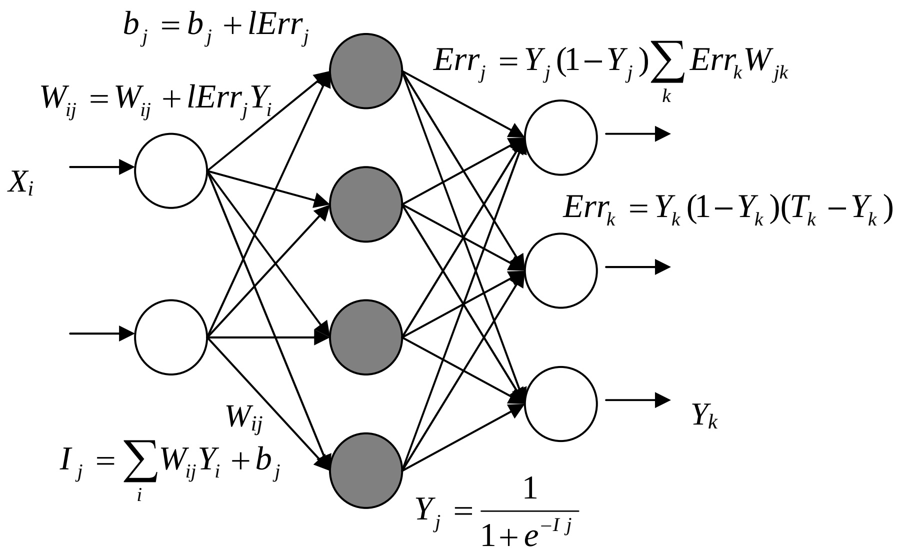

Fig.5.7 Backpropagation formulas of BPN

5.2.2 Construction of artificial neural network in laser structuring

The parameters in laser writing step such as the laser power, number of repetition, repetition rate, bite size and focal length have influence on laser structuring results. These parameters are controllable in the actual operation and are non-linear. A model of this non-linear system may help the industrial applicability of the laser structuring technique. The Artificial Neural Network technique is a useful tool for predicting outcome results and optimizing the operation parameters of such a non-linear model. Two ANN models were constructed in this section. One was to predict the geometry of circuit spaces after laser writing (ANN prediction model) and the other was to select optimum process parameters which can achieve acceptable geometry of circuit space in laser writing step (ANN optimization model).

Five parameters -- laser power, number of repetition, repetition rate, bite size and the defocused focal length -- were selected as the input of both the ANN models.

According to the previous analysis of the laser writing process by Taguchi methodology, the four laser parameters -- laser power, repetition rate, number of repetition and bite size are important factors to fabrication results. The defocused focal length is selected as this factor also has some influences on fabrication results. In the ANN prediction model, the output parameters include the width *d* and the depth *z* of circuit spaces and the resolidification height *h* as shown in Fig.5.8. BP networks were selected in our research.

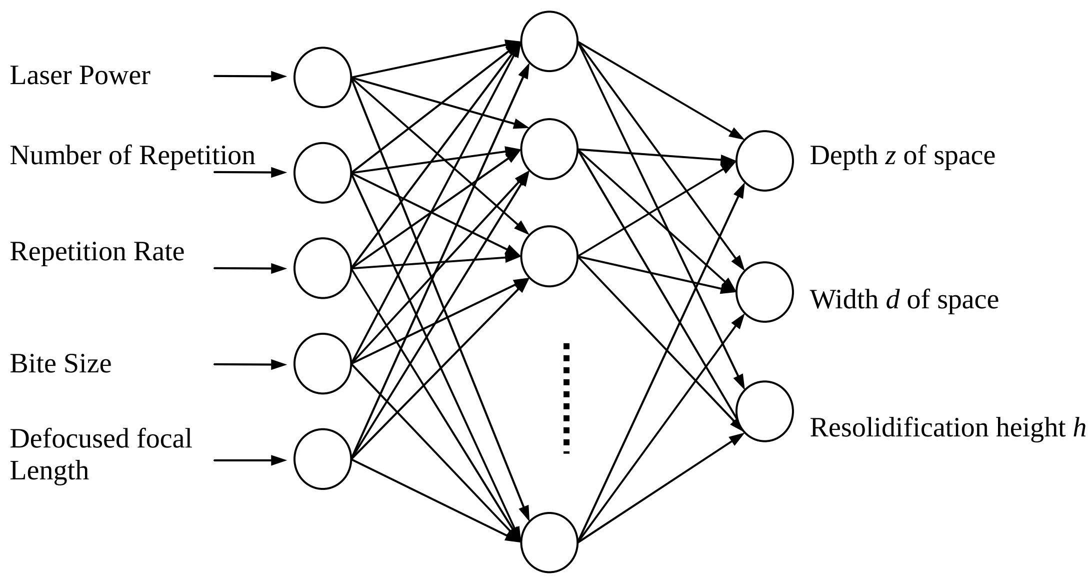

Fig.5.8 Structure of ANN prediction model of laser structuring

On the basis of the ANN prediction model which was used to predict the geometry of circuit spaces after the input of control parameters, a more complicated ANN model which was used to optimize the input parameters and get optimum output was constructed. The optimum results of circuit spaces are achieved through observation of experimental results. The optimum outputs of space geometry include: the depth of space should be controlled in the range of 2 to 10 μm (constraint by the thickness of tin layer and copper layer); the width of space should be under 30 μm and the resolidification height should be less than 3 μm in order to achieve small geometry of circuits and reduce the amount of melting materials. The structure of the ANN optimization model and the constraint of the target characteristic parameters are shown in Fig.5.9. If the process parameters can be optimized to achieve optimum fabrication results, the industrial applicability of laser structuring technique can be hoped to expand widely.

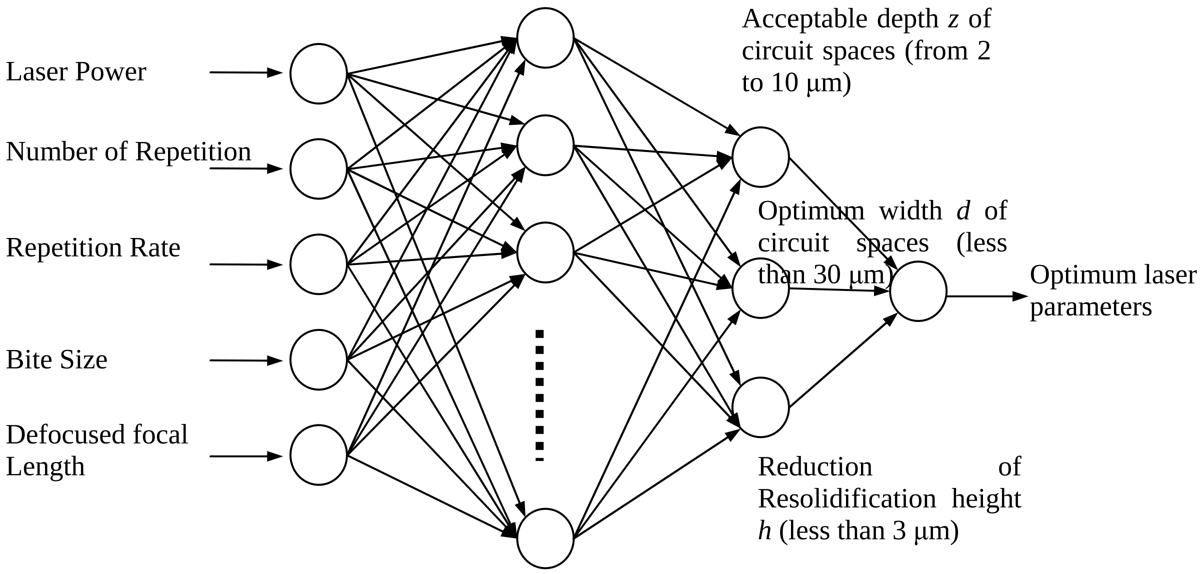

Fig.5.9 ANN model in the optimization of process parameters in laser structuring

The main idea of ANN is to learn the relationship between an input vector x and a target y. This learning is realized by sample training which makes the network adjust its parameters so that the network is able to simulate output values to input vectors. The network needs to be trained before it can predict anything. A sufficiently large and reliable data set should be given when training ANN model so that it can try to find the hidden rules that govern the relation between the variables used as input and the value that comes out.

A set of desired data often referred to as training data were needed for the training of ANN model. The data used were collected by the experimental set up in the laboratory. The experimental set up is designed by planning series of experiments with changing variables. The designed experiments can describe the process in the most efficient way in order to find optimal variable settings for further evaluation. In case of high number of input factors, Taguchi methodology is recommended for the design of experiments. Using this method, it is possible to reduce the large number of necessary experiments. The Taguchi engineering approach has the ability of maximizing the information coming from a small database of data. Therefore, reliable and valuable information over the ranges of the processes is provided from a limited number of experiments. The data for the training of ANN model in laser structuring are shown in Table 5.7. The data used were collected by the experimental set up in the laboratory based on the Taguchi methodology.

Table 5.7 27 training data of input and output

TRIAL NO.	INPUT					OUTPUT		
	Laser power (W)	Number of repetition	Repetition rate (kHz)	Bite size (μm)	Focal length (μm)	Widths (μm)	Depths (μm)	Height (μm)
1	0.15	1	6	3	0	23	4.230	1.742
2	0.15	1	8	6	15	16	2.688	0.599
3	0.15	1	10	9	30	15	2.164	0.619
4	0.15	2	6	6	30	25	6.758	2.095
5	0.15	2	8	9	0	20	4.422	0.611
6	0.15	2	10	3	15	17	4.790	1.970
7	0.15	3	6	9	15	27	7.650	2.456
8	0.15	3	8	3	30	21	7.901	5.281
9	0.15	3	10	6	0	16	5.412	1.082
10	0.25	1	6	3	30	29	11.230	3.889
11	0.25	1	8	6	0	22	4.694	1.478
12	0.25	1	10	9	15	18	3.239	1.032
13	0.25	2	6	6	15	33	10.039	2.149
14	0.25	2	8	9	30	26	6.338	2.195
15	0.25	2	10	3	0	21	8.716	3.434
16	0.25	3	6	9	0	35	12.825	3.371
17	0.25	3	8	3	15	26.5	10.054	6.365
18	0.25	3	10	6	30	23	8.009	3.008
19	0.35	1	6	3	15	33	11.692	3.783
20	0.35	1	8	6	30	27	6.767	1.700
21	0.35	1	10	9	0	21	4.160	0.753
22	0.35	2	6	6	0	35	12.723	2.215
23	0.35	2	8	9	15	31	9.437	2.837
24	0.35	2	10	3	30	26	10.066	7.025
25	0.35	3	6	9	30	35	13.000	3.411
26	0.35	3	8	3	0	34	11.828	6.788
27	0.35	3	10	6	15	27	11.485	4.032

MATLAB_ NN Tool box was used for the design, the implementation and the simulation of the network. During training, all weights and biases were adjusted according to the difference between the targeted and the actual output. The training process of the network was a cyclic process and the weights and biases of the nodes of the network were adjusted until an accurate mapping was obtained. This trained neural network can then predict the values of the objective for any new set of design variables.

5.2.3 ANN in the prediction of laser structuring results

The ANN used in this work was back propagation (BP) network with three layers. Laser power, number of repetition, repetition rate, bite size and defocused focal length of laser were processed to extract features, which would be inputs into the neural network. The standard BP network was improved with adaptive learning rate, momentum and Nguyen–Widrow weight initialization method by MATLAB_NN tool box.

In most situations, there is no way to determine the best number of hidden nodes without training several networks and estimating the generalization error of each. The number of hidden nodes of ANN prediction model was determined by training a set of models with different number of hidden nodes. In this work, the training results were thought acceptable when MSE (mean square error) value reached the level of 10^{-8}. The MSE value decreased with the increase of the number of nodes in the hidden layer as shown in Fig.5.10. If the number of nodes in the hidden layer was not large enough, the training results cannot reach the desired level (in Fig.5.10a-c). After training with different number of nodes in the hidden layer, the number of nodes was determined at fifty-four as shown in Fig.5.10d.

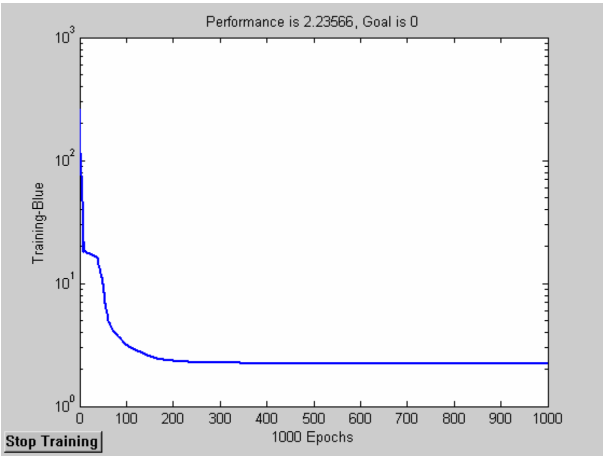

(a)

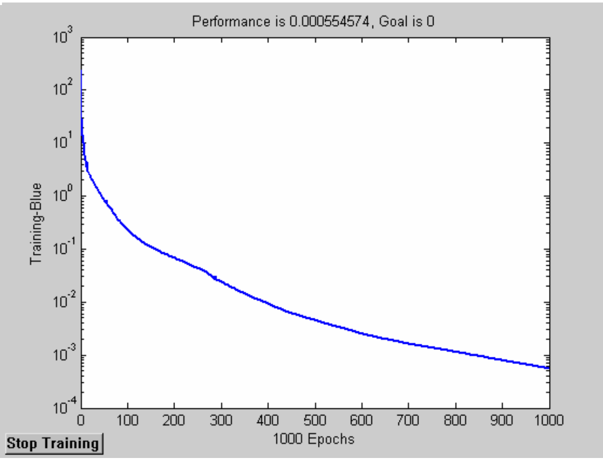

(b)

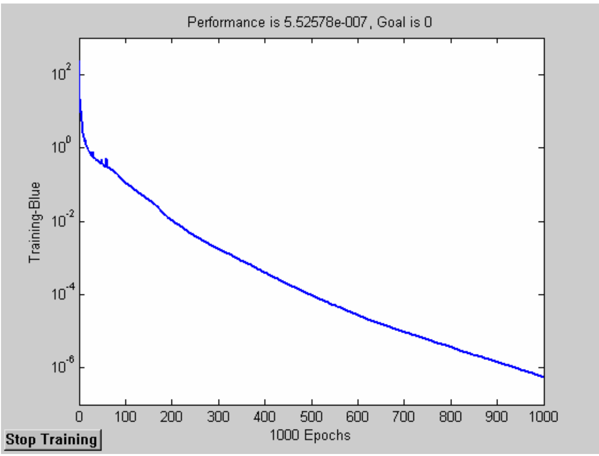

(c)

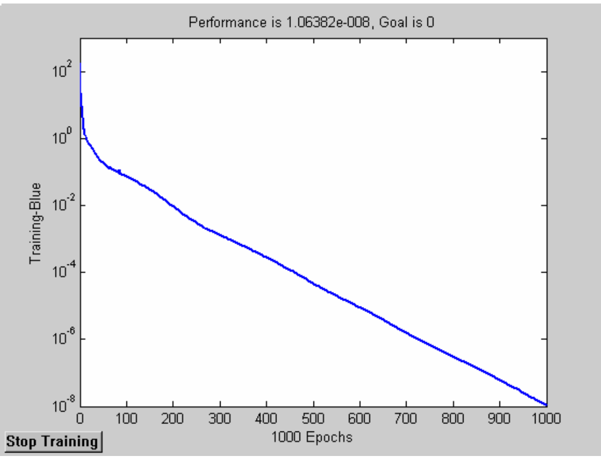

(d)

Fig.5.10 The influences of the number of nodes in the hidden layer on the training results with the number of nodes is (a) 14, (b) 40, (c) 52, (d) 54.

The MSE and epochs results in the training of ANN prediction model with different number of nodes in the hidden layer are shown in Table 5.8. The number of nodes in the hidden layer should not be set at a too large number, because the increase of the nodes in the hidden layer will cost the usage of RAM (random access memory). If the ANN model can reach the desired accurate level (MSE), it is preferable to select the nodes in the hidden layer at a comparably low value.

Table 5.8 The MSE and epochs in the training of the ANN prediction model with different number of nodes in the hidden layer

	Number of nodes in the hidden layer			
	14	40	52	54
MSE	2.23566	0.00055	5.52578×10^{-7}	1.06382×10^{-8}
Epochs	1000	1000	1000	1000

After training the ANN model with different number of nodes in the hidden layer, transfer function and network type, the prediction model for laser writing step in laser structuring technique is shown in Fig.5.11. The number of nodes in the input layer, hidden layer and output layer is five, fifty-four and three respectively. The transfer functions are ‘Tansig’ in the hidden layer and ‘Purelin’ in the output layer. W{1,1}, W{2,1} and B{1}, B{2} are weights and bias of nodes. The training and structure parameters of the ANN prediction model are shown in Table 5.9.

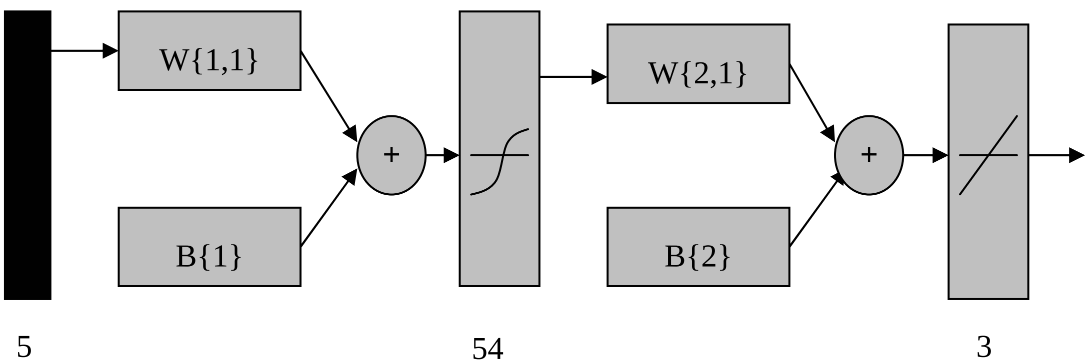

Fig.5.11 ANN prediction model of laser writing step

Table 5.9 The structure parameters of ANN prediction model

	ANN prediction model
Input	Laser power
	Number of repetition
	Repetition rate
	Bite size
	Defocused focal length
Output	Width of circuit spaces *d*
	Depth of circuit spaces *z*
	Resolidification height *h*
Layers	2
Hidden neurons	54
Transfer functions	Tansig / Purelin
Train epochs	1000
MSE goal	1.00×10^{-8}
Number of train data	27

The ANN prediction model was construct to predict the geometry of circuit spaces after laser writing step in laser structuring technique according to the input process parameters. The training results of the ANN model are compared with the experimental results in Fig.5.12. It is clear that the prediction results of ANN model are good in all the three aim functions-- the width of space d, the depth of space z and the resolidification height h.

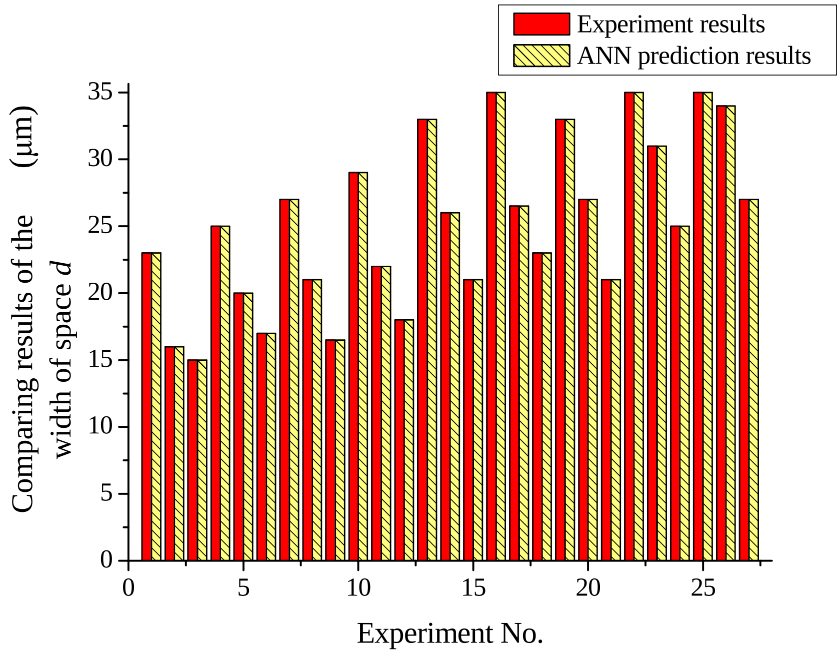
Experiment results
ANN prediction results
Comparing results of the width of space d (μm)
Experiment No.

(a)

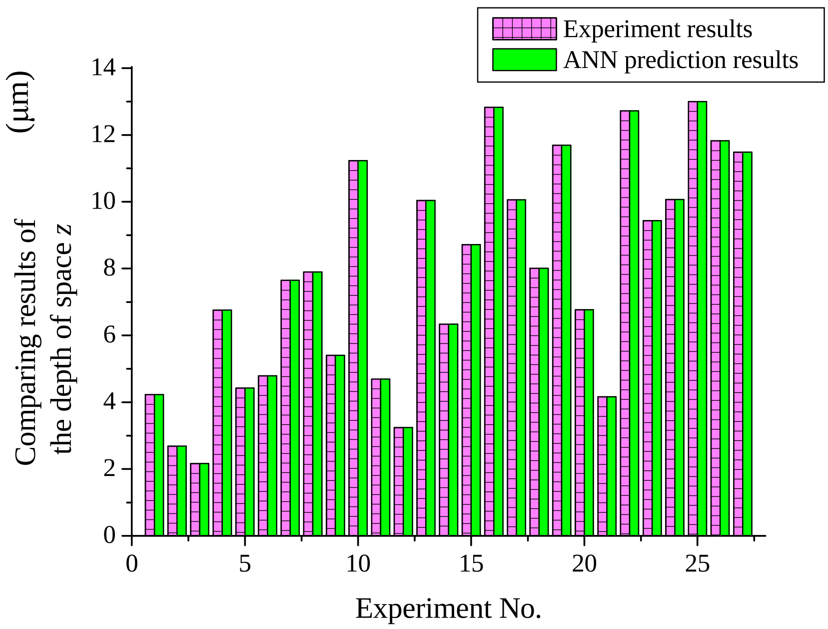
Experiment results
ANN prediction results
Comparing results of the depth of space z (μm)
Experiment No.

(b)

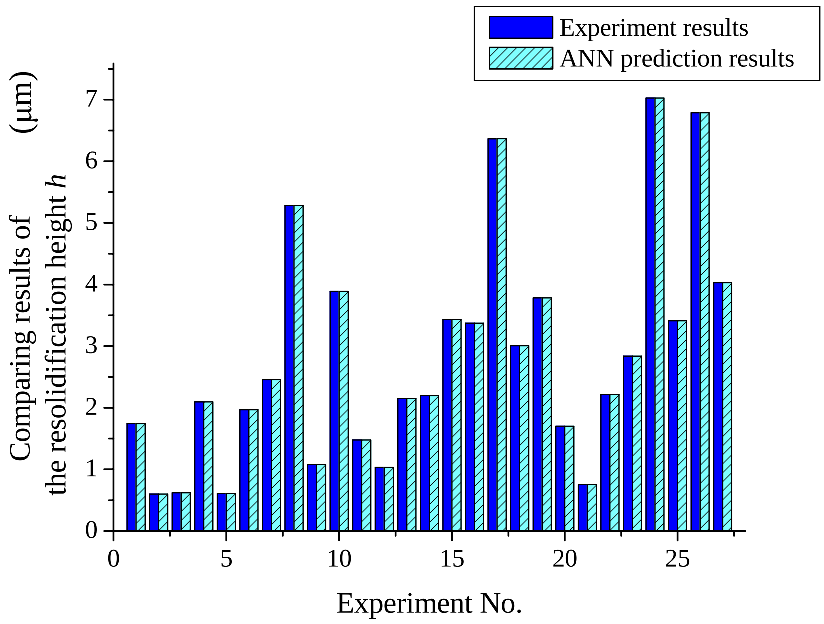

(c)

Fig.5.12 The comparison of experimental results and ANN prediction results in (a) the space width *d*, (b) the space depth *z* and (c) the resolidification height *h*.

5.2.4 ANN in the optimization of process parameters in laser structuring

The ANN prediction model can be used to predict the results of space geometry after inputting a set of process parameters. However, whether the output results of circuit spaces reached the requirement of acceptable space depth *z*, space width *d* and resolidification *h* cannot be examined by this model. So, a more complicated ANN model that can optimize the output results was construct. In this model, after inputting a set of process parameters, the results of the ANN model would tell whether this set of process parameters and fabrication results were acceptable under the pre-designed requirement.

The geometry of circuit spaces is determined by three characteristic parameters—d, z and h. The width d of circuit spaces should be small in order to reduce the final total size of circuit line and circuit space. The depth z of circuit spaces should be larger than the thickness of tin layer and smaller than the total thickness of tin and copper layer as shown in Fig.5.13. If the depth of space structured by laser is too shallow, the tin layer may be not etched by laser totally and will influence the copper etching process. If the depth of space is too deep, the dielectric material under copper layer will be damaged. The resolidification height should also be considered because it is the reflection of the amount of melting materials. If the amount of melting materials is large, the value D_d (the distance between two outer edges of circuit space as shown in Fig.5.13) will be larger than the measured space width d (the distance between two highest spots of circuit space). The larger value D_d enlarges the final width of circuit spaces after etching process. The resolidification height also influences the etching time in copper etching step. Because the etching time depends on the thickness 'z-h', when the depth of space z is the same, if the value of the resolidification h is large, the thickness 'z-h' will be small. The small value of the thickness 'z-h' will cause more time in the etching step. So it is better to achieve smaller resolidification height h.

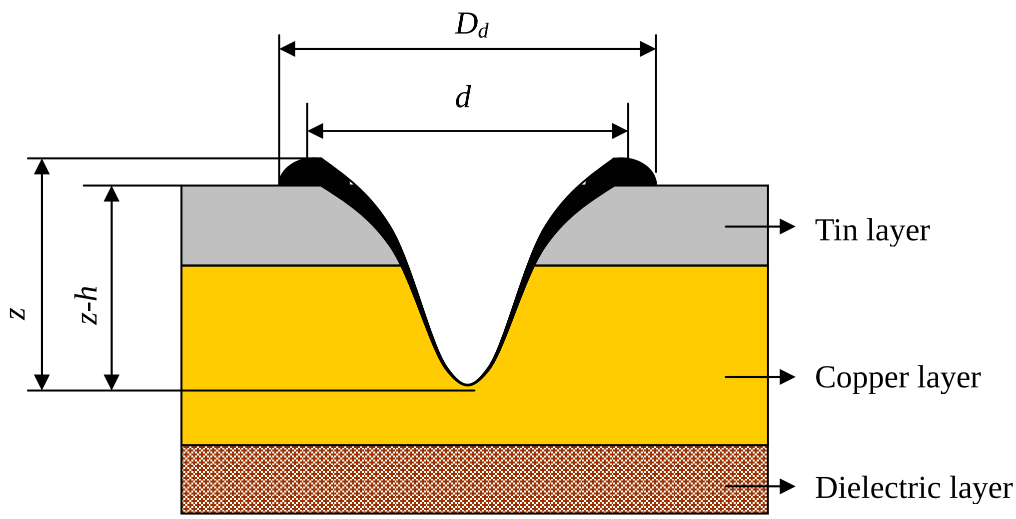

Fig.5.13 Pre-designed requirement for the selection of *d*, *z* and *h*

On the basis of the previous experimental results, the requirements of these three factors are as follows. The width of circuit spaces should be under 30 μm, the depth of circuit spaces should be between two to ten micrometers, and the resolidification heights should be under 3 μm. When all these three results reached the pre-designed requirement above, it can be said that the fabrication results were good. The ANN optimization model was built and used to optimize the input parameters and get the acceptable output results under these requirements.

In the ANN optimization model, the outputs are designed as status values ‘0’ or ‘1’ instead of the real numbers. When training the ANN optimization model, it hopes to get much higher accuracy and make the output reach the status values (‘0’ or ‘1’) infinitely. The output of the ANN optimization model is designed according to the rule shown in Fig.5.14.

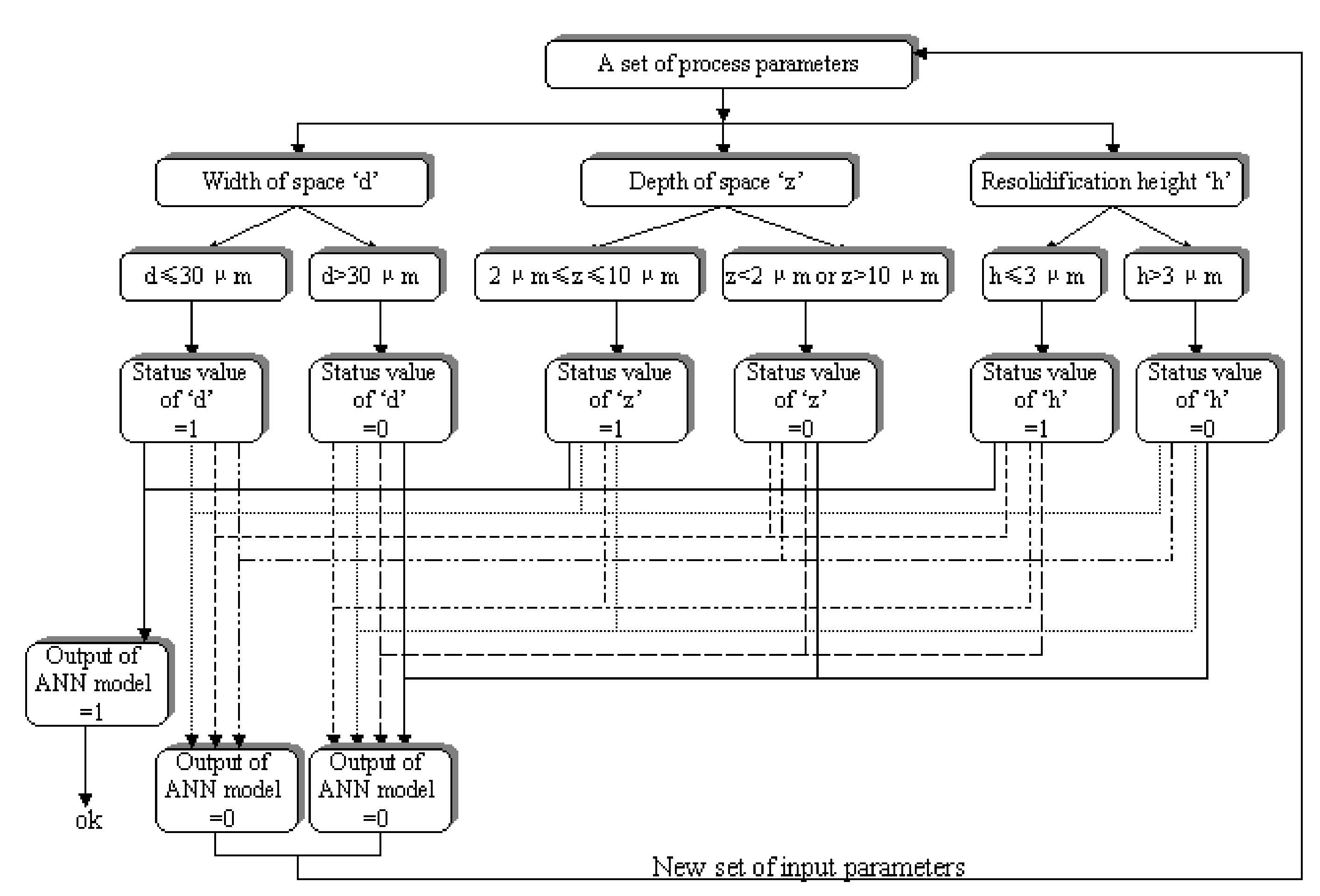

Fig.5.14 The optimization of process parameters in ANN optimization model

As shown in Fig.5.15, ANNs are trained with different number of nodes in the hidden layer from fifty to one hundred and forty. When the number of nodes is too small, it cost more training time and more epochs and cannot reach the required output level. After experiments, the number of nodes in the hidden layer was selected as one hundred and thirty.

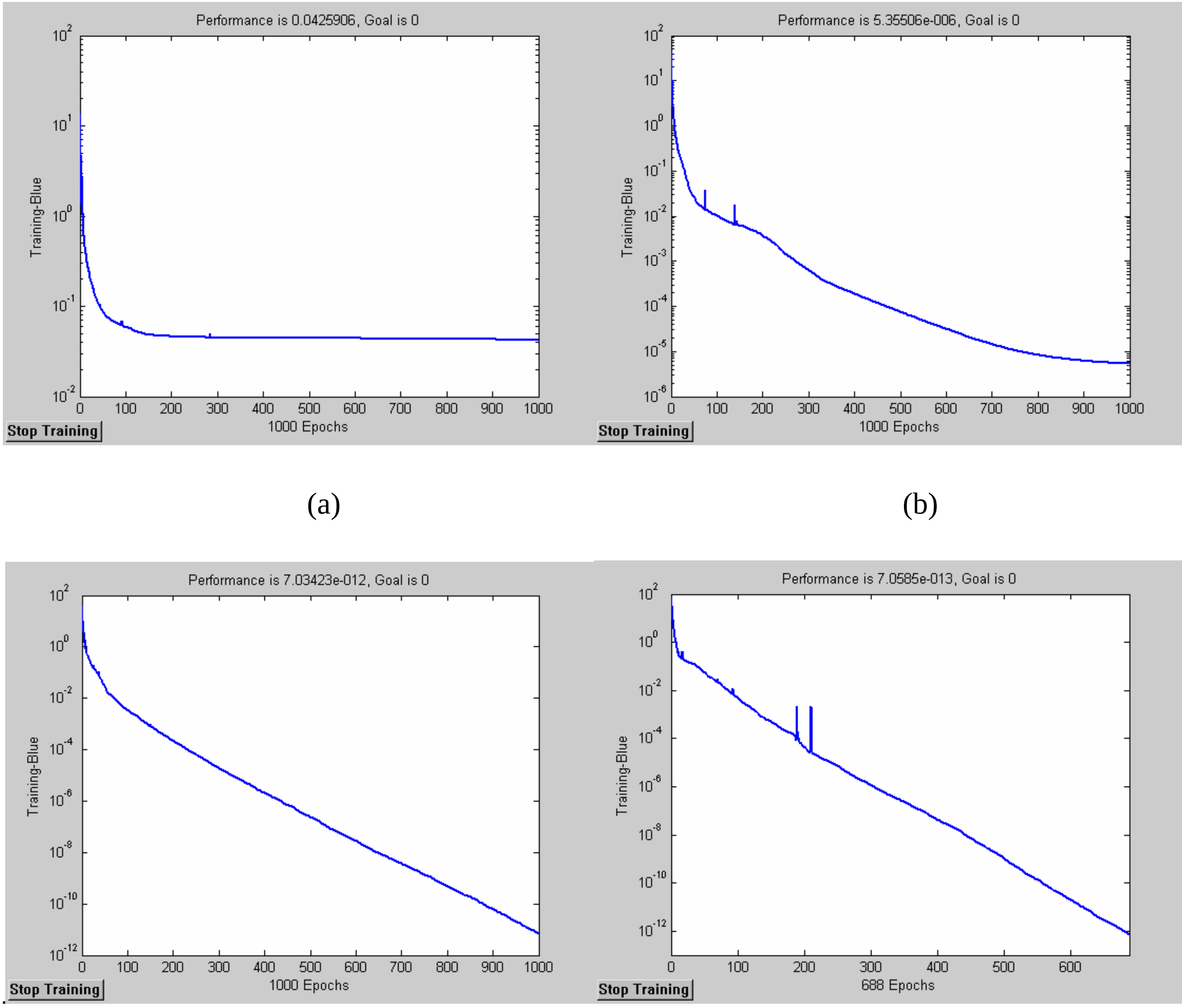

(a) (b)

(c) (d)

Fig.5.15 The influences of the number of nodes in the hidden layer on the training results with the number of nodes is (a) 50, (b) 120, (c) 130 and (d) 140.

In the Table 5.10, it shows the MSE and epochs in the training of ANN optimization model with different number of nodes in the hidden layer. It should be noticed that, when the number of nodes increases from one hundred and twenty to one hundred and thirty, the MSE values decrease from 5.35×10^{-6} to 7.03×10^{-12}. When ten more nodes are added on the base of one hundred and thirty, the MSE values only decrease from 7.03×10^{-12} to 7.05×10^{-13}. With the increase of number of nodes in the hidden layer, the MSE values decrease more slowly. Except for the consideration of the cost of RAM, it is also not recommended to make the ANN architecture too complex by adding the number of nodes in the hidden layer. So the number of nodes in this work was selected at one hundred and thirty.

Table 5.10 The MSE and epochs in the training of the ANN optimization model with different number of nodes in the hidden layer

	Numbers of neurons in the hidden layer			
	50	120	130	140
MSE	0.04259	5.35506×10^{-6}	7.03423×10^{-12}	7.0585×10^{-13}
Epochs	1000	1000	1000	688

The ANN optimization model for laser structuring is shown in Fig.5.16 after training the ANN model with different number of nodes in hidden layer, transfer function and network type. The nodes in the input layer, hidden layer and two output layers are five, one hundred and thirty, three and one respectively. W{1,1}, W{2,1} and B{1}, B{2} are weights and bias of nodes. The transfer function are ‘Tansig’ in hidden layer, ‘Purelin’ and ‘AND’ in output layer. Only when three output values in second last layer are all ‘1’ (acceptable output), the status value in the last layer can be got at ‘1’ under the calculation of function ‘AND’. The training and structure parameters of the optimization model are shown in Table 5.11.

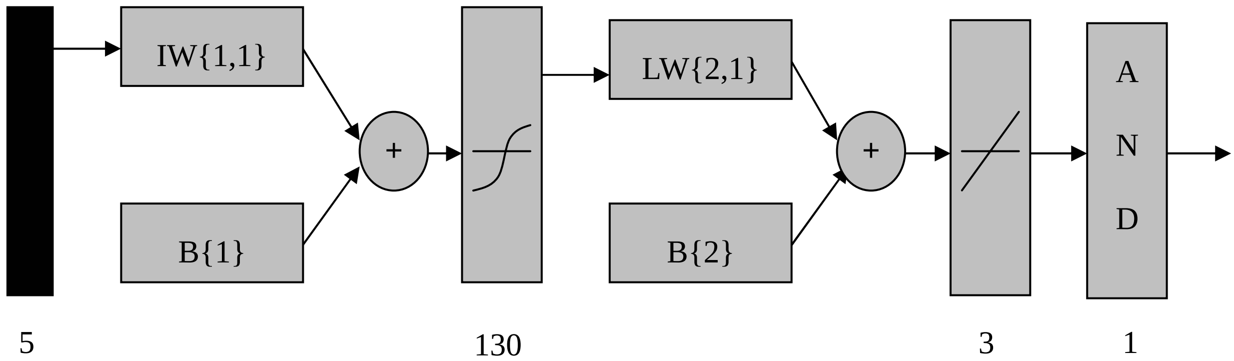

Fig.5.16 ANN optimization model of laser structuring

Table 5.11 The structure parameters of ANN optimization model

	Optimization ANN model
Input	Laser power
	Number of repetition
	Repetition rate
	Bite size
	Defocused focal length
Output in second last layer	Status value of space width ‘0’ or ‘1’
	Status value of space depth ‘0’ or ‘1’
	Status value of resolidification height ‘0’ or ‘1’
Output in last layer	Optimum results of the geometry of circuit spaces
Layers	3
Hidden neurons	130
Transfer functions	Tansig/purelin/AND
Train epochs	1000
Performance goal	1.00×10^{-11}
Number of training data	27

The training results of the ANN optimization model are compared with the experimental results in Fig.5.17. The stars represent the status values of experimental results and the continuous line represents the output of the ANN optimization model. When the status value is ‘1’, it represents that the geometry of circuit space under this set of input parameters satisfy the pre-designed requirements. When the status value is ‘0’, it represents that the results are unacceptable and this set of input parameters should not be used.

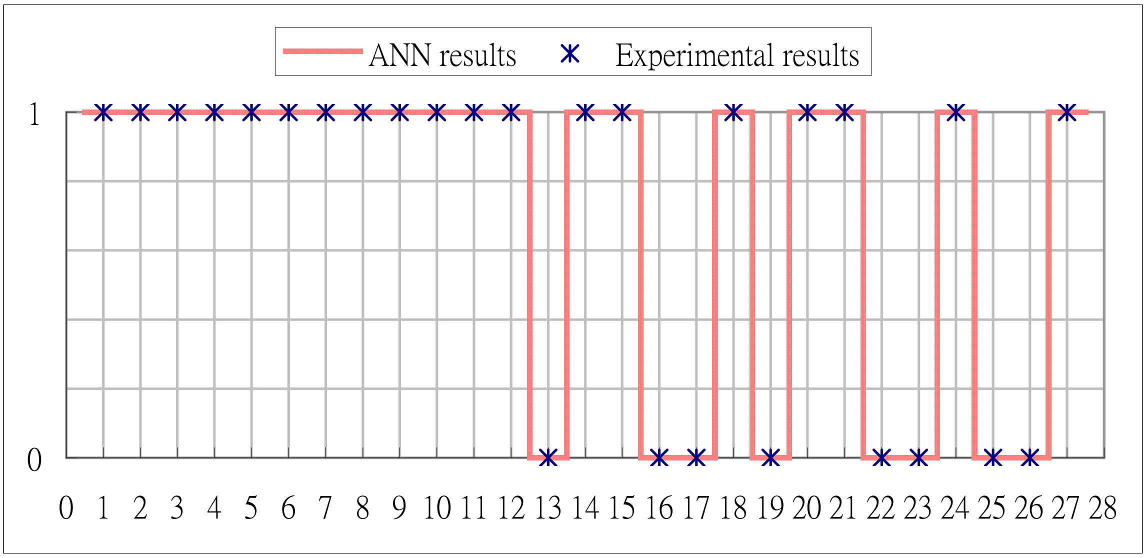

(a)

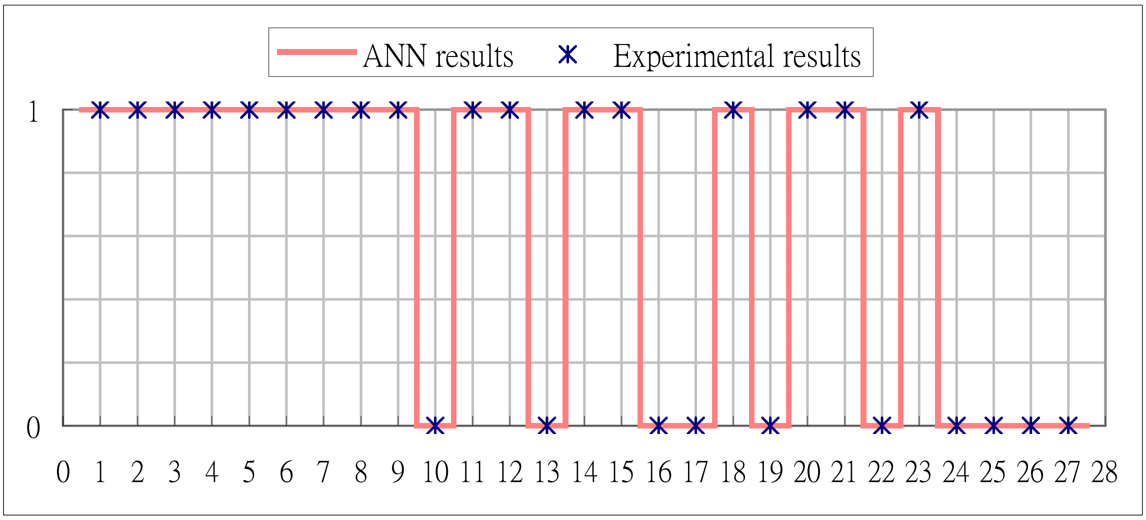

(b)

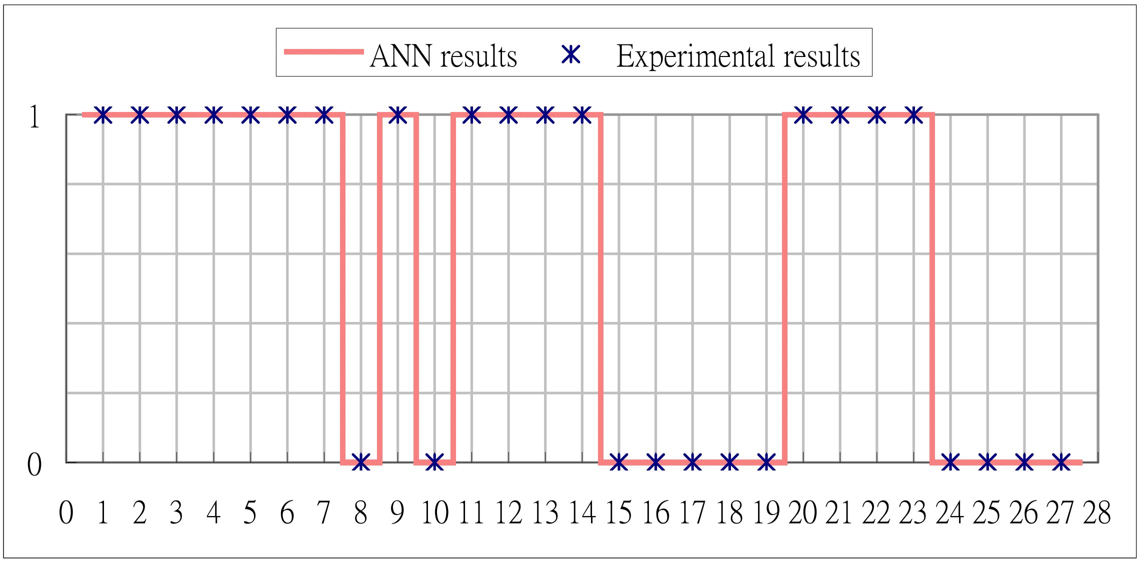

(c)

Fig.5.17 The comparisons of the experimental results and results of ANN optimization model in (a) the width of circuit spaces, (b) the depth of circuit spaces and (c) the resolidification height.

The final results of the ANN optimization model are shown in Fig.5.17. The final results are got in the consideration of all the three output results in the second last layer. When all the three output status values are ‘1’, the input set of parameters is considered to be acceptable. If one, two or three of these three status results are ‘0’, the input set of parameters is considered failed. In Fig.5.18, it shows the ultimate optimization results under the input parameters of training data.

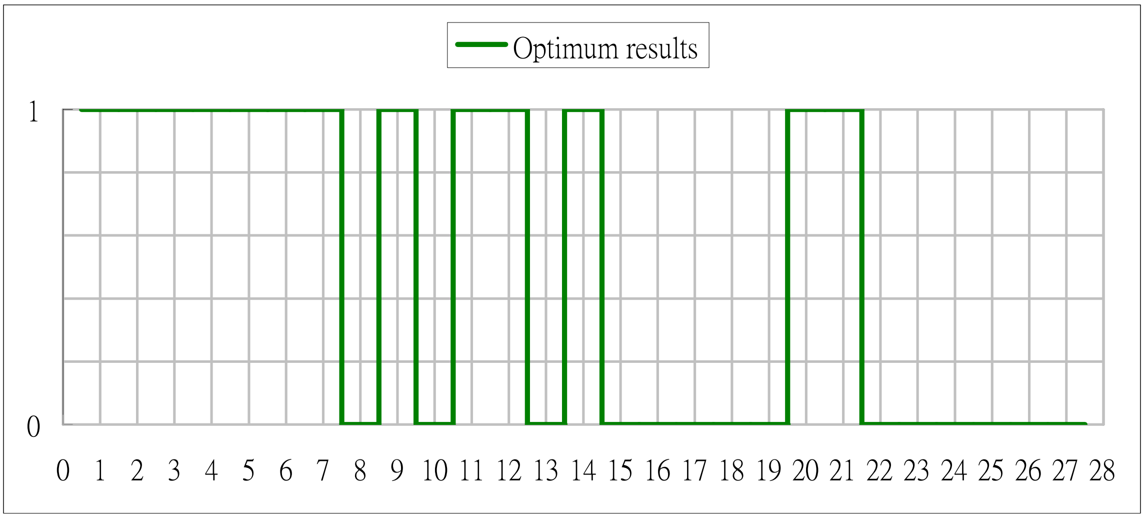

Fig.5.18 The final results of ANN optimization model

In the ANN optimization model, the pre-designed requirements of space geometry included: the depth of space was controlled in the range of 2 to 10 μm (constraint by the thickness of tin layer and copper layer); the width of space was under 30 μm and the resolidification height was less than 3 μm (less amount of melting materials). In order to get small geometry of circuits and reduce the amount of melting materials, it is better to reduce the value of the width of circuit space (the smaller the better) and the resolidification height (the smaller the better). The best geometry of circuit space (with min *d* and min *z*) is described by the constraint function (13).

$$\min d = \begin{cases} d \le 30 \\ 2 \le z \le 10 \\ h \le 3 \\ f(P_{out}, R_s, R_r, d_b) \end{cases} ; \min h = \begin{cases} d \le 30 \\ 2 \le z \le 10 \\ h \le 3 \\ g(P_{out}, R_s, R_r, d_b) \end{cases} \quad (13)$$

where $f(P_{out}, R_s, R_r, d_b)$ and $g(P_{out}, R_s, R_r, d_b)$ are the functions used to describe the complex relations between process parameters and characteristic parameters of circuit space.

The optimum settings of process parameters can be achieved with Taguchi methodology. According to the ANOVA analysis in section 5.1.5, the laser power, number of repetition and repetition rate are the most important factors that will influence the width of circuit space. The resolidification height is caused mainly by laser power, number of repetition and bite size. The best combination of process parameters for both the effects on the width of space and the resolidification height are (as shown in Fig.5.19): laser power=0.15 W, number of repetition=1, repetition rate=10 kHz, bite size=9 μm.

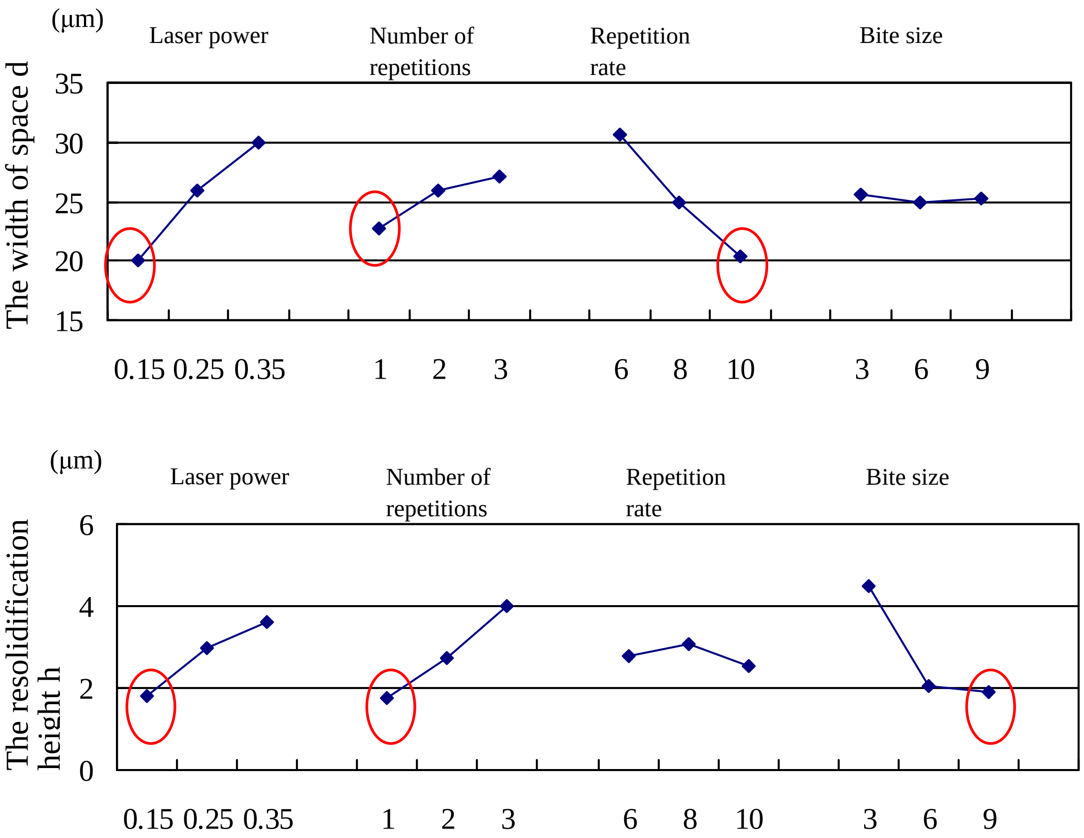

Fig.5.19 Effects of process parameters on the width of space and the resolidification height

This combination of process parameters which can achieve optimum value of *d* and *h* was tested by the ANN optimization model to see if the depth of space was also in the acceptable range (2 μm≤z≤10 μm). The output of the ANN optimization model for the inputs (laser power=0.15 W, number of repetition=1, repetition rate=10 kHz, bite size=9 μm, focal length=0-30 μm) was the status value '1'. That is to say, with this combination of the process parameters, the best geometry of circuit space can be achieved (with the minimum value of *d* and *h*, and 2 μm≤z≤10 μm). This result was in good agreement with experimental result (d=15 μm, z=2.164 μm, h=0.619 μm) which was the best circuit geometry of all the experimental results.

5.2.5 Check the validity of ANN models with experimental findings

Once ANN model has been trained, it has good predictive capability and ability to accurately describe the laser writing process. Since ANNs are learning to associate the inputs with the outputs, the network may get over-trained. That means that the network will not determine general rules, but rather will learn data by heart. Therefore, to keep independent check of the ANN performance, relevant verification and test data sets, different from training data set, should be created. The test data set for the verification of ANN prediction model and ANN optimization model are shown in Table 5.12. There are eight samples of inputs and outputs that are different from the training data.

Table 5.12 Experiments for the test of the ANN model

	Power (W)	Number of repetitions	Repetition rate (kHz)	Bite size (μm)	Focal length (μm)	Results		
						d (μm)	*z* (μm)	*h* (μm)
1	0.3	1	9	3	10	22.82	6.64	2.08
2	0.35	2	7	5	10	34.53	10.83	3.56
3	0.25	2	8	7	10	26.41	7.49	1.49
4	0.2	2	9	5	20	19.24	4.80	0.47
5	0.35	2	8	3	20	30.52	10.48	4.93
6	0.35	1	7	7	20	31.91	8.79	1.71
7	0.2	2	7	7	30	26.24	6.03	2.05
8	0.3	1	8	9	30	25.62	5.75	1.21

The most outstanding advantage about neural networks is their ability to generalize the findings to new sceneries. Once a neural network is ‘trained’ to a satisfactory level it may be used as an analytical tool on other data (this is called test mode). In the test mode, the training is stopped and the weights of nodes kept constant. New inputs are set to the input layer where they filter into and are processed by the middle layers as though training is taking place. However, at this point the output is retained and no backpropagation occurs. That is to say, after training, ANN model can generate the output by using the input and its weights.

After the test by the new data set, the prediction results and optimization results are shown in Fig.5.20 and Fig.5.21. In Fig.5.20, the prediction results of the width of circuit spaces, the depth of circuit spaces and resolidification height from ANN model and the experimental results are compared. Each experimental result was obtained by the calculation of the average value of five experiments under the same process parameters. The average value was used to compare with ANN prediction results. The measurement of experimental results was taken in the middle of each circuit space (the length of circuit space was 5 cm on each specimen in all experiments). In the ANN prediction model, the errors between the prediction results and experimental results were within ten percent. From Fig.5.21, after the optimization of output results, it can be concluded that from the eight experiment data, experiment one and experiment four are good in the selection of process parameters and are good in the fabricated geometry of circuit spaces. These results follow closely with the experimental findings.

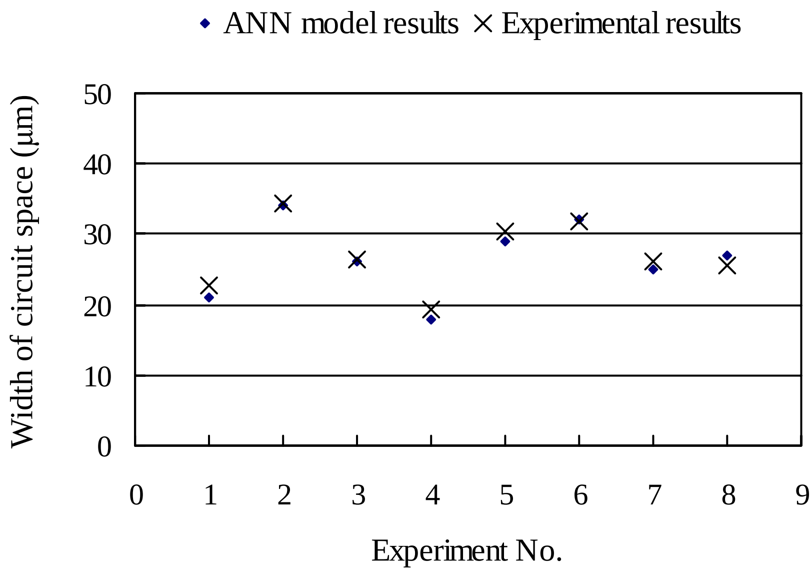

(a)

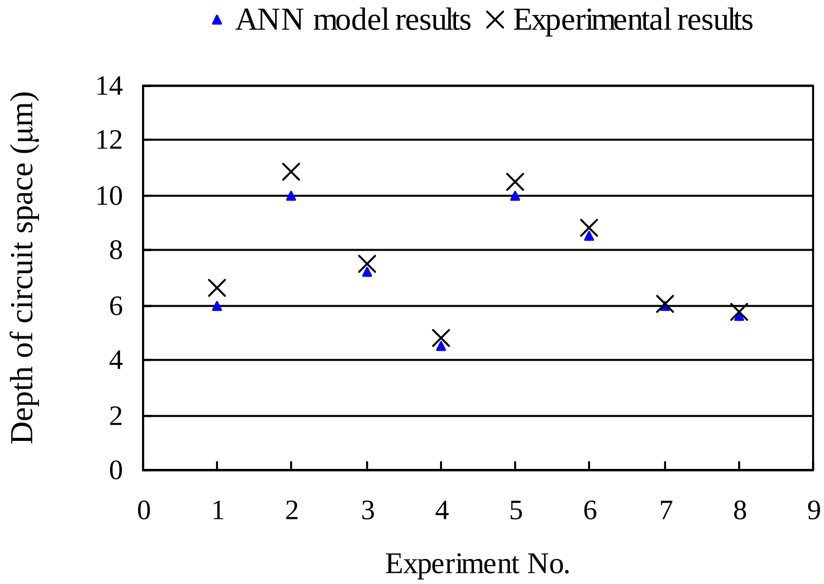

(b)

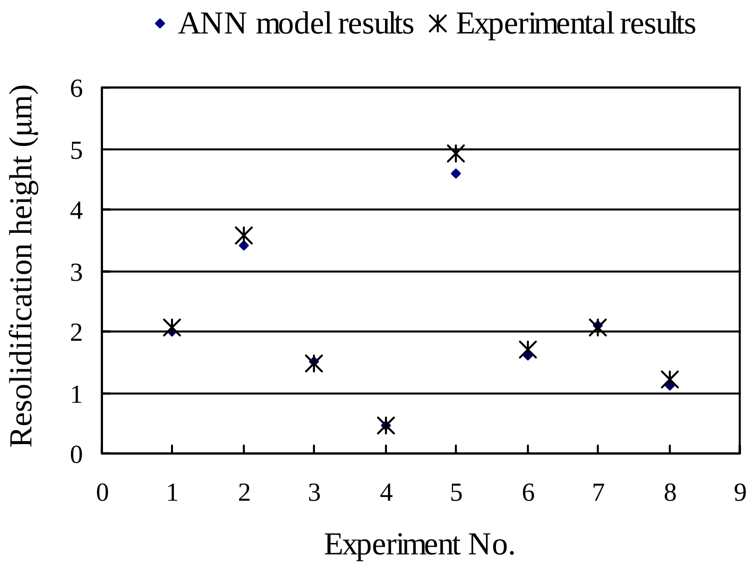

(c)

Fig.5.20 Comparisons of ANN prediction results and experimental results of test data in (a) the width of circuit space, (b) the depth of circuit space, (c) the resolidification height.

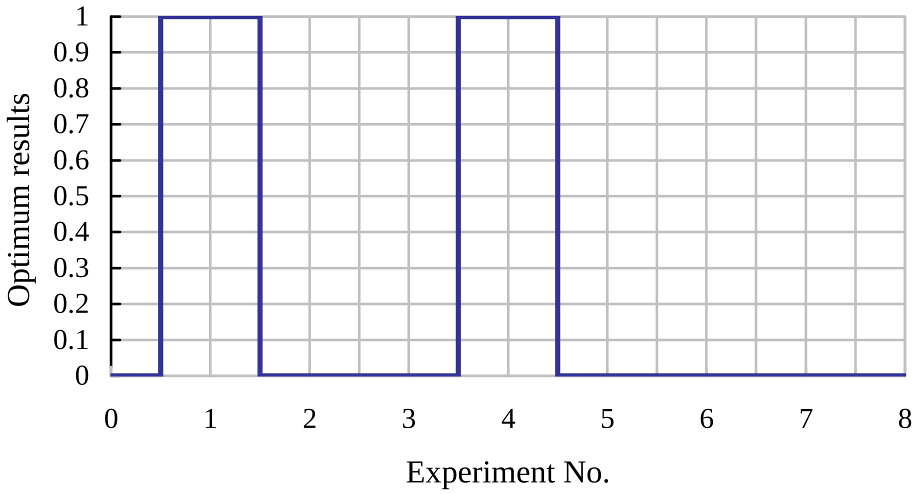

Fig.5.21 Optimization results of test experiments

By using the ANN prediction model, we can predict the geometry of circuit spaces only by inputting new set of process parameters to the input layer. These results simulated by ANN model are comparable to experimental results. After testing the ANN model, the prediction results are reasonably accurate. Through ANN optimization model, it demonstrates that if one set of input parameters is good in the simulation process, they can be selected as process parameters in experiment and in real production. It costs less time, money and energy in the simulation process than in the real experiment. The results in this work show that the ANN prediction model and ANN optimization model are helpful in the guidance of laser structuring process in the future research.

CHAPTER 6

MATHEMATICAL ANALYSIS AND MODELLING OF LASER STRUCTURING PROCESS

6.1 Analysis of laser writing process

6.1.1 Absorption of laser radiation by metals

For an opaque solid, the incident radiation absorbed is

$$A = 1 - R \tag{1}$$

where A and R are the absorptivity and reflectivity at normal incident. A and R can be calculated from measurements of optical constants or the complex refractive index. For a complex refractive index m',

$$m' = n - ik^* \tag{2}$$

the reflectivity at normal incidence is (Born and Wolf, 1975)

$$R = \frac{(n-1)^2 + k^{*2}}{(n+1)^2 + k^{*2}} \tag{3}$$

The absorptivity is then

$$A = \frac{4n}{(n+1)^2 + k^{*2}} \tag{4}$$

In general, n and k^* for metallic materials are functions of wavelength and temperature.

In the interaction of laser and material, it is assumed that the workpiece is semi-infinite and the material is a homogeneously absorbing medium. The energy Q_a

absorbed by material in the depth direction can be written

$$Q_a(z,t) = I_0 t(1-R)\alpha e^{-\alpha z} \tag{5}$$

where I_0 is the output power density from the laser, and α is the linear absorption coefficient of the solid.

The relation between α and refractive index is given by

$$\alpha = \frac{4\pi k^*}{\lambda} \tag{6}$$

where k^* is the imaginary term in the complex refractive index m' and λ is the wavelength of incident light.

The heating process of material can in general be described in terms of two characteristic lengths, namely α^{-1} (the optical absorption depth) and L_d (the heat diffusion length). The heat diffusion length L_d is approximately equal to $(2Dt)^{1/2}$ (D, the thermal diffusivity, is given by $D=k/c\rho$, while k, c and ρ represent the thermal conductivity, specific heat and density respectively). In cases where L_d is much greater than the optical absorption depth α^{-1}, as it is for most metals at most laser wavelengths, the heat source term becomes a surface source of energy since α becomes large. The temperature of material in y direction with the laser irradiance I_0 is shown as follows (Duley, 1996):

$$T(y,t) = \left[\left(\frac{I_0}{k\sqrt{Dt}}\right) ierfc\left(\frac{y}{2\sqrt{Dt}}\right)\right](1-R) \tag{7}$$

where $erf(s) = \frac{2}{\sqrt{\pi}}\int_0^s e^{-x^2}dx$ is the error function and $erfc(s)$ is the complementary error function 1-$erf(s)$.

6.1.2 The phases of material in the laser ablation process of laser structuring

When the laser intensity is 10^5-10^7 W/cm^2, the melting temperature at the material surface is reached very rapidly. When the laser intensity is 10^6-10^8 W/cm^2, the material is vaporized rapidly with high intensity, mostly in the pulsed operation.

At lower laser flux densities (in the range of 10^6-10^8 W/cm^2), the amount vaporized depends more on the thermal conductivity of the material than on the latent heat of vaporization. In the low-power regime, the greater thermal conductivity of the metal leads to greater heat conduction into the interior so that relatively little metal is vaporized. As the laser flux density increases, it reaches a value at which the heat is supplied too fast to be conducted away. The dominant factor then becomes the latent heat of vaporization (Ready, 1971). The flux density I_c for which the crossover occurs from the region in which the effect of the thermal conductivity is negligible is given approximately by

$$I_c \geq 2L\rho D^{1/2}\tau^{-1/2} \tag{8}$$

where L is the latent heat per unit mass, ρ is the density, D is the thermal diffusivity, and τ is the laser pulse duration. The I_c for materials (tin and copper) are shown in Fig.6.1. When laser intensity reaches 8.2×10^7 W/cm^2 and 2.6×10^8 W/cm^2, tin and copper are vaporized instantly with the negligible influences of thermal conductivity.

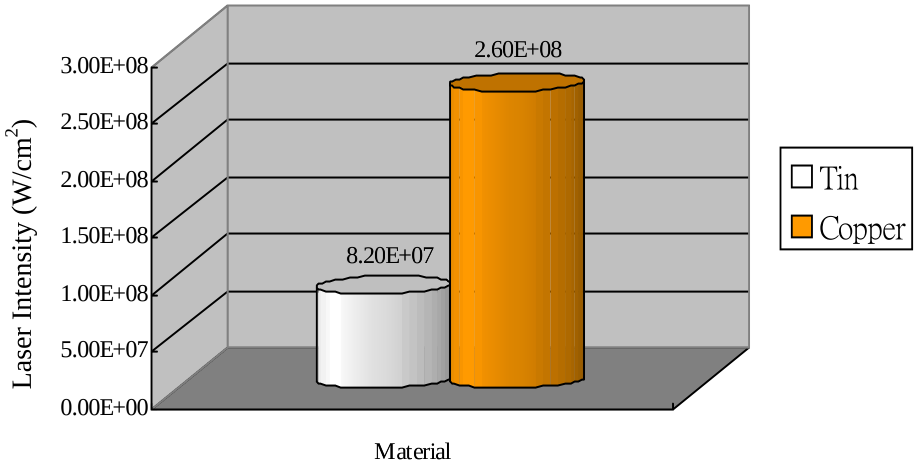

Fig.6.1 The laser Intensity I_c for Tin and Copper

In laser writing process of LS, the laser beam of Nd:YAG is Gaussian spatially, so

$$G(r) = \exp(-2r^2 / w^2) \tag{9}$$

where *r* is the distance in the direction transverse to the direction of propagation; and *w* is the focal spot radius for a laser beam. Then the pulse energy *E* can be expressed as

$$E = I_0 \int_0^{\tau} \int_0^{\infty} F(t) G(r) 2\pi r dr dt \tag{10}$$

where *t* represents time, and *F*(*t*) is the time-dependent function of pulse laser, I_0 is the laser irradiance at the center of the focal spot. The spatial profile of pulse energy *E* is determined mainly by I_0 (the laser irradiance at the center of focal spot) and *r* (distance to the center of laser spot). The laser spatial profile with different laser irradiation is shown in Fig.6.2. It can be seen from Fig.6.2, the maximum laser intensity is at the center of laser spot. When the distance r increases from the center to the edge of the laser spot, the laser intensity decreases accordingly. In laser structuring process, as the laser intensity I_0 of Nd:YAG laser is always above 1×10^8 W/cm^2, the energy at the center of the laser beam is large enough to vaporize material. However, the laser intensity at the edge of the laser beam will ablate material in melting stage instead of vaporization. So in laser structuring process, resolidification layers always exist at the edge of circuit spaces (at the edge of laser beam accordingly).

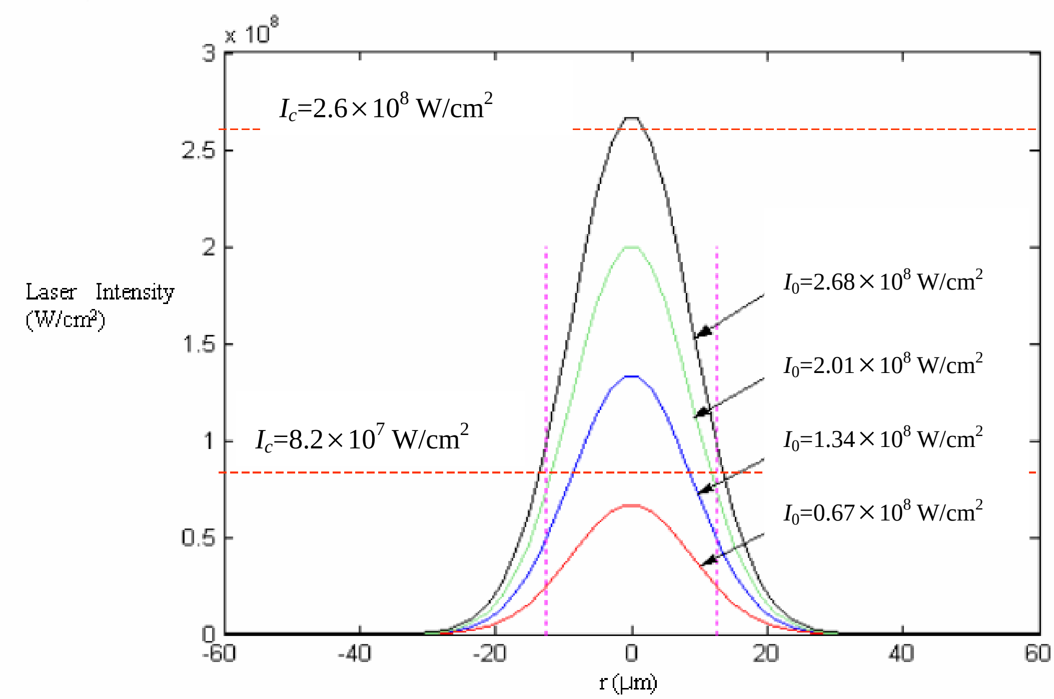

Fig.6.2 Laser spatial profile with different laser intensity I_0

6.1.3 Time distribution in laser writing process during two consecutive laser pulses

In order to build a model of laser writing step, first, it is needed to analyze the whole laser ablation process. As the laser parameters and the phases of materials all change with the variation of time, the time is an important parameter to analyze the whole laser ablation process.

When the material is heated by laser beam from the beginning of the pulse duration, the time needed to reach the evaporation point t_b for various materials is given by Ready (1971)

$$t_b = \frac{\pi k \rho c (T_v - T_0)^2}{4 I_a^2} \tag{11}$$

Here k, c, ρ and I_a are the thermal conductivity, heat capacity per unit mass, density and laser intensity absorbed by material, respectively, and T_v and T_0 are the vaporization temperature and initial temperature. This situation is most relevant to metals and metallic-type media. Therefore, such formula is useful in applications where evaporation of metals is performed, e.g., in laser structuring.

If the deposition of energy from the laser beam induces a phase change in the workpiece, and if the deposition of energy continues after melting, or evaporation occurred, the heating models must include the various latent heats of reaction, as well as the thermal properties of the materials with the variation of temperature. The time needed to evaporate materials copper and tin with the changes of different initial temperature is shown in Fig.6.3. When heated by laser in the room temperature (about 293K), the time t_b of copper and tin is in the level of 1×10^{-10} s and 1×10^{-9} s.

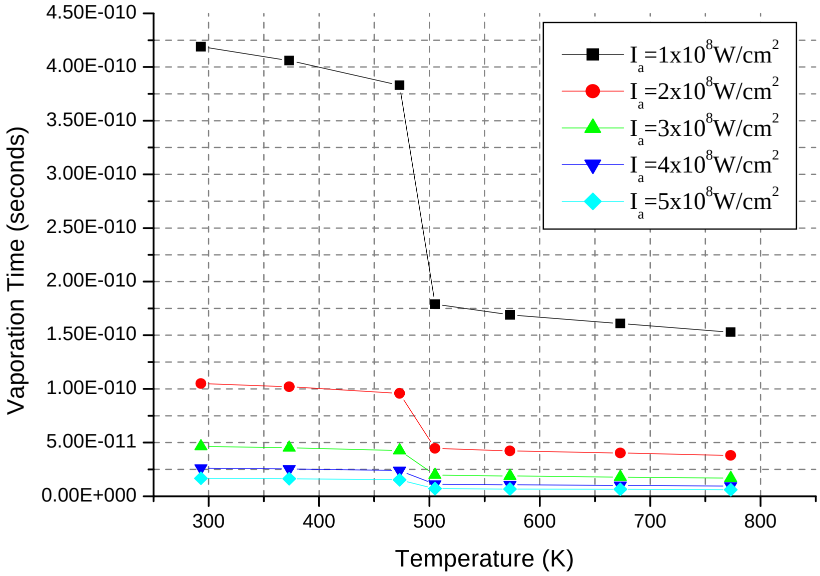

(a)

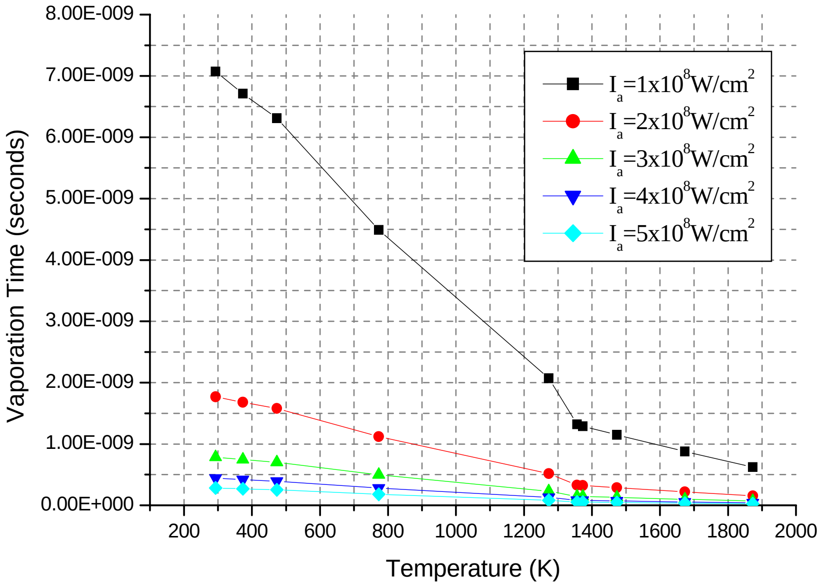

(b)

Fig.6.3 (a)The time to reach the evaporation point of copper at different initial temperature;

(b)The time to reach the evaporation point of tin at different initial temperature.

When materials reach the evaporation point, the ablation velocity and ablation time can be calculated. During the laser ablation process, assume that the laser power *W* is distributed uniformly over some area of the surface *S* and is applied normally to the surface. In a time interval δt the amount of energy dissipated in $W\delta t$ and the depth of the spaces increases by δz.

After introducing the following normalized variables by Andrews and Atthey (1975) where *l* is some characteristic length

$$\eta = \frac{\nu t}{l}, \quad \xi = \frac{z}{l}$$

The complete solution of $d\xi / d\eta$ to first order is (where $\varepsilon = \dfrac{cT_v}{L_v}$)

$$\frac{d\xi}{d\eta} = \left[1 + \varepsilon\left\{erfc\left(\eta^{1/2}/2\right)/2 - (\pi\eta)^{-1/2} e^{-\tau/4}\right\}\right]\left[(2/\pi)\left\{1 + \varepsilon/(\pi\eta)^{1/2}\right\}\right]\arcsin\left\{\left(1 - \pi\varepsilon^2/4\eta\right)^{1/2}\right\} \tag{12}$$

The relations between $d\xi / d\eta$ and $d(z)/dt$ is as follows:

$$\frac{d\xi}{d\eta} = \frac{d\left(z/l\right)}{d\left(\nu t/l\right)} = \frac{d(z)}{d(\nu t)} = \frac{1}{\nu}\frac{d(z)}{dt} \tag{13}$$

Then the velocity v_s (in depth direction) in structuring process is

$$v_s = \frac{d(z)}{dt} = \nu\frac{d\xi}{d\eta} \tag{14}$$

$$\nu = \frac{W}{(cT_v + L_v)\rho S} = \frac{(W/L_v\rho S)}{(1+\varepsilon)} = \frac{I_a}{L_v\rho(1+\varepsilon)}$$

After the preheating process, the value of $d\xi / d\eta \approx 1$, then

$$v_s \approx v = \frac{I_a}{L_v \rho (1 + \varepsilon)} \tag{15}$$

The time t to ablation the depth z of material can be calculated by

$$t = z / v_s = \frac{z L_v \rho (1 + \varepsilon)}{I_a} \tag{16}$$

When the laser intensity is from 1×10^8 W/cm^2 to 9×10^8 W/cm^2, the ablation time for different depth of tin and copper is shown in Fig.6.4.

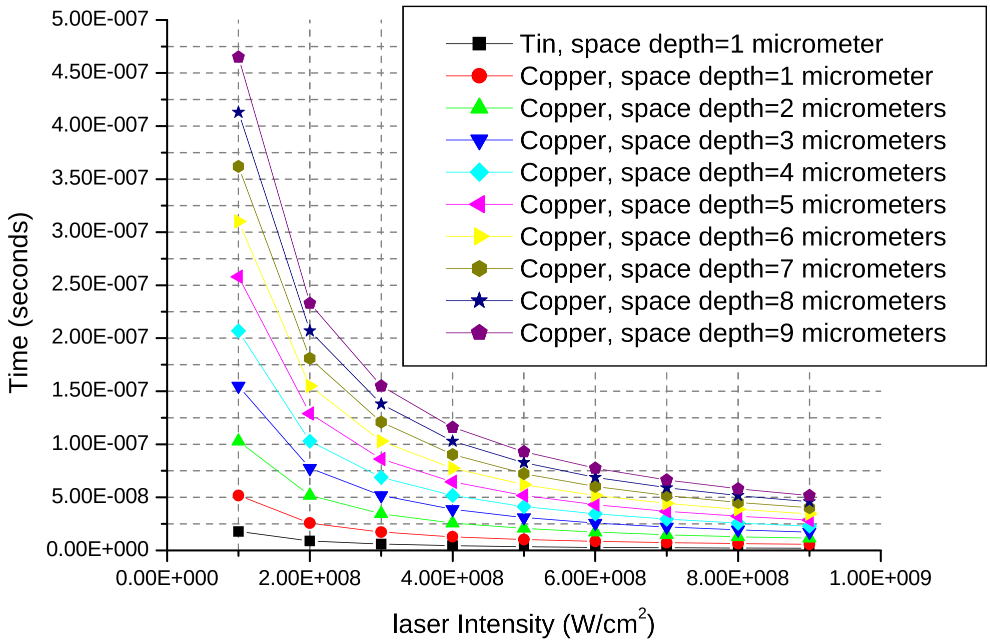

Fig.6.4 Time to structure different depth of spaces with the changes of laser intensity

As shown in section 6.1.2, the intensity at the center of laser beam can cause vaporization of material. While at the same time, the lower intensity at the edge of laser beam ablates material by melting and vaporizing simultaneously. When material is melted, whether it will flow in the scanning direction with the moving of laser beam is discussed in the following part.

For metals the solidification velocities are of the order of 10 to 10^3 m/s (Bauerle, 2000). The time of solidification can be calculated as follows (Bauerle, 2000):

$$t_s = \frac{h_l^{\max 2}}{4\omega^2 D}\left(1 + \frac{2\omega l_T}{h_l^{\max}}\right) \tag{17}$$

in which $l_T \approx 2(D\tau)^{1/2}$. D is thermal diffusivity; τ is the duration of laser pulse. According to Dieter Bauerle, the physically reasonable values of ω are within $0.25<\omega<1$; $h_l^{\max}$ is the maximum melt depth. The time of solidification of copper and tin with different melt depth is shown in Fig.6.5. The solidification time is in the order of 10^3 ns.

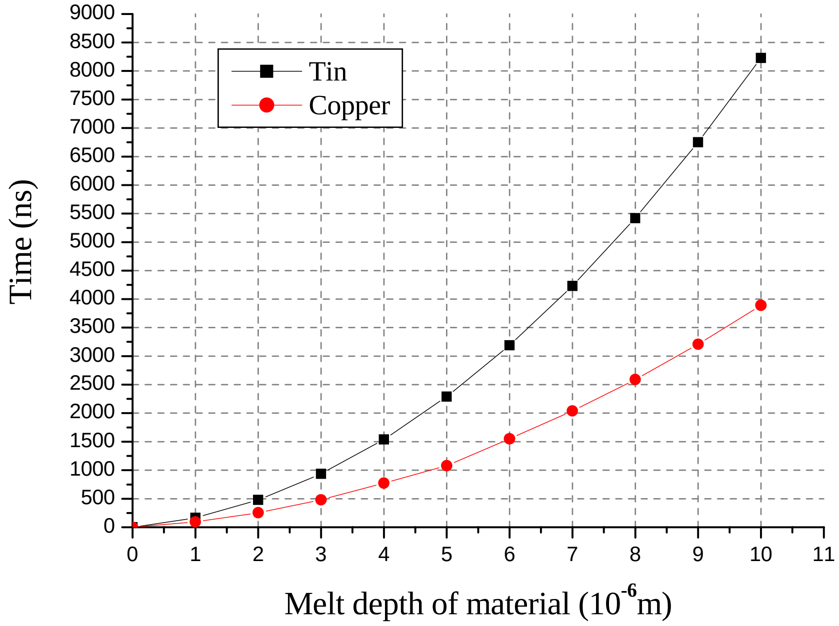

Fig.6.5 The time of solidification of materials with different melt depth

During the time between two consecutive laser pulses, the laser writing process is described in Fig.6.6. In the laser writing process, it is assumed that the laser intensity absorbed by material I_a is from 1×10^8 W/cm^2 to 8×10^8 W/cm^2; The depth z of material ablated by laser beam is 1×10^{-6} m and 4×10^{-6} m in tin layer and copper layer separately; The maximum melt depth is from 1 μm to 10 μm; There are 10^3-10^4 pulses in one second (repetition rate=1 kHz-10 kHz). Then the time distribution during two consecutive laser pulses in laser writing process is shown in Fig.6.6.

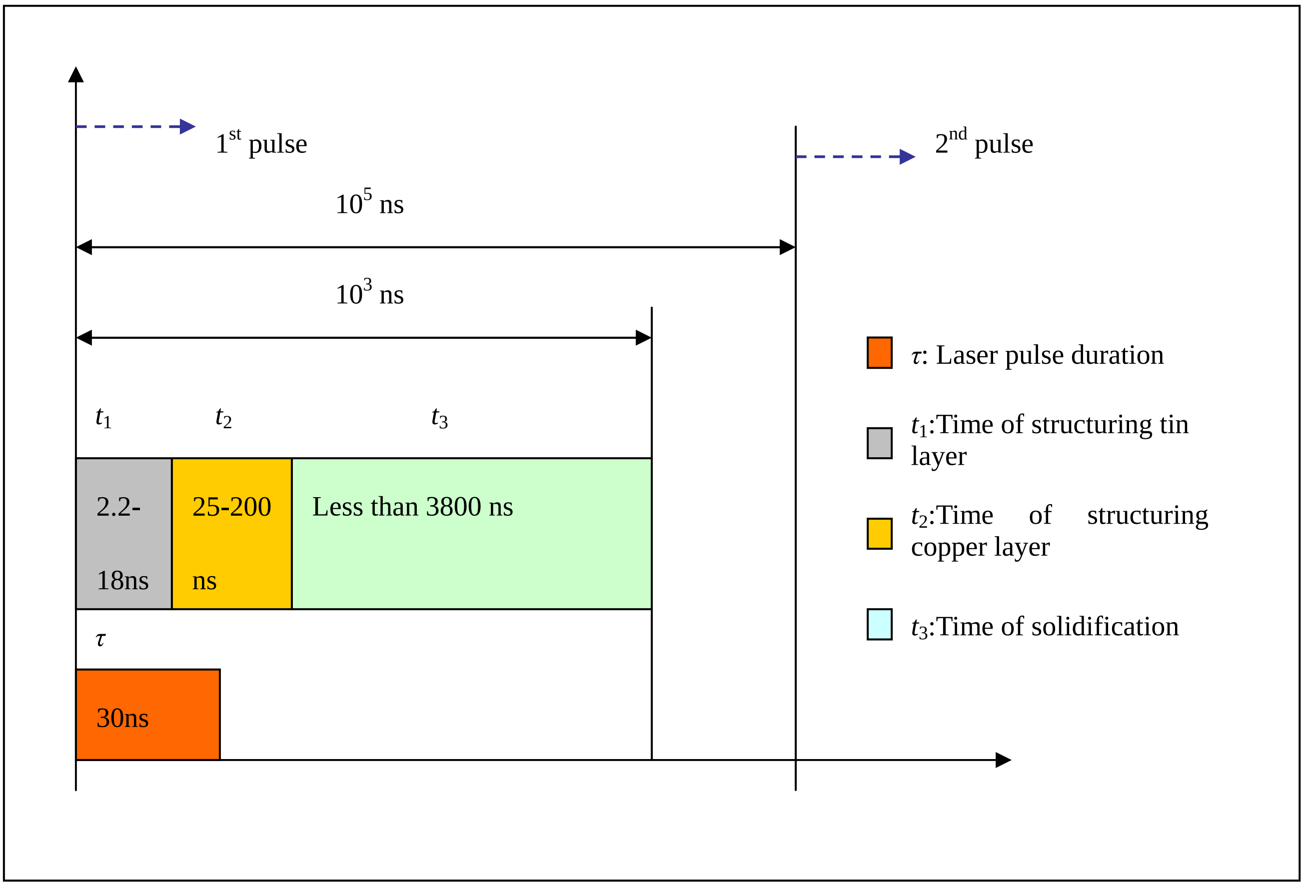

Fig.6.6 Time distribution in laser writing process during two consecutive laser pulses

6.2 Laser parameters' influences on the absorption of laser intensity during laser writing process

In section 4.2, the relationship between laser parameters (Nd:YAG laser, 355 nm wavelength) and the dimension of circuit space was studied with experiments. The variation of the dimension of circuit space is mainly caused by the laser irradiance absorbed by materials. In this section, the relationship between laser parameters (laser power, repetition rate, number of repetition, bite size and focal length of laser) and the irradiance absorbed by material is studied by mathematical approach. The mathematical approach can be used to explain the experimental results in section 4.2.

6.2.1 Consideration of the effect of laser power and repetition rate on the laser irradiance

The depth of circuit spaces vaporized by laser pulse energy at any instant t can be expressed as

$$z(t) = \frac{(1-R)E(t)}{h_m \rho S} \tag{18}$$

where $E(t)$ is the total energy dissipated by the source in the time interval (0,t), h_m is the heat required to vaporize the unit mass of material, ρ is the density of the material, R is the reflectivity of the material and S is the surface area under irradiation (Andrews, 1976). Thus, from the Equation (18), it is clear that the depth of spaces depends on the total energy supplied to the surface of the material. The energy of laser beam E (per pulse) is mainly determined by the laser power (P_{out}) and repetition rate (R_r). The relations among these three parameters are as follows

$$ER_r = P_{out} \tag{19}$$

The energy per pulse (E) can be calculated by

$$E = P_{out} / R_r \tag{20}$$

The laser power per pulse (W) is calculated by

$$W = E / \tau \tag{21}$$

τ is the pulse duration. The irradiance I_0 of laser at the central of the laser beam at the focal plane is expressed by

$$I_0 = \frac{2P}{\pi w^2} \tag{22}$$

w is the radius of the laser beam. Then from Equation (20), (21) and (22), it can be concluded that

$$I_0 = \frac{2P_{out}}{\pi w^2 \tau R_r} \tag{23}$$

From Equation (23), I_0 will increase with the increase of P_{out} and decrease with the increase of R_r. When only considering the parameters of laser power and repetition rate, the Equation (18) can be changed into

$$z(t) = \frac{(1-R)I_0}{h_m \rho} = \frac{2(1-R)P_{out}}{h_m \rho \pi w^2 \tau R_r} \tag{24}$$

The depth of space structured by laser will increase with the increase of P_{out} and increase with the decrease of R_r which are compared with the experimental results in section 4.2.1 and 4.2.3.

6.2.2 Consideration of the effect of bite size on the absorptivity of laser irradiance

The whole energy absorbed by material $E(t)$ in Equation (18) is determined not only by laser power P_{out} and repetition rate R_r but also by many other factors such as the bite size of laser d_b, number of repetitions R_s and so on. In the laser writing process, the laser beam structures a series of continuous cavities that turn into the circuit spaces between circuit lines on materials. The distance between the centers of two connected laser spots is the bite size of laser beam d_b. As shown in Fig.6.7, the bite size d_b will have an effect on the depth of circuit spaces. When the bite size is small, the material absorbs more energy at one point than in the situation when the bite size is comparatively large. r_0 is the half width of circuit space ($r_0 \approx w$ in most cases, where w is the radius of laser beam).

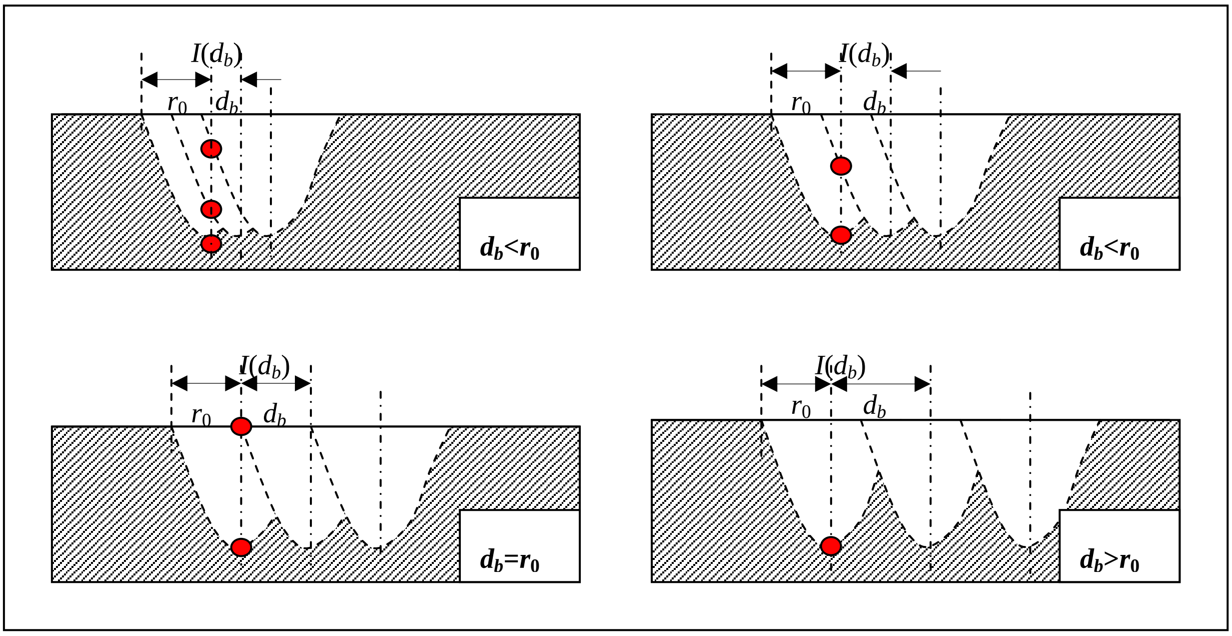

Fig.6.7 The influence of bite size d_b on the laser irradiance $I(d_b)$

When bite size d_b is considered, the depth of circuit spaces is controlled by the irradiance $I(d_b)$ determined by I_0 and d_b. When $d_b \geq r_0$, $I(d_b) = I_0$ (in Fig.6.7); when $d_b < r_0$, $I(d_b)$ is shown as follows

$$I(d_b) = \sum_{n=0}^{m} I_0 e^{\left[\frac{-2(nd_b)^2}{r_0^2}\right]} \tag{25}$$

$$md_b < r_0, m = 1,2,......$$

The irradiance absorbed by material (I_a) then can be calculated by

$$I_a(d_b) = I_0(1-R_T) + (1-R_C)\left\{ I_0 e^{\left(\frac{-2d_b^2}{r_0^2}\right)} + I_0 e^{\left[\frac{-2(2d_b)^2}{r_0^2}\right]} + ... + I_0 e^{\left[\frac{-2(md_b)^2}{r_0^2}\right]} \right\} \tag{26}$$

$$md_b < r_0, m = 1,2,......$$

where R_T is the reflectivity of the tin electroplating layer and R_C is the reflectivity of the copper layer. Normally, the tin layer will be ablated away after the first pulse of laser beam and the following pulses will irradiate directly onto the copper.

When $d_b < r_0$ and $md_b < r_0$, the value of bite size will influence the depth of spaces. The smaller the value of d_b, the larger the number of *m* when r_0 is fixed at the same value. The larger of the number *m* means the more laser energy will irradiated on the same spot of material (Equation (26)). Then when $d_b < r_0$, the depth of space increases with the decrease of bite size. When $d_b < r_0$ and $md_b > r_0$, or $d_b \geq r_0$, the bite size will not influence the energy absorbed by material any more. In conclusion, the depth of circuit spaces structured by laser will decrease with the increase of bite size at first and then remain the same when $d_b > r_0$, as shown by the experimental results given in section 4.2.4.

6.2.3 Consideration of the effect of the number of repetitions on the absorptivity of laser irradiance

In the above section, the situation is that the laser only writes once along the required pattern. When the number of repetitions (R_s) is more than once, the influence of R_s at one point can be obtained by

$$I_a(j) = \sigma(1-R_T)I_0 + \sigma(j-1)(1-R_C)I_0 \qquad (27)$$

j is the number of repetitions, σ is the correction factor ($0<\sigma<1$). Combining (26) and (27), the irradiance absorbed by material is

$$I_a = I_0(1-R_T) + \sigma(1-R_C)\sum_{n=1}^{m} I_0 e^{\left[\frac{-2(nd_b)^2}{r_0^2}\right]} + \sigma(j-1)(1-R_C)\sum_{n=0}^{m} I_0 e^{\left[\frac{-2(nd_b)^2}{r_0^2}\right]} \qquad (28)$$

$$md_b < r_0, m = 1,2,......$$

Laser irradiance I_a absorbed by the material will increase with the increase of number of repetitions as shown in Equation (28) which are compared with the experimental results in section 4.2.2.

6.2.4 Focal length's influence on the laser irradiance

The Equation (28) is obtained when the focal plane of the laser beam is directly on the surface of material ($I(r, z_1)$, z_1=0). In this section, the situation when the laser spot on the material is not on focal plane is considered ($I(r, z_1)$, $z_1 \neq 0$).

The radius r of the laser beam at distance z_1 from the focal plane is (Ifflander, 2001)

$$r(z_1) = r_0 \left[1 + \left(\frac{z_1}{z_r} \right)^2 \right]^{1/2} \tag{29}$$

where r_0 is the radius of laser beam on focal plane, z_r is the Rayleigh length.

$$2z_r = \frac{4\pi r_0^2}{\lambda} \tag{30}$$

As shown in Fig.6.8, the central intensity $I(0, z_1)$ can be determined as the following

$$\frac{I(0, z_1)}{I(0,0)} = \frac{r_0^2}{r^2(z_1)} \tag{31}$$

Then the laser intensity at the distance z_1 from the focal plane is

$$I(0, z_1) = \frac{I(0,0)}{1 + (z_1 / z_r)^2} \tag{32}$$

where $I(0,0)$ is the central intensity in the laser beam on focal plane. When distance z_1 increases, the $I(0, z_1)$ will decrease at the same time and $r(z_1)$ will increase as shown in Equation (29).

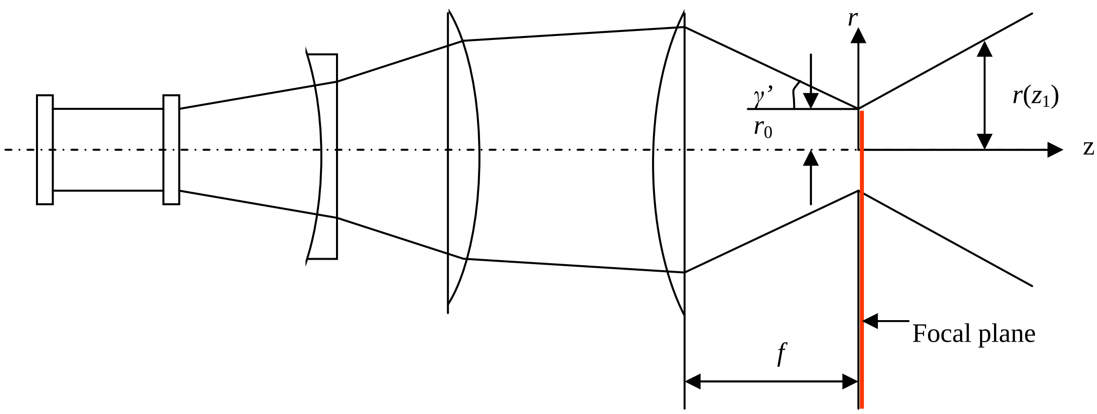

Fig.6.8 Laser beam propagation

Then the laser irradiation at distance z_1 from laser focal plane can be calculated by

$$I(r, z_1) = I(0, z_1)\exp\left(-2r^2 / r(z_1)^2\right) \qquad (33)$$

6.3 Models in the prediction of the geometry of circuit spaces in laser writing process

6.3.1 Formation of space in laser writing process

Some models have been used to explain and predict the effects produced by laser-induced heating and ablation of materials. These thermal models are often quite complicated, involving nonlinear optical and thermodynamical processes such as absorption, reflection, carrier and thermal diffusion, melting and evaporation, energy of reaction, and indeed the reaction mechanism itself. There does not yet exist a universal model describing laser induced heating, and in general, many researchers only modeled the effect for a small range of materials that optical and thermal properties are similarly described. In many cases, however, several simplifying assumptions with little loss in accuracy can be used in order to provide analytical solution in each case.

With the analysis in section 6.1, the laser structuring of circuit spaces can be described in Fig.6.9. The center intensity of the laser beam is high enough to ablate tin and copper by vaporization. At the edge of the laser beam, material is ablated away by melting and vaporization simultaneously. The melting layer of material will cool down and form a solidification layer at the edges of circuit spaces.

The geometry of circuit spaces is an important factor in laser structuring. So in this section, the emphasis of the model is on the description of the space geometry. The laser used is Q-switched Nd:YAG laser and the material is a two-layer metal (tin and copper).

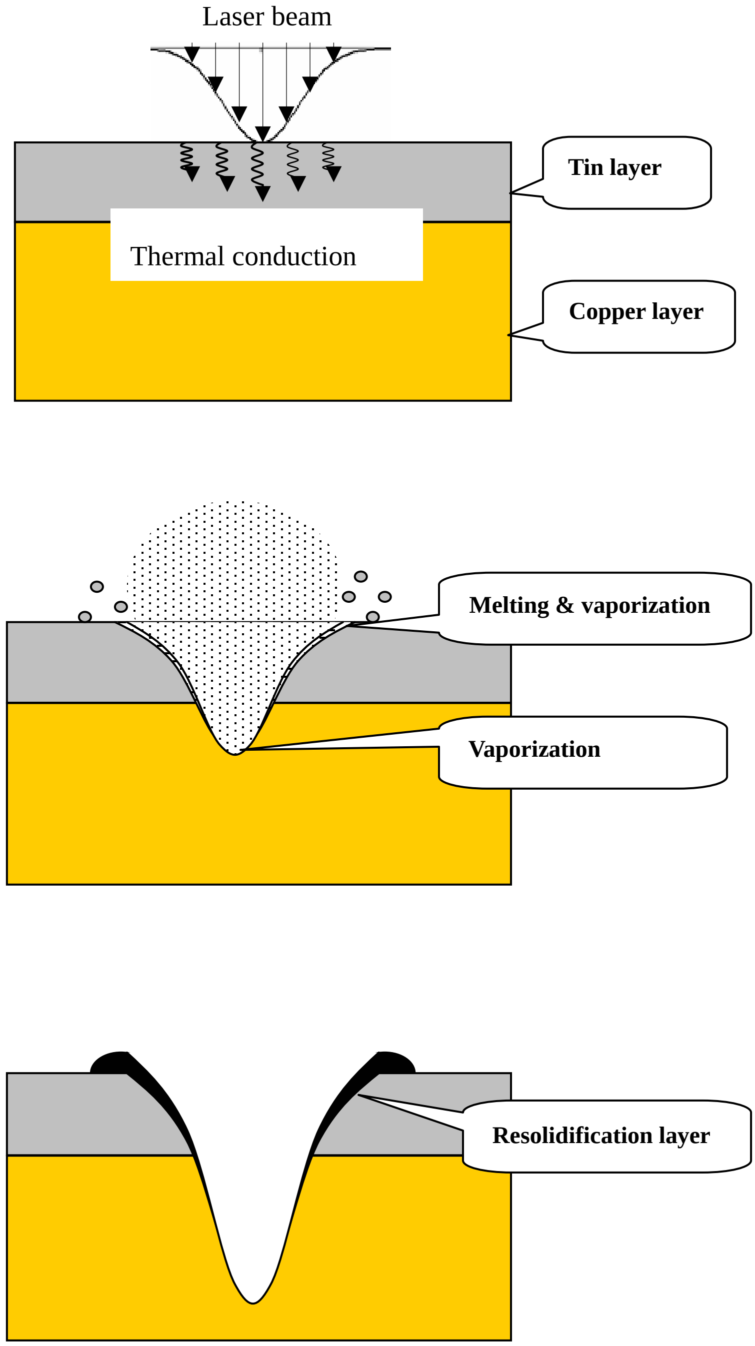

Absorption of laser radiation by the law $I(z) = I_0(1-R)e^{-\alpha z}$ at the light penetration depth $\delta=1/\alpha\approx 10^5\ \mathrm{cm}^{-1}$ for metals

Vaporization after absorption the latent heat L_v at the center of circuit spaces

Vaporization & melting at the edge of the circuit spaces

Circuit paces formed with resolidification layer

Fig.6.9 The description of the formation of circuit spaces under laser irradiance

6.3.2 1-D analytical model of the depth of circuit spaces

The depth of circuit space varies greatly with the changes of laser parameters. 1-D analytical model is used here to calculate the depth of circuit space with the changes of laser parameters.

Assume that the power W of laser is applied normally to the surface S. The intensity of the laser at the center of the laser beam is I_0 and the intensity absorbed by material at the center of laser beam is I_a In a time interval δt the amount of energy dissipated is $W\delta t$ and the depth of circuit space increases by δz. Hence the volume of the material evaporated is $S\delta z$ and by conservation of energy, we have

$$h_m \rho S \, \delta z = W \, \delta t \tag{34}$$

where h_m is the heat required to vaporize unit mass of material and ρ is the density of the material. The speed at which the cavity develops is obtained letting $\delta t \rightarrow 0$

$$\frac{dz}{dt} = \frac{W/S}{h_m \rho} \tag{35}$$

The speed at the center of the space is then

$$\frac{dz}{dt} = \frac{I_a}{h_m \rho} \tag{36}$$

The depth at the center of the space at any instant t (z=0 at t=0) is

$$z(t) = \frac{1}{h_m \rho} \int_0^t I_a \, dt \tag{37}$$

Thus, in the evaporation-controlled limit, the depth of circuit space depends only on the total energy absorbed by material (I_a).

In practice there will always be some conduction of heat into the material, so the evaporation-controlled speed (36) represents an upper limit on the rate of penetration.

In order to solve the problem of getting the velocity and space depth, we have to solve the one-dimensional unsteady heat conduction equation

$$\frac{\partial T^2}{\partial z^2} = \frac{1}{D}\frac{\partial T}{\partial t} \tag{38}$$

for the temperature $T(z,t)$ inside the material, where $D=k/\rho c$ is the thermal diffusivity, k, ρ, and c are the thermal conductivity, density and specific heat, respectively. At the moving boundary, $d' = z(t)$. One boundary condition at the moving boundary is obtained by applying the principle of conservation of energy there,

(rate of energy absorption by surface)

= (rate of energy conversion into latent heat of evaporation)+(rate of heat conduction into the material)

$$I_a = L_v \rho \frac{dz}{dt} - k\frac{\partial t}{\partial (d')} \tag{39}$$

where L_v is the latent heat of evaporation per unit mass. Another boundary condition is that the temperature of the moving boundary is approximately equal to the boiling point, so that on $d' = z(t)$

$$T = T_v \tag{40}$$

For penetrating materials the presence of the far face is relatively unimportant and it is reasonable to remove the far face to infinity, where

$$T = 0 \tag{41}$$

For completeness it is also necessary to state boundary conditions at the other phase boundary (between the solid and the liquid and between the liquid and vapor). However, for many materials of interest the ratio of the latent heats of fusion and evaporation is small compared with unity and the discontinuity at the melting boundary can be ignored to a good approximation (Andrews and Atthey, 1975).

In the laser writing process, we assume the boundary is moving close to the evaporation-controlled limiting speed. In this case the characteristic heat lost by conduction to that by latent heat of evaporation is

$$\left|\frac{k(\partial T/\partial(d'))}{L_v\rho[dz/dt]}\right| = \frac{k\ O(T_v/l)}{L_v\rho\ O(I_a/h_m\rho)} \tag{42}$$

where l is some characteristic length for temperature decay into the material, given by

$$l = \frac{D}{(I_a/h_m\rho)} \tag{43}$$

Substituting for l and D, putting $h_m = L_v + cT_v$, we have

$$\left|\frac{k(\partial T/\partial(d'))}{L_v\rho[dz/dt]}\right| = O(\varepsilon) \tag{44}$$

where

$$\varepsilon = \frac{cT_v}{L_v} = \frac{heat\,required\ to\ heat\ material\ to\ boiling\ po\text{int}}{heat\ reuired\ at\ the\,boiling\ \ po\text{int}\ \ for\ evaporation} \tag{45}$$

ε is a constant for the material and is typically small compared with unity for many materials. The ε value of copper and tin is listed in Table 6.1.

Table 6.1 The ε value of copper and tin

Material	Heat capacity cT_v (kJ/kgm)	Latent heat of evaporation L_v (kJ/kgm)	Latent heat of Fusion L_f (kJ/kgm)	Ratio of latent heat L_f/L_v	ε
Copper	999.075	4770	205	0.043	0.209
Tin	503.94	1945	60.7	0.031	0.259

A simple perturbation solution in terms of small parameter, $\varepsilon = cT_v / L_v$, to determine the motion of the boundary is developed. In order to distinguish different orders of approximation it is convenient to introduce the following normalized variables

$$\phi = \frac{T}{T_v}, \quad \zeta = \frac{d'}{l}, \quad \eta = \frac{\nu t}{l}, \quad \xi = \frac{z}{l}$$

Taking ν to be the speed of boundary in the evaporation-controlled limit, we have from equation (36)

$$\nu = \frac{I_a}{(cT_v + L_v)\rho} = \frac{(I_a / L_v \rho)}{(1+\varepsilon)} \tag{46}$$

When consideration the influences of laser power, number of repetition, repetition rate and bite size of laser, the Equation (46) is

$$\nu = \frac{2P_{out}\{(1-R_T) + \sigma(1-R_C)\sum_{n=1}^{m} e^{\left[\frac{-2(nd_b)^2}{r_0^2}\right]} + \sigma(j-1)(1-R_C)\sum_{n=0}^{m} e^{\left[\frac{-2(nd_b)^2}{r_0^2}\right]}\}}{L_v \rho (1+\varepsilon)(R_r \tau \pi r_0^2)}$$

$$md_b < r_0, m = 1,2,...... \tag{47}$$

where P_{out} is the laser power, R_r is the repetition rate of laser, j is the number of repetitions, d_b is the bite size of laser.

The complete solution of dimensionless velocity $d\xi / d\eta$ by Andrews and

Atthey to first order in ε is

$$\frac{d\xi}{d\eta} = \left[1+\varepsilon\left\{erfc\left(\eta^{1/2}/2\right)/2-\left(\pi\eta\right)^{-1/2}e^{-\tau/4}\right\}\right]\left[(2/\pi)\left\{1+\varepsilon/(\pi\eta)^{1/2}\right\}\right]\arcsin\left\{\left(1-\pi\varepsilon^{2}/4\eta\right)^{1/2}\right\} \tag{48}$$

The dimensionless velocity in the writing of copper and tin with different laser intensity is shown in Fig.6.10.

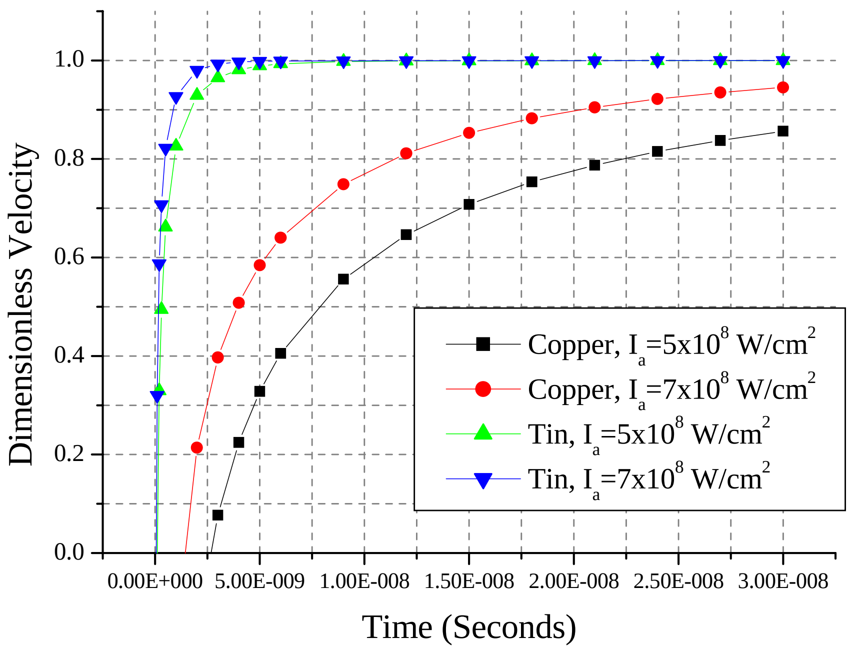

Fig.6.10 The dimensionless velocity in the structuring of copper and tin

The depth of space can be obtained on the base of the velocity of laser writing.

$$\xi = \int_{0}^{\frac{\tau v^2}{D}} \left[\frac{d\xi}{d\eta}\right] d\eta \tag{49}$$

where $d\xi/d\eta$ is expressed in Equation (48), ν can be calculated in Equation (47), τ is the pulse duration, D is the thermal diffusivity.

In order to obtain the depth of circuit spaces, the integral calculus is used to calculate the area under the function of velocity. An integral is a mathematical object that can be interpreted as an area or a generalization of area. The area of a surface is the amount of material needed to “cover” it completely.

Then the area under function $F(\eta)$ (as shown in Fig.6.11) can be written as

$$\xi = \lim_{n\to\infty}(\xi_1 + \xi_2 + \xi_3 + ... + \xi_n) = \lim_{n\to\infty}\sum_{i=1}^{n}\xi_i \tag{50}$$

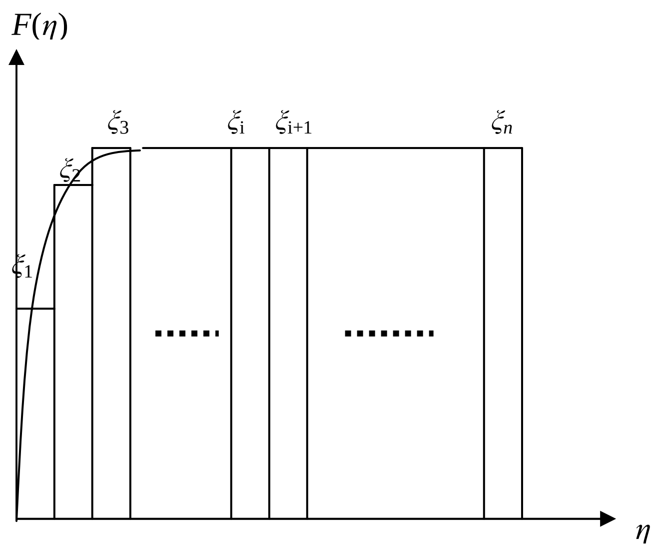

Fig.6.11 The approach to obtain the area of the region under function $F(\eta)$

The Riemann Integral method was used in solving the problem of calculating the area under the function of velocity. The Riemann Integral of the function $F(\eta)$ is written

$$\xi = \int_0^{\tau v^2/D} F(\eta)d\eta = \lim\sum_{i=1}^{n}\left(\frac{\xi_i + \xi_{i-1}}{2}\right)\Delta\eta_i\,, \quad \eta_n = \frac{\tau v^2}{D} \tag{51}$$

After the calculation of ξ, the parameter z can be got from

$$\xi = \frac{z}{l} \quad (l = \frac{D}{(I_a / h_m \rho)}) \tag{52}$$

Then $z(t, t = \tau)$ can be expressed as (with the combination of Eq.47, Eq.48, Eq.51 and Eq.52)

$$z(t, t = \tau) = d' = l\xi \tag{53}$$

The results of the depth of circuit spaces obtained from the analytical model (between the depth of circuit spaces and laser parameters) are compared with experimental results in Fig.6.12. The depth of space was measured by Boeckeler VIA-video The experimental results were the average value of five times of repeated experiments. From the comparison results, it shows that the analytical results and experimental results agree very well with the changes of laser power, number of repetitions, repetition rate and bite size. The errors of the analytical results are within ±10%. The experimental results were fabricated under the following laser parameters:

(1) Laser power and the depth of space: laser power=0.1-0.4 W, repetition rate=10 kHz, velocity=50 mm/s, bite size=5 μm and number of repetition=1;

(2) Number of repetitions and the depth of space: laser power=0.1 W, repetition rate=10 kHz, velocity=50 mm/s, bite size=5 μm and number of repetitions=1-4;

(3) Bite size and the depth of space: laser power=0.2 W, repetition rate=5 kHz, bite size=5-21 μm (velocity=bite size $\times$ repetition rate) and number of repetition=1;

(4) Repetition rate and the depth of space: laser power=0.1 W, repetition rate=2-10 kHz, bite size=5 μm (velocity=bite size $\times$ repetition rate) and number of repetition=1;

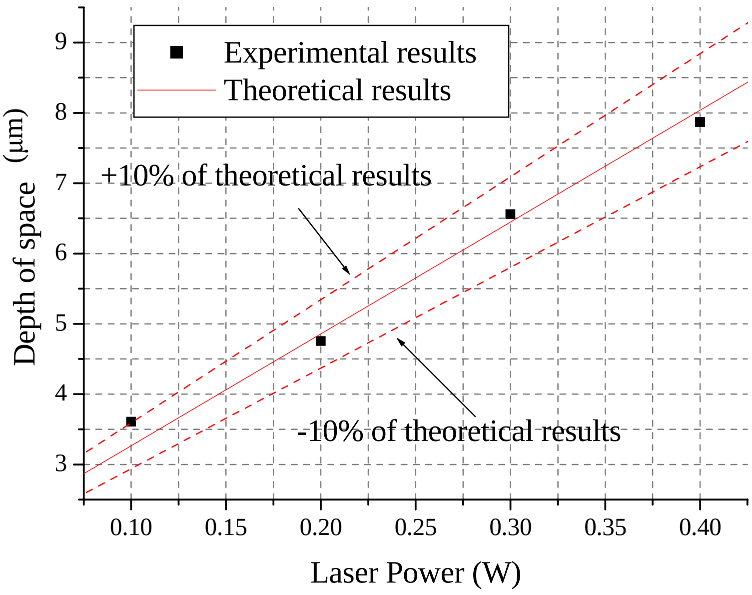
Experimental results
Theoretical results
+10% of theoretical results
-10% of theoretical results
Depth of space (μm)
Laser Power (W)
9
8
7
6
5
4
3
0.10
0.15
0.20
0.25
0.30
0.35
0.40

(a)

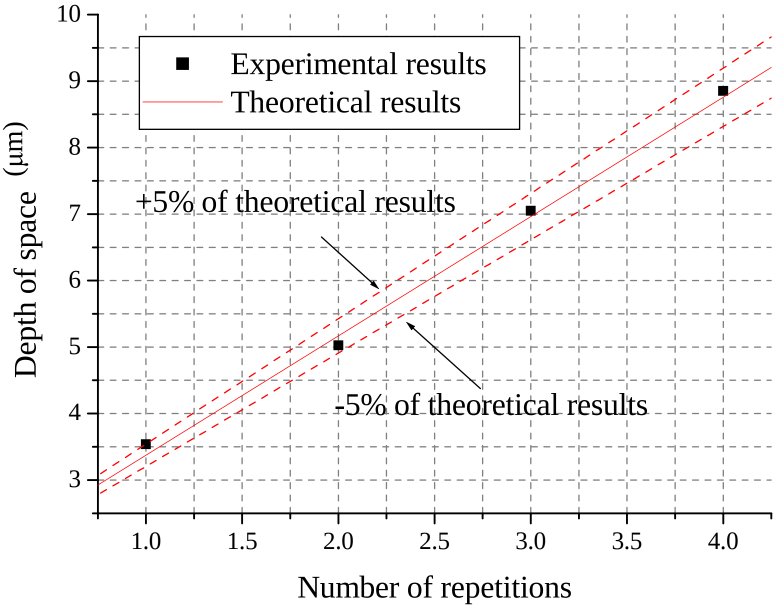
Experimental results
Theoretical results
+5% of theoretical results
-5% of theoretical results
Depth of space (μm)
Number of repetitions
10
9
8
7
6
5
4
3
1.0
1.5
2.0
2.5
3.0
3.5
4.0

(b)

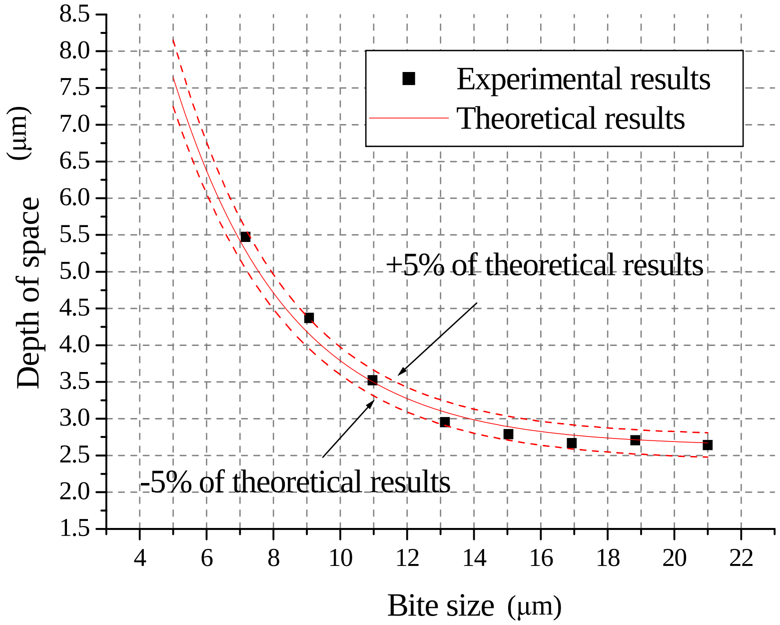

(c)

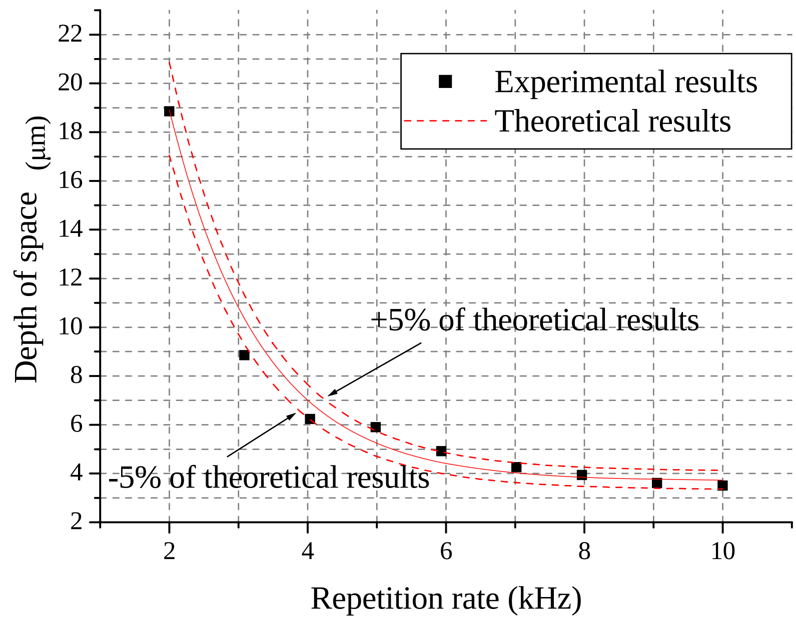

(d)

Fig.6.12 The comparisons of analytical results and experimental results

6.3.3 Combination of analytical model and ANN prediction model in the prediction of 2-D cross-sectional profiles of spaces

In this section, a 2-D model for the description of the cross-sectional profile of circuit spaces was built that combined a mathematical description of the Gaussian profile and the artificial neural network results.

The artificial neural network can predict the depth of space, width of space and resolidification height. These three parameters are important but cannot give us an entire view of the cross-sectional profile of space. Then on the basis of the characteristic parameters of space (the depth of space z, the width of space d and the resolidification height h), a 2-D profile of space is predicted with the help of mathematical method. The flowchart for the final prediction of the 2-D cross-sectional profile of circuit spaces is shown in Fig.6.13.

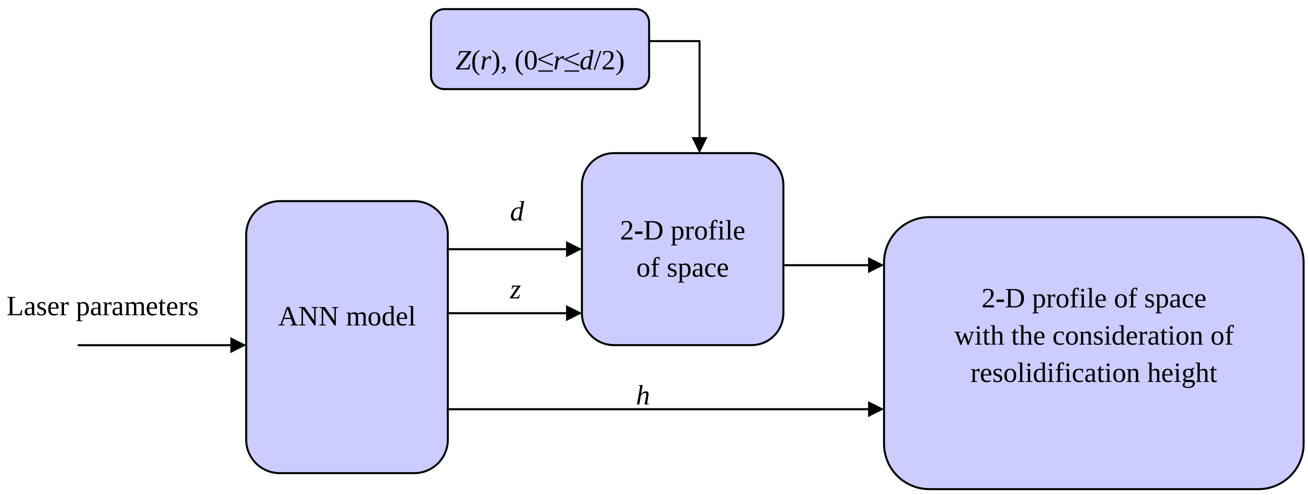

Fig.6.13 The flowchart of the prediction of 2-D profile of space

The laser used in practice to structure spaces typically produces a Gaussian intensity distribution, which is axi-symmetric. The function $Z(r)$ employing the axisymmetry to describe the relations between $Z(r)$ and r ($0 \le r \le d/2$), is given by

$$Z(r) = \frac{z}{(I_a - I_a^{\min})} \left(I_a e^{\left(\frac{-2r^2}{(d/2)^2} \right)} - I_a^{\min} \right) \tag{54}$$

where z is the depth of circuit spaces got from ANN model, r is the distance from the center of laser beam, d is the width of space, $I_a^{\min}$ is the minimum intensity to initiate vaporization of material, I_a is the laser intensity absorbed by material. The parameter $I_a^{\min}$ can be calculated as follows.

In the situation when $(Dt)^{1/2} >> \alpha^{-1}$, which may be encountered with strongly absorbent media such as metals, the temperature profile of material is given by

$$T(y,t) = T_0 + \frac{I_a (Dt)^{1/2}}{k} ierfc\left(\frac{y}{2(Dt)^{1/2}} \right) \tag{55}$$

where D is the thermal diffusivity, k is the thermal conductivity, y is a coordinate extending from the sample surface into the material, T_0 is the initial temperature, the *ierfc* is the integral of the error function. Then the temperature at the material surface is given by Duely (1996)

$$T(0,t) = T_0 + 2\frac{I_a}{k}\left(\frac{Dt}{\pi} \right)^{1/2} \tag{56}$$

The minimum absorbed laser intensity, $I_a^{\min}$, necessary to initiate significant material evaporation within a laser pulse length, τ, can be calculated from

$$I_a^{\min} = \frac{T_v - T_0}{2\left(\frac{1-R}{k} \right)\left(\frac{Dt}{\pi} \right)^{1/2}} \tag{57}$$

The minimum absorbed laser intensity for initiate the vaporization of material tin and copper is shown in Fig.6.14.

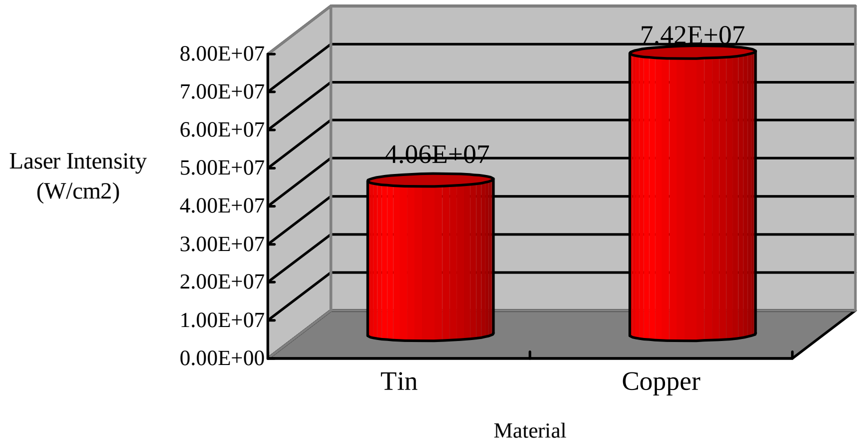

Fig.6.14 The minimum laser intensity necessary to initiate tin and copper evaporation

After the combination of Equation (54), (57) and the prediction results of ANN model, the 2-D model of the profile of the circuit spaces is obtained. In Fig.6.15, the results of 2-D model and the experimental results are compared. The four experimental results were obtained by a contact type measuring system—Talysurf PGI 1240 Measurement System. The four cross-sectional profiles of spaces were fabricated under the following laser parameters:

(1) laser power=0.15 W, number of repetition=2, repetition rate=6 kHz, bite size=6 μm;

(2) laser power=0.25 W, number of repetition=1, repetition rate=6 kHz, bite size=3 μm;

(3) laser power=0.35 W, number of repetition=1, repetition rate=8 kHz, bite size=6 μm;

(4) laser power=0.35 W, number of repetition=3, repetition rate=8 kHz, bite size=3 μm;

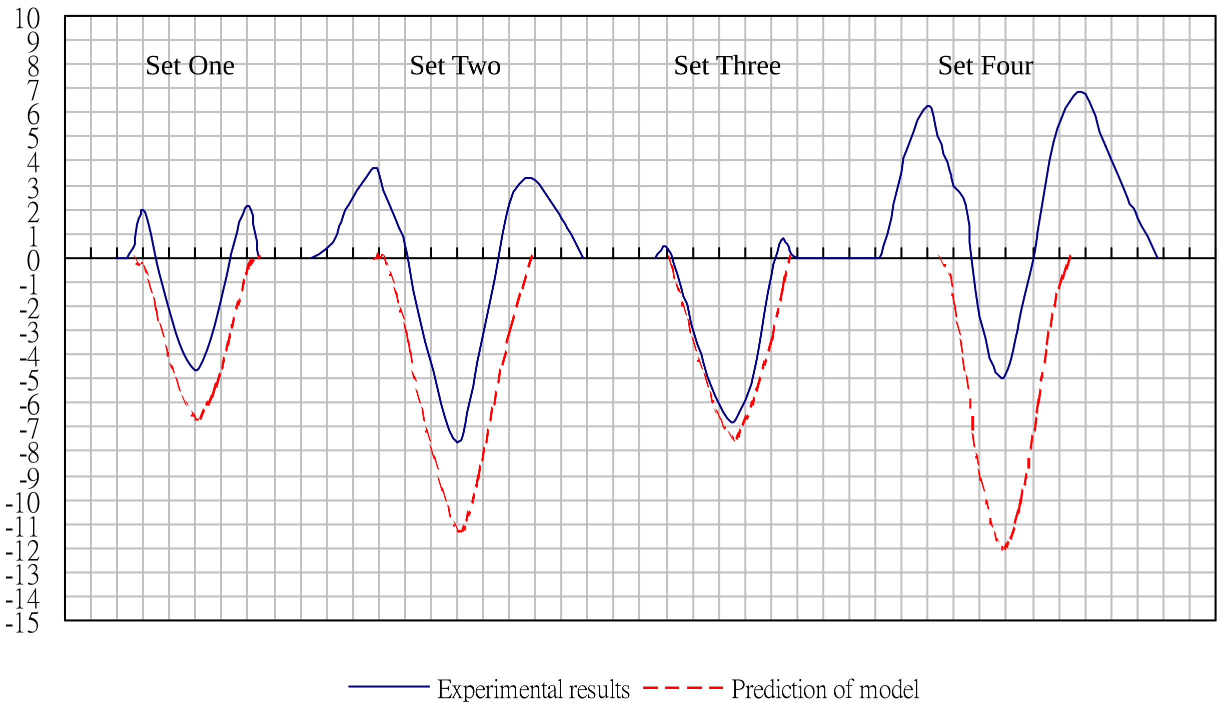

Fig.6.15 Comparison of experimental results and model prediction results under four sets of laser parameters

In this comparison, the situation of resolidification height was not considered. From the comparisons results from Fig.6.15, the cross-sectional profiles of spaces will vary a lot when the resolidification height is large. Thus, the resolidification height cannot be ignored and should also be added in the 2-D model.

After consideration of the resolidification height h got from ANN model, the function $Z(r)$ can be expressed by

$$\begin{cases} Z(r) = h + \dfrac{z}{(I_a - I_a^{\min})}\left(I_a e^{\left(\frac{-2r^2}{(d/2)^2}\right)} - I_a^{\min} \right) \\[2ex] Z\left(\dfrac{d}{2} + x\right) = Z\left(\dfrac{d}{2} - x\right) \qquad x[0, \dfrac{d}{2} - r'] \\[2ex] r' = \sqrt{-\dfrac{w^2}{2}\ln\left[\dfrac{\dfrac{(z-h)(I_a - I^{\min})}{z} + I^{\min}}{I_a}\right]} \end{cases} \tag{58}$$

where r' is the distance from the center of space to the place where the resolidification height begins, h is the resolidification height.

In Fig.6.16, the four experiments cross-sectional profiles of spaces with resolidification height were compared with the results of amended 2-D model. The prediction results of the model agree well with the experimental results after the consideration of resolidification height. After comparing Fig.6.15 and Fig.6.16, it can be seen that, the amended model shows its advantages especially when resolidification height were large as in Fig.6.16b and d. The amended model is good in the prediction of the 2-D cross-sectional profile of circuit spaces.

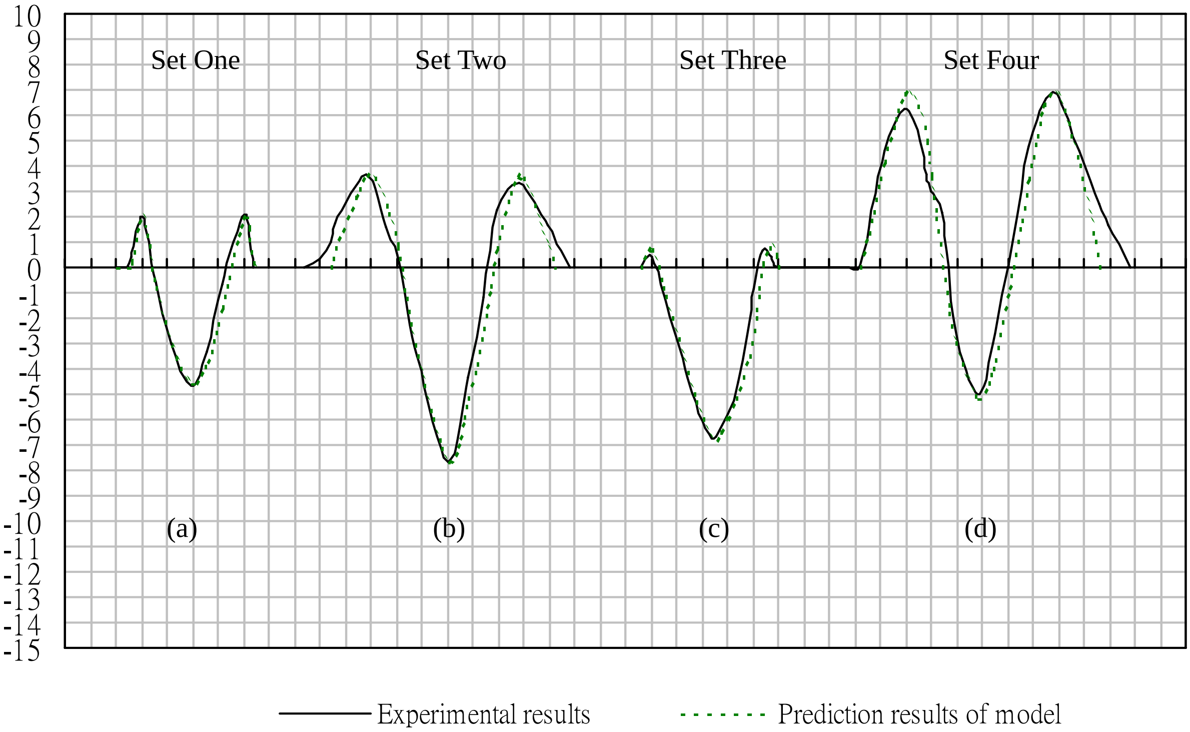

Fig.6.16 Comparisons between the model prediction results and experimental results of the 2-D cross-sectional profiles of circuit spaces with consideration of resolidification height *h* under four sets of laser parameters

The prediction results of *d*, *z* and *h* in this 2-D model are determined by the input process parameters of the ANN prediction model. If one set of process parameters is selected, the 2-D geometry of the circuit space under this set of parameters can be calculated. This new approach gives a quick and convenient way to figure out the 2-D geometry of circuit space by knowing the process parameters.

6.4 Analysis of copper etching process in chemical solution

6.4.1 Copper etching by $Cu(NH_3)_4Cl_2$ in ammoniacal solutions

Copper etching in ammoniacal solution is generally used in the manufacture of printed circuit boards. The process involves the oxidation of metallic copper by an ammoniacal cupric complex leading to an ammoniacal cuprous complex. Concomitantly, the cuprous complex is oxidized by oxygen in order to regenerate the starting cupric complex.

The copper that is dissolved in solution already is the catalyst that is used to dissolve the copper metal on the board. The metal is dissolved by being “Oxidized”, which means that it loses electrons, which changes it from a yellow/gold-colored metal to a blue compound. The electrons are initially removed from the metal by the copper in solution. This oxidation process can happen because copper can exist in three ways, as metal, as cupric salts (which are the blue compounds), and as a third form cuprous salts (which is halfway between the yellow metal and the blue salts) Cuprous salts are typically white.

1. Metal - copper with a correct amount of electrons;
2. Cuprous salts, Cu^{+}(white) - copper missing one electron;
3. Cupric salts, Cu^{2+}(blue) - copper missing two electrons.

The initial metal dissolving reaction is that Cu (metal) reacts with Cu^{2+}(Blue) to give 2 Cu^{+}(cuprous) (as shown in Fig.6.17). The cuprous salts are then immediately oxidized (electrons removed) by the oxygen in the air, and in the process the oxygen is converted into water in the etchant. All of this is facilitated by the ammonia etchant, because the cuprous (Cu^{+}) compounds are not soluble except in the presence of the ammonia (NH_3). And the overall reactions are these:

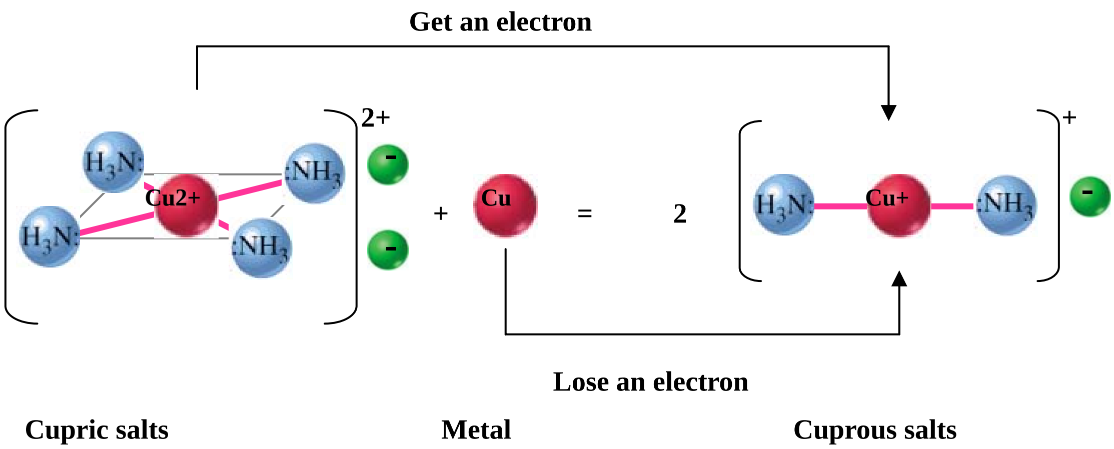

Fig.6.17 The oxidation process of copper into solutions

Then the air reacts with the Cuprous to change it to the Cupric:

$$2Cu(NH_3)_2\,Cl + 2NH_3 + 2NH_4Cl + O \rightarrow 2Cu(NH_3)_4\,Cl_2 + H_2O \qquad (59)$$

(Cuprous) (ammonia etchant) (Air) (Cupric, Blue)

In this alkaline environment, both cuprous and cupric ions are complexed by ammonia. Cuprous chloride is re-oxidized by oxygen from the air to provide cupric ions for the further oxidation of copper.

6.4.2 An analytical method in the prediction of the depth of circuit spaces during etching step

In this section, we develop a one-dimensional analytical model for the prediction of the depth of circuit spaces in the etching process.

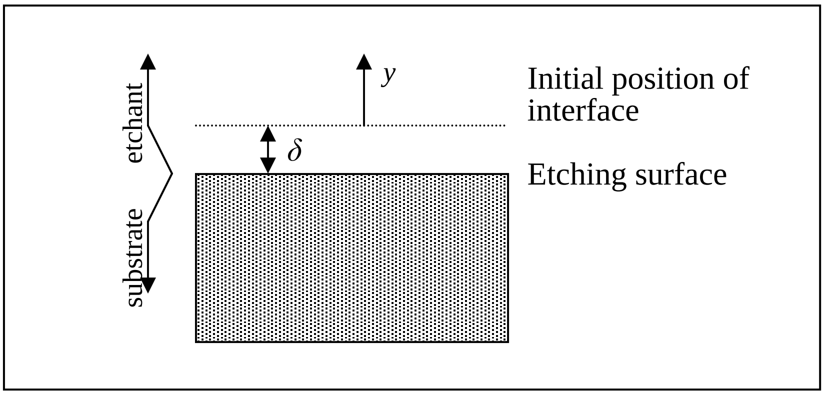

Fig.6.18 Geometry for one-dimensional etching

In Fig.6.18, it shows a one-dimensional geometry that partly occupied by the solid to be etched and the remaining part is filled with etching liquid. The etching direction is measured by the coordinate *y*, which assumes the value zero at the initial (t=0) position of the interface. At any subsequent time, the location of the interface is denoted by $y = -\delta$. According to the Fick's second law of diffusion in the region $y > -\delta$

$$\frac{\partial C}{\partial t} = \frac{\partial}{\partial y}\left(D_e \frac{\partial C}{\partial y} \right) \quad (t \geq 0, y > -\delta) \tag{60}$$

where C (mol/m^3), D_e (m^2/s), t are the concentration of the etchant, the diffusion coefficient of the etchant and the time. The initial condition is

$$C = C^b, \delta = 0 \quad \text{at} \quad t = 0 \tag{61}$$

the first of the two conditions prevailing for all $y \geq 0$. Subsequently, the bulk concentration C^b will be approached at a sufficiently large distance from the interface

$$C \to C^b \text{ when } y \to \infty \ (t>0) \tag{62}$$

Since $-d\delta/dt$ is the inward-directed velocity at which the interface proceeds into the solid, a simple mass balance shows that

$$\frac{d\delta}{dt} = \sigma_e \frac{\partial C}{\partial y} \quad \text{at} \quad y = -\delta \quad (t>0) \tag{63}$$

where σ_e is given by

$$\sigma_e = \frac{D_e M_s}{m\rho_s} \tag{64}$$

Here, M_s is the molecular weight of the solid, ρ is its density, and m represents the number of molecules of active etching component required to dissolve one molecule of the solid.

The solution can be written as follows (Kuiken, Kelly & Notten, 1986)

$$C = C^b \frac{\int_{-\gamma}^{\frac{y}{2}(D_e t)^{1/2}} e^{-x^2} dx}{\int_{-\gamma}^{\infty} e^{-x^2} dx} \tag{65}$$

where γ is a constant that is implicitly given by

$$2\gamma e^{\gamma^2} \int_{-\gamma}^{\infty} e^{-x^2} dx = 1/\beta \tag{66}$$

The dimensionless parameter β appears to be important in the mathematical description of etching processes. It may be written as follows

$$\beta = \frac{m\rho_s}{C^b M_s} \tag{67}$$

Once the essential chemical or electrochemical reaction determining a particular etching process is known, one may calculate β from the known values of the physical quantities that appear on the right hand side of equation (67). The speed of the etch front is inversely proportional to β. In general the initial etchant concentration is higher, the etch rate should be higher. It is clearly evident from the definition of β as it is inversely proportional to the initial etchant concentration. So high initial etchant concentration leads to lower value of β which leads to the faster movement of the etch front as mentioned above.

In diffusion-controlled etching the reaction rate at the interface is infinitely fast compared to diffusion of etchant to the interface. Therefore, for a given diffusion coefficient of etchant, if $\kappa >> D_e$, κ is the rate constant of reaction, then the etching process can be assumed diffusion-controlled. The position of the moving interface can be obtained by (Kuiken, Kelly & Notten, 1986; Westberg, 1996)

$$\delta = 2\gamma(D_e t)^{1/2} \tag{68}$$

In the reaction-controlled etching, the reaction rate is finite. The position of the moving interface of reaction-controlled etching can be obtained by (Westberg, 1996; Rath, 2005)

$$\delta = 2\gamma^2 k_r t \tag{69}$$

where k_r is a constant determined by a chemical reaction.

In Fig.6.19, the changes of depth during etching process are compared with diffusion-controlled etching and reaction-controlled etching. In both of these cases, the diffusion constant is consider as 10^{-5} cm^2/s, and dimensionless parameter β=1. In reaction-controlled etching, the etch depth increases in a linear way. In diffusion-controlled etching, the etch depth increases fast at first and then does not vary much with the increase of etching time. In Fig.6.20, it shows the comparison of etch depth for five β values in reaction-controlled etching process. It is seen that as the value of β increases, the etch depth decreases. This is because β is inversely proportional to the initial etchant concentration for a given etchant-substrate combination.

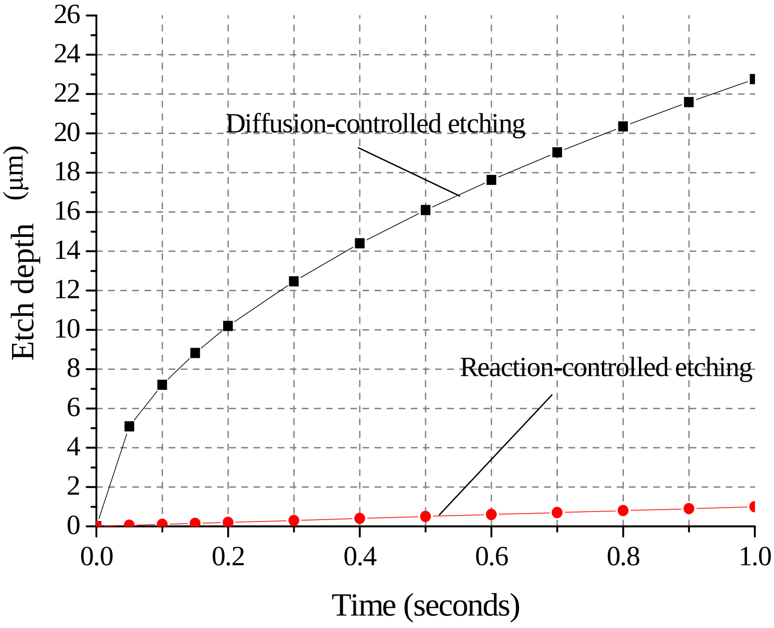

Fig.6.19 Comparison of etch depth for one seconds in diffusion-controlled and reaction-controlled etching with D=10^{-5} cm^2/s and β=1.

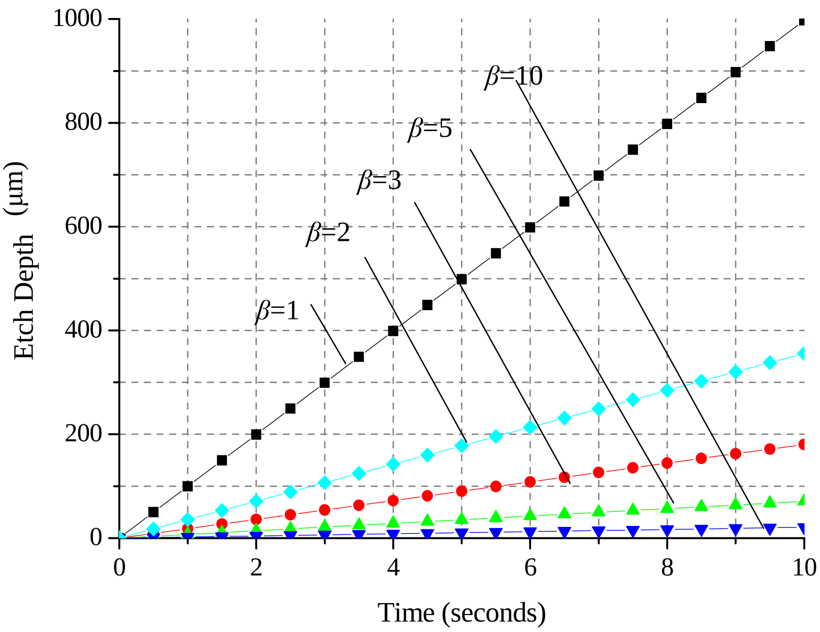

Fig.6.20 Etch depths in reaction-controlled etching with β=1, β=2, β=3, β=5 and β=10.

In the copper etching process of laser structuring, the diffusion constant D_e is about 10^{-5} cm^2/s and the reaction rate of constant κ is in the region of 10^{-5} cm^2/s. In this situation, κ is not much larger than D_e as in the diffusion-controlled etching. The etching process here is a reaction-controlled etching. The value β of copper etching by $Cu(NH_3)_4Cl_2$ solution is calculated by Equation (67) and is shown in Table 6.2. In this typical etching system, etchant is constructed by $CuCl_2/NH_3/H_2O$. The concentration of Cu^{2+} was 2 mol/L.

Table 6.2 Some important parameters in the copper etching system

Solid		Cu
Etchant		$CuCl_2/NH_3/H_2O$
Rate-determing	Species	Cu^{2+}
	Concentration	2M
m		1
β		70
γ		0.00806

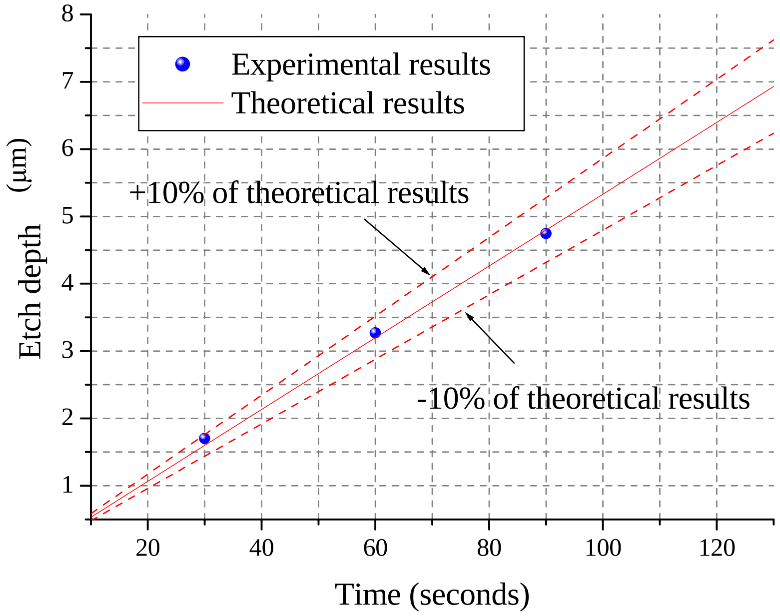

Fig.6.21 The comparisons of etch depth with analytical results and experiment results

In Fig.6.21, the results of the depth got from analytical model are compared with experimental results. As shown in Fig.6.21, the differences between the experimental results and the analytical results are within ±10%. Thus, this analytical model is good in the prediction of copper etching depth. Then the copper etching process can be controlled with this model to predict the depth of space during etching process.

CHAPTER 7

QUALITY AND RELIABILITY OF LASER STRUCTURING

7.1 Experiment set up of quality and reliability test

7.1.1 Open/short test

Many drawbacks which may be overlooked in the past should be paid attention to with the small circuit feature size. In order to guarantee final electrical performance of each circuit, open/short tests have been required to guarantee the electrical quality of fine circuit lines and circuit spaces. When the size of circuit features shrink below 50 μm circuit lines/spaces, small defects of lines and circuit spaces may cause open/short problems as shown in Fig.7.1.

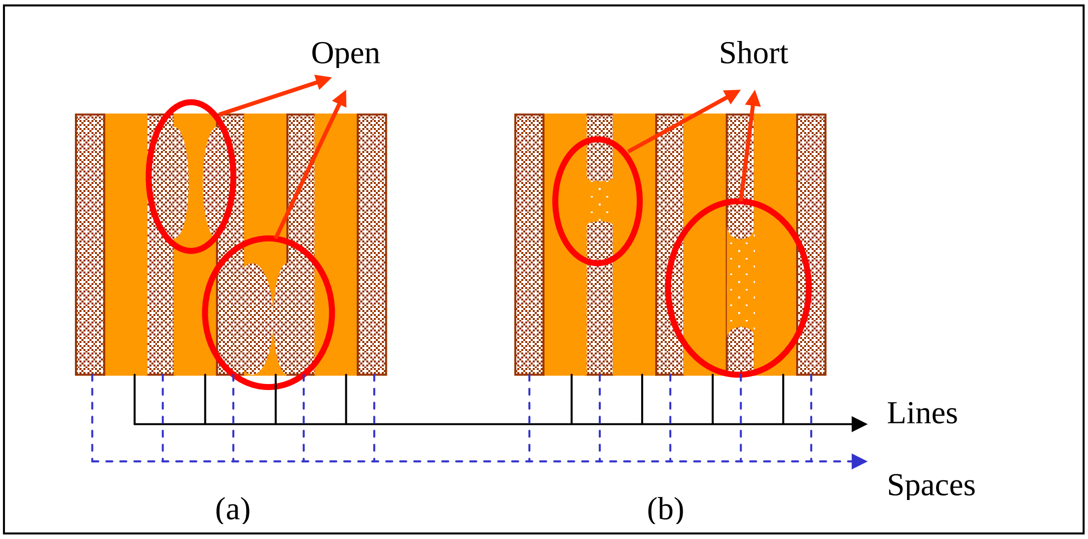

Fig.7.1 Defects of open and short

The specimen in this experiment is designed as shown in Fig.7.2. A multimeter is used to test the open/short of fine lines and circuit spaces in this section which is commonly used to measure voltage and resistance between two points. The steps to measure the resistance of circuit lines/spaces with a digital multimeter were as follows:

1.The multimeter was set to a resistance range greater than the expected resistance of the specimen;

2.The multimeter probes were touched together to check that the meter reads zero;

3.The probes were put across the components (as shown in Fig.7.2).

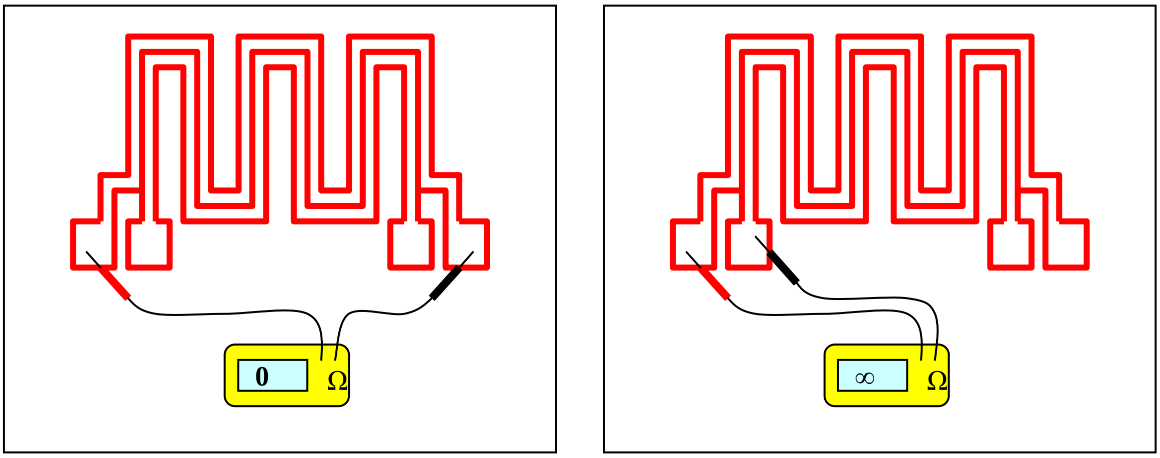

(a) (b)

Fig.7.2 Open (a) and short (b) test of circuit lines/spaces fabricated by laser structuring

If there is no "open" in the fine circuit lines, the resistance of the circuit lines should be near zero. Copper has the best electrical conductivity of any metal, except silver. A good electrical conductivity is the same as a small electrical resistance. If the circuit lines are open, the resistance of circuit lines includes the resistance of copper lines and the resistance of epoxy resin at the open spot of copper lines. Epoxy resin is an insulator and the resistance of it is much larger than copper. So in this case, the resistance of circuit lines will be large when there is open in the circuit lines.

The short between circuit lines can also be tested with the multimeter. If there is no short between circuit lines, the resistance between circuit lines should be near ∞ (infinitely large) because of the high resistance of dielectric material between circuit lines. If short exists, the resistance between circuit lines will decrease obviously because of the low resistance of copper remaining between circuit lines.

When the resistance of circuit lines is near zero and the resistance between circuit lines is near ∞, the circuit lines and circuit spaces are acceptable under the open/short tests.

7.1.2 Peel test

A copper foil on epoxy resin substrates are commonly used for fine circuit lines and high-density electronic interconnection applications. The basic adhesion is the interfacial bond strength, which depends on the interfacial properties or interaction (electrostatic, chemical, van der Waals) and mechanical interlocking. The peel strength test is the most commonly used method to determine the adhesion of copper on the base material of PCB. In laser structuring process, the materials are exposed to chemical environments in the copper etching and tin stripping steps. Circuit fabrication can degrade adhesion of copper to base material. As there is no chemical bonding between copper and epoxy, the peel strength of a copper layer on any epoxy surface depends mainly on the structure on their interface.

IPC TM-650 2.4.8.1 (peel strength industrial test standard for thin laminates) describes the procedure for the peel test. Each test requires a minimum of two strips measuring 3.18 mm wide per specimen as shown in Fig.7.3. The tab to be clamped onto the load applicator is to be no longer than 12.72 mm long. The specimen is fixed to maintain a peel at an angle of 90°. A force is applied in the vertical direction at 50.88 mm per minute, and the specimen must be peeled for a minimum of 25.44 mm. The actual width of the test strip is then measured and recorded along with the minimum load. The width of the conductor is measured and recorded to calculate the peel strength.

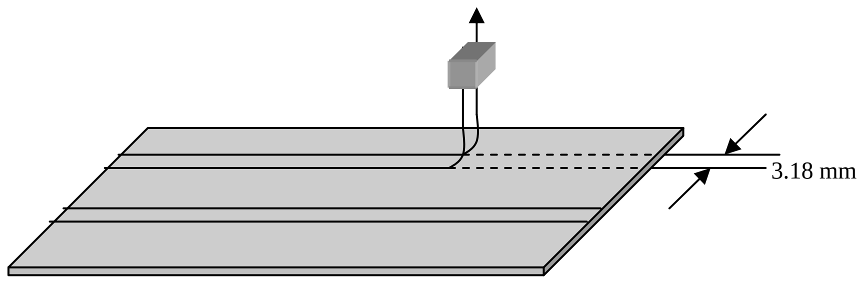

Fig.7.3 The specimen of peel test

The IPC TM-650 2.4.8.1 test is used to test the adhesion strength of a foil on another material. In this work, the peel test was used to test the adhesion of a copper layer on dielectric material. Then a further test of the adhesion of fine circuit lines fabricated by laser structuring on basis material was carried out. The aim of this test was to see whether the fine circuit lines would adhere onto the base material tightly after they had been subjected to laser writing and chemical influences in the LS process. Special structures were arranged on these test circuits to enable a representative sample of layout to be studied. The test samples are described in

Fig.7.4. The adhesion of fine circuit lines on base material was checked by the cross section image measured by a Boeckeler VIA-video.

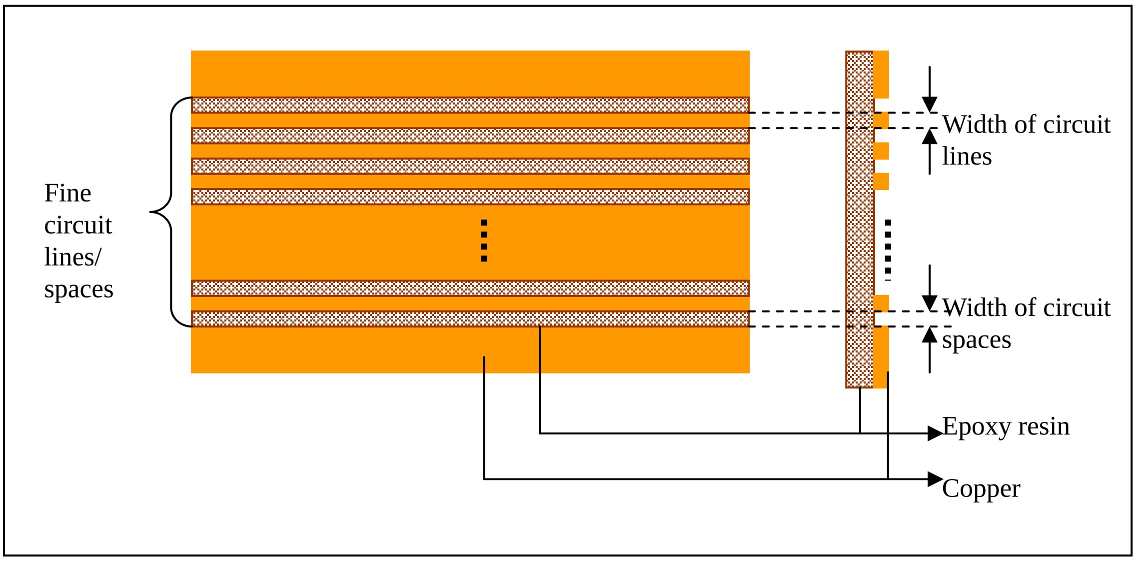

Fig.7.4 Specimen of the adhesion of fine circuit lines

7.1.3 Surface insulation test (SIR test) under thermal and humidity cycling

Metal migration between isolated conductors may produce electrical shorts. In simple terms, shorts occur when the space between the conductors is bridged by re-deposited metal ions. The added presence of moisture can cause ionic residues to disassociate into either negatively or positively charged species and create conductive solutions, known as electrolytic solutions. When there is a voltage bias between cathode and anode, an ionic species will grow from one conductor to another. Metallic salts will conduct electricity and create shorts across the spaces. SIR testing was performed to determine whether the circuit lines/spaces used in an assembly are likely to produce unacceptable current leakage levels, or shorts due to metal migration between conductors.

The surface insulation resistance test was used here as a test method to examine the insulation between fine circuit lines under humidity, bias voltage, pressure and thermal cycling. The specimen of intermeshing comb structures is shown in Fig.7.5 to test the insulation resistance between fine circuit lines fabricated by laser structuring. Each comb (a and b) consisted of several fingers which were separated and insulated from each other by the laser-structured spaces.

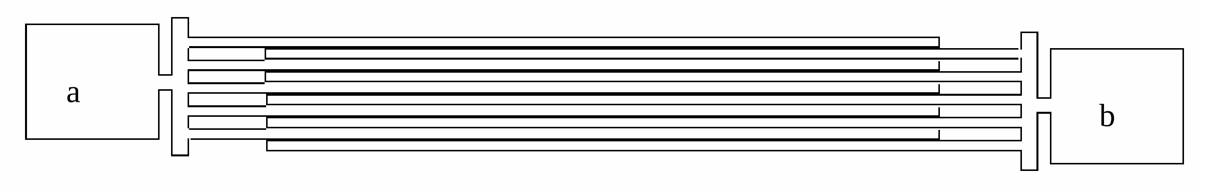

(a)

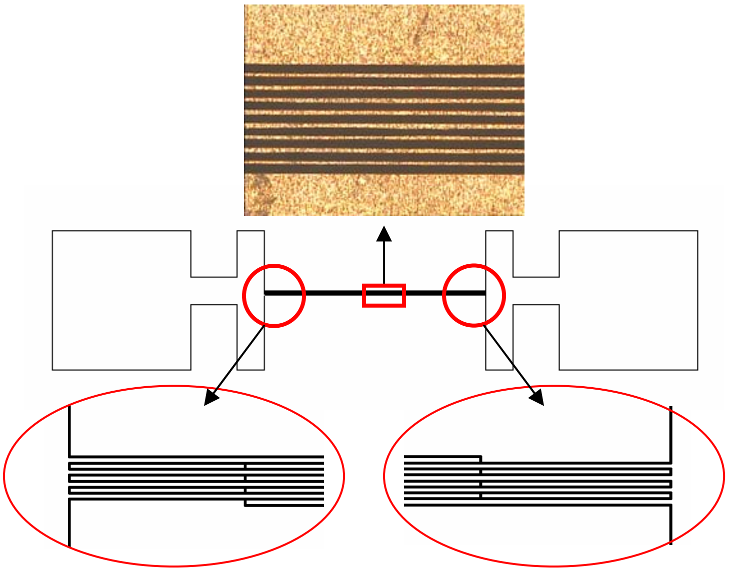

(b)

Fig.7.5 Specimen of surface insulation test

(a) The structure of the SIR specimen

(b) The SIR specimen

Before the SIR test, the specimen was tested by multimeter first as shown in

Fig.7.6. If a, b, and c were insulated (resistance is near ∞ ohm) from each other, then the specimen was ready for the SIR test.

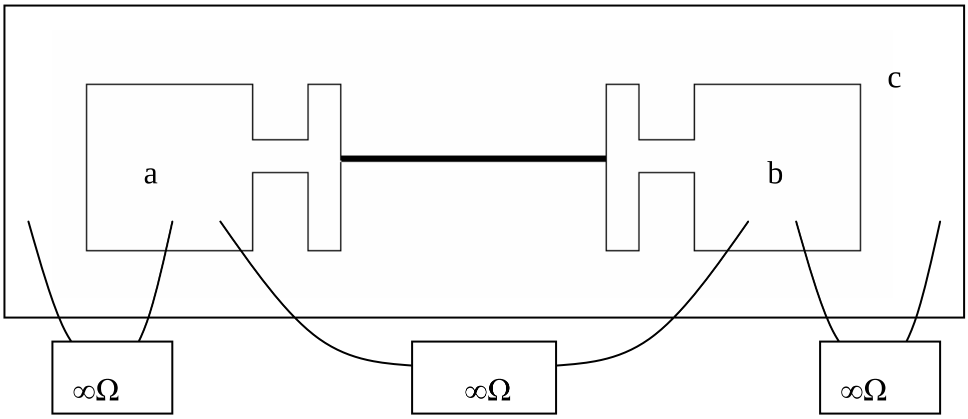

Fig.7.6 Preparation step before SIR test

The IPC test method of surface insulation under high humidity and heat conditions (2.6.3.3A), is listed below: 20 cycles of temperature ranging form 25+5/-2 °C to 65±2 °C, 85—93% relative humidity, 100 ± 10% volts and 160 hours in total.

(1) 25→65 °C, time spans 150 minutes (9000 seconds) ±5 minutes (300 seconds)

(2) 65±2°C, time spans 180 minutes (10800 seconds) ±5 minutes (300 seconds)

(3)65±2°C→25°C, time spans 150minutes (10800 seconds) ±5 minutes (300 seconds)

This test used a high temperature (65 °C), high relative humidity (about 85%), under high atmospheric pressure conditions (up to 4 atm). The high atmospheric pressure conditions can decrease the test time needed to get useful results.

The SIR test system (ion migration evaluation system) used in this research integrated with two modules. They were Environmental Chamber PL-2KPH and Measurement Unit AMI-050-P. The ion migration evaluation system systemizes the environmental test chamber and measurement/evaluation system. It offered continuous, accurate and effective ways to collect insulation resistance data by applying stress voltage over specimens under specific temperature and humidity condition.

7.2 Results and analysis of open/short test

Table 7.1 shows the open/short test results with different widths of circuit lines and circuit spaces and etching time. The originally designed widths of circuit lines (before etching step) were 55 μm, 50 μm, 45 μm, 40 μm and 35 μm. Etching time in the etching step was selected at 240 seconds, 300 seconds, 360 seconds and 420 seconds The etching rate was about 1.5 μm/min according to the calculation results of etching model. In order to etch through the copper layer (less than 9 μm), the etching time was selected above 240 seconds in the light of previous experiments. After etch etching step, the widths of circuit lines decreased with the increase in etching time. When etching time was 240 seconds, the copper between the circuit lines were not etched away totally and the resistance between circuit lines were not infinitely large (∞). So the short tests failed in these cases. After increasing the etching time (300 seconds, 360 seconds and 420 seconds), the resistance between circuit lines were shown as ∞. It showed that the short tests succeeded when etching time was above 300 seconds. When etching time was above 300 seconds, the widths of circuit spaces were above 40 μm.

Table 7.1 The open/short tests of circuit lines/spaces with different pre-designed line widths under the etching time of 240, 300, 360, and 420 seconds

Line width before etching (μm)	Etching Time (seconds)	Width of Line/space after etching (μm)	Quality of open test of circuit lines	Quality of short test between circuit lines	Quality of open/short test
55	240	41±5/37±5	√	×	×
	300	38±5/40±5	√	√	√
	360	35±5/43±5	√	√	√
	420	32±5/46±5	√	√	√
50	240	36±5/37±5	√	×	×
	300	33±5/40±5	√	√	√
	360	30±5/43±5	√	√	√
	420	27±5/46±5	√	√	√
45	240	31±5/37±5	√	×	×
	300	28±5/40±5	√	√	√
	360	25±5/43±5	√	√	√
	420	22±5/46±5	×	√	×
40	240	26±5/37±5	√	×	×
	300	23±5/40±5	×	√	×
	360	20±5/43±5	×	√	×
	420	17±5/46±5	×	√	×
35	240	21±5/37±5	×	×	×
	300	18±5/40±5	×	√	×
	360	15±5/43±5	×	√	×
	420	12±5/46±5	×	√	×

From Table 7.1, it is clear that the circuit lines/spaces passed the open/short tests are the original designed circuit lines with the width of 55 μm and the etching time of 300 seconds, 360 seconds and 420 seconds; the width of 50 μm and the etching time of 300 seconds, 360 seconds and 420 seconds; the width of 45 μm and the etching time of 300 seconds and 360 seconds. The results of these experiments were that the widths of circuit lines/spaces were 38±5/40±5 μm, 35±5/43±5 μm, 32±5/46±5 μm, 33±5/40±5 μm, 30±5/43±5 μm, 27±5/46±5 μm, 28±5/40±5 μm and 25±5/43±5 μm. The widths of circuit lines passed the open test were above 25 μm and the widths of spaces between circuit lines passed the short test were above 40 μm. That is to say, the minimum width of circuit lines and circuit spaces with good results of open/short test was 25 μm and 40 μm.

The final widths of circuit spaces varied about ±5 μm after laser writing and copper etching steps (the widths of circuit lines varied about ±5 μm at the same time). The variation of the width of circuit spaces was caused by fabrication process and the width of circuit lines varied accordingly. If the width of circuit line was 30 μm at average after the etching step, the maximum and minimum widths of circuit lines were about 35 μm and 25 μm. When the variance of the widths of the circuit lines is ±5 μm, the variance of the width of the circuit line is ±20% and the variance of the width of the circuit space is ±12.5%. According to IPC 6011, a tolerance of ±20% in the line and space widths is considered acceptable for the fine circuit lines/spaces. The variation of line width is caused in laser writing step and copper etching step.

In the laser writing step, there are two main causes in the variation of the widths of final lines and circuit spaces, these are the bite size of the laser and the splashing problem. As shown in Fig.7.7a, in the laser writing step, the width of circuit spaces was not the same, which is caused by the moving of the laser (bite size of laser). The variation of the width of space increases with the increase of bite size. So the bite size is always selected at the value that is equal or less than laser radius (Zhang & Yung, 2006). The second reason is the splashing of copper during laser writing process. The splashing liquid copper may cause the tin layer to melt. When the tin layer melts, it cannot act as resist in copper etching process and causes enlargement of widths of spaces. Besides these two main reasons, the uniformity of the thickness of tin layer and the little vibration of laser power during laser writing step can also cause variation of the width of circuit spaces.

In the copper etching process, the main cause of variation of the width of lines and circuit spaces is the cracking problem of the tin layer as shown in Fig.7.7b. When the copper under the tin layer is etched away, the tin layer, which is very thin in thickness, will crack without the support of the copper under it. The cracked tin may cover the copper material in some places and prevent the copper from being etched away in the following time. Then the width of circuit spaces in such a place will be smaller than in other places.

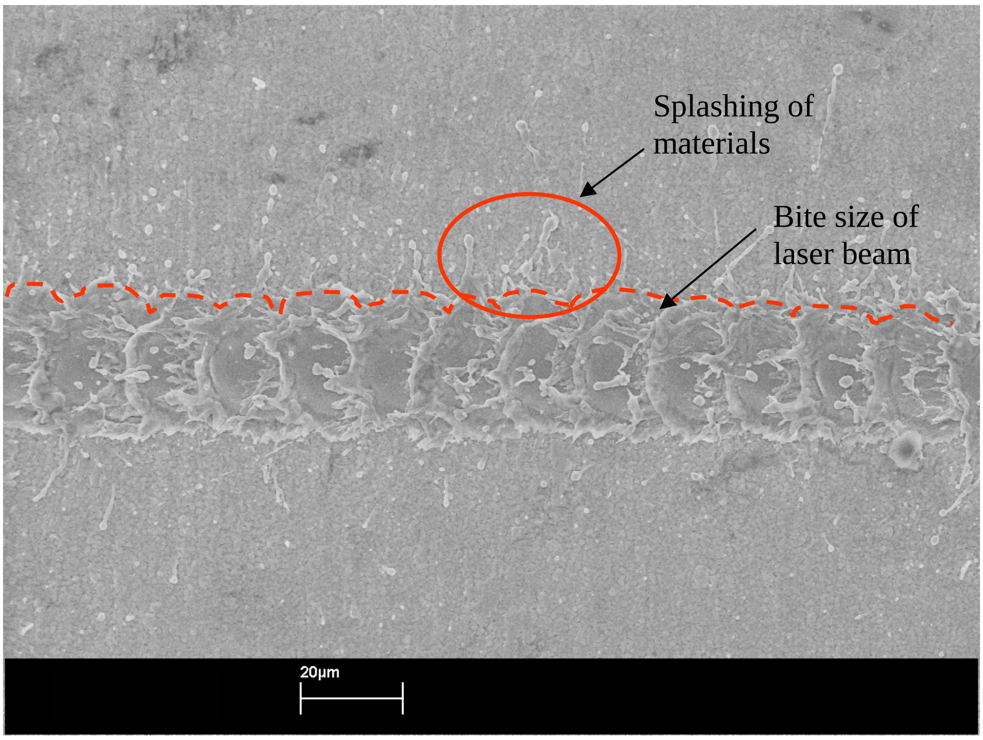

(a)

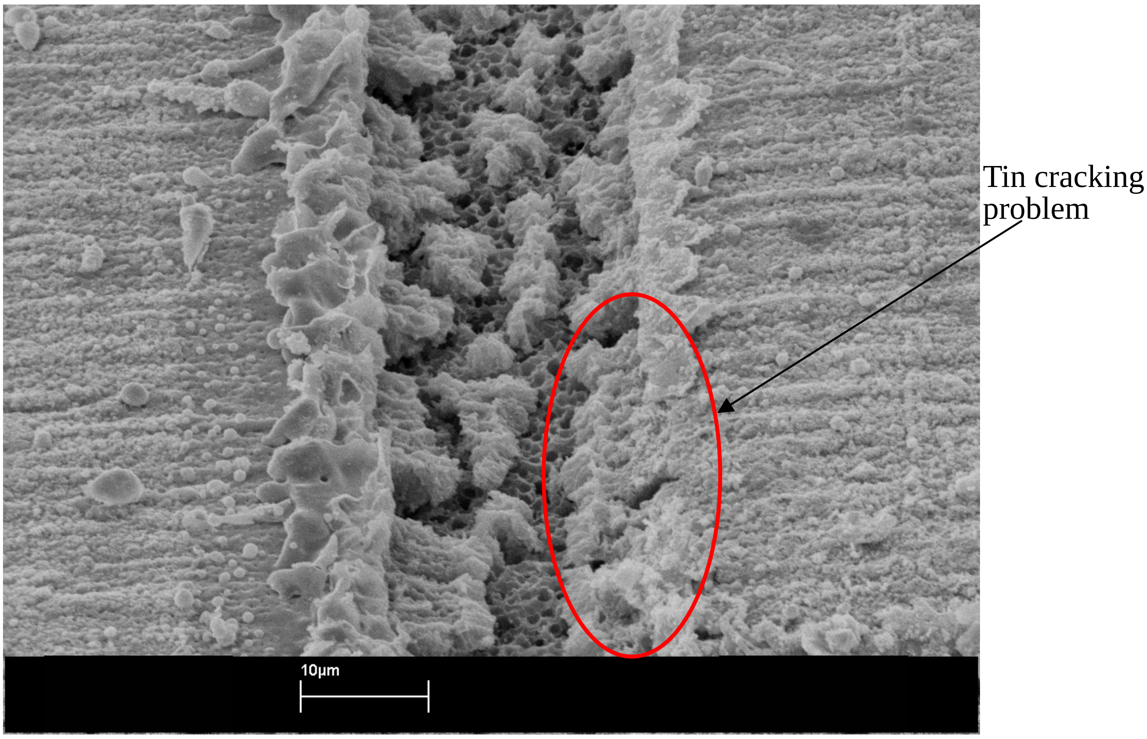

(b)

Fig.7.7 The causes of variation of the widths of circuit lines and circuit spaces in (a) the laser writing step and (b) the copper etching step

Opens in the circuit lines and shorts between the circuit lines are shown in Fig.7.8. In Fig.7.8a, the width of the circuit line with circle is thinner than that of other places. In Fig.7.8b, the places circled with line still have copper left after the etching step. These two situations are both caused by variation of the widths of circuit lines and circuit spaces. The variation of the widths of lines and circuit spaces caused by bite size can be reduced by the decrease of bite size value. The splashing problem can be lessened by selecting proper laser parameters-such as low laser power and small number of repetitions. The influences of tin crack problem on variation of the widths of lines and circuit spaces can be reduced by decreasing the etching time in etching step. By keeping attention to the problems above, the emergence of open/short problems can also be decreased.

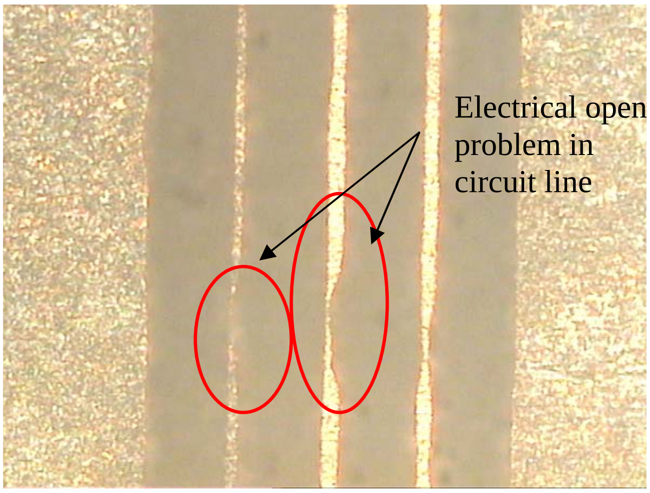

(a)

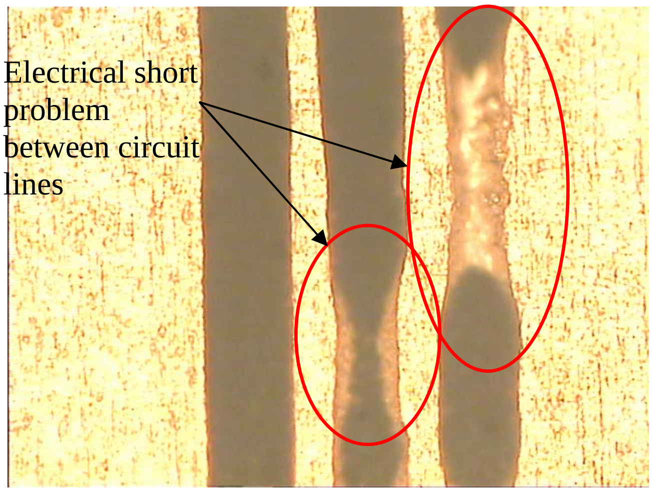

(b)

Fig.7.8 (a) The failure of the open test

(b) The failure of the short test

The aim of the open test of the circuit line was to guarantee that the circuit lines were continuous after etching step. Because the width of the circuit line was very small, the circuit line could easily get broken in the etching step. After the open tests of the circuit lines, it can be concluded that the results of the open tests were acceptable when the widths of circuit lines were above 25±5 μm. When the widths of circuit lines were under 25 μm, part of circuit lines were disconnected and the whole circuit lines were discontinuous. With the decrease in the width of the original designed circuit lines and the increase in etching time, the phenomenon of discontinuous lines was more obvious.

7.3 Results and analysis of peel test

The cross section view and the top view of the basic material (FR4 laminate) used in this research are shown in Fig.7.9. The interface between copper layer and epoxy resin layer was not smooth. The surface of the copper layer was pretreated to make it more easily adhere to epoxy resin layer. The roughness between the two materials can improve the adherence of these two materials.

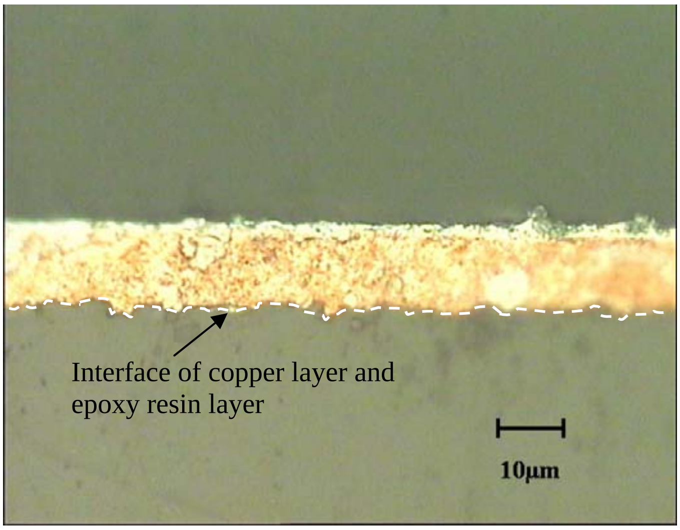

(a)

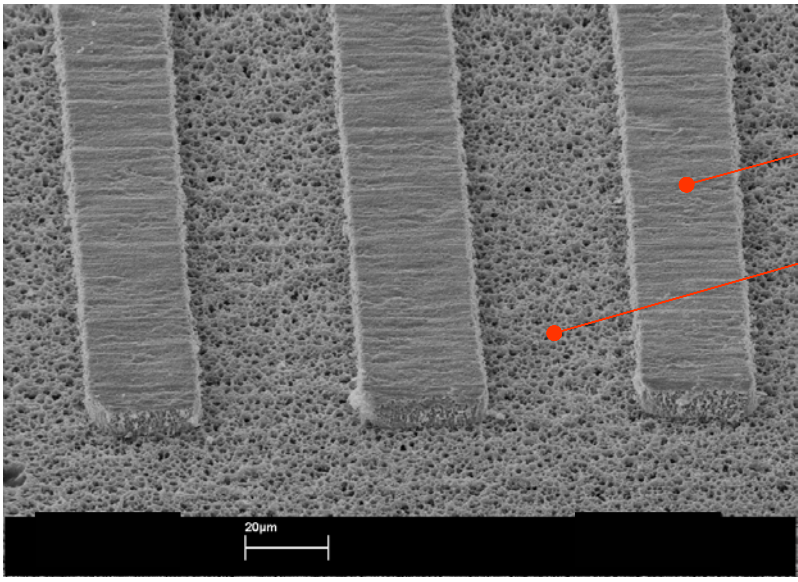

(b)

Fig.7.9 The interface between copper layer and epoxy resin layer:

(a) From cross section view, (b) From the top view

The test results of the IPC TM-650 2.4.8.1 about the adhesion of the copper layer on an epoxy resin layer, are shown in Table 7.2. These results were selected from four different samples. According to the IPC calculation formula

$$\text{kg/mm (lbs/in)} = L_M / W_S \tag{1}$$

where L_M = Minimum load, W_S = Measured width of peel strip. The minimum loading of these four samples was from 0.2858 kg to 0.2994 kg. All the conductor widths were the same at 3.18 mm. The calculation results of peel strength were also listed in Table 7.2.

Table 7.2 The results of the peel strength test

	Loading (kg)	Conductor width (mm)	Peel strength (kg/mm)
1	0.2994	3.18	0.094
2	0.2994	3.18	0.094
3	0.2858	3.18	0.090
4	0.2948	3.18	0.093

The maximum and minimum peel strengths of these samples were 0.094 kg/mm and 0.090 kg/mm. The variation of the peel strength among these samples was very small. That is to say, the quality of the adhesion of copper layer on the epoxy resin layer was stable. All of the values of the peel strength were above IPC specifications (IPC-FC-241C/18) of 0.036 kg/mm for thin materials and 0.071 kg/mm for thick materials (Bergstresser, 2003). The test of peel strength of the copper layer was performed in order to guarantee the adhesion quality of fine circuit lines. High copper peel strength allows for thinner etched line widths.

Fig.7.10 shows the adhesion situation of copper lines on base material with different line width after etching step has been completed in laser structuring. The micrographs in Fig.7.10 were taken after the peel test of base materials. In Fig.7.10a-d, when the widths of circuit lines are from 24 μm to 10 μm, the cross section of the lines shows that the copper circuit lines remain intact on the dielectric layer. While in Fig.7.10e-f, when the widths of circuit lines are under 10 μm, the copper circuit lines are found to be separate from the dielectric layer. During and after the fabrication process, when the width of the circuit lines decreases, the fine copper lines will more easily leave the dielectric layer.

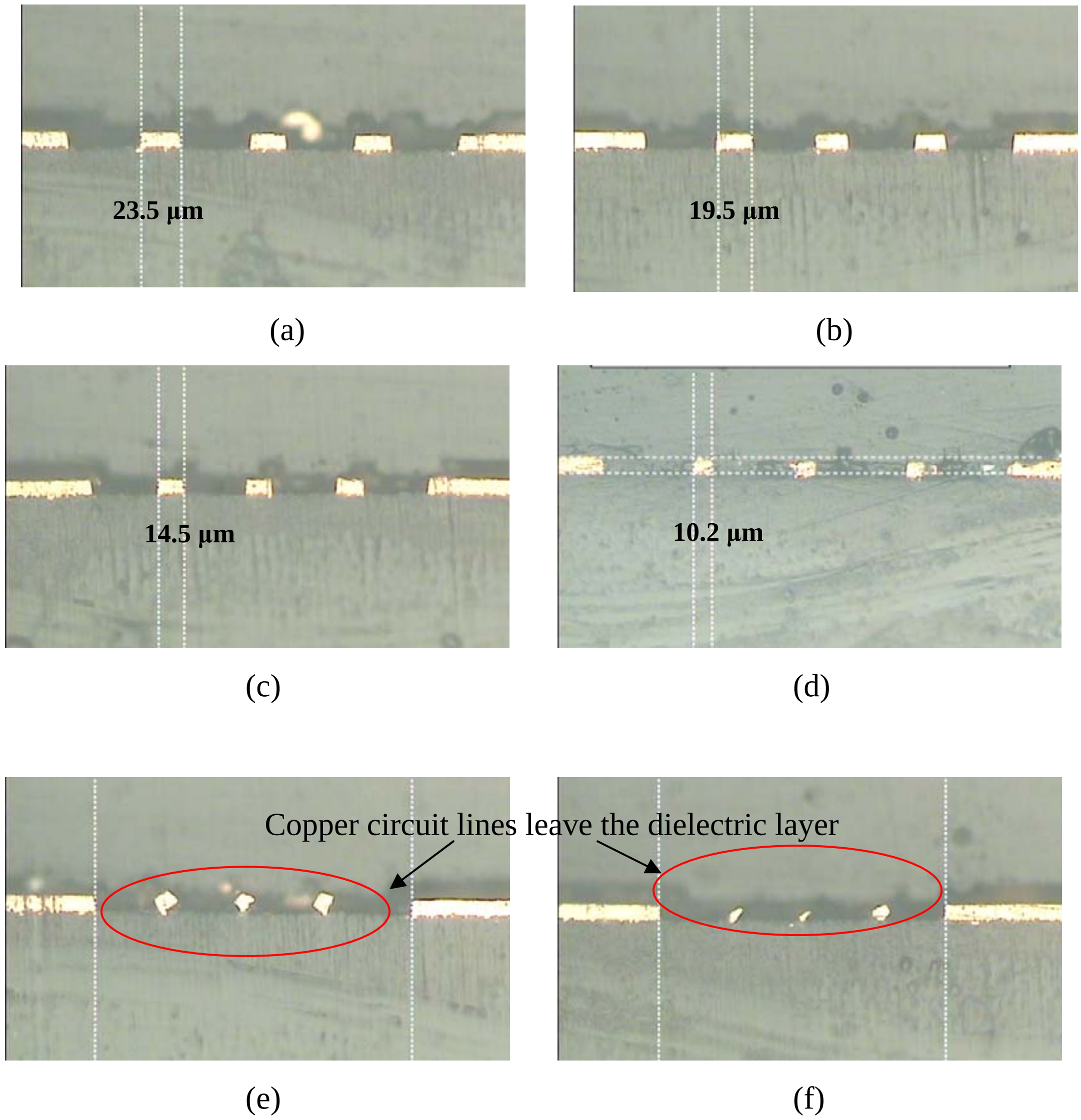

Fig.7.10 The adhesion situation of copper circuit lines on the dielectric layer, after the copper etching process, when the width of circuit lines is (a) 23.5 µm; (b) 19.5 µm; (c) 14.5 µm; (d) 10.2 µm and (e)-(f) under 10 µm.

When the copper circuit lines leave the dielectric material, the productions are unacceptable. So the adhesion quality of circuit lines fabricated by laser structuring is acceptable only when the width of circuit lines is above 10 µm.

7.4 Results and analysis of SIR test

Before the SIR test, the elements between circuit lines were tested with EDX. The EDX results of the elements between circuit lines after laser writing, copper etching and tin stripping steps are shown in Fig.7.11. Because the specimen in SEM was carried out Au coated, the element Au in EDX mapping can be neglected. The element between circuit lines was mainly the copper (after copper etching step). The resistance between circuit lines can reach 10^9 ohm even with this small amount of copper as shown in Table 7.3.

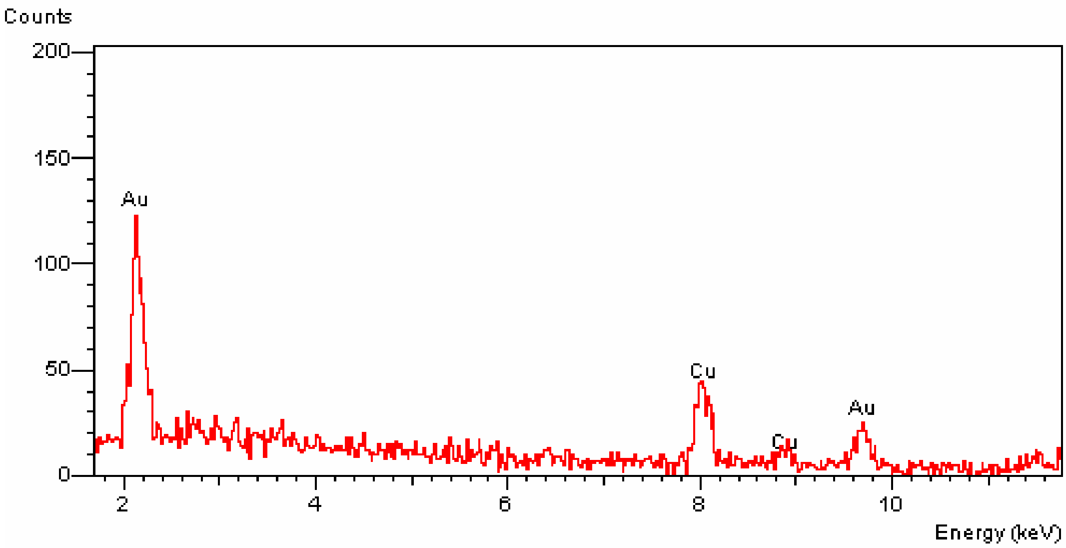

Fig.7.11 EDX analysis of the elements between circuit lines

In Table 7.3, the counts of copper and tin detected by EDX within the same detecting time are listed. The counts detected in the same period of time are comparable. All these data were measured from the circuit spaces between circuit lines after different fabrication step. After the laser writing step (before the copper etching and tin stripping), the amount of copper and tin are much higher than those after etching and stripping step. When there are copper and tin left between circuit lines, the resistance between circuit lines is zero. After the copper etching and tin stripping steps, the amounts of copper and tin decrease obviously. Even there is small amount of copper left in circuit spaces, the insulation between circuit lines is good (above 10^9 ohm) in normal environment.

Table 7.3 The resistance and elements between copper lines

	Resistance between copper lines (ohm)	Elements between copper lines (counts within the same detecting time period)	
		Copper	Tin
Laser structured specimen before etching	0	700	560
Laser structured specimen after etching (etching time = 300 seconds, with tin stripping)	10^9	55	--

The SIR test of circuit line/space was carried out in order to test the insulation between circuit lines under humidity, bias voltage, pressure, and thermal cycling. In this test, the width of circuit lines was 25 μm. The width of circuit spaces varied from 40 μm to 55 μm. Before the SIR test, the specimen should have passed the open/short test first. The minimum width of circuit line and spaces that can pass open/short test was 25 and 40 μm respectively. The experiments of SIR tests were divided into three groups according to the width of circuit space. We took 10^6 ohm as the acceptable value of the resistance between circuit lines. When the insulation resistance between circuit lines was under 10^6 ohm, the SIR test was considered to have failed.

In group one, when the width of circuit spaces were at 40 μm to 45 μm, the insulation resistance between circuit lines was above 10^6 ohm at the beginning of the

SIR test. However, the SIR test failed in the middle of the test duration when the specimens were under high humidity, bias voltage, pressure, and thermal cycle for a period. The high humidity induced short circuit problem between circuit lines under bias voltage when the width of circuit space was small. When the width of circuit spaces were at 45 μm to 50 μm and above 50 μm (in group two and group three), the insulation resistance between circuit lines was above 10^6 ohm from the beginning to the end of the test. These results are listed in Table 7.4.

Table 7.4 The results of SIR test

	Width of spaces (μm)	Width of lines (μm)	SIR test results	Resistance range (ohm)
Group 1	40-45	25	Failure in the middle of the test	-
Group 2	45-50	25	Good	10^8
Group 3	>50	25	Good	10^9

Some of the SIR test results were shown in Fig.7.12. The curve lines in the figures show the resistance between circuit lines in the experiment process. When the resistance was under 10^6 ohm, the SIR machine would stop recording the resistance value.

In Fig.7.12a, when the width of circuit spaces was 40 μm, the resistance between circuit lines varied greatly and dropped under the required level in the twentieth hour in a quick speed. In Fig.7.12b, when the width of circuit spaces was 43 μm, the SIR test ended in the fiftieth hour. The decreasing rate of the resistance was a little slower compared with the first case. The resistance remained above required level and did not vary too much when the width of circuit spaces was 46 μm (in Fig.7.12c) and when the width of circuit spaces was 50 μm (in Fig.7.12d). The resistance in Fig.7.12d was a little larger than the average value in Fig.7.12c.

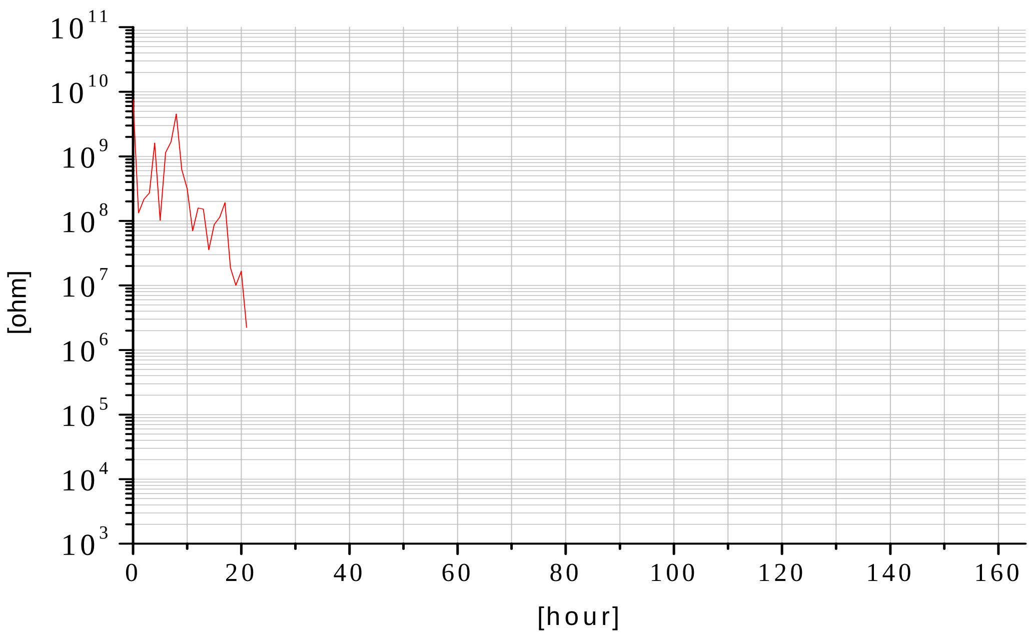

(a)

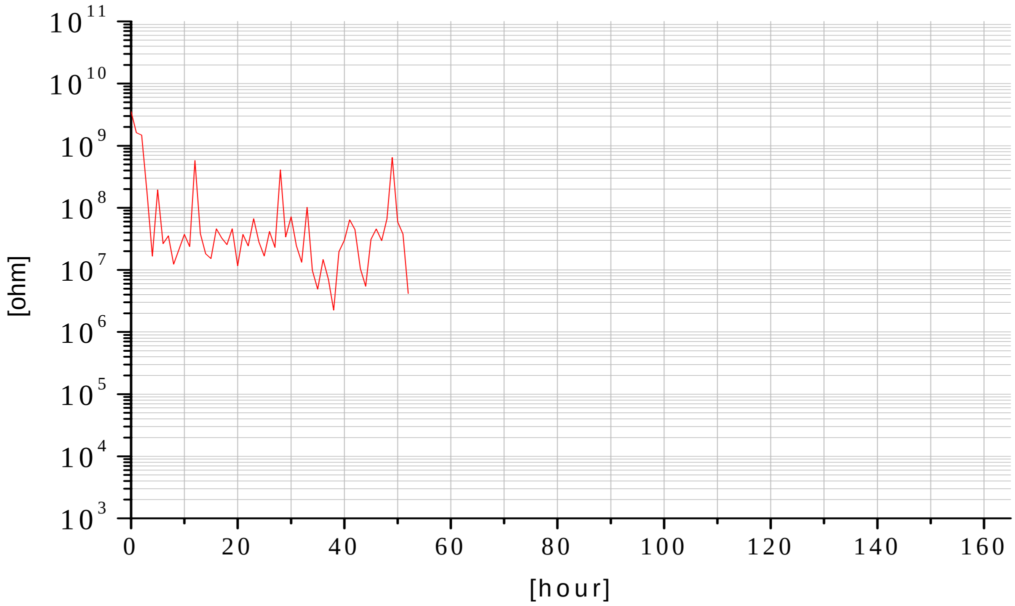

10^{11}
10^{10}
10^{9}
10^{8}
10^{7}
10^{6}
10^{5}
10^{4}
10^{3}
[ohm]
0
20
40
60
80
100
120
140
160
[hour]

(b)

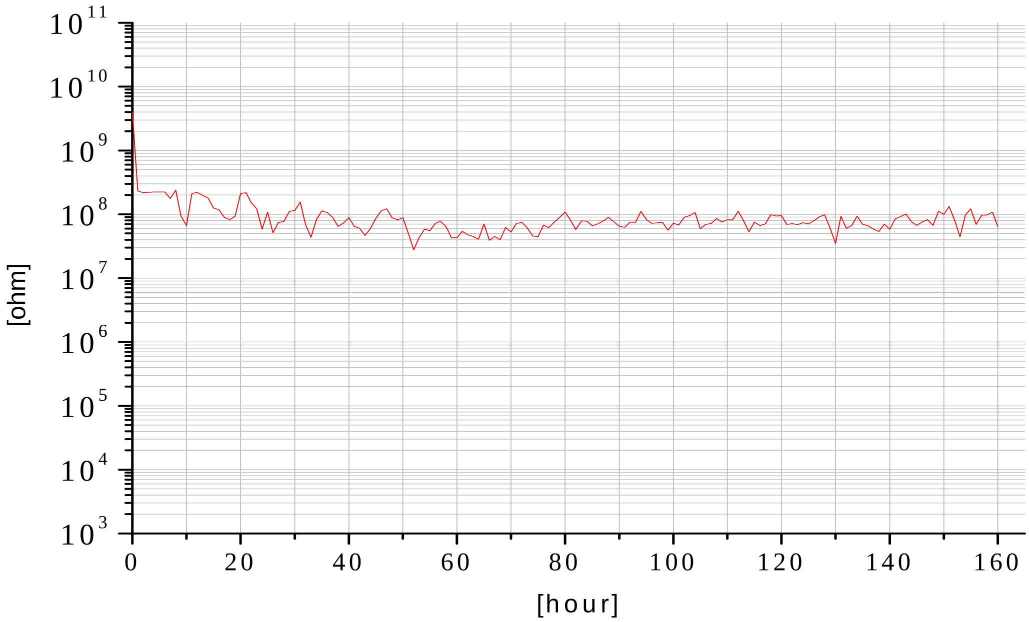

10^{11}
10^{10}
10^{9}
10^{8}
10^{7}
10^{6}
10^{5}
10^{4}
10^{3}
[ohm]
0
20
40
60
80
100
120
140
160
[hour]

(c)

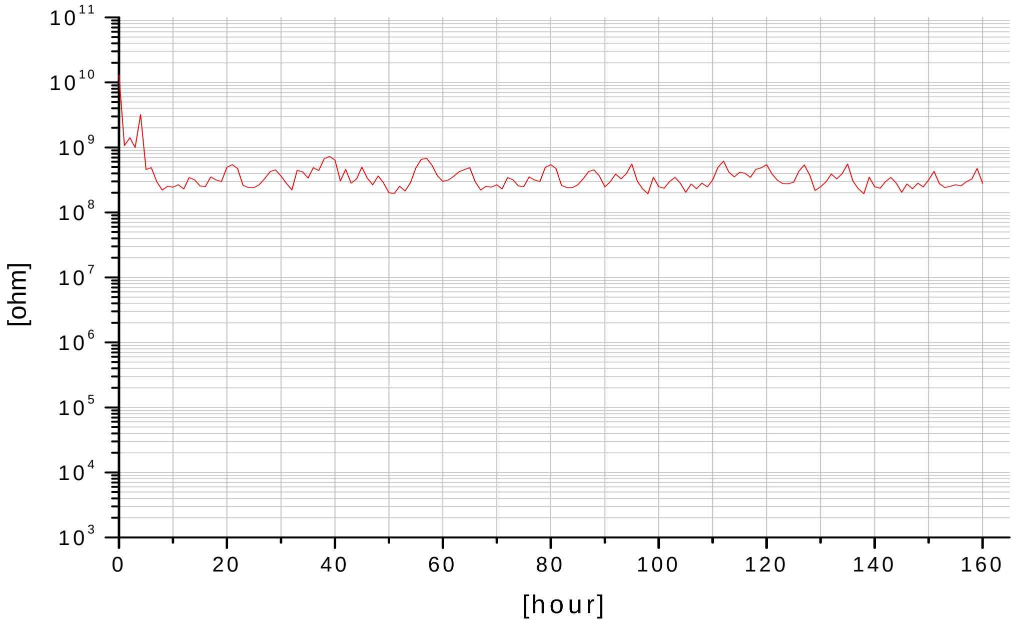

(d)

Fig.7.12 SIR test of the fabrication results of LS with the width of circuit lines and circuit spaces is (a) 25 μm and 40 μm; (b) 25 μm and 43 μm; (c) 25 μm and 46 μm and (d) 25 μm and 50 μm.

From the experimental results, it can be concluded that the resistance between circuit lines decreased dramatically under humid and thermal-cycling environment when the width of circuit spaces was not big enough. In conclusion, the minimum widths of circuit lines and circuit spaces with good quality and reliability fabricated by laser structuring were 25 μm and 45 μm, respectively (Zhang & Yung, 2006).

In Fig.7.13, it shows the final fabrication results of laser structuring with the 25 μm and 45 μm widths of circuit lines and circuit spaces. After the optimization of laser parameters and the control of etching time, the final fabrication results of circuit lines and circuit spaces are neat in profile and are good in quality and reliability.

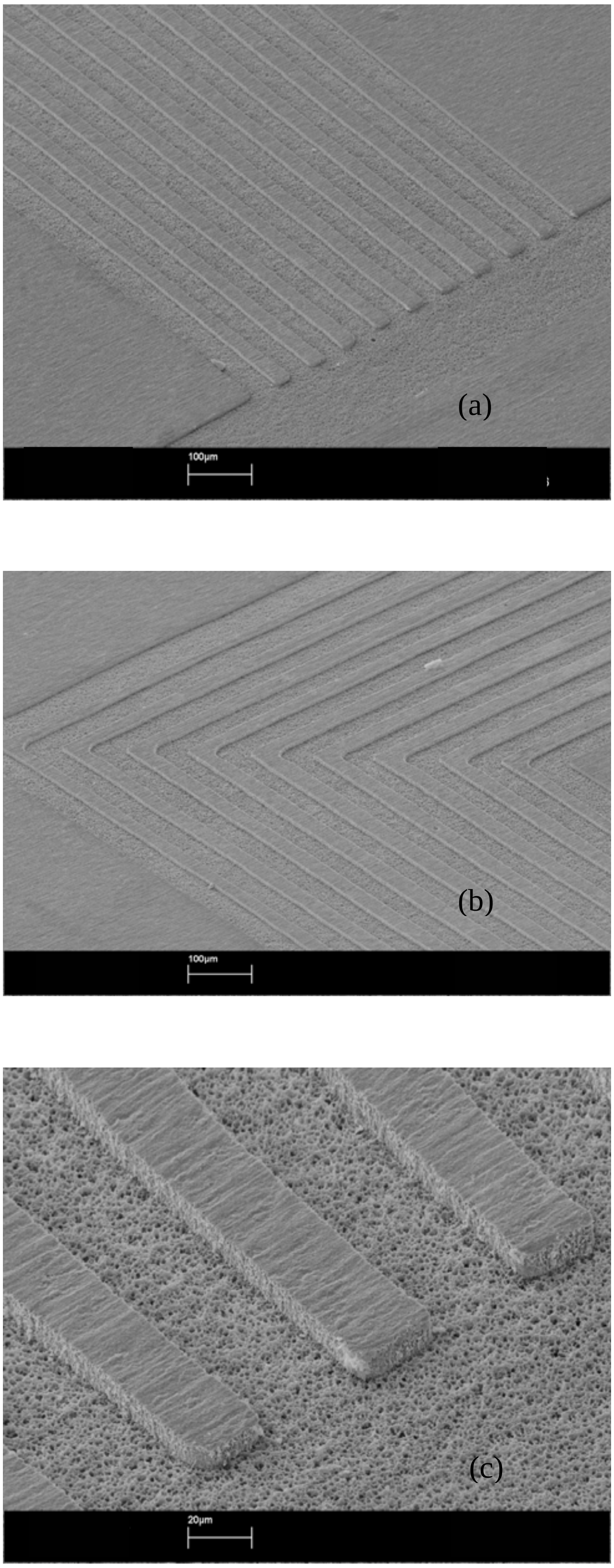

Fig.7.13 Circuit lines and circuit spaces (25 μm and 45 μm) fabricated by laser structuring

CHAPTER 8

CONCLUSIONS, CONTRIBUTIONS AND SUGGESTIONS FOR FUTURE RESEARCH

8.1 Conclusions

This study focuses on the control, prediction and optimization of circuit geometry by studying relations between the process parameters and fabrication results in laser structuring technology. The effects of laser parameters on the geometry of circuits were carried out by experiments and analyzed by mathematical method. The geometry of circuit space can efficiently be controlled by investigating the main factors that influence the characteristic parameters of circuit space with Taguchi methodology. ANN was firstly used in the study of laser structuring technique. With ANN models, the optimization of process parameters in laser writing step can be realized and the 2-D cross-sectional profile of circuit space can be calculated with the combination of ANN model and mathematical method. At last, quality and reliability tests of fine circuit lines and circuit spaces fabricated with laser structuring were also included. The main conclusions are summarized as follows.

8.1.1 Influences of laser parameters on laser structuring results

The effects of laser parameters (Frequency-tripled Nd:YAG laser, 355 nm wavelength) in laser writing step were investigated with experiments. The quantitative relations between laser parameters and fabrication results were achieved.

These experimental results will provide the range of process parameters for the further study of laser writing step with Taguchi methodology and can provide useful information for the real production in industry.

In the laser writing step, the laser parameters will directly influence the geometry of circuit spaces. Some frequently used laser parameters are therefore discussed here, including laser power (P_{out}), number of repetitions (R_s), repetition rate (R_r) and bite size (d_b). Laser power and repetition rate directly influenced the laser energy per pulse E, where $E = P_{out} / R_r$. So the energy absorbed by material (and the depth of circuit space) increased with the increase of laser power and the decrease of repetition rate. The depth of circuit spaces increased with the increase of number of repetitions, but at the same time the problem of splashing materials also increased. So the number of repetition was always selected at a low value to avoid the amount of splashing material. With the increase of the bite size, the depth of circuit spaces decreased first. When the bite size was equal to or larger than the radius of laser beam, the depth of circuit spaces maintained nearly at the same value. Velocity of laser structuring also increased with the increase of bite size when the repetition rate was fixed. However the bite size should not be set at a large value because of considerations of the uniformity of the width of circuit spaces (the variation of the width of circuit spaces in the laser writing and copper etching steps would cause the variation of the width of circuit lines). In this work, the bite size was selected less than the radius of laser beam. By doing this, the variation of the width of circuit space in laser writing step was less than 13%.

For comparison purpose, Excimer laser (KrF, 248 nm wavelength) was used as another laser source in laser structuring technique. Excimer laser shows its advantages when the total width of circuit line and circuit space is under 60 μm, a small dimension that cannot be achieved using Nd:YAG laser. When the total width of circuit line and circuit space is above 60 μm, it was more efficient to use Nd:YAG laser as a laser source whose scanning velocity was about 120 times faster than the Excimer laser. Different with the Nd:YAG laser, the Excimer laser can change the spot size of the laser beam to a small dimension conveniently by inserting a mask. When the Excimer was used as the laser source, the aperture on the middle of the mask let the uniform laser energy pass through it. The material under the irradiation of the laser beam then absorbed almost the same energy. This will contribute to the flatter profile at the bottom of the circuit spaces with the Excimer laser than with the Nd:YAG laser, which had the Gaussian beam output. In the etching process, with the increase in the etching time, the speed of etching were almost the same after being structured by the two lasers.

8.1.2 Main effective factors to the geometry of circuit spaces

Laser writing is the key step in the fabrication of fine circuit lines and circuit spaces in laser structuring technique. The process parameters in laser writing step will directly influence the geometry of circuit spaces (the space width d, the space depth z, the resolidification height h). Laser power and number of repetitions were the most important parameters in laser writing step. They had influences on all the characteristic parameters of the geometry of circuit spaces -- the width of circuit space d, the depth of circuit space z and the resolidification height h. Repetition rate and bite size should also be considered as important factors in laser writing step. The thickness of tin layer and defocused focal length were of minor importance and can be neglected.

The key factors that affected the geometry of circuit spaces were found out with the Taguchi methodology. According to the analysis of variance (ANOVA), we can get the conclusions as follows. The widths of circuit spaces d were mainly controlled by laser power, number of repetition and repetition rate. The most effective factors to the depths of circuit spaces z were laser power, number of repetition, repetition rate and bite size. Among these four parameters, laser power had the greatest influence and then were number of repetition, repetition rate and bite size in the order of priority. The resolidification height h can be reduced by select lower laser power, smaller number of repetition and larger bite size that were the main three factors affecting the resolidification height. The thickness of tin layer and the focal length have minor influence on the experimental results. The interaction between laser power and number of repetition, laser power and repetition rate, laser power and bite size can also be neglected according to the analysis of the ANOVA.

8.1.3 Models in laser writing step

The prediction of the geometry of circuit space in laser writing step was realized by analytical model and ANN model in this work.

In this work, an analytical model previously developed for laser materials processing by Andrews and Atthey (1975) has been further developed to include the consideration of laser parameters (frequency-tripled Nd:YAG laser) and the two-layer structure of material (tin and copper) in laser structuring process. This model is developed by engineering judgement with analytical basis and can give a clear relationship between process parameters and the depth of circuit space.

Artificial neural network (ANN) was also used for the prediction of circuit geometry and the selection of optimum process parameters in laser writing step. ANN model is more convenient for the prediction of all characteristic parameters of circuit space and can be used in more complex situation. However, ANN model has a “black box nature”. ANN model cannot give analytical description between input process parameters and output results. The inputs of the ANN models were the process parameters (laser power, number of repetition, repetition rate, bite size and focal length). The outputs were the three characteristic parameters of circuit geometry for the ANN prediction model and the optimum results of circuit geometry for the ANN optimization model. The layers, hidden nodes and train epochs were two, fifty-four, and one thousand for the ANN prediction model and three, one hundred and thirty, and one thousand for the ANN optimization model respectively. The training data used were collected through a set of experiments designed by Taguchi methodology to provide reliable and valuable information over ranges of the processes from a limited number of experiments. The prediction results and optimization results were further tested by a set of new experiments. In the ANN prediction model, the errors between the prediction results and experimental results were within ±10%. The optimum results from the ANN optimization model also matched the experimental results very well.

The artificial neural network was also combined with mathematical method (the mathematical description of the Gaussian profile) to build a 2-D model for the description of the cross-sectional profile of the circuit spaces in laser writing step.

The advantage of this model is that it can calculate the 2-D circuit space with the consideration of resolidification height which reflects the melt materials during laser writing step. After combining the results predicted for the characteristic parameters of the geometry of the circuit space by the ANN model and the mathematical description of the Gaussian profile, the cross-sectional profile of the circuit spaces got from the 2-D model matched well with experimental results.

8.1.4 Quality and reliability tests of fine circuit lines and circuit spaces fabricated in laser structuring

The quality and reliability of circuit lines and circuit spaces fabricated with laser structuring will influence the further usage of this technique. After the laser writing and copper etching steps (tin layer also stripped away), the final circuit lines and circuit spaces fabricated by laser structuring were tested using the quality and reliability tests - open/short test, peel test and surface insulation resistance test (SIR test).

The minimum width of circuit lines and circuit spaces that passed the open/short test was as narrow as 25±5 μm and 40±5 μm. The failure cause of the open/short test was the variation of the width of circuit lines and circuit spaces which was caused by the bite size of laser and splashing problem in laser writing step and cracking problem of tin layer in the copper etching step. When the variance of the widths of the circuit lines (circuit spaces) is ±5 μm, the variance of the width of the circuit line is ±20% and the variance of the width of the circuit space is ±12.5%. According to IPC 6011, a tolerance of ±20% in the line and space widths is considered acceptable for the fine circuit lines/spaces. The variation of the widths of lines and circuit spaces caused by bite size can be reduced by the decrease of bite size value. The splashing problem can be lessened by selecting proper laser parameters - such as low laser power and small number of repetitions. The influences of tin cracking problem on the variation of the widths of circuit lines and circuit spaces can be reduced by decreasing the etching time in etching step. By keeping attention to the problems above, the emergence of open/short problem can also be minimized.

In the peel test of the base material (FR4 used in this work), the maximum and minimum peel strengths were 0.094 kg/mm and 0.090 kg/mm. All of the values of the peel strength were above IPC specifications (IPC-FC-241C/18) of 0.036 kg/mm for thin materials and 0.071 kg/mm for thick materials. On the base of this material, the minimum width of circuit lines that would remain intact after laser structuring was 10 μm.

The SIR test was used to test the insulation between circuit lines under humidity, bias voltage, pressure and thermal cycling. According to the IPC test method, the experiment was set at 20 cycles of temperature ranging from 25+5/-2°C to 65±2°C, 85-93% relative humidity, 100 ± 10% volts and 160 hours in total. When the widths of circuit spaces were above 45 μm, the resistance between isolated copper lines was above 10^6 ohm from the beginning to the end of the SIR test. In this work, the minimum width of circuit spaces that can pass the SIR test was 45 μm.

As a conclusion, the minimum widths of circuit lines and circuit spaces with good quality and reliability fabricated by laser structuring were 25 μm and 45 μm.

8.2 Suggestions for the future research

For laser structuring technique, the first candidate for future study should be the usage of a mask on the Nd:YAG laser. The radius of laser beam on focal plane is an important factor especially in miniaturization manufacturing because it will influence the total size of circuits. By inserting a mask with aperture, the radius of the laser spot can be reduced and the final size of the circuit lines/spaces can be reduced accordingly. On the other hand, by using a mask, the energy at the edge of the laser beam will be blocked, which will always cause the melting of materials because of the comparatively low energy. The reduction of the melting materials is recommended. So the Nd:YAG laser with a mask has greater advantages in the fabrication of smaller widths of circuit lines/spaces and neat pattern in the laser structuring technique.

The complement of ANN model should also be considered in the future work. In this work, the range of the input parameters of the ANN model are selected when the laser structured depth of circuit space is less than ten micrometers, which is constraint by the thickness of copper layer. When the thickness of copper layer on the printed circuit board is thick enough, the range of the process parameters, which will be used as training data for the ANN model, can be enlarged. The enlargement of the range of input parameters will rich the knowledge of ANN model and make the ANN model have a wider skill in the prediction of fabrication results.

In addition, in laser structuring technique, using a two-layer material structure, the lasers of high intensity and short pulse duration used in the process of laser ablation of materials are different from those used in other laser ablation techniques, such as laser welding and laser cutting. Based on heat transfer theory, the laser structuring technique may be further studied by the Finite Element Modeling (FEM) method. Laser structuring can be described as a laser-material interaction process. The set of appropriate differential equations in finding the 3-D profile of circuit space and circuit line should include heat conductivity equation, energy conservation equation and boundary conditions. In the FEM simulation process, the 3-D profile of the circuit spaces and the resolidification problem should be put on the emphasis.

8.3 Statement of originality and contribution to knowledge

Laser structuring is a new technique in the fabrication of fine circuit lines/spaces. Most of the previous work only introduced laser structuring as a new method in the fabrication of fine circuit lines and mentioned that the width of circuit line can be reduced under 50 μm or below with this technique. However, the control of process parameters and the minimum achievable width of circuit line/space were not available. As a new technique, laser structuring is still immature.

In the laser writing step of laser structuring, the laser-material interaction is different from other laser-material fabrication process such as laser welding, laser cutting and laser drilling. In laser structuring, the laser source is in the UV regime of the spectrum and the base material is a two-layer metal (tin and copper, tin electroplated on FR4 laminate). In this work, the influences of process parameters on the depth of circuit space in laser structuring technology were studied with experiments. Other substrate materials such as PI/Ceramic can also be used as the basic material in laser structuring and can be supposed to achieve the same experimental results of the geometry of circuit space during laser-material interaction process. This is because, in laser structuring technology, laser beam only removes tin layer and a small layer of copper. The underlying dielectric layer remains untouched. So the experimental results of the geometry of circuit space on FR4 laminate can be considered to have a wider guidance to other materials.

The geometry of circuit space (characteristic parameters of circuit space d, z, h) should be controlled in a specific range that is constraint by the thickness of base material, the requirement of the small width of circuit space and the requirement of the less melting materials. The main parameters that influence the characteristic parameters of circuit space were investigated with Taguchi methodology. The good results of the three characteristic parameters of circuit space ($d \leq 30$ μm, 2 μm$\leq z \leq$10 μm, $h \leq 3$ μm, achieved from experimental experience) can be achieved by selecting proper process parameters especially the main factors to each characteristic parameter.

ANN model was firstly used in laser structuring technique for the prediction of circuit geometry and the selection of optimum process parameters. Experiments can be used for the prediction of circuit geometry and the determination of which set of process parameters are good to get optimum fabrication results. However, ANN models are more convenient as a simulation method in these aspects. From the experimental results, it seems that ANN is a useful tool in the simulation and optimization of laser structuring process. The 2-D cross-sectional profile of circuit space with the consideration of resolidification height can be predicted with a new method which combined the ANN prediction model and the mathematical description of the Gaussian profile.

After the laser writing and copper etching step, the final circuit lines and spaces were achieved and tested with quality and reliability tests. By selecting proper process parameters to avoid the emergence of quality and reliability failures, the minimum width of circuit lines and circuit spaces fabricated by laser structuring technique was achieved at 25/45 μm.

References:

1. Adalsteinsson, D., Sethian, J.A., “A level set approach to a unified model for etching, deposition and lithography I: Algorithms and two-dimensional simulations”, J. Comput. Phys. 120, 1995, pp.128-144.
2. Adhikary, B.B. and Mutsuyoshi, H., “Prediction of shear strength of steel fiber RC beams using neural networks”, Construction and Building Materials, Volume 20, Issue 9, November 2006, pp.801-811.
3. Al-Haik, M.S., Hussaini, M.Y. and Garmestani, H., “Prediction of nonlinear viscoelastic behavior of polymeric composites using an artificial neural network”, International Journal of Plasticity, Volume 22, Issue 7, July 2006, pp.1367-1392.
4. Allmen, M. V., “Laser Drilling Velocity in Metals”, Journal of Applied Physics, Volume 48, 1976, pp.5460-5463.
5. Amla, T., “Conductive Anodic Filament Growth Failure”, Proceedings of the technical conference of IPC printed circuits EXPO, March 2002, S08-2.
6. Anderson, D., McNeil, G., Artificial Neural Networks Technology, 2002 August, Data and Analysis Center for Software, NY.
7. Andrews, J.G. and Atthey, D.R., “On the Motion of an Intensely Heated Evaporating Boundary”, Journal of Inst. Maths Applics, 1975, pp.59-72.
8. Armon, E., Zvirin, Y., Laufer, G. and Solan, A., “Metal drilling with a CO_2 laser beam. I. Theory”, Journal of Applied Physics, 65(12), 1989, pp.4995-5002.
9. Ayata, T., Savusog, A., and Arcaklıog, E., “Predictions of temperature distributions on layered metal plates using artificial neural networks”,

Energy Conversion and Management, Volume 47, Issues 15-16, September 2006, pp.2361-2370.

10. Bandyopadhyay, S., Gokhale, H., “A statistical approach to determine process parameter impact in Nd:YAG laser drilling of IN718 and Ti-6Al-4V sheets”,Optics and Lasers in Engineering, Volume 43, Issue 2, February 2005, pp.163-182.
11. Barclay, B., Morrell, M., “Laser Direct Imaging: A User’s Perspective”, Circuit Tree, October 1, 2001, http://www.circuitree.com.
12. Basu, B. and Srinivasan, J., “Numerical study of steady-state laser melting problem”, International Journal of Heat and Mass Transfer, 1988, 31, pp.2331-2338.
13. Bauerle, D., Laser Processing and Chemistry, Springer-Verlag Berlin Heidelberg 2000, Germany, Third Edition.
14. Bendell, A., Taguchi Methods Applications in World Industry, IFS Publications, Bedford, 1989.
15. Bender, M., Otto, M., Hadam, B., Spangenberg, B. and Kurz, H., “Multiple Imprinting in UV based Nanoimprint Lithography: Related Materials Issues”, Microelectronic Engineering, 61-62, 2002, pp.407-413.
16. Bergstresser, T., Hilburn, R., “Adhesiveless Copper on Polyimide Substrate with Nickel-Chromium Tiecoat”, IPC Printed Circuit Expo 2003, Long Beach, CA, 2003.
17. Bernard, W. and Smith, F.W., “Pattern-Recognizing Control Systems”, Computer and Informations Sciences Symposium Proceedings, Spartan Books, Washington, DC, 1963.

18. Bernard, W., “Pattern Recognition and Adaptive Control”, Applications and Industry, September 1964.

19. Bogaerts, A., Chen, Z. Y., Gijbels, R., Vertes, A., “Laser ablation for analytical sampling: what can we learn from modeling”, Spectrochimica Acta Part B 58, 2003, pp.1867-1893.

20. Bogaerts, A., Chen, Z.Y., “Effect of laser parameters on laser ablation and laser-induced plasma formation: A numerical modeling investigation”, Spectrochimica Acta Part B: Atomic Spectroscopy, Volume 60, Issues 9-10, October 2005, pp.1280-1307.

21. Born, M., Wolf, E., Principles of Optics, Pergamon, New York, 1975.

22. Boutinguiza, M., Pou, J., “Drilling of slate tiles by CO_2 laser”, Optics & Laser Technology, Volume 37, Issue 5, July 2005, pp.348-356.

23. Bransch, H. N., “Welding with High-power CW and Pulsed Nd:YAG lasers,” Photonics Spectra, September 1991, pp.107.

24. Bruneau, S., Hermann, J., “Ultra-fast laser ablation applied to deep-drilling metals”, Applied Surface Science, Volume 248, Issues 1-4, 30 July 2005, pp.299-303.

25. Bruch, J.C., Papadopoulos, J.C.A., Sloss, J.M., “Parallel computing used in solving wet chemical etching semiconductor fabrication problems”, Math. Sci. Appl. 1, 1993, pp.282-292.

26. Buchner, C., Wijinaendts van Resandt, R.W., “The Future of Lithography in HDI and PCB Industries”, PCB Fabrication, February 2004, pp.18-20.

27. Camon, H. and Gue, A.M., “Modelling of anisotropic etching in silicon-based sensor application”, Sensors and Actuators A, 33, 1992,

pp.103-105.

28. Casalino, G., Filippis, L.A.C., "A technical note on the mechanical and physical characterization of selective laser sintered sand for rapid casting", Journal of Materials Processing Technology, Volume 166, Issue 1, 15 July 2005, pp.1-8.

29. Casalino, G., Curcio, F., "Investigation on Ti6Al4V laser welding using statistical and Taguchi approaches", Journal of Materials Processing Technology, Volume 167, Issues 2-3, 30 August 2005, pp.422-428.

30. Chan, C. L., Mazumder, J. and Chen, M. M., "Effect of surface tension gradient driven convection in a laser melt pool: Three-dimensional perturbation model", Journal of Applied Physics, 64(11), 1988, pp.6166-6174.

31. Choi, J.W., Lee, K.E., "Adhesion Strength and Peeling Angle Measured on the Polyimide/Cr Interfaces", Journal of Materials Research Society 2000, Volume629, FF5.10.1-FF5.10.6.

32. Christou, A., Integrating Reliability into Microelectronics Manufacturing, John Wiley and Sons, Inc., 1994.

33. Cole, E. I., "Local thermal probing to detect open and shorted IC interconnections", Microelectronics Reliability 39, 1999, pp.681-693.

34. Cus, F. and Zuperl, U., "Approach to optimization of cutting conditions by using artificial neural networks", Journal of Materials Processing Technology, Volume 173, Issue 3, 20 April 2006, pp.281-290.

35. Darchen, A., Drissi-Daoudi, R., "Electrochemical investigations of copper etching by Cu(NH3)4Cl2 in ammoniacal solutions", Journal of Applied

Electrochemistry 27, 1997, pp.448-454.

36. Dietz, K., “Alkaline Etching”, http://www.circuitree.com, 02/01/2005.

37. Drissi-Daoudi, R., Irhzo, A., Darchen, A., “Electrochemical investigations of copper behavior in different cupric complex solutions: Voltammetric study”, Journal of Applied Electrochemistry 33, 2003, pp.339-343.

38. Dudirham, J.J., Damme, R.M.J., “Space-time Discontinuous Galerkin Method for Wet-Chemical Etching of Microstructures”, The Proceedings of European Congress on Computational Methods in Applied Sciences and Engineering, 2004.

39. Duley, W.W., “UV lasers: effects and applications in materials science”, New York, NY:Cambridge University, 1996, 78 ff (4).

40. Dumitru, G., “Metallographical analysis of steel and hard metal substrates after deep-drilling with femtosecond laser pulses”, Applied Surface Science, Volumes 208-209, 15 March 2003, pp.181-188.

41. Edward, I.C., “Local thermal probing to detect open and shorted IC interconnections”,Microelectronics and Reliability, Volume 39, Issue 5, May 1999, pp.681-693.

42. Endelt, B., Nielsen, K.B. and Danckert, J., “ New framework for on-line feedback control of a deep-drawing operation”, Journal of Materials Processing Technology, in Press, available online 12 June 2006.

43. Endert, H., Patzel, R., Basting, D., “Excimer laser: a new tool for precision micromaching”, Opt Quantum Electron 1995, 1995, 27: pp.1319-35.

44. Fathi, A. and Aghakouchak, A.A., “Prediction of fatigue crack growth rate in welded tubular joints using neural network”, International Journal of Fatigue,

in Press, available online 18 May 2006.

45. Fausett, L., Fundamentals of neural networks: architectures, algorithms, and applications, Prentice-Hall, London, 1994.

46. Fishburn, J.M., Withford, M.J., “Study of the fluence dependent interplay between laser induced material removal mechanisms in metals: Vaporization, melt displacement and melt ejection”, Applied Surface Science, in Press, available online 8 September 2005.

47. Ganesh, R. K., Faghri, A., “A generalized thermal modeling for laser drilling prcess--I. Mathematical modeling and numerical methodology”, Journal of Heat Mass Transfer, Volume40, No.14, 1997, pp.3351-3360.

48. Gurney, K., An Introduction to Neural Networks, UCL Press, London, 1997.

49. Hauder, M., “Electromigration resistance of sputtered silver lines using different patterning techniques”, Microelectronic Engineering Volume 60, Issues 1-2 , January 2002, pp.51-57.

50. Haykin, S., Neural Networks, 2nd Edition, Upper Saddle River, N.J., Prentice Hall, 1999.

51. Henderson, C.L., “Quality and Reliability”, Semiconductor Reliability, 2001.

52. Higgins, L., Schreiner, A., “Laser Structuring as an Enabling Technology for HDI and PSGA,” Proc. Fifth Pan Pacific Microelectronics Symposium, 2000, pp.23-32.

53. Ho, J. R., Grigoropoulos, C. P. and Humphrey, J. A. C., “Computational Study of Heat Transfer and Gas Dynamics in the Pulsed Laser Evaporation of Metals”, Journal of Applied Physics, val. 78, 1995, pp.4696-4709.

54. Horn, H., Beil, S., Wesner, D. A., Weichenhain, R. and Kreutz, E. W.,

"Excimer laser pretreatment and metallization of polymers", Nuclear Instruments and Methods in Physics Research Section B: Beam Interactions with Materials and Atoms, Volume 151, Issues 1-4, 2 May 1999, pp.279-284.

55. Ifflander, R., Solid-State Lasers for Materials Processing, Springer-Verlag Berlin Heidelberg, Germany, 2001.

56. Jacobs, R.A., 1988. Increased rates of convergence through learning rate adaptation. Neural Networks1, pp.295-307.

57. Jain, K., Zemel, M., Klosner, M., "Large-area Excimer Laser Lithography and Photoablation Systems," Microlithography World 11, August 2002, pp.8–10.

58. Jalonen, P., "A new concept for making fine line substrate for active component in polymer", Microelectronics Journal 34, 2003, pp.99-107.

59. Jeng, J.Y., Mau, T.F, Leu, S.M., "Prediction of laser butt joint welding parameters using back propagation and learning vector quanization networks", Journal of Materials Processing Technology 99, 2000, pp207-218.

60. Jeong, S.H., Greif, R., Russo, R.E., "Numerical modeling of pulsed laser evaporation of aluminum targets", Applied Surface Science 127-129, 1998, pp.177-183.

61. Jonnalagadda, K., "Reliability of via-in-pad structures in mechanical cycling fatigue", Microeletronics Reliability 42, 2002, pp.253-258.

62. Kaneko, K., Noda, T., Sakata, M., Uchiyama, T., "Observation and numerical simulation for wet chemical etching process of semiconductor", Proceedings of 4th ASME–JSME Joint Fluids Engineering Conference, Honolulu, USA,

2003.

63. Kar, A. and Mazumder, J., "Two-Dimensional Model for Material Damage due to Melting and Vaporization during Laser Irradiation", Journal of Applied Physics, Volume 68, 1990, pp.3884-3891.

64. Karnakis, D.M., "High power single-shot laser ablation of silicon with nanosecond 355 nm", Applied Surface Science, Available online 25 October 2005.

65. Karatas, C., Keles, O., Uslan, I. and Usta, Y., "Laser cutting of steel sheets: Infuence of workpiece thickness and beam waist position on kerf size and stria formation", Journal of Materials Processing Technology, Volume 172, Issue 1, 20 February 2006, pp.22-29.

66. Kerr, C., "Sustainable technologies for the regeneration of acidic tin stripping solutions used in PCB fabrication", Circuit World, 30/3, 2004, pp.51-58.

67. Keusseyan, R.L., Amey, D.I. and Horowitz, S.J., "New Low Cost Interconnection Materials For High Frequency MCM Applications", 1998 International Conference on Multichip Modules and High Density Packaging, pp.206-211.

68. Kim, D., Oh, B. and Lee, H., "Effect of liquid film on near-threshhold laser ablation of a solid surface", Applied Surface Science, 2004, pp.138-147.

69. Kimpfel, "Fine line production: the issues for PCB manufacturers", Printed Circuit Europe, May-June 1999, pp.12-14.

70. Kordas, K., Pap, A.E., Toth, G., "Laser soldering of flip-chips", Optics and Lasers in Engineering, Volume 44, Issue 2, February 2006, pp.112-121.

71. Kou, S., Wang, Y. H., “Three-dimensional convection in laser melted pools”, Metallurgical Transactions A, 17A, 1986, pp.2265-2270.

72. Krause, J., “High- precision PCB technology”, Printed Circuit Europe, 1st Quarter 2000, pp.16-19.

73. Krause, J., “High- Precision Working”, PC FAB, March 2000, pp.24-28.

74. Kuiken, H. K., Kelly, J. J., “Etching profiles at resist edges- Mathematical models for diffusion-controlled cases”, Journal of Electrochemistry Society 133, 1986, pp.1217-1226.

75. Kuiken, H.K., “Etching: a two-dimensional mathematical approach”, Proc. R. Soc. Lond. A 392, 1984, pp.199-225.

76. Kuo, T.Y., Lin, H.C., “Effects of pulse level of Nd:YAG laser on tensile properties and formability of laser weldments in automotive aluminum alloys”, Materials Science and Engineering: A, Volume 416, Issues 1-2, 25 January 2006, pp.281-289.

77. Lam, Y.C., Chai, J.C., Rath, P., “A fixed grid method for chemical etching”, Int. Commun. Heat Mass Transfer 31(8), 2004, pp.1123–1131.

78. Laude, L.D., “Excimer lasers”, Kluwer Academic, 1994.Li, J., and Ananthasuresh, G.K., “A quality study on the excimer laser micromachining of electro-thermal-compliant micro devices”, Journal of Micromechanics and Microengineering, 2001, pp.38-47.

79. Lee, H.K., Han, H.S., “Optimization of Nd:YAG laser welding parameters for sealing small titanium tube ends”, Materials Science and Engineering: A, Volume 415, Issues 1-2, 15 January 2006, pp.149-155.

80. Li, Q., Zheng, Y.J., “A novel high-peak power double AO Q-switches pulse

Nd:YAG laser for drilling”, Optics & Laser Technology, Volume 37, Issue 5, July 2005, pp.357-362.

81. Li, Q., Yu, J.Y., “BP neural network prediction of the mechanical properties of porous NiTi shape memory alloy prepared by thermal explosion reaction”, Materials Science and Engineering: A, Available online 10 February 2006.

82. Li, W.J., Shih, J.C., Mai, J.D., “Numerical simulation for the sacrificial release of MEMS square diaphragms”, in: 1st International Conference on MSMSSA, San Jose, USA, April 1998.

83. Low, D.K.Y., Li, L., “An investigation into melt flow dynamics during repetitive pulsed laser drilling of transparent media”, Optics & Laser Technology, Volume 33, Issue 7, October 2001, pp.515-522.

84. Luo. H, Zeng. H, Hu. L.J., Zhou. Z.D., “Application of artificial neural network in laser welding defect diagnosis”, Journal of Materials Processing Technology, July 2005.

85. Magna, A.L., Arrigo, G.D., Garozzo, G., Spinella, C., “Computational analysis of etched profile evolution for the derivation of 2D dopant density maps in silicon”, Mater. Sci. Eng. B 102 (1-3), 2003, pp.43-48.

86. Mao, X.L., Zeng, X.Z, “Time-resolved plasma properties for double pulsed laser-induced breakdown spectroscopy of silicon”, Spectrochimica Acta Part B: Atomic Spectroscopy, Volume 60, Issues 7-8, 31 August 2005, pp.960-967.

87. Martin, B., “Characterisation of cw Nd:YAG laser keyhole dynamics”, Optics & Laser Technology 33, 2001, pp.201-207.

88. McCulloch, Warren S., and Pitts, Walter H., “A Logical Calculus of the Ideas

Immanent in Neural Nets", Bulletin of Mathematical Biophysics, Volume 5, 1943.

89. McKee, T., "Nd:YAG lasers", LIA handbook of laser materials processing, 2001, pp.535-536.

90. McKeever, M. R., "Laser Direct Imaging—Trends for the Next Generation of High Performance Resists for Electronic Packaging", Proceedings of the technical conference of IPC printed circuits EXPO, April 2000, S12-1.

91. McKenney, D. J. and Numakura, D. K., "Design of Quality Assurance System for High Density Flex Circuits", Proceedings of the technical conference of IPC printed circuits EXPO, April 2001, S12-2.

92. McKesson, D., "Miracles in Tin stripping", RD Chemical Co., Mountain View, CA, http://www.pcbfab.com/tinstrip.html, Page last updated on 12/09/99.

93. Meier, D. J., "UV Laser Direct Patterning of HDI Applications", Proceedings of the technical conference of IPC printed circuits EXPO, April 2001, S04-3.

94. Metev, S. M., Veiko, V. P., Laser assisted microtechnology, Springer Series in Materials Science, Volume 19, 1994.

95. Moen, R.D., Improving Quality Through Planned Experimentation, McGraw-Hill, Inc., New York, 1991.

96. Morgan, E., Chemometrics: Experimental Design, Wiley, New York, 1997.

97. Neves, B., "Test Setup, Procedures and Patterns for Conductive Anodic Filament and Electrochemical Migration Testing", Proceedings of the technical conference of IPC printed circuits EXPO, March 2002, S08-1.

98. Notten, P.H.L., Kelly, J.J., Kuiken, H.K., "Etching profiles at resist edges—II.

Experimental confirmation of models using GaAs”, Journal of Electrochem. Soc. 133, 1986, pp.1226-1232.

99. Ohlig, B., “Meeting HDI Resolution and Registration Requirements”, Proceedings of the technical conference of IPC printed circuits EXPO, April 2000, S12-2.

100. Olabi, A.G., Casalino, G., Benyounis, K.Y. and Hashmi, M.S.J., “An ANN and Taguchi algorithms integrated approach to the optimization of CO_2 laser welding”, Advances in Engineering Software, Volume 37, Issue 10, 2006, pp.643-648.

101. Orr, N.S. and Cummins, F., Neural Networks, http://www.willamette.edu, 1999.

102. Paek, U., Gagliano, F. P., “Thermal Analysis Laser Drilling Processes”, IEEE Journal of Quantum Electronics, Volume QE-8, 1972, pp.112-119.

103. Pan, L.K., Wang, C.C., Hsiao, Y.C. and Ho, K.C., “Optimization of Nd:YAG laser welding onto magnesium alloy via Taguchi analysis”, Optics & Laser Technology, Volume 37, Issue 1, February 2005, pp.33-42.

104. Pandey, N.D., Shan, H.S. and Bharti, A., “Percussion drilling with laser: hole completion criterion”, The International Journal of Advanced Manufacturing Technology, Volume 28, pp.863-868.

105. Pantsar, H., Kujanpaa, V., “Effect of oxide layer growth on diode laser beam transformation hardening of steels”, Surface and Coatings Technology, Volume 200, Issue 8, 24 January 2006, pp.2627-2633.

106. Parker, D.B., “Optimal Algorithms for Adaptive Networks: Second Order Back Propagation, Second Order Direct Propagation and Second Order

Hebbian Learning”, Proc. of the 1st ICNN, Volume II, 1987.

107. Partha, A., Zemel, M. and Jain, K., “A Comparison of PCB Imaging Technologies”, Proceedings of the technical conference of IPC printed circuits EXPO, April 2001, S-15-02.

108. Qiu, W., Watson, J., Thonpson, D. S., Deans, W. F., “Modelling the interaction between laser and target material in laser microspectral analysis”, Optics and Laser Technology, Volume26, No. 3, 1994, pp.157-166.

109. Rath, P., Chai, J.C., “A fixed-grid approach for diffusion and reaction-controlled wet chemical etching”, International Journal of Heat and Mass Transfer 48, 2005, pp.2140-2149.

110. Rath, P., Chai, J.C., “Modeling two-dimensional diffusion-controlled wet chemical etching using a total concentration approach”, International Journal of Heat and Mass Transfer, 2005, pp.1480-1488.

111. Rao, B.T., Kumar, H., Nath, A.K., “Processing of concretes with a high power CO_2 laser”, Optics & Laser Technology, Volume 37, Issue 5, July 2005, pp.348-356.

112. Ready, J. F., “Effects of High Power Laser Radiation”, Academic Press, New York, 1971.

113. Rodriguez, E., “Plasma dynamics studies during the preparation of PbTe thin film on glass substrate”, Vacuum, available online 2 August 2005.

114. Roelants, E., “Laser Direct Structuring as an Innovative Alternative for Traditional Lithography”, IPC- Expo2002 Long Beach Proceedings: 2002, S03-3-1-9.

115. Rohde, H. and Verboven, P., “Precision Cutting and Drilling with a Nd:YAG

Slab Laser", 1995 International symposium for electromachining ISEM XI, 1995, pp.777-783.

116. Rowlands, H., Antony, J., Knowles, G., "An application of experimental design for process optimization", The TQM Magazine, Volume 12 No.2, 2000, pp.78-83.

117. Rominger, S., "Predicting Reliabililty Of Printed Wiring Boards With Variable Parameters Using Finite Element Modeling", Proceedings of the technical conference of IPC printed circuits EXPO, April 2000, S06-2.

118. Ross, P.J., Taguchi Techniques for Quality Engineering, McGraw-Hill Book Company, New York, 1989.

119. Rumelhart, D.E., Hinton, G.E., Williams, R.J., "Learning representations by back-propagating errors", Nature 323, 1986, pp.533-536.

120. Rumelhart, D.E., Hinton, G.E., and Williams, R.J., "Learning Internal Representations by Error Propagation", Institute for Cognitive Science Report 8506, San Diego, University of California, 1985.

121. Scaroni, J., Design News, July 1985, pp.17-20.

122. Schlesinger, M., "Electroplating", Electrochemistry Encyclopedia, September, 2002.

123. Sciti, D., Bellosi, A., "Laser-induced surface drilling of silicon carbide", Applied Surface Science, Volume 180, Issues 1-2, 1 August 2001, pp.92-101.

124. Shimizu, K., Komatsu, K., "Controlled Surface Etching Process for Fine Line/Space Circuits", Proceedings of the technical conference of IPC printed circuits EXPO, March 2002, S07-3.

125. Shin, C.B., Economou, D.J., "Effect of transport and reaction on the shape

evolution of cavities during wet chemical etching”, J. Electrochem. Soc. 136 1989, pp.1997-2004.

126. Siau, S., Vervaet, A., “Adhesion Strength of the Epoxy Polymer/Copper Interface for Use in Microelectronics“, Journal of Electrochemics Society, Volume 152, Issue 6, 2005, pp. c442-c455.

127. Siegel, J., Epurescu, G., Perea, A., Gordillo-Vázquez, F.J., Gonzalo, J. and Afonso, C.N., “High spatial resolution in laser-induced breakdown spectroscopy of expanding plasmas”, Spectrochimica Acta Part B: Atomic Spectroscopy, Volume 60, Issues 7-8, 31 August 2005, pp.915-919.

128. Smith, L., “An Introduction to Neural Networks”, University of Stirling, 1996.

129. Solana, P., Kapadia, P., “An analytical model for the laser drilling of metals with absorption within the vapor”, Journal of Phys. D: Appl. Phys. 32, 1999, pp.942-952.

130. Spawr, W. J., “Appropriate lasers and optics in surface treatment”, Handbook of Laser Materials Processing, 2001, pp.271.

131. Srinivasan, J., Basu, B., “A numerical study of thermocapillary flow in a rectangular cavity during laser melting”, International Journal of Heat and Mass Transfer, Volume29, April 1986, pp.563-572.

132. Stauffer, L., Würsch, A., Gächter, B., Siercks, K., Verettas, I., Rossopoulos, S. and Clavel, R., “A surface-mounted device assembly technique for small optics based on laser reflow soldering”, Optics and Lasers in Engineering, Volume 43, Issues 3-5, March-May 2005, pp.365-372.

133. Steen, W. M. and Kamalu, J. N., “Laser Cutting”, Laser Materials Processing,

North-Holland Pub. Company, New York, 1983 Volume3.

134. Stergiou, C. and Siganos, D., “Neural Networks”, http://www.doc.ic.ac.uk.

135. Stone, D. E., “Laser Direct Imaging- A Cost Effective Choice”, Proceedings of the technical conference of IPC printed circuits EXPO, April 2001, S18-3.

136. Sudirham, J.J. and Damme, R.M.J., “Space–time discontinuous Galerkin method for wet-chemical etching of microstructures”, Proceedings of European Congress in Applied Sciences and Engineering, ECCOMAS, Jyvaskyla, Finland, 2004.

137. Sun, Z., Wan, K.T. and Dillard, D.A., “A theoretical and numerical study of thin film delamination using the pull-off test”, International Journal of Solids and Structures 41, 2004, pp.717-730.

138. Suna, B. K., O’Keefe, T. J., “Growth of electrolytic copper dendrites and their adhesion to an epoxy resin”, Surface and Coating technology 106, 1998, pp.44-52.

139. Tadic, E., “Hair’s Breadth Structures for Future Product Designs”, SMT Ausgabe 1-2/2000, 12ff.

140. Taff, I., “Direct Imaging- Major Trends and Impact on PCB Manufacturers”, Proceedings of the technical conference of IPC printed circuits EXPO, April 2001, S04-1.

141. Taguchi, G., Introduction to Quality Engineering, Asian Productivity Organisation, Tokyo, 1986.

142. Tam, S.C., “Optimization of laser deep-hole drilling of Inconel 718 using the Taguchi method”, Journal of Materials Processing Technology, Volume 37, Issues1-4, February 1993, pp.741-757.

143. Tam, S.C., Lim, L.E.N., Quek, K.Y., "Application of Taguchi methods in the optimization of the laser-cutting process", Journal of Materials Processing Technology, Volume 29, Issues 1-3, January 1992, pp.63-74.

144. Tan, B., Venkatkrishnan, K., "Laser drilling of thick material using femtosecond pulse with a focus of dual-frequency beam", Optics & Laser Technology, Volume 35, Issue 3, April 2003, pp.199-202.

145. Tan, X.Y., Zhang, D.M., "Vaporization effect studying on high-power nanosecond pulsed laser deposition", Physics B: Condensed Matter, Volume 358, Issues 1-4, 15 April 2005, pp.86-92.

146. Terliuc, G. and Benron, H., "Thermal Direct Imaging and HDI- Advanced Registration Accuracy and High Yields with Conventional DES Process", proceedings of the technical conference of IPC printed circuits EXPO, April 2000, S12-3.

147. Thawari, G., "Influence of process parameters during pulsed Nd:YAG laser cutting of nickel-based superalloys", Journal of Materials Processing Technology, Volume 170, Issues 1-2, 14 December 2005, pp.229-239.

148. Thompson, E., "Fabrication of step and flash imprint lithography templates using commercial mask processes", Proceeding of The SPIE's Int. Symp. on Microlithogaphy: Emerging Lithographic Technologies VII, Santa Clara, CA, February 2003.

149. Tobar, M.J., "Laser transformation hardening of a tool steel: simulation-based parameter optimization and experimental results", Surface and Coatings Technology, available online 27 December 2005.

150. Toelants, E., "Laser Direct Structuring as an Innovative Alternative for

Traditional Lithography", Proceedings of the technical conference of IPC printed circuits EXPO, March 2002, S03-3.

151. Tohde, H. and Dausinger, F., "Investigation of the dynamical process during the formation of a micro through hole", ECLAT'96, pp.675-682.

152. Tunna, L., O'Neill, W., Khan, A. and Sutcliffe, C., "Analysis of laser micro drilled holes through aluminium for micro-manufacturing applications", Optics and Lasers in Engineering, Volume 43, Issue 9, September 2005, pp.937-950.

153. Vaucher, C., Jaquet, R., "Laser Direct Imaging and Structuring", www.circuitree.com, august 2002.

154. Vuik, C., Cuvelier, C., "Numerical solution of an etching problem", J. Comput. Phys. 59, 1985, pp.247–263.

155. Wang, X.F., Lu, X.D., "Research on the temperature field in laser hardening", Optics & Laser Technology, Volume 38, Issue 1, February 2006, pp.8-13.

156. Wang, X.Y., Ng, G.K.L., Chen, G.N., Hu, Sh.G. and Su, Y.P., "EPMA microanalysis of recast layers produced during laser drilling of type 305 stainless steel", Thin Solid Films, Volumes 453-454, 1 April 2004, pp.84-88.

157. Waxler, S., "Direct Imaging Implementation: Real World Case Studies", Proceedings of the technical conference of IPC printed circuits EXPO, April 2000, S12-4.

158. Westberg, D., Paul, O., "Surface micromachining by sacrificial aluminium etching", Journal of Micromech. Microeng. 6, 1996, pp.376-384.

159. Wheeler, J.A., "Laser Direct Imaging A Solution for Fine Line Imaging", Proceedings of the technical conference of IPC printed circuits EXPO,

March 2002, S03-4.

160. Xu, L.J., Xing, J.D., Wei, S.Z., Zhang, Y.Z. and Long, R., “Optimization of heat treatment technique of high-vanadium high-speed steel based on back-propagation neural networks”, Materials & Design, in Press, available online 19 May 2006.

161. Yang, L.J., “Plasma surface hardening of ASSAB 760 steel specimens with Taguchi optimisation of the processing parameters”, Journal of Materials Processing Technology, Volume 113, Issues 1-3, 15 June 2001, pp.521-526.

162. Yang, H.J., Hwang, P.J., “A study on shrinkage compensation of the SLS process by using the Taguchi method”, International Journal of Machine Tools & Manufacture 42, 2002, pp.1203-1212.

163. Zacharia, T., Eraslan, A. H., David, S. A., “Three-dimensional transient model for arc welding process”, Metallurgical Transactions B, 20B, 1989, pp.645-659.

164. Zemel, M., “X-Y Scaling Compensation Technology for Fine-Line PCB Imaging with High-Precision Alignment”, IPC Printed Circuit Expo, Proc. of Technical Conf., Long Beach, CA, Mar. 26-28, 2002, S03-1-1.

165. Zhang, B., Yung, K.C., “Frequency-tripled Nd:YAG laser ablation in laser structuring process”, Optics and Lasers in Engineering, Volume 44, Issue 8, August 2006, pp.815-825.

166. Zhang, B., Yung, K.C., “Feasibility of the 248 nm Excimer laser in the laser structuring of fine circuit lines on printed circuit board”, International Journal of Advanced Manufacturing Technology, accepted January 2006.

167. Zhang, B., Yung, K.C., “Analysis of process parameters of laser structuring

with Taguchi method", Optics and Laser Technology, submitted.

168. Zhang, B., Yung, K.C., "The quality and reliability of fine circuit lines fabricated by laser structuring technique", Industrial Engineering Research, Vol. 3 (1), 2006, pp.10-19.

169. Zhang, S., Baets, J. D., Calster, A. V., "A two-layer high density printed circuit board and its reliability", Microelectronics Rliability 39, 1999, pp.1337-1341.

170. Zhang, D.M., Tan, X.Y., "Thermal regime and effect studying on the ablation process of thin films prepared by nanosecond pulsed laser", Physical B: Condensed Matter, Volume 357, Issues 3-4, 15 March 2005, pp.348-355.

171. Zhang, Y., Faghri, A., "Vaporization, melting and heat conduction in the laser drilling process", International Journal of Heat and Mass Transfer 42, 1999, pp.1775-1790.

172. Zorich, R., Handbook of Quality Integrated Circuit Manufacturing, Academic Press, Inc., 1991.

Appendix A: Journal and conference publications arising from this research

Journal papers

1. Zhang, B., Yung, K.C., "Frequency-tripled Nd:YAG laser ablation in laser structuring process", Optics and Lasers in Engineering, Volume 44, Issue 8, August 2006, pp. 815-825.
2. Zhang, B., Yung, K.C., "Feasibility of the 248 nm Excimer laser in the laser structuring of fine circuit lines on printed circuit board", International Journal of Advanced Manufacturing Technology, accepted January 2006.
3. Zhang, B., Yung, K.C., "Analysis of process parameters of laser structuring with Taguchi method", Optics and Laser Technology, submitted.
4. Zhang, B., Yung, K.C., "The quality and reliability of fine circuit lines fabricated by laser structuring technique", Industrial Engineering Research, Volume 3 (1), 2006, pp.10-19.

Conference paper

1. Zhang, B., Yung, K.C., "Studies of frequency tripled Nd:YAG laser in laser structuring process", 24th International Congress on Applications of Lasers & Electro-Optics, Miami, Florida, USA, October 31 2005, pp.315-324.